

Nonlocal Models of Complex Systems

Lead Guest Editor: András Rontó

Guest Editors: Alexander Domoshnitsky, Robert Hakl, Nino Partsvania,
and Manuel Zamora





Nonlocal Models of Complex Systems

Complexity

Nonlocal Models of Complex Systems

Lead Guest Editor: András Rontó


Guest Editors: Alexander Domoshnitsky, Robert Hakl, Nino Partsvania, and Manuel Zamora



Copyright © 2020 Hindawi Limited. All rights reserved.

This is a special issue published in "Complexity." All articles are open access articles distributed under the Creative Commons Attribution License, which permits unrestricted use, distribution, and reproduction in any medium, provided the original work is properly cited.

Chief Editor

Hiroki Sayama , USA

Associate Editors

Albert Diaz-Guilera , Spain
Carlos Gershenson , Mexico
Sergio Gómez , Spain
Sing Kiong Nguang , New Zealand
Yongping Pan , Singapore
Dimitrios Stamovlasis , Greece
Christos Volos , Greece
Yong Xu , China
Xinggang Yan , United Kingdom


Academic Editors

Andrew Adamatzky, United Kingdom
Marcus Aguiar , Brazil
Tarek Ahmed-Ali, France
Maia Angelova , Australia
David Arroyo, Spain
Tomaso Aste , United Kingdom
Shonak Bansal , India
George Bassel, United Kingdom
Mohamed Boutayeb, France
Dirk Brockmann, Germany
Seth Bullock, United Kingdom
Diyi Chen , China
Alan Dorin , Australia
Guilherme Ferraz de Arruda , Italy
Harish Garg , India
Sarangapani Jagannathan , USA
Mahdi Jalili, Australia
Jeffrey H. Johnson, United Kingdom
Jurgen Kurths, Germany
C. H. Lai , Singapore
Fredrik Liljeros, Sweden
Naoki Masuda, USA
Jose F. Mendes , Portugal
Christopher P. Monterola, Philippines
Marcin Mrugalski , Poland
Vincenzo Nicosia, United Kingdom
Nicola Perra , United Kingdom
Andrea Rapisarda, Italy
Céline Rozenblat, Switzerland
M. San Miguel, Spain
Enzo Pasquale Scilingo , Italy
Ana Teixeira de Melo, Portugal

Shahadat Uddin , Australia
Jose C. Valverde , Spain
Massimiliano Zanin , Spain


Contents

A Case Study on Computer-Based Analysis of the Stochastic Stability of Mechanical Structures Driven by White and Colored Noise: Utilizing Artificial Intelligence Techniques to Design an Effective Active Suspension System

Aydin Azizi 


Research Article (8 pages), Article ID 7179801, Volume 2020 (2020)

Orthopedic Boot-Tree 3D Design by means of the Integral Curves of Solutions of Differential Equations

Merab Shalamberidze, Zaza Sokhadze , and Malvina Tatvidze


Research Article (6 pages), Article ID 4252790, Volume 2020 (2020)

Applications of Artificial Intelligence Techniques to Enhance Sustainability of Industry 4.0: Design of an Artificial Neural Network Model as Dynamic Behavior Optimizer of Robotic Arms

Aydin Azizi 


Research Article (10 pages), Article ID 8564140, Volume 2020 (2020)

A Case Study on Designing a Sliding Mode Controller to Stabilize the Stochastic Effect of Noise on Mechanical Structures: Residential Buildings Equipped with ATMD

Aydin Azizi 



Research Article (17 pages), Article ID 9321928, Volume 2020 (2020)

Differential Transform Algorithm for Functional Differential Equations with Time-Dependent Delays

Josef Rebenda  and Zuzana Pátíková



Research Article (12 pages), Article ID 2854574, Volume 2020 (2020)

Multiobjective Optimization Model of Production Planning in Cloud Manufacturing Based on TOPSIS Method with Combined Weights

Zhiru Li, Wei Xu , Huibin Shi, Qingshan Zhang , and Fengyi He

Research Article (15 pages), Article ID 7503176, Volume 2019 (2019)

Distributed Control and the Lyapunov Characteristic Exponents in the Model of Infectious Diseases

M. Bershadsky, M. Chirkov, A. Domoshnitsky , S. Rusakov, and I. Volinsky 




Research Article (12 pages), Article ID 5234854, Volume 2019 (2019)

Nonlocal Symmetry and Bäcklund Transformation of a Negative-Order Korteweg–de Vries Equation

Jinxi Fei, Weiping Cao , and Zhengyi Ma 


Research Article (10 pages), Article ID 5479695, Volume 2019 (2019)

Oscillation Criteria for Third-Order Emden–Fowler Differential Equations with Unbounded Neutral Coefficients

George E. Chatzarakis, Said R. Grace , Irena Jadlovská, Tongxing Li , and Ercan Tunç 

Research Article (7 pages), Article ID 5691758, Volume 2019 (2019)

An Application of (3+1)-Dimensional Time-Space Fractional ZK Model to Analyze the Complex Dust Acoustic Waves

Lei Fu and Hongwei Yang 

Research Article (15 pages), Article ID 2806724, Volume 2019 (2019)

Research Article

A Case Study on Computer-Based Analysis of the Stochastic Stability of Mechanical Structures Driven by White and Colored Noise: Utilizing Artificial Intelligence Techniques to Design an Effective Active Suspension System

Aydin Azizi 

School of Engineering, Computing and Mathematics, Oxford Brookes University, Wheatley Campus, Oxford No. 33 1HX, UK

Correspondence should be addressed to Aydin Azizi; aydin.azizi@brookes.ac.uk

Received 16 April 2019; Revised 6 November 2019; Accepted 29 January 2020; Published 25 April 2020

Academic Editor: András Rontó

Copyright © 2020 Aydin Azizi. This is an open access article distributed under the Creative Commons Attribution License, which permits unrestricted use, distribution, and reproduction in any medium, provided the original work is properly cited.

The goal of this research is to design an Artificial Intelligence controller for the active suspension system of vehicles. The Ring Probabilistic Logic Neural Network (RPLNN) architecture has been adopted to design the proposed controller, and the pavement condition has been modelled utilizing Gaussian white noise. The results show that the proposed RPLNN controller has an effective performance to reduce the unwanted stochastic effect of the road profile.

1. Introduction

1.1. Background. During the car transportation due to conversion of absorbed energy by suspension and tire of the vehicle to thermal energy, an energy loss happens. Utilizing an effective suspension system gives an opportunity to reduce the energy loss and save energy [1], and saving energy means reducing the fuel consumption. In recent years, many researchers focus on reducing the undesirable effects of the pavement and decrease the fuel consumption rate by designing effective suspension systems [2].

In 2012, Ismail et al. [3] proposed an Artificial Neural Network (ANN) model for a light-duty diesel engine powered using blends of various biodiesel fuels with conventional fossil diesel. Cay et al. [4] utilized ANN to predict the brake specific fuel consumption. In 2014, Roy et al. [5] modelled the performance and emission parameters of a single-cylinder four-stroke engine under CNG-diesel dual-fuel mode by ANN. In 2015, the performance, emission, and combustion characteristics of a single-cylinder, four-stroke variable compression ratio engine were predicted with the aid of ANN by Muralidharan and Vasudevan [6]. As an intelligent technique,

particle swarm optimization has been adopted by Olivera et al. [7] to reduce vehicle emissions and fuel consumption in the city. In 2016, Lotfan et al. [8] combined ANN and nondominated sorting genetic algorithm II to model and reduce CO and NOx emissions from a direct injection dual-fuel engine. ANN has been utilized by Perrotta et al. [9] in 2017 to model fuel consumption of trucks. In 2018, Azizi [10] proposed a PID controller to control fuel consumption rate based on the changing pavement condition. Although the result of the research shows that the proposed PID controller can reduce the fuel consumption, but the vibration at the beginning of the control procedure because of the input control signal for few seconds is high.

The current research aims to design an effective Artificial Intelligence (AI) architecture to decrease the effect of the road profile which shows itself as imposed vibration on vehicle. It means less fuel consumption and higher parts life can be achieved by filtering such a noise. In this research, Gaussian white noise has been adopted to model the road profile. Different from previous works, the aim of the current research is presenting an effective approach to eliminate the mentioned fluctuation and

control the fuel consumption rate even at the beginning of the control process [11, 12]. For this purpose, Ring Probabilistic Logic Neural Network (RPLNN) which is an effective paradigm and has been utilized by researchers as a function optimizer, prediction tool, and plant simulator [13–16] is adopted here to be trained by the PID controller proposed by Azizi et al. [10]. In this paper, MATLAB software and Simulink toolbox have been utilized to develop a simulation-based model of the active suspension system of the vehicle and design an effective RPLNN controller to investigate and reduce the effect of the imposed vibration from the road profile. The proposed simulator is capable of simulating the vertical displacement of the vehicle before and after utilizing the AI controller, also it is capable of analyzing these vibrations by examining the different values of the system parameters. The results show that the proposed RPLNN controller has a superior performance than the PID controller and has an effective performance to reduce the imposed vibration by the road profile and reducing the fuel consumption rate.

After the brief introduction and literature review about the research topic, the remaining parts of the paper is organized in three more sections. First, in Section 2, mathematical modeling of a proposed active suspension of a quarter car model proposed RPLNN algorithm, and the simulation-based model set up have been discussed in detail. In Section 3, which is the results section, the designed simulator has been verified by analyzing the effect of the proposed controller's effect on system vertical displacement. Finally, in Section 4, the summary of the research has been given and possible future works have been suggested.

2. Methodology

Fuel consumption rate can be affected by two important factors: vehicle handling performance and vehicle suspension system [17]. In conventional method, a passive suspension system which is a combination of springs and dampers has been utilized to reduce the imposed vibrations to the vehicle from the pavement profile. It is important to know that, since the damping ratio cannot be adjusted, so such a system is not able to eliminate the imposed vibration. Nowadays, by advancement in technology active suspension systems which are equipped with effective controllers are being utilized to reduce the effect of pavement conditions. [18].

The ultimate goal of this research has been defined as to design an effective AI controller to reduce the undesirable effect of the road profile on vehicles. The steps of the proposed methodology in this research have been defined in the following order. The first step is introducing the quarter car model equipped with an active suspension system. The second step is utilizing RPLNN algorithm to design an efficient controller as a part of the active suspension system. The third step is utilizing MATLAB software to train the proposed AI controller. The next step is simulating the proposed set up utilizing Simulink, and the last step is testing

and analyzing the performance of the proposed RPLNN controller and comparing it with the performance of the PID controller.

2.1. Active Suspension Controller Model. The quarter car model, which is a model to investigate the dynamic vibration of a vehicle with regards to the road profile as the input of the model, has been illustrated in Figure 1. It is important to know that, in such a model some parameters such as geometrical information, pitching, and rolling angles have not been neglected, but most of the important features such as the change of the load has been considered.

In the current work, to generate the mathematical model, the state space method which is one of the well-known approaches in control engineering has been adopted [20].

To generate the state space representation, the first step is analyzing the quarter car model (Figure 1), which has been carried out by the following equations:

$$M_1 \ddot{x}_1(t) + D [\dot{x}_1(t) - \dot{x}_2(t)] + k_1 [x_1(t) - x_2(t)] = u, \quad (1)$$

$$M_2 \ddot{x}_2(t) - D [\dot{x}_1(t) - \dot{x}_2(t)] + k_1 [x_2(t) - x_1(t)] + k_2 [x_2(t) - x_0(t)] = -u. \quad (2)$$

M_1 (300 kg) and M_2 (40 kg) are the sprung and unsprung masses, respectively. K_1 (15000 N/m) and D (1000 N/m) are stiffness and damping coefficients of spring and damper of the suspension system, respectively. K_2 (150000 N/m) is the stiffness coefficient of the spring which is the model of the tire of the vehicle. The vertical displacements of the sprung mass, unsprung mass, and pavement condition have been shown by $X_1(t)$, $X_2(t)$, and $X_0(t)$, respectively, and the parameter U represents the controlled force.

Now, the state variables with respect to the dynamic equations (1) and (2) and can be defined as follows:

$$\begin{aligned} x_1 &= x_2(t), \\ x_2 &= x_1(t), \\ x_3 &= \dot{x}_2(t), \\ x_4 &= \dot{x}_1(t). \end{aligned} \quad (3)$$

By substituting state variables presented on equation (3) in equations (2) and (3), we will get the following expressions:

$$\dot{x}_4 = -\frac{D}{M_1}x_4 + \frac{D}{M_1}x_3 - \frac{K_1}{M_1}x_2 + \frac{K_1}{M_1}x_1 + \frac{u}{M_1}, \quad (4)$$

$$\dot{x}_3 = \frac{D}{M_2}x_4 - \frac{D}{M_2}x_3 - \frac{K_1}{M_2}x_1 + \frac{K_1}{M_2}x_2 - \frac{K_2}{M_2}x_1 + \frac{K_2}{M_2}x_0 - \frac{u}{M_2}, \quad (5)$$

In general state space variables, change can be defined as follows:

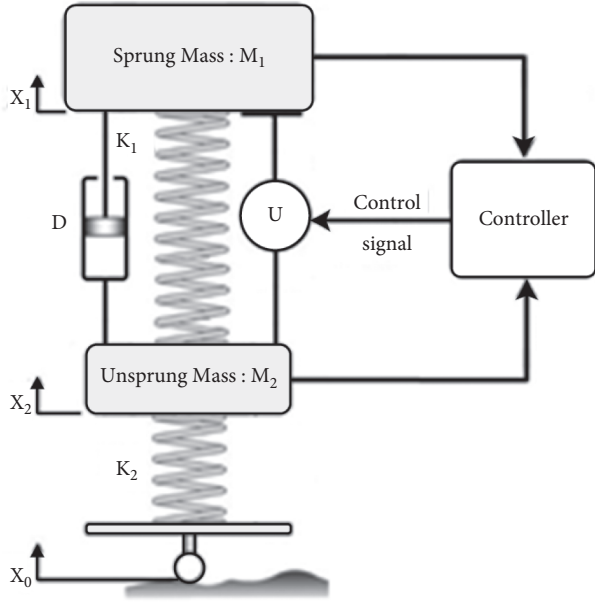


FIGURE 1: Quarter car model equipped with the active suspension system [19].

$$\frac{dX}{dt} = AX + BU, \quad (6)$$

$$X = [x_1 \ x_2 \ x_3 \ x_4]^T. \quad (7)$$

So, based on equations (4) and (5) matrixes A and B of equation (6) will be as follows:

$$A = \begin{bmatrix} 0 & 0 & 1 & 0 \\ 0 & 0 & 0 & 1 \\ \frac{k_1 + k_2}{M_2} & \frac{k_1}{M_2} & \frac{D}{M_2} & \frac{D}{M_2} \\ \frac{k_1}{M_1} & \frac{k_1}{M_1} & \frac{D}{M_1} & \frac{D}{M_1} \end{bmatrix}, \quad (8)$$

$$B = \begin{bmatrix} 0 & 0 \\ 0 & 0 \\ \frac{k_2}{M_2} & \frac{1}{M_2} \\ 0 & \frac{1}{M_1} \end{bmatrix}.$$

The system input variable matrix is

$$U = [x_0(t) \ u]^T. \quad (9)$$

The vehicle suspension system output matrix equation is

$$Y = CX + DU \quad (10)$$

In this paper, the output has been defined as the difference of the vertical displacement of the sprung and unsprung masses:

$$Y = x_2(t) - x_1(t). \quad (11)$$

So, based on equation (11) matrixes C and D of equation (10) will be as follows:

$$C = [-1 \ 1 \ 0 \ 0], \quad (12)$$

$$D = [0 \ 0].$$

After introducing the mathematical model of the quarter car model, the next step is investigation of one of the inputs of this mathematical model which is the pavement condition.

2.2. White Noise Road Input Signal. Mathematical modeling of the pavement condition due to its Gauss-distributed stochastic behavior is too hard. To fulfill this task, the Gaussian white noise which shows randomness behavior can be utilized as the representative of the statistical pavement power spectral density. As shown in equation (13), the relationship of the random road input signal and the Gaussian white noise per ISO/TC108/SC2N67 can be modelled mathematically as shown in the following equation [21]:

$$\frac{q(s)}{w(s)} = \frac{2\pi n_0 \sqrt{G_q(n_0)v}}{s + 2\pi f_0}. \quad (13)$$

where $q(s)$ is the random road input signal, $w(t)$ is the Gaussian white noise, n_0 is Reference Spatial frequency, $G_q(n_0)$ is the Road roughness coefficient, and f_0 is the Filter lower-cut-off frequency.

After introducing the quarter car mathematical model and the Gaussian white noise as one the input signals of it, the next step is the design of the controller utilizing the RPLNN algorithm.

2.3. Ring Probabilistic Logic Neural Networks Controller. Probabilistic Logic Neuron (PLN) is a weightless neuron which its output can be defined as one, zero, or "don't care" states [22]. Because of the "don't care" state, the PLNs have flexibility to bind together and design a fast-learning weightless neural networks [14]. Based on this property the RPLNN has been proposed by Menhaj et al. [23] as a novel algorithm to model, control, and optimize complex plants. The proposed design consists of PLNs in which the output of the last one is fed by the input of the first one (see Figure 2).

In 2016, Azizi et al. [15, 22] utilized RPLNN structure as an optimizer tool to optimize weightless neural networks and RFID networks. Later, the RPLNN structure has been developed and utilized as a part of the hybrid optimizers [13, 14, 16, 24, 25].

In the current research, different from previous works, the weightless RPLNN has been utilized to be trained by the

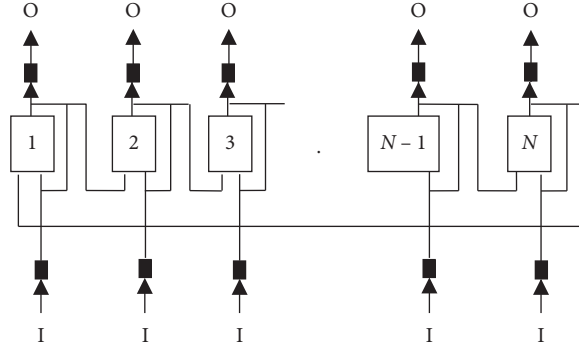


FIGURE 2: RPLNN structure [13].

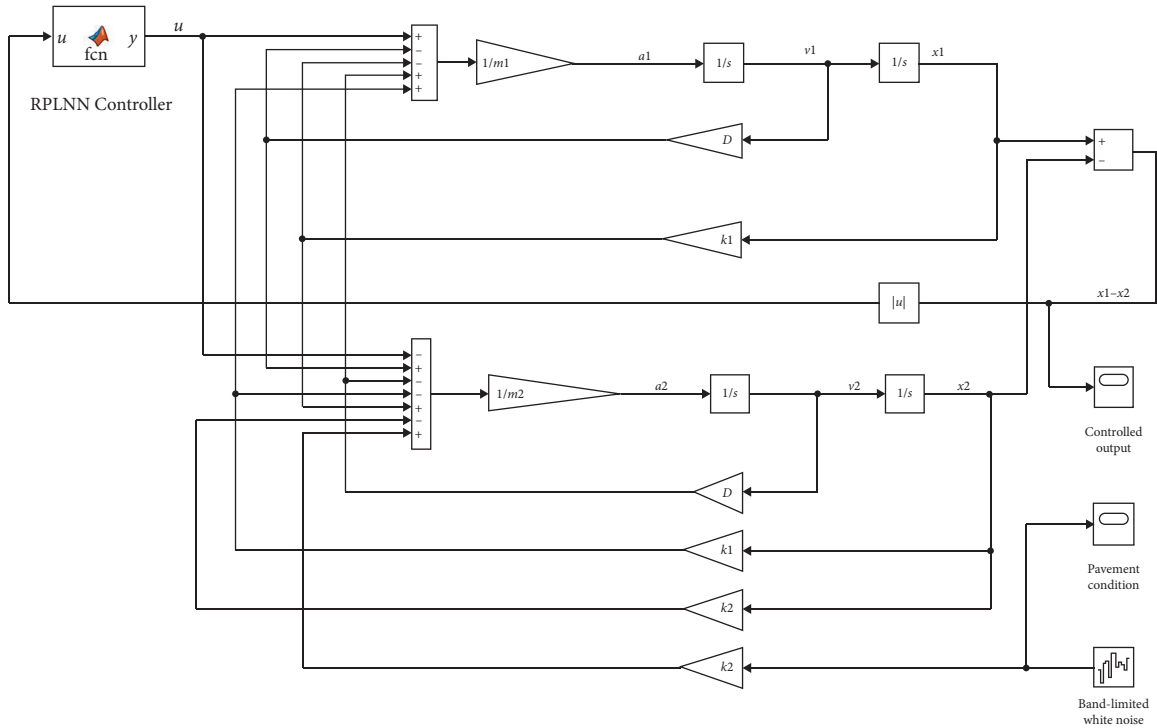


FIGURE 3: MATLAB Simulink Model of the Noise Cancellation system for the quarter car model.

proposed PID controller in previous reserach [10], so after the accomplishment of the training process, the proposed RPLNN has been utilized as the controller to reduce the vertical vibration of the vehicle due to the road conditions which can be considered as Gaussian white noise input.

The input of the RPLNN will be the vertical displacement of the vehicle, and the output will be the actuator's force. It means that the proposed controller regulates the active suspension system's force considering the vibration due to road condition.

To fulfill this task, it is essential to define an objective function. Since the proposed algorithm gives a fitter result in each iteration, so it can be called as an evolutionary algorithm. Here, since the aim is reducing the difference between the vertical displacements of the sprung and unsprung masses, so the objective function can be defined as the error function (see equation (14)). In this case by minimizing the

objective function the RPLNN controller will be able to adjust the active suspension force. It is important to know that to train the RPLNN controller the reference modelis the data of the PID controller, which has been proposed by Azizi at el. [10, 26]:

$$E(t) = x_1(t) - x_2(t). \quad (14)$$

3. Results

As seen in Figure 3, the proposed quarter car model has two inputs: the first one is the road condition which is taken as random input and has been modelled by Gaussian white noise function, and the second input is the generated force by the RPLNN controller to reduce the effect of the imposed noise to the vehicle.

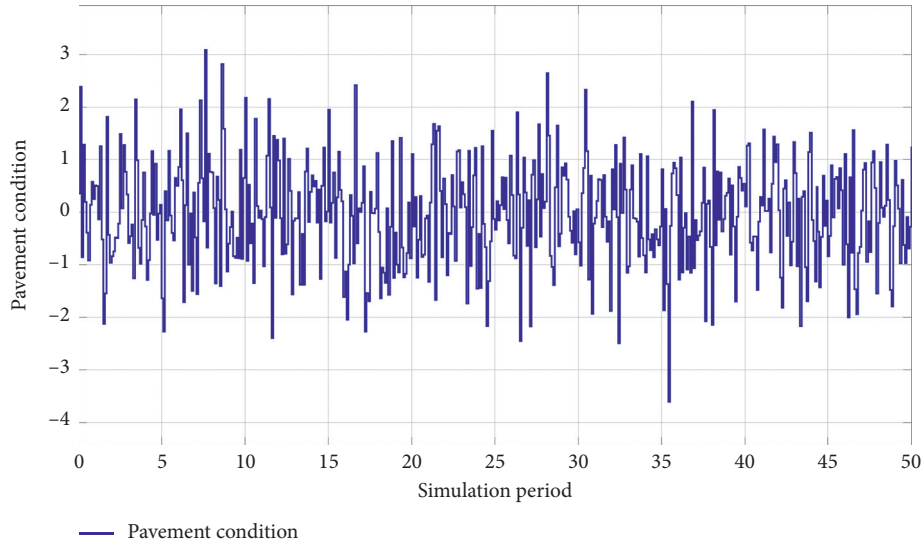


FIGURE 4: Pavement condition.

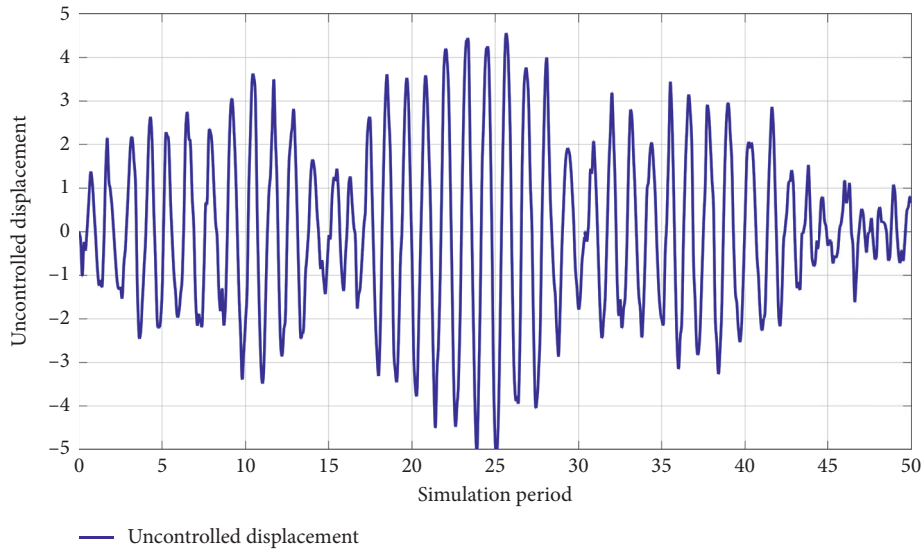


FIGURE 5: Uncontrolled displacement.

As seen in Figure 4, first input, which is the road condition, has been modelled by Gaussian white noise and the effect of this noise, which is the vertical displacement of the car, has been shown as uncontrolled displacement in Figure 5.

As seen in Figure 5, the quarter car model fluctuates based on the road input signal. Since it is the uncontrolled behavior, so by comparing Figures 4 and 5, it can be observed that the vehicle completely follows the road condition which can result in increasing the fuel consumption and compromising passenger's safety.

As it is mentioned previously, the reference model which has been utilized to train the RPLNN is the data of the PID controller which has been presented in Figures 6 and 7.

The RPLNN controller has been trained offline by running the training for 100 iterations. As seen in Figure 8, at the end of the training procedure the error function value

has been reduced to 0.001. The output of the system by utilizing RPLNN controller has been calculated and shown in Figure 9.

By comparing Figures 5 and 9, which are the indicators of the behavior of the system equipped and not equipped with RPLNN controller, it can be observed that the system equipped with the RPLNN controller reduces the effect of the pavement on the vehicle and reduces the vibrations.

Noise cancellation results utilizing PID and RPLNN controllers have been shown in Figures 9 and 10, respectively. By comparing these two figures, it can be observed that both controllers are able to reduce the undesired effect of the pavement profile on the vehicle. It is important to mention that although both controllers are able to reduce the vertical vibrations in the same simulation period, but since the active suspension system equipped with the RPLNN

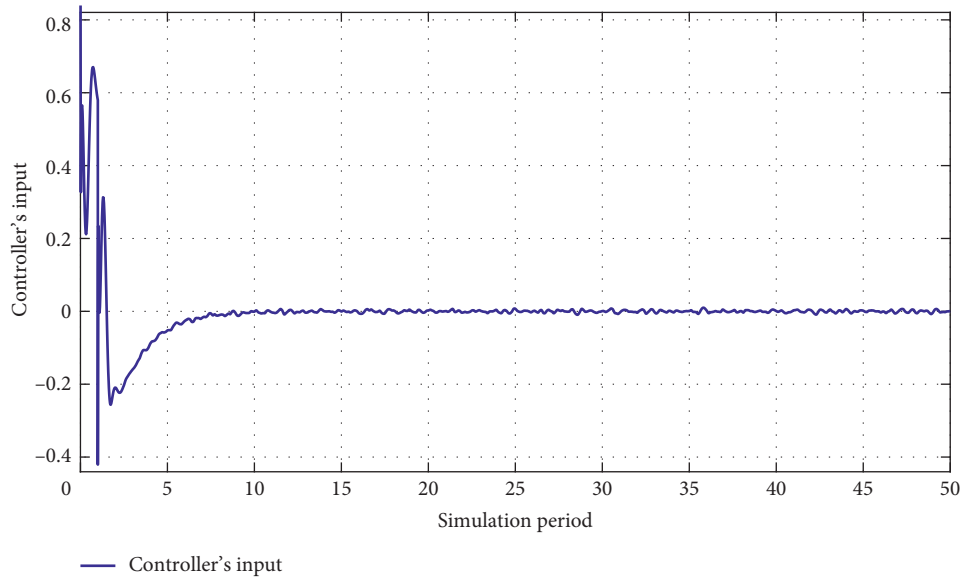


FIGURE 6: Reference Input data (PID controller) of the controller.

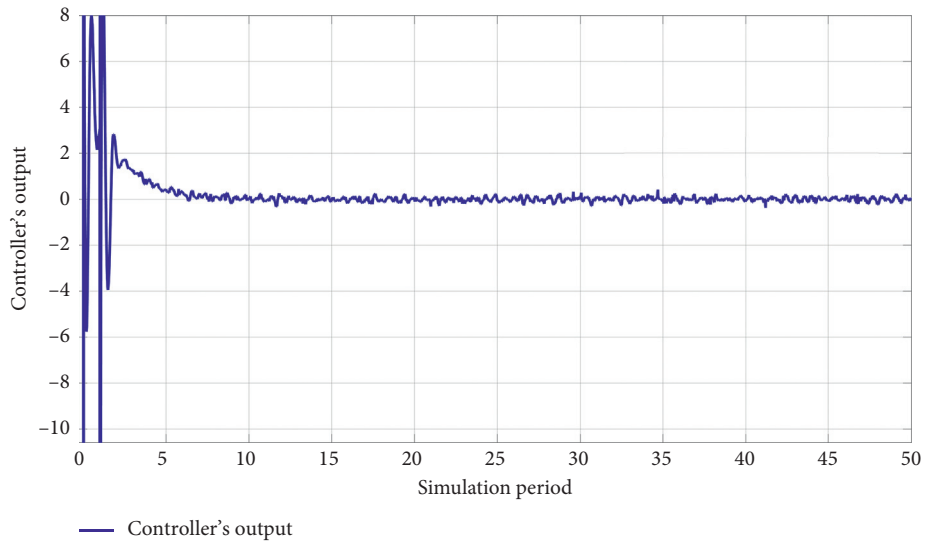


FIGURE 7: Reference output data (PID controller) of the controller.

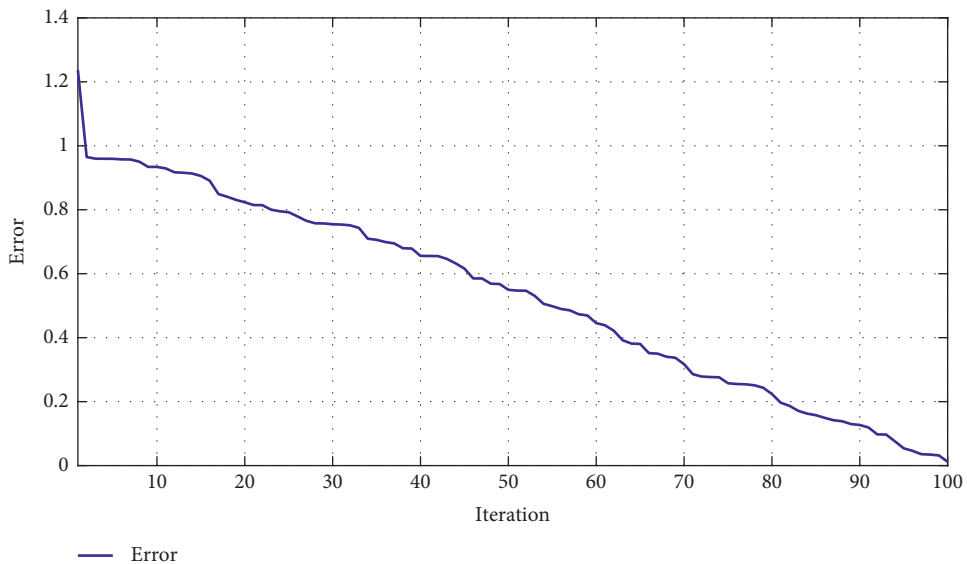


FIGURE 8: Error in each training iteration.

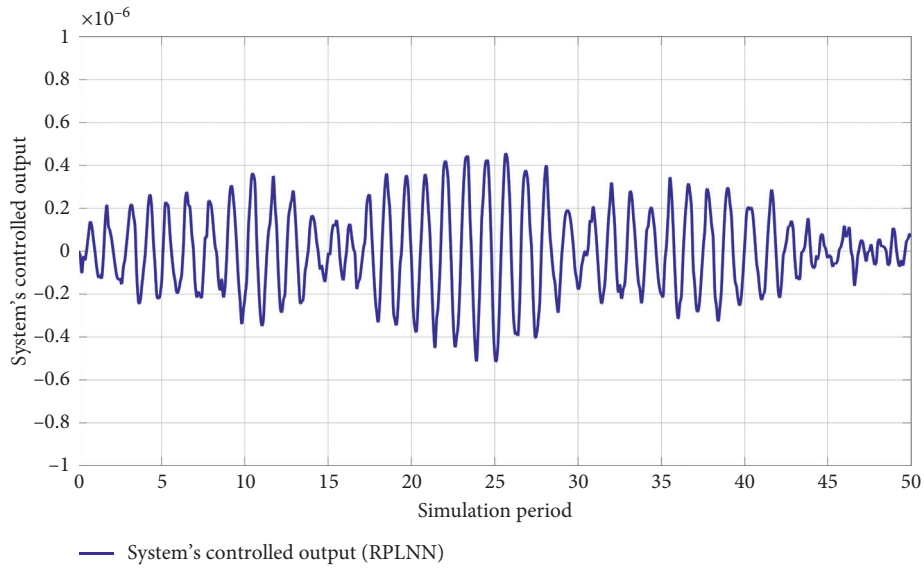


FIGURE 9: Noise cancellation utilizing the RPLNN controller.

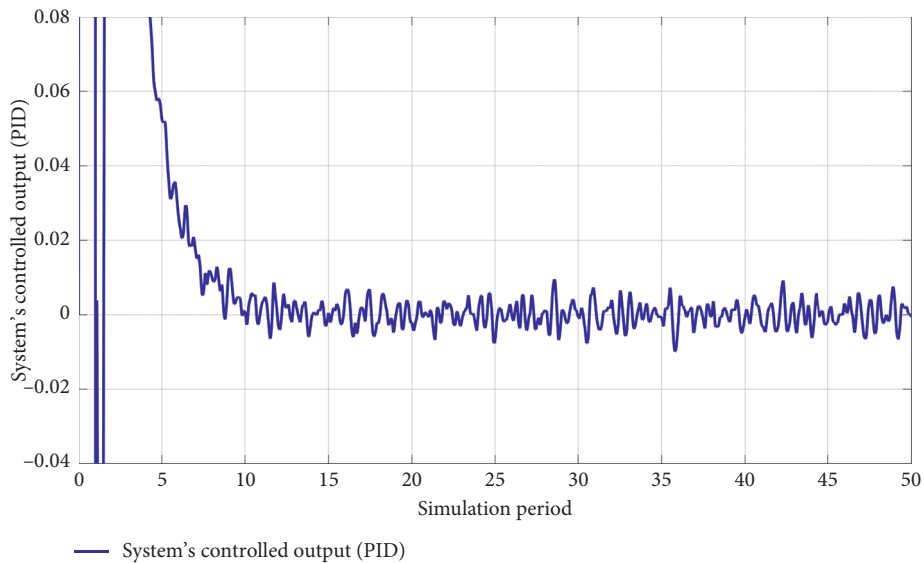


FIGURE 10: Noise cancellation utilizing PID controller.

controller has not shown an overshoot response, so it has a superior performance than the PID controller.

To have a better overview on the performance of the proposed RPLNN controller, the behavior of the system, once equipped with PID and then with RPLNN controllers, has been observed and compared.

As seen in Figure 9, at the first stages of the control process, the system equipped with PID controller reacts to the ground excitation with overshoot controlled response, and after three seconds starts to cancel the noise properly. However, as seen in Figure 10, by adopting the RPLNN controller system from the beginning of the control process shows a smooth response and prepares a convenient and safe ride for passengers.

Finally, it can be concluded that utilizing RPLNN controller, due to decreasing the imposed fluctuations to the

vehicle from the road profile (which has been considered as Gaussian white noise), is an effective solution to be considered as noise cancellation tool, also it is obvious that, due to the reduction of vertical vibrations, the lifetime of the car parts has been increased.

4. Conclusion and Future Work

In the current research, to reduce the imposed vibrations to the quarter car model via the ground excitation an effective artificial intelligence controller for the active suspension system has been designed and modeled. The RPLNN algorithm has been utilized to design the proposed controller, and the road input signal has been modelled by utilizing Gaussian white noise. The proposed setup has been modelled by MATLAB and Simulink. The results show that the

proposed RPLNN controller is able to reduce the undesired effect of the road condition on the vehicle, which ultimately results in decreasing the fuel consumption and increasing the lifetime of the parts of the vehicle. The performance of the RPLNN controller has been compared with the PID controller and results show that the RPLNN controller has a superior performance. As future work, other AI algorithms such as Fuzzy Logic and Neural Networks can be utilized as controllers, also adopting nonlinear models to evaluate the performance of the designed controller will be an alternative important topic to be investigated.

Data Availability

The related data are presented within the manuscript.

Conflicts of Interest

The authors declare they have no conflicts of interest.

Acknowledgments

This study was funded by the Research Council of Oman under Grant no. ORG/CBS/14/008.

References

- [1] J. Palmer and S. Sljivar, *Vehicle Fuel Consumption Monitor and Feedback Systems*, Google Patents, Long Beach CA, USA, 2017.
- [2] A. Azizi and P. G. Yazdi, "Introduction to fuel consumption optimization techniques," in *Computer-Based Analysis of the Stochastic Stability of Mechanical Structures Driven by White and Colored Noise*, pp. 1–12, Springer, Berlin, Germany, 2019.
- [3] H. M. Ismail, H. K. Ng, C. W. Queck, and S. Gan, "Artificial neural networks modelling of engine-out responses for a light-duty diesel engine fuelled with biodiesel blends," *Applied Energy*, vol. 92, pp. 769–777, 2012.
- [4] Y. Çay, A. Çiçek, F. Kara, and S. Sağıroğlu, "Prediction of engine performance for an alternative fuel using artificial neural network," *Applied Thermal Engineering*, vol. 37, pp. 217–225, 2012.
- [5] S. Roy, R. Banerjee, A. K. Das, and P. K. Bose, "Development of an ANN based system identification tool to estimate the performance-emission characteristics of a CRDI assisted CNG dual fuel diesel engine," *Journal of Natural Gas Science and Engineering*, vol. 21, pp. 147–158, 2014.
- [6] K. Muralidharan and D. Vasudevan, "Applications of artificial neural networks in prediction of performance, emission and combustion characteristics of variable compression ratio engine fuelled with waste cooking oil biodiesel," *Journal of the Brazilian Society of Mechanical Sciences and Engineering*, vol. 37, no. 3, pp. 915–928, 2015.
- [7] A. C. Olivera, J. M. García-Nieto, and E. Alba, "Reducing vehicle emissions and fuel consumption in the city by using particle swarm optimization," *Applied Intelligence*, vol. 42, no. 3, pp. 389–405, 2015.
- [8] S. Lotfan, R. A. Ghiasi, M. Fallah, and M. H. Sadeghi, "ANN-based modeling and reducing dual-fuel engine's challenging emissions by multi-objective evolutionary algorithm NSGA-II," *Applied Energy*, vol. 175, pp. 91–99, 2016.
- [9] F. Perrotta, T. Parry, and L. C. Neves, "Application of machine learning for fuel consumption modelling of trucks," in *Proceedings of the Big Data (Big Data) IEEE International Conference on, 2017*, IEEE, Boston, MA, USA, pp. 3810–3815, December 2017.
- [10] A. Azizi, "Computer-based analysis of the stochastic stability of mechanical structures driven by white and colored noise," *Sustainability*, vol. 10, no. 10, p. 3419, 2018.
- [11] A. Azizi and P. G. Yazdi, "Introduction to noise and its applications," in *Computer-Based Analysis of the Stochastic Stability of Mechanical Structures Driven by White and Colored Noise*, pp. 13–23, Springer, Berlin, Germany, 2019.
- [12] A. Azizi and P. G. Yazdi, "Noise control techniques," in *Computer-Based Analysis of the Stochastic Stability of Mechanical Structures Driven by White and Colored Noise*, pp. 61–73, Springer, Berlin, Germany, 2019.
- [13] A. Azizi, "Hybrid artificial intelligence optimization technique," in *Applications of Artificial Intelligence Techniques in Industry 4.0*, pp. 27–47, Springer, Berlin, Germany, 2019.
- [14] A. Azizi, "Introducing a novel hybrid artificial intelligence algorithm to optimize network of industrial applications in modern manufacturing," *Complexity*, vol. 2017, Article ID 8728209, 18 pages, 2017.
- [15] A. Azizi, A. Barenji, R. Barenji, and M. Hashemipour, "Modeling mechanical properties of FSW thick pure copper plates and optimizing it utilizing artificial intelligence techniques," *Sensor Netw Data Commun*, vol. 5, no. 142, p. 2, 2016.
- [16] A. Azizi, *Applications of Artificial Intelligence Techniques in Industry 4.0*, Springer, Berlin, Germany, 2018.
- [17] Y. Zhang, K. Guo, D. Wang, C. Chen, and X. Li, "Energy conversion mechanism and regenerative potential of vehicle suspensions," *Energy*, vol. 119, pp. 961–970, 2017.
- [18] I. Maciejewski, T. Krzyzynski, and H. Meyer, "Modeling and vibration control of an active horizontal seat suspension with pneumatic muscles," *Journal of Vibration and Control*, vol. 24, pp. 5938–5950, 2018.
- [19] A. Azizi and P. G. Yazdi, "Mechanical structures: mathematical modeling," in *Computer-Based Analysis of the Stochastic Stability of Mechanical Structures Driven by White and Colored Noise*, pp. 37–59, Springer, Berlin, Germany, 2019.
- [20] D. J. Inman, *Vibration with Control*, John Wiley & Sons, Hoboken, NJ, USA, 2017.
- [21] A. Azizi and P. G. Yazdi, "White noise: applications and mathematical modeling," in *Computer-Based Analysis of the Stochastic Stability of Mechanical Structures Driven by White and Colored Noise*, pp. 25–36, Springer, Berlin, Germany, 2019.
- [22] A. Azizi, A. Vatankhah Barenji, and M. Hashmipour, "Optimizing radio frequency identification network planning through ring probabilistic logic neurons," *Advances in Mechanical Engineering*, vol. 8, no. 8, p. 1687814016663476, 2016.
- [23] M. B. Menhaj and N. Seifpour, "Function optimization by RPLNN," in *Proceedings of the 2002 International Joint Conference on Neural Networks*, pp. 1522–1527, Honolulu, HI, USA, May 2002.
- [24] A. Azizi, "Modern manufacturing," in *Applications of Artificial Intelligence Techniques in Industry 4.0*, pp. 7–17, Springer, Berlin, Germany, 2019.
- [25] A. Azizi, "RFID network planning," in *Applications of Artificial Intelligence Techniques in Industry 4.0*, pp. 19–25, Springer, Berlin, Germany, 2019.
- [26] A. Azizi and P. G. Yazdi, "Modeling and control of the effect of the noise on the mechanical structures," in *Computer-Based Analysis of the Stochastic Stability of Mechanical Structures Driven by White and Colored Noise*, pp. 75–93, Springer, Berlin, Germany, 2019.

Research Article

Orthopedic Boot-Tree 3D Design by means of the Integral Curves of Solutions of Differential Equations

Merab Shalamberidze,¹ Zaza Sokhadze ,² and Malvina Tatvidze³

¹Department of Design and Technology, Akaki Tsereteli State University, Tamar Mepe Str. No. 59, Kutaisi 4600, Georgia

²Department of Mathematics, Akaki Tsereteli State University, Tamar Mepe Str. No. 59, Kutaisi 4600, Georgia

³Department of Chemical Technology, Akaki Tsereteli State University, Tamar Mepe Str. No. 59, Kutaisi 4600, Georgia

Correspondence should be addressed to Zaza Sokhadze; z.sokhadze@gmail.com

Received 29 July 2019; Revised 16 December 2019; Accepted 16 January 2020; Published 30 March 2020

Academic Editor: András Rontó

Copyright © 2020 Merab Shalamberidze et al. This is an open access article distributed under the Creative Commons Attribution License, which permits unrestricted use, distribution, and reproduction in any medium, provided the original work is properly cited.

For the preparation of orthopedic shoes, it is necessary to design boot-trees, where pathological abnormalities of club feet are taken into account as much as possible. For the normal functioning of the club foot, we have to develop such an internal shape of special-purpose footwear, which is comfortable for the patient. This paper describes the methods and issues of the 3D design for constructing the geometric shapes of the main cross sections of the orthopedic boot-tree. In the research process, the authors' team of this article relied mainly on the patient database, containing the anthropometric, strain-gauge, and pedographic data on club and pathological feet. To construct the shapes of the main cross sections of the orthopedic boot-tree, we have used the integral curves to the suitable second-order differential equations. By means of a computer program, we executed turning and connection of sections of the obtained curves, on the basis of which we have the shapes of transverse-vertical cross sections of the orthopedic boot-tree. This paper also describes the main longitudinal-vertical section and the print of the orthopedic boot-tree in 3D format. By using a program of 3D design (Delcam), a skeleton of the orthopedic boot-tree was constructed in the spatial format.

1. Introduction

In the special-purpose shoe industry, considerable attention is paid to design special-purpose boot-trees. It is well known that geometrically, the orthopedic boot-tree has a complex shape and its description using mathematical investigation methods is a long enough and arduous process. In general, the technical side of the boot-tree design is diverse. In the process of the boot-tree design, it is necessary to take into account the size and shape of the foot.

The algorithm describing a geometrical shape of the surface of the boot-tree was considered in academic writings of different researchers [1–5]. To describe a geometrical shape of the boot-tree, they have used the following methods of mathematical investigation: radius-graphical, biquadratic spline, and bicubic interpolating spline. These methods are

quite complex, labor-intensive, and time-consuming in the process of boot-tree design.

The authors' team of this article conducted the anthropometric, strain-gauge, and pedographic investigations of club and pathological feet. A database of patients has been created, where pathological abnormalities of each patient's feet are specified. Based on biomechanics of the movement of foot, it is necessary to transform the obtained parameters and on that basis to determine curvilinear lines describing the surface of the boot-tree. In particular, it is necessary to construct the shapes of transverse-vertical, longitudinal-vertical, and longitudinal-horizontal cross sections of orthopedic shoes. Development of a new algorithm describing a geometric surface of the boot-tree and its use in practice is one of the main and pressing problems in the orthopedic shoe industry.

2. Research Methods

The authors' team of this article decided to describe a geometrical shape of the orthopedic boot-tree by means of the integral curves of solutions of the singular Dirichlet boundary value problem. The issue will be completed in a relatively short time, and the result will be much more accurate.

The goal of our work is to design the appropriate shapes of transverse-vertical cross sections of the orthopedic boot-tree for patients with club and pathological feet. To achieve this goal, it would not be sufficient to use the simple functional relationships. We consider the particular cases of the singular Dirichlet boundary value problem. The multiplicity of solutions of these problems allows us in choosing a shape of orthopedic shoes we are seeking for club and pathological feet.

An important novelty of research consists in obtaining the approximate shapes of transverse-vertical cross sections of the orthopedic boot-tree by means of the integral curves of solutions of the singular Dirichlet boundary value problem.

In the work [6], Rachunkova et al. consider the singular Dirichlet boundary value problem:

$$u''(t) + \frac{a}{t}u'(t) - \frac{a}{t^2}u(t) = f(t, u(t), u'(t)), \quad (1)$$

$$\begin{aligned} u(t) &= 0, \\ u(T) &= 0, \end{aligned} \quad (2)$$

where $a \in (-\infty; 1)$ and f satisfies the local Caratheodory condition for a set $[0, T] \times D$, $D = (0; +\infty) \times R$.

This paper dwells on studying the existence of solution of (1)-(2) problems, and besides, Lemma 3.1 [6] in this article clearly shows the solution of (1)-(2) problems, particularly:

$$u(t) = c_1 t + c_2 t^{-a} + t \int_t^T S^{-a-2} \left(\int_s^T \xi^{a+1} f(t, u(\xi), u'(\xi)) d\xi \right) d\xi, \quad (3)$$

where $c_1, c_2 \in R$, $t \in [0, T]$.

Our goal is to write clearly the solution for the different cases of a function $f(t, u(t), u'(t))$ presented on the right side of the equation (1), and also using the formula (3) for different values of a , and then to construct the integral curves of these solutions that will allow us for obtaining the desirable shapes of transverse-vertical cross sections of the orthopedic boot-tree.

Let us consider the first particular case of (1) and (2) problems:

$$u'' + \frac{2}{t}u' - \frac{2}{t^2}u = t, \quad (4)$$

$$\begin{aligned} u(1) &= 0, \\ u'(1) &= c, \end{aligned} \quad (5)$$

i.e., we put $f(t, u(t), u'(t)) = t$, $a = -2$, and $t \in [0, 1]$, and the solutions of (4) and (5) problem is as follows:

$$u(t) = \frac{t^3}{2} - \frac{1}{3}ct^{-2} - \left(1 - \frac{1}{3}c\right)t + \frac{1}{2}. \quad (6)$$

If $c=0$, then we have $u(t) = (t^3/2) - t + (1/2)$.

Figure 1 illustrates the appropriate integral curve graphics for obtained solutions. Let us consider the same particular case of (1) and (2) problems:

$$u'' + \frac{a}{t}u' - \frac{a}{t^2}u = t^2, \quad (7)$$

$$\begin{aligned} u(1) &= 0, \\ u'(1) &= c, \end{aligned} \quad (8)$$

viz, with provision $f(t, u(t), u'(t)) = t$, $a = -2$, and $t \in [0, 1]$, the solution of (7) and (8) problems is as follows:

$$u(t) = \left(-\frac{1}{3} - \frac{1}{3}c\right)t + \frac{1}{3}c\frac{1}{t^2} + \frac{2}{3}t - \frac{t^2}{2} + \frac{t^4}{6}. \quad (9)$$

If $c=0$, then we have $u(t) = (t^4/6) - (t^2/2) + (1/3)t$.

Figure 2 illustrates the appropriate integral curve graphics for obtained solutions.

Thus, by means of the integral curves of the solution to suitable second-order differential equations, it is possible to describe the shapes of the transverse-vertical cross section of the orthopedic boot-tree.

By means of the abovementioned mathematical investigation method and the integral curves of solutions of differential equations with deviating argument, we constructed the shapes (boot-tree print) of transverse-vertical, main longitudinal-vertical, and longitudinal-horizontal cross sections of the orthopedic boot-tree [7–11].

3. Discussion of Research Findings

Based on the 3D scanning results of abnormal and club feet, the right-side terms of equations (4) and (6) were chosen because various parts of the integral curves of the solutions to these equations are as close as possible to the shapes of the foot presented in the patient database.

Using the abovementioned methods of mathematical research, we constructed the shapes of the following transverse-vertical cross sections: $0.4D$, $0.8D$, and $0.9D$ (where D is the length of the foot). The following shapes of transverse-vertical cross section have been constructed for women's orthopedic boot-tree, size 38.

To obtain the shape of the mentioned cross section, we have used mainly the patient database. To construct the transverse-vertical cross section of the orthopedic boot-tree ($0.4D$), it was divided previously into eight parts and each enumerated section was described by means of the integral curves of solutions of differential equations given in the following. From the integral curves, we choose those eight parts that are identical to the geometric shapes of transverse-vertical cross section of the orthopedic boot-tree on $0.4D$, in particular:

(1) AB curve corresponds that part of the solution of the equation $u(t) = (t^3/2) + (1/3)ct^{-2} - (1 - (1/3)c)t +$

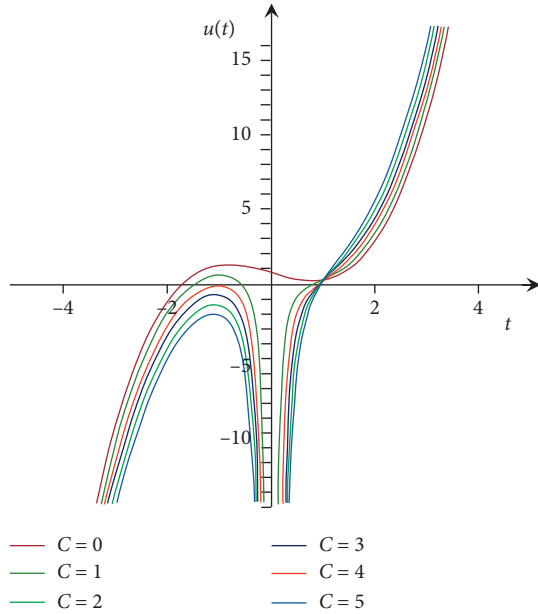


FIGURE 1: Integral curve graphics for solutions of (4) and (5) problems.

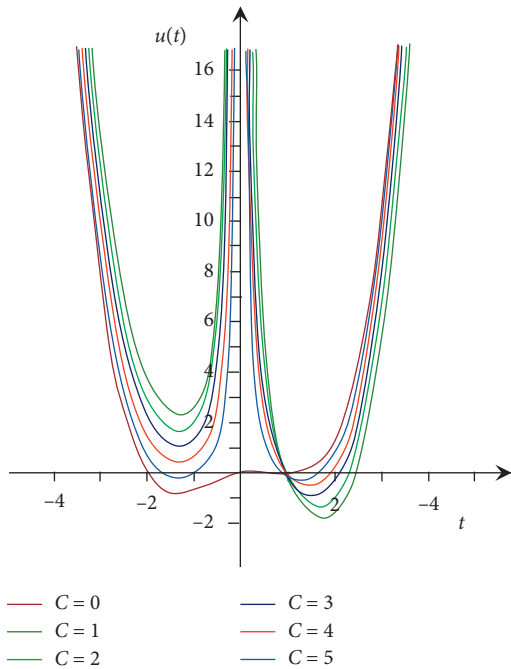


FIGURE 2: Integral curve graphics for solutions of (4) and (5) problems.

(1/2), for which $c=0$ and corresponds to a set $[-2,2; -2,95] \times [-1,3; 1]$;

- (2) BC curve corresponds that part of the solution of the equation $u(t) = -(1/3) - (1/3)c)t + (1/3)c(1/t^2) + (2/3)t + (t^2/2) + (t^4/6)$, for which $c=5$ and corresponds to a set $[-1,95; 1,3] \times [-2,4; 3,1]$;
- (3) CD curve corresponds that part of the solution of the equation $u(t) = -(1/3) - (1/3)c)t + (1/3)c(1/t^2) +$

$(2/3)t + (t^2/2) + (t^4/6)$, for which $c=3$ and corresponds to a set $[-0,8; 4] \times [-0,44; 13,2]$;

- (4) DE curve corresponds that part of the solution of the equation $u(t) = -(1/3) - (1/3)c)t + (1/3)c(1/t^2) + (2/3)t + (t^2/2) + (t^4/6)$, for which $c=0$ and corresponds to a set $[3; 3,8] \times [2,6; 2,6]$;
- (5) EF curve corresponds that part of the solution of the equation $u(t) = (t^3/2) + (1/3)ct^{-2} - (1 - (1/3)c)t + (1/2)$, for which $c=0$ and corresponds to a set $[-0,8; 1] \times [0,3; 0,2]$;
- (6) FN curve corresponds that part of the solution of the equation $u(t) = (t^3/2) + (1/3)ct^{-2} - (1 - (1/3)c)t + (1/2)$, for which $c=2$ and corresponds to a set $[-2,3; -7,1] \times [-1,4; -2,7]$;
- (7) NM curve corresponds that part of the solution of the equation $u(t) = -(1/3) - (1/3)c)t + (1/3)c(1/t^2) + (2/3)t + (t^2/2) + (t^4/6)$, for which $c=5$ and corresponds to a set $[-2,9; 2,9] \times [-2,7; 4,1]$;
- (8) MA curve corresponds that part of the solution of the equation $u(t) = (t^3/2) + (1/3)ct^{-2} - (1 - (1/3)c)t + (1/2)$, for which $c=4$ and corresponds to a set $[1,55; 1,9] \times [3; 11,9][3; 9, 11]$.

By means of a computer program, we executed turning and connection of these curves, on the basis of which we obtained a shape of the transverse-vertical cross section of the orthopedic boot-tree on $0.4D$, as shown in Figure 3.

Likewise, we have constructed the shapes of transverse-vertical cross sections of the orthopedic boot-tree on $0.8D$ and $0.9D$.

To construct a shape of transverse-vertical cross sections of the boot-tree on $0.8D$, we have divided it previously into six parts. Each enumerated section was described by means of the integral curves of solutions of differential equations given in the following. From the integral curves, we choose those six parts that are identical to the geometric shapes of transverse-vertical cross section of the orthopedic boot-tree on $0.8D$, in particular:

- (1) AB curve corresponds that part of the solution of the equation $u(t) = -(1/3) - (1/3)c)t + (1/3)c(1/t^2) + (2/3)t + (t^2/2) + (t^4/6)$, for which $c=2$ and corresponds to a set $[-2,1; -6] \times [-1,1; -2,1]$;
- (2) BC curve corresponds that part of the solution of the equation $u(t) = (t^3/2) + (1/3)ct^{-2} - (1 - (1/3)c)t + (1/2)$, for which $c=0$ and corresponds to a set $[-1,7; -0,5] \times [-2,6; 2,7]$;
- (3) CD curve corresponds that part of the solution of the equation $u(t) = (t^3/2) + (1/3)ct^{-2} - (1 - (1/3)c)t + (1/2)$, for which $c=0$ and corresponds to a set $[1,8; 1] \times [2,8; 7,4]$;
- (4) DE curve corresponds that part of the solution of the equation $u(t) = -(1/3) - (1/3)c)t + (1/3)c(1/t^2) + (2/3)t + (t^2/2) + (t^4/6)$, for which $c=0$ and corresponds to a set $[-1,5; 0,5] \times [-1,9; 1]$;
- (5) EF curve corresponds that part of the solution of the equation $u(t) = -(1/3) - (1/3)c)t + (1/3)c(1/t^2) +$

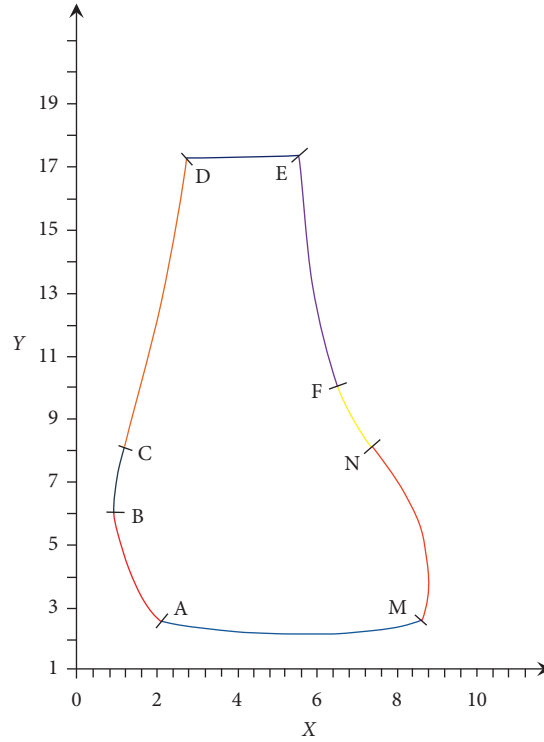


FIGURE 3: A shape of the transverse-vertical cross section of the orthopedic boot-tree on $0.4D$.

$c(1/t^2) + (2/3)t + (t^2/2) + (t^4/6)$, for which $c=0$ and corresponds to a set $[1,6; 0,5] \times [2,1; 3]$;

- (6) FA curve corresponds that part of the solution of the equation $u(t) = (-1/3) - (1/3)c)t + (1/3)c(1/t^2) + (2/3)t + (t^2/2) + (t^4/6)$, for which $c=1$ and corresponds to a set $[1,4; 1,3] \times [2,9; 14,2]$.

Here, too, by means of a computer program, we constructed a shape of the transverse-vertical cross section of the orthopedic boot-tree on $0.8D$, as shown in Figure 4.

To construct a shape of transverse-vertical cross sections of the boot-tree on $0.9D$, we have divided it previously into four parts. Each enumerated section was described similarly, and it is given as follows:

- (1) AB curve corresponds that part of the solution of the equation $u(t) = (-1/3) - (1/3)c)t + (1/3)c(1/t^2) + (2/3)t + (t^2/2) + (t^4/6)$, for which $c=0$ and corresponds to a set $[-2,2; -2,1] \times [0,4; 0,3]$;
- (2) BC curve corresponds that part of the solution of the equation $u(t) = (t^3/2) + (1/3)ct^{-2} - (1 - (1/3)c)t + (1/2)$, for which $c=3$ and corresponds to a set $[-2; 4] \times [-2,6; 8]$;
- (3) CD curve corresponds that part of the solution of the equation $u(t) = (t^3/2) + (1/3)ct^{-2} - (1 - (1/3)c)t + (1/2)$, for which $c=0$ and corresponds to a set $[-1,6; -0,8] \times [-2,5; 2,05]$;
- (4) DA curve corresponds that part of the solution of the equation $u(t) = (-1/3) - (1/3)c)t + (1/3)c(1/t^2) + (2/3)t + (t^2/2) + (t^4/6)$, for which $c=1$ and corresponds to a set $[1,4; 1] \times [2,85; 13,05]$.

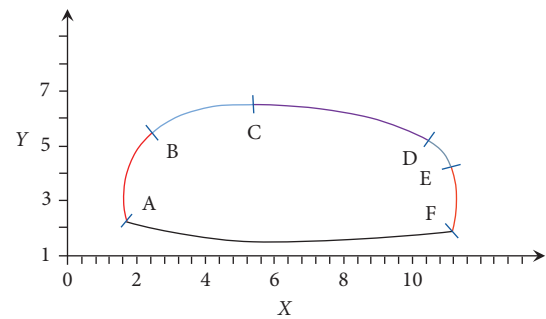


FIGURE 4: A shape of the transverse-vertical cross section of the orthopedic boot-tree on $0.8D$.

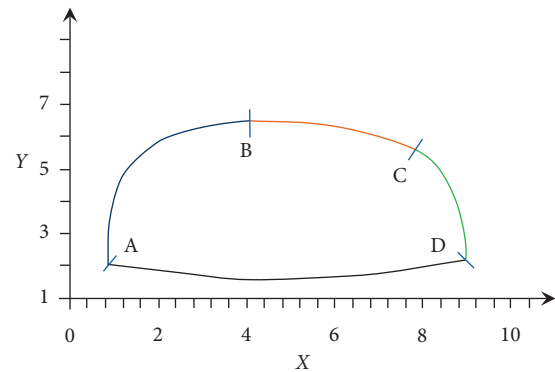


FIGURE 5: A shape of of the transverse-vertical cross section of the orthopedic boot-tree on $0.9D$.

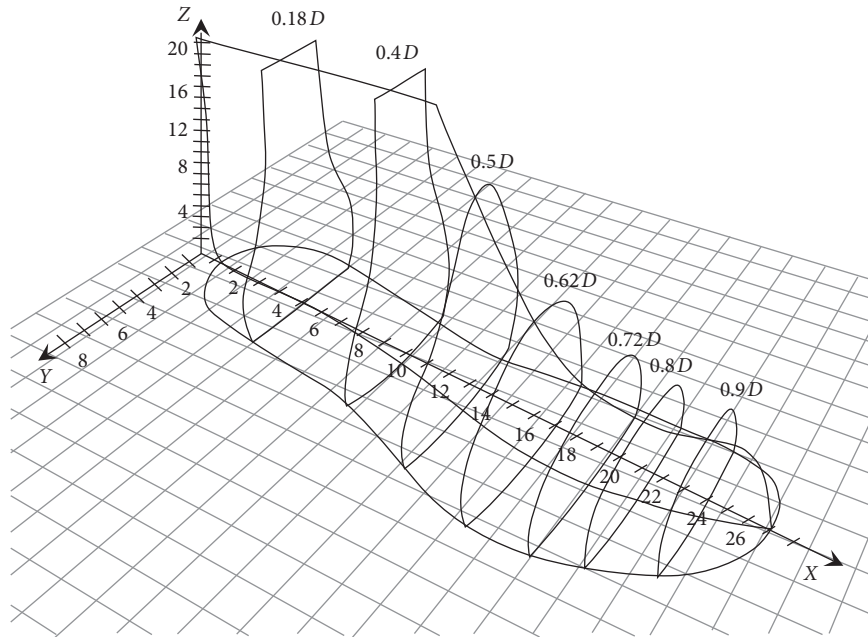


FIGURE 6: A skeleton of the orthopedic boot-tree in 3D format.

Figure 5 illustrates a shape of the transverse-vertical cross section of the orthopedic boot-tree on $0.9D$.

By using a program of 3D design (Delcam), Figure 6 illustrates the main transverse-vertical, longitudinal-vertical, and longitudinal-horizontal (boot-tree print) cross sections in the spatial format.

4. Conclusions

Thus and so, based on the patient database, the authors' team of this article has constructed the shapes by means of the integral curves of solutions to suitable second-order Euler differential equations. This method allows for describing with high accuracy the shapes of the main cross section of the orthopedic boot-tree. It also enables us to change the shapes of the main transverse-vertical, longitudinal-vertical, and longitudinal-horizontal cross sections of the orthopedic boot-tree an unlimited number of times, while changing the sizes of orthopedic boot-trees. The latter is particularly relevant during the production of orthopedic shoes, when we deal with patients having nonstandard or club and pathological feet.

Data Availability

The data used to support the findings of this study are available from the corresponding author upon request.

Conflicts of Interest

The authors declare that they have no conflicts of interest.

Acknowledgments

The work was fulfilled with the financial support of the Shota Rustaveli National Science Foundation of Georgia (Grant FR no. 217386).

References

- [1] V. A. Fukin, *Radius-Graphical Method For Designing An Internal Shape of Footwear*, vol. 381, Light Industry, Atlanta, GA, USA, 1980.
- [2] V. A. Fukin, V. V. Kostyleva, and V. P. Lyba, *Boot-Tee Design*, vol. 268, Legpromizdat, Moscow, Russia, 1987.
- [3] V. A. Fukin, *Theoretical Bases of Designing An Internal Shape of Footwear*, vol. 356, MGUDT, Moscow, Russia, 2nd edition, 2000.
- [4] K. S. Yu, "Automated engineering design and production of machine-tool attachments for manufacture of footwear and prosthetic and orthopedic appliances," Ph. D. thesis for academic degree of Doctor of Science in Engineering, vol. 392, MGUDT, Moscow, Russia, 2004.
- [5] K. N. Zamarashkin, *Mathematical Methods of Footwear and Machine-Tool Attachments Design*, vol. 312, SPGUTD, Saint Petersburg, Russia, 2004.
- [6] I. Rachunkova, A. Spielaurer, S. Stanek, and E. B. Weinmuller, "The structure of a set of positive solutions to Dirichlet BVPs with time and space singularities," *Georgian Mathematical Journal*, vol. 1, pp. 95–127, 2013.
- [7] M. Shalamberidze, Z. Sokhadze, and M. Tatvidze, "Construction of the transverse-vertical shapes of the orthopedic boot tree by means of the solution to singular dirichlet boundary value problem," *Bulleten of the Georgian National Academy of Sciences*, vol. 12, no. 1, pp. 27–32, 2018.
- [8] M. Shalamberidze, Z. Sokhadze, and M. Tatvidze, "Construction of the orthopedic shoe tree main transverce-vertical cross-sections by means of the integral curves," *Bulleten of the Georgian National Academy of Sciences*, vol. 12, no. 3, pp. 23–30, 2018.
- [9] M. Shalamberidze and Z. Sokhadze, "Constructing a shape of orthopedic boot-tree print by means of the solution to differential equation with deviating argument," *International Scientific Journal. Theoretical & Applied Science*, vol. 61, no. 5, pp. 122–126, 2018.

- [10] M. Shalamberidze, Z. P. Sokhadze, and N. Z. Lomtadze, "Constructing the transverse-vertical geometrical shape of the orthopedic shoe-tree in section 0,5D using the solutions of singular dirichlet boundary problems," *Theoretical & Applied Science*, vol. 74, no. 6, pp. 501-504, 2019.
- [11] M. Shalamberidze, Z. Sokhadze, and M. Tatvidze, "Construction of the orthopedic boot tree print and main longitudinal vertical section by means of the solution of differential equations," *Bulleten of the Georgian National Academy of Sciences*, vol. 13, no. 2, pp. 17-21, 2019.

Research Article

Applications of Artificial Intelligence Techniques to Enhance Sustainability of Industry 4.0: Design of an Artificial Neural Network Model as Dynamic Behavior Optimizer of Robotic Arms

Aydin Azizi 

School of Engineering, Computing and Mathematics, Oxford Brookes University, Wheatley Campus, Oxford OX33 1HX, UK

Correspondence should be addressed to Aydin Azizi; aydin.azizi@brookes.ac.uk

Received 16 April 2019; Revised 6 November 2019; Accepted 19 December 2019; Published 21 March 2020

Guest Editor: Robert Hakl

Copyright © 2020 Aydin Azizi. This is an open access article distributed under the Creative Commons Attribution License, which permits unrestricted use, distribution, and reproduction in any medium, provided the original work is properly cited.

Industrial robots have a great impact on increasing the productivity and reducing the time of the manufacturing process. To serve this purpose, in the past decade, many researchers have concentrated to optimize robotic models utilizing artificial intelligence (AI) techniques. Gimbal joints because of their adjustable mechanical advantages have been investigated as a replacement for traditional revolute joints, especially when they are supposed to have tiny motions. In this research, the genetic algorithm (GA), a well-known evolutionary technique, has been adopted to find optimal parameters of the gimbal joints. Since adopting the GA is a time-consuming process, an artificial neural network (ANN) architecture has been proposed to model the behavior of the GA. The result shows that the proposed ANN model can be used instead of the complex and time-consuming GA in the process of finding the optimal parameters of the gimbal joint.

1. Introduction

In the definition of the sustainable economic model, natural resources such as energy and material are considered as limited resources. Industrial robots can be utilized as a potential solution for the issue by increasing the productivity and reducing the wastes which results in the reduction in emission and contributing to sustainability [1]. In the past decade, designing more precise and accurate robots has been a point of research interest of many scientists. In particular, many research studies have been concentrated to utilize artificial intelligence (AI) techniques to contribute to economic and environmental sustainability [2–4].

A variety of novel techniques such as ring probabilistic logic neural networks (RPLNNs) [5], genetic algorithms (GA), particle swarm (PS), hybrid algorithms, and agent-based algorithms have been presented by researchers to provide an approximate solution of the synthesis of mechanisms [5, 6]. In 2017, Soldberg [7] investigated the possibility of object detection in agricultural robots via deep

neural networks. Jin et al. [8] presented the special form of neural networks to optimize the redundant manipulators. Fuzzy wavelet ANN approach has been utilized by Yen et al. [9] in 2017 to control the industrial robot manipulator using fuzzy wavelet neural networks. Also, in 2018, they adopted recurrent fuzzy wavelet neural network approach to control the manipulator [10].

In this paper, an ANN architecture has been adopted to model the behavior of the GA optimizer in the process of finding the optimal parameters of robotic arms equipped with a gimbal driver. The research presents a novel approach in the training process of ANN by adopting data of genetic algorithms (GAs) to train the proposed ANN, so at the end of the training process, the proposed ANN acts as a function optimizer instead of GA. In this research, MATLAB software has been utilized to generate the ANN model and perform the GA optimization process. It is important to highlight the point that other effective optimization techniques such as PSO, bee colony, and RPLNN can be adopted to train the proposed ANN, and GA has been utilized just as an example of an optimization technique.

2. Methodology

The ultimate aim of this research is to develop an ANN model as a function approximator which is able to model the dynamic behavior of the GA optimizer in the process of finding the optimal parameters of gimbals in robotic arms.

Different from previous works, the designed ANN has not been trained by the general extracted data from the mathematical model of the robotic arm, but its reference model is the GA as the parameter optimizer of the gimbals equipped robotic arm model. It means that the proposed ANN should act as a function optimizer and will eliminate the need of utilizing optimization techniques.

To reach this goal at the first step, the behavior of the gimbals should be modeled mathematically, and the next step is utilizing the introduced gimbals in 3 different well-known robotic arms and introducing the related mathematical models. The third step is to find the optimum design parameters utilizing GA which is one of the well-known AI evolutionary techniques. The last step which is the novelty part of this research is to design and train an ANN to act instead of the optimization algorithm, GA. The proposed approach has been illustrated as a flowchart in Figure 1.

To fulfill the task, the rest of the manuscript has been prepared in the following sequence: a brief introduction of gimbals mechanisms is presented in the next section. Also, the resistivity ellipsoid is formulated to measure the manipulability of robotic arms. Next, to be able to apply maximum force in a desired direction, genetic algorithm (GA) as one of the well-known evolutionary optimization techniques has been employed to optimize the highly nonlinear fitness function. As GA is very time-consuming, an artificial neural network (ANN) as the novelty of this research has been utilized to learn the relation between the inputs and outputs of GA. The ANN is trained using the optimization results obtained from GA in several randomly generated configurations. Thus, the trained ANN could replace the whole optimization process and act as a function optimizer. This way enables utilizing the trained ANN model to obtain the optimized results for new configurations instead of the GA optimizer. To have a better perception of the effectiveness of this method, three simple robotic arms are selected to investigate the task.

2.1. The Gimbal Drive. In Figure 2, a regular one-degree-of-freedom gimbals drive is shown. Following is the governing equation on gimbals mechanism [11]:

$$\theta_{\text{out}} = \theta_{\text{of_out}} + \tan^{-1}(\tan \theta_c \cos \theta_{\text{in}}), \quad (1)$$

where θ_{in} is the input angle (angle of rotation of vertical shaft), θ_{out} is the output angle (angle of rotation of the horizontal shaft/frame), θ_c is the gradient of the truncated cylinder, and $\theta_{\text{of_out}}$ is the offset angle at the output. It can be deduced that the gradient of the truncated cylinder, θ_c , is a design parameter because it sets the range of output angle.

Verity is that, for any input value (θ_{in}), there exist two possible output configurations (θ_{out}), which is another

advantage of the gimbals mechanism. The effect of the reduction ratio should be considered too. We also should notice that the gradient of θ_c is a design parameter because it will set the range of the output angle.

To study manipulability modality, the classical criterion of resistivity ellipsoid is formulated for manipulators with traditional revolute joints. It is compared to the same modality of the same arm in which some joints are substituted with gimbals transmissions.

To have the maximum achievable force at the manipulator tip point, the classical hypothesis is to assume that the Euclidian norm of the joint torques remains unity [11]:

$$\tau^T \cdot \tau = 1. \quad (2)$$

The relation of the task-space force F and the vector of joint torques τ is given by [11]

$$\tau = J^T F, \quad (3)$$

where J is the Jacobian of the whole manipulator.

By substituting (3) in (2), one obtains the following equation:

$$F^T J J^T F = 1. \quad (4)$$

Relation (4) changes the hypersphere of the joint forces (2) into a hyperellipsoid that is called the resistivity ellipsoid. This method is largely employed to evaluate the manipulability qualities of robotic arms.

Here, achieving greater force in a specified direction by using the gimbals mechanism is the main goal. The task-space force vector is expressed as [11]

$$F = f \begin{bmatrix} dx \\ dy \\ dz \end{bmatrix} = f \hat{F}, \quad (5)$$

where f is the magnitude of F and $[dx \ dy \ dz]^T$ are the unit vectors on the direction of f along X , Y , and Z axes, respectively, and to maintain conciseness, substitute by \hat{F} . Substituting (5) in (4) yields the following equation [11]:

$$f^2 (\hat{F}^T J J^T \hat{F}) = 1. \quad (6)$$

Thus, the magnitude of the applicable force in a desired direction at a specific point of manipulator's workspace should be determined. Comparing the magnitudes of the applicable force, f , for different types of manipulators, would lead to recognizing the efficient robot design and whether using gimbals transmission instead of the traditional revolute joints improves robot's manipulability or not.

2.1.1. Case Studies

(1) *RRR Arm.* To get numerical examples, three case studies have been performed. First, a spatial robot with three revolute joints (RRR or 3R) shown in Figure 3 is investigated to analyze the advantages of gimbals drive in robot joint transmission. For convenience,

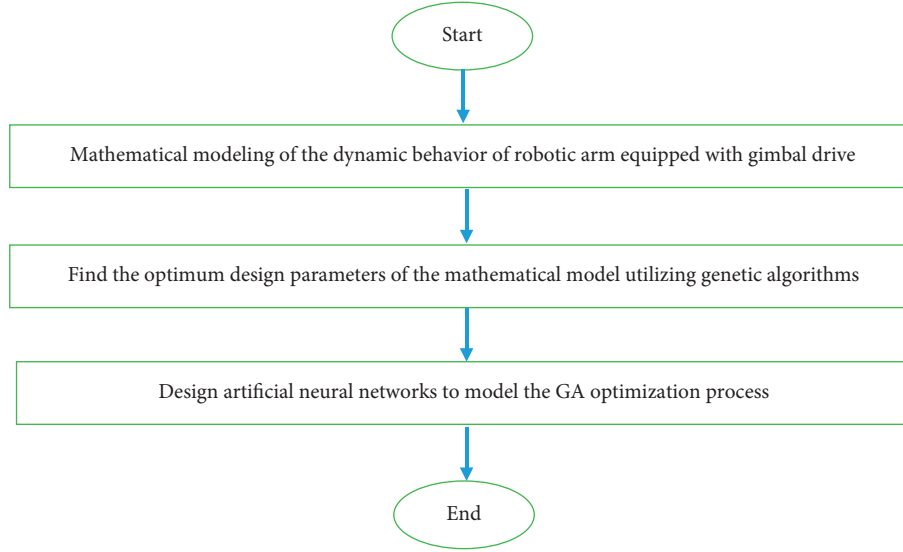


FIGURE 1: Flowchart of the proposed methodology.

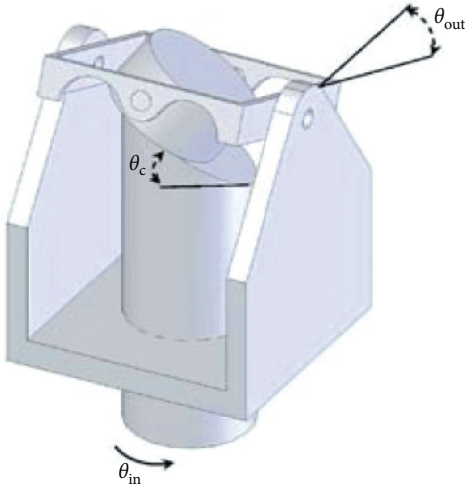


FIGURE 2: The gimbal drive [11].

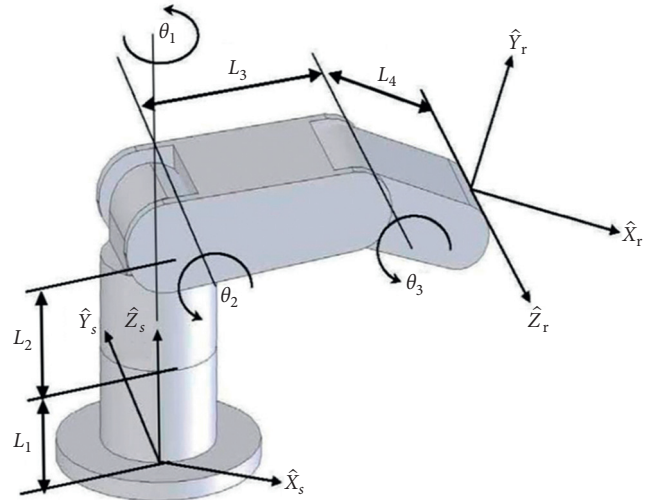


FIGURE 3: RRR spatial robot arm [11].

$$\begin{aligned} c_{m\dots n} &= \cos(\theta_m + \dots + \theta_n), \\ s_{m\dots n} &= \sin(\theta_m + \dots + \theta_n), \end{aligned} \quad (7)$$

are used instead, respectively. Assuming $L_1 = L_2 = L_4 = 0.5$ m and $L_3 = 1$ m, the Jacobian matrix of the 3R spatial robot is given by [11]

$$J = \begin{bmatrix} -\frac{1}{2}s_1c_{23} - s_1c_2 & \frac{1}{2}c_1s_{23} - c_1s_2 & \frac{1}{2}c_1s_{23} \\ \frac{1}{2}c_1c_{23} + c_1c_2 & -\frac{1}{2}s_1s_{23} - s_1s_2 & -\frac{1}{2}s_1s_{23} \\ 0 & \frac{1}{2}c_{23} + c_2 & \frac{1}{2}c_{23} \end{bmatrix}. \quad (8)$$

Now it is desired to use gimbal transmissions at joints 2 and 3. To obtain a new Jacobian matrix, one shall substitute

for θ_2 and θ_3 of the 3R spatial robot. Assuming $\theta_{of_out} = 0$ and $\theta_c = 45^\circ$, the Jacobian matrix for the manipulator with gimbal transmissions at joints 2 and 3 becomes [11]

$$J_G = \begin{bmatrix} R_1 & R_2 & R_3 \\ R_4 & R_5 & R_6 \\ R_7 & R_8 & R_9 \end{bmatrix}, \quad (9)$$

where J_G is the Jacobian of the manipulator when a gimbal transmission is used at joints 2 and 3. Using manipulability ellipsoid, f in the simple and gimbal equipped 3R spatial robots has been compared by Mohammadi et al. [11].

(2) *Stanford Arm*. A simplified version of Stanford arm shown in Figure 4 has been investigated here. The Jacobian matrix for this arm, assuming $L_1 = 1$ m and $L_2 = 0.5$ m, is as follows [11]:

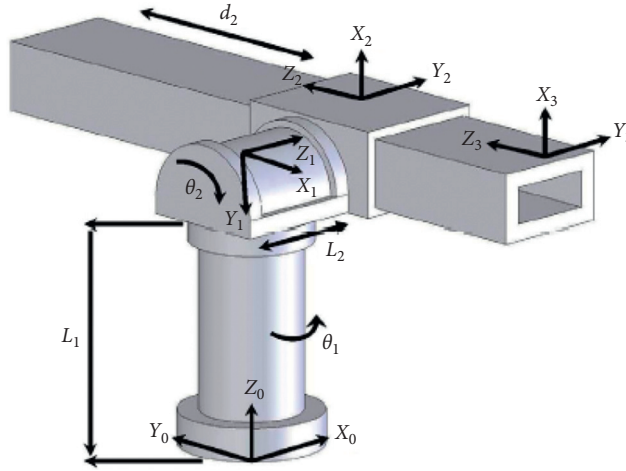


FIGURE 4: Stanford arm [11].

$$J = \begin{bmatrix} d_3 c_1 c_2 - \frac{1}{2} s_1 & -d_3 s_2 s_1 & s_1 c_2 \\ -d_3 c_2 c_1 - \frac{1}{2} c_1 & -d_3 c_1 s_2 & c_1 c_2 \\ 0 & -d_3 c_2 & s_2 \end{bmatrix}. \quad (10)$$

Using gimbal drive at joint 2, the new Jacobian matrix is obtained by substituting from (1) for θ_2 in (11). Assuming $\theta_{of_out} = 0$ and $\theta_c = 45^\circ$, the following Jacobian matrix is derived [11]:

$$J_G = \begin{bmatrix} R_1 & R_2 & R_3 \\ R_4 & R_5 & R_6 \\ R_7 & R_8 & R_9 \end{bmatrix}. \quad (11)$$

$$J_G = \begin{bmatrix} \frac{-s_1 c_2 d_3}{(1+c_2^2)^{(1/2)}} - \frac{1}{2} c_1 & \frac{-c_1 s_2 d_3}{(1+c_2^2)^{(1/2)}} + \frac{c_1 c_2^2 d_3 s_2}{(1+c_2^2)^{(3/2)}} & \frac{c_1 c_2}{(1+c_2^2)^{(1/2)}} \\ \frac{c_1 c_2 d_3}{(1+c_2^2)^{(1/2)}} - \frac{1}{2} s_1 & \frac{-s_1 s_2 d_3}{(1+c_2^2)^{(1/2)}} + \frac{s_1 c_2^2 d_3 s_2}{(1+c_2^2)^{(3/2)}} & \frac{s_1 c_2}{(1+c_2^2)^{(1/2)}} \\ 0 & \frac{c_2 s_2 d_3}{(1+c_2^2)^{(3/2)}} & \frac{1}{(1+c_2^2)^{(1/2)}} \end{bmatrix}. \quad (12)$$

where J_G is the Jacobian of the manipulator where a gimbal transmission is used at joint 2. Using manipulability ellipsoid, we compare f in the simple and gimbal equipped Stanford arm with traditional revolute joints and the arm equipped with gimbal transmissions at revolute joint 2. To this end, d_3 (the joint variable of the arm's mere prismatic joint) is set to 1 m. The direction of the desired force vector is assumed to be $dx = dy = dz = 1$ [11].

(3) *RPR Planar Arm*. Figure 5 shows a revolute-prismatic-revolute (i.e., RPR) planar manipulator. The Jacobian matrix

for the arm, assuming $L_1 = 1$ m and $L_2 = 0.5$ m, is as follows [11]:

$$J = \begin{bmatrix} -c_{13} L_2 - s_1 L_1 + c_1 d_2 & s_1 & -c_{13} L_2 \\ -s_{13} L_2 - c_1 L_1 + s_1 d_2 & -c_1 & -s_{13} L_2 \\ 0 & 0 & 0 \end{bmatrix}. \quad (13)$$

Gimbal transmission is used at joint 3 by replacing the traditional revolute joint. To obtain a new Jacobian matrix, one shall substitute from (1) for θ_3 of the robot. Assuming

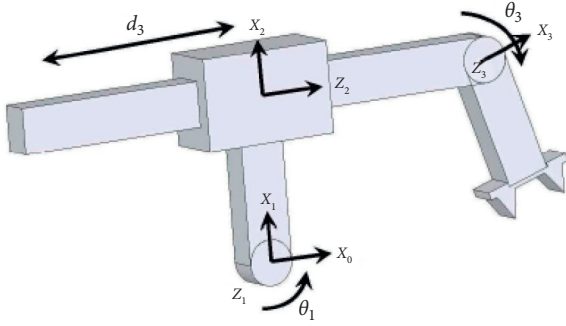


FIGURE 5: RPR arm [11].

$\theta_{of_out} = 0$, the Jacobian matrix for the manipulator with gimbal transmission at joint 3 becomes [11]

$$J_G = \begin{bmatrix} R_1 & R_2 & R_3 \\ R_4 & R_5 & R_6 \\ R_7 & R_8 & R_9 \end{bmatrix}, \quad (14)$$

where J_G is the Jacobian of the manipulator when a gimbal transmission is used at joint 3. To maintain conciseness, the elements of J_G are not shown here.

2.2. Genetic Algorithms. Genetic algorithm is one of the well-known evolutionary optimization techniques, which has been adopted by many researchers to optimize complex problems [12–14]. Briefly, the optimization process by GA can be divided into 6 steps as follows [15]:

- (1) Creating population of possible answers
- (2) Evaluation of fitness function
- (3) Creating the next generation of possible answers
- (4) Applying crossover
- (5) Applying mutation
- (6) Repeat steps 2–5

In this research, genetic algorithm has been utilized to find optimal parameters of the gimbal joints (truncation angles). For this purpose, the population generation techniques as listed above have been explored to generate the new population of the weight matrices. This process continues until the selection of the last weight matrix or matrices has been performed. In this simulation, a population of weight matrices is produced randomly when the GA starts. In each generation, the matrices of this population have been modified through discrete crossovers and uniformly random mutations, and their fitness values have been evaluated. The cycle of reconstructing the new population with better individuals and restarting the search is repeated until a better solution is found.

The fitness function has been defined as maximizing the applicable force magnitude, f , by minimizing the parameters of equation (6) [16]. To this end, to generate the fitness function for each of the three robotic manipulators (RRR, RPR, and Stanford), it is needed to substitute Jacobian matrix of each of the case studies, equations (9), (12), and

(14) in equation (6) [16]. Then, the optimization process has been started with a population of 20 individuals and has been run for 1000 times. As it is shown in Table 1, the probability of happening of crossover and mutation has been assumed as 0.4 and 0.01, respectively.

2.3. Neural Networks. Artificial neural networks have been utilized to different engineering and science fields such as control, data processing [17], robotics [18], function approximation [19], and pattern and speech recognition [20]. An ANN consists of interconnecting neurons which have been categorized into three layers which are, namely, input layer, hidden layer, and output layer [21]. There could be more than one hidden layer in an ANN making it more flexible and accurate to learn at the cost of learning time and effort.

Based on the type of connections between these neurons, artificial neural networks can be divided into two different groups: weighted artificial neural networks and weightless artificial neural networks [22]. This research focuses on utilizing weighted neural networks as a function optimizer.

As seen in Figure 6, parameters of the networks should be adjusted to enable the network to act as the plant (reference model). It means that by giving the same input to the ANN and the plant, the output of the network should be similar to the output of the plant. The first step in training a feed-forward network is to create the network object. It requires three arguments and returns the network object. The first argument is a matrix of sample R-element input vectors. The second argument is a matrix of sample S-element target vectors. The sample inputs and outputs are used to set up network input and output dimensions and parameters. The third argument is an array containing the sizes of each hidden layer (the output layer size is determined from the targets). In this research, the mentioned unknown function is the GA optimizer. The proposed ANN consists of a sigmoid hidden layer and a linear output layer.

Parameters of the ANN have been adjusted to enable the ANN to act as the GA optimizer (reference model) which optimizes the performance index of gimbal equipped robotic arm. It means that by giving the same input to the ANN and the GA, the output of the network should be like the output of the GA which is the evaluated fitness function. It means that the proposed ANN has a single input-single output (SISO) architecture. Levenberg–Marquardt algorithm has been adopted here to train the proposed ANN to model the dynamic behavior of the GA optimizer of the gimbal equipped robotic arms. The input of ANN is a Jacobian matrix with the dimension of 3×3 and its output is the matrix of the calculated maximum force with the demotion of 1×1 .

Levenberg–Marquardt algorithm computes the approximate Hessian matrix, which has dimensions n -by- n . Gradient descent is the process of making changes to weights and biases, where the changes are proportional to the derivatives of network error with respect to those weights and biases. This is done to minimize network error. When the performance function has the form of a sum of squares (as is

TABLE 1: Parameters used for the genetic algorithm [16].

Population size	20
Generations	1000
Crossover probability	0.4
Mutation probability	0.01

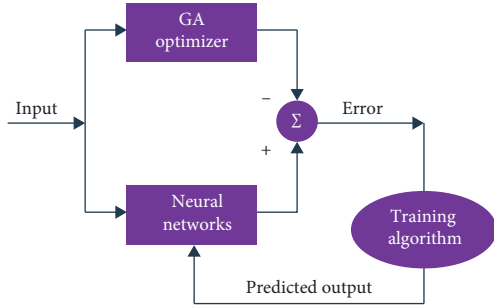


FIGURE 6: Proposed neural network model.

typical in training feed-forward networks), then the Hessian matrix can be approximated as

$$H = J^T J, \quad (15)$$

where J is the Jacobian matrix that contains first derivatives of the network errors with respect to the weights and biases and e is a vector of network errors. The gradient can be computed as

$$g = J^T e. \quad (16)$$

3. Results

As described previously to find the maximum value of f in each of the introduced case studies, GA optimization technique has been adopted in this research. The process has been started with a population of 20 individuals and has been run for 1000 times and the probability of happening of crossover and mutation has been assumed as 0.4 and 0.01, respectively. The results for normalized fitness function values of each of the robotic arms in each iteration of the GA optimization process have been shown in Figure 7. It can be observed that the optimization process for all the three cases works properly and normalized fitness values have been increased in each iteration.

Table 2 shows the results achieved by running GA for four different joint values and directions based on the fitness function of RRR arm which is used to evaluate and optimize the maximum values for f , and also it compares the amount of maximum force in gimbal equipped RRR robot with the robot with revolute joints. It is shown that in these points, the amount of force delivered by the gimbal equipped robot is greater than the same quantity for the robot that uses revolute joints. Thus, it can be reasoned that gimbal drive has improved the manipulability of the robot. Here, the values of θ_{c_2} and θ_{c_3} are restricted to 10 to 85 degrees so that the design becomes feasible.

Table 3 shows the results achieved by running GA for four different joint values and directions based on the fitness function of RPR arm which is used to evaluate and optimize

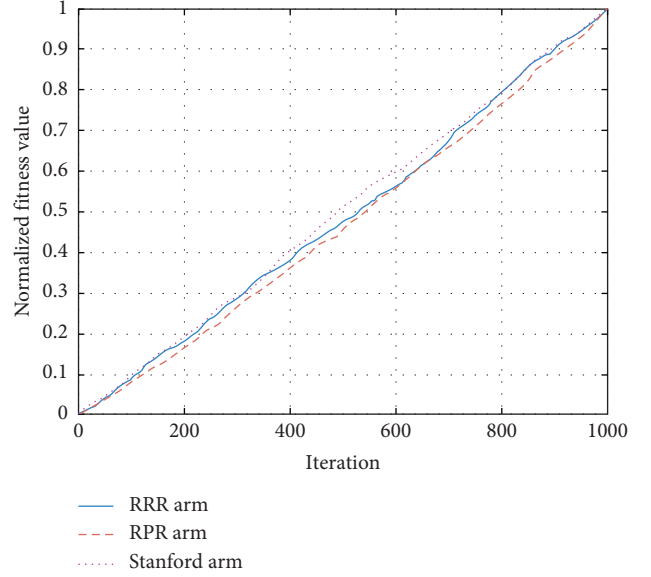


FIGURE 7: Normalized fitness function values in each step of GA optimization.

TABLE 2: GA optimization results for RRR arm [11].

Trial	1	2	3	4	Mean
θ_1	0	0	45	90	
θ_2	45	30	-15	15	
θ_3	-45	-30	30	30	
dx	0	1	1	1	
dy	0	1	1	1	
dz	1	1	0	1	
θ_{c_2}	85	85	10	85	66.25
θ_{c_3}	15.2	13.6	10	12.56	12.84
F for gimbal equipped arm	80.31	15.06	50.49	21.89	
F for simple arm	10.47	1.11	2.76	1.16	

TABLE 3: GA optimization results for RPR arm [11].

Trial	1	2	3	4	Mean
θ_1	0	30	45	90	
d_2	0.5	1	1	0.5	
θ_3	30	15	45	-30	
dx	1	0	1	1	
dy	1	1	1	1	
θ_c	49.10	61.37	35.8	85	57.81
F for gimbal equipped arm	1.09	0.81	1.97	1.41	
F for simple arm	0.97	0.76	1.41	1.29	

the maximum values for f . It can be inferred from results that implementation of gimbal drive in joint 2 has increased the maximum achievable force at the tip point of the manipulator. Here, the value of the truncation angle is bound to ensure design feasibility between 49 and 85 degrees.

Table 4 shows the results achieved by running GA for four different joint values and directions based on the fitness function of Stanford arm which is used to evaluate and optimize the maximum values for f . The amount of maximum force in gimbal equipped robot has been compared to

TABLE 4: GA optimization results for Stanford arm [11].

Trial	1	2	3	4	Mean
θ_1	0	90	90	90	
θ_2	0	0	90	90	
d_3	0.185	0.185	0.185	0.885	
dx	1	1	0	1	
dy	1	1	0	1	
dz	1	1	1	1	
θ_c	85	69	10	10	43.5
F for gimbal equipped arm	1.53	1.35	1	1.53	
F for simple arm	1.51	1.34	1	1.21	

the robot with traditional revolute joints and shows that in these points, the amount of force exerted by the gimbal equipped robot is greater than the same quantity for the robot that uses traditional revolute joints. Thus, it can be reasoned that gimbal drive has considerably improved the manipulability of the robot. Here, the value of the truncation angle is bound to ensure design feasibility between 10 and 85 degrees.

Now, by having the optimized results of the GA, the training of the proposed ANN can be performed. Basically, since the GA has been utilized to optimize three different case studies which have different Jacobian matrixes, three different ANNs have been trained for each of the robotic arms. It is important to know that since the number of the hidden layer's neurons should be chosen arbitrary, in this research the effect of increasing the hidden layer neurons has been investigated for 15, 20, and 25 neurons, and also the training mean square error limit has been defined as 0.9. Figure 8 shows the ANN training results for RRR arm with assuming 15, 20, and 25 neurons in the hidden layer.

From Figure 8, it can be observed that by increasing the number of neurons from 15 to 20, training of the ANN has been finalized in fewer steps, but the training mean square error has been increased and it makes the simulation result worse. On the other hand, by increasing the number of neurons from 20 to 25, training of the ANN has been finalized in fewer steps, and the training mean square error has been decreased even it is less than the case with 15 neurons and it makes the simulation result better.

Training results for RPR arm with assuming 15, 20, and 25 neurons in the hidden layer have been illustrated in Figure 9.

In Figure 9, although the results show that the trainings were successful, they do not follow the previous path as described for RRR. The difference is in the accuracy of the simulations results which indicate that by increasing the neurons in the hidden layer, training time and iterations will be reduced, but the mean square error of the ANN with 15 neurons is the lowest one, so the related ANN has a superior performance in comparison with the other two.

Training results for Stanford arm with assuming 15, 20, and 25 neurons in the hidden layer have been illustrated in Figure 10.

The results shown in Figure 10 are completely different from the results of RRR and RPR; also, the designed ANN shows different behavior. Like the previous two cases, it can

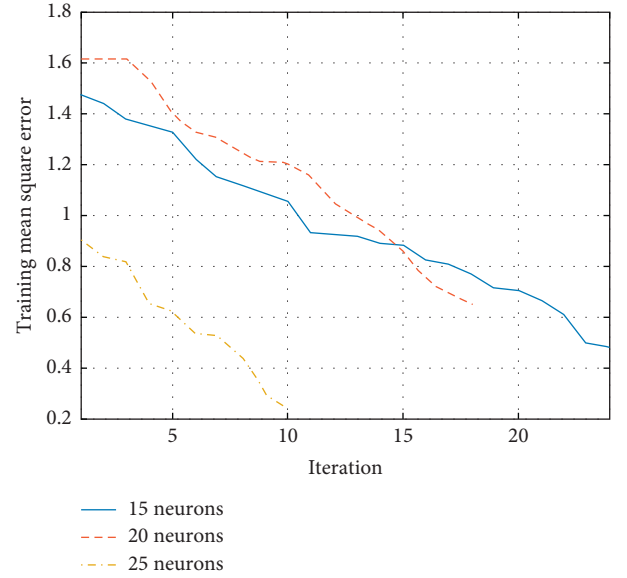


FIGURE 8: ANN training results for RRR arm with assuming 15, 20, and 25 neurons in the hidden layer.

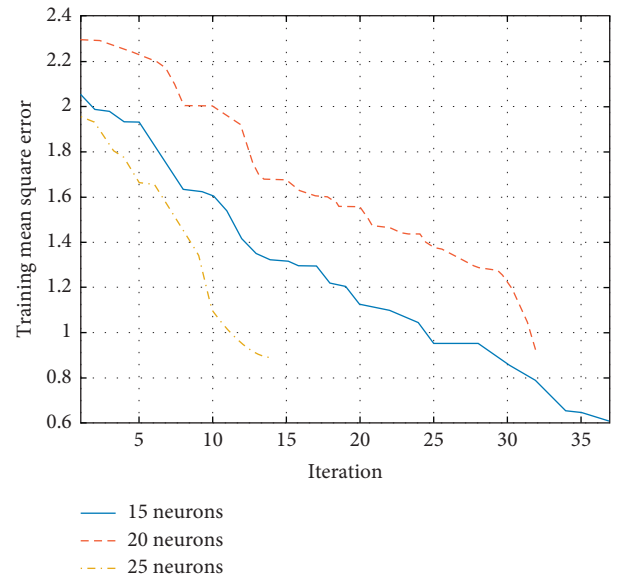


FIGURE 9: ANN training results for RPR arm with assuming 15, 20, and 25 neurons in the hidden layer.

be observed that by increasing the number of neurons in the hidden layer, the training iterations have been increased. Here, different from the results for RPR and RRR, the training mean square error has been decreased by increasing the number of neurons in the hidden layer. It means that the ANN with 25 neurons in the hidden layer has the best performance than the other two.

The summary of all these observations has been shown in Tables 5–7. The results indicate that the behavior of the proposed ANN cannot be predicted by the number of hidden layer's neurons, but one thing is obvious, and it is the fact of the proposed ANN working properly.

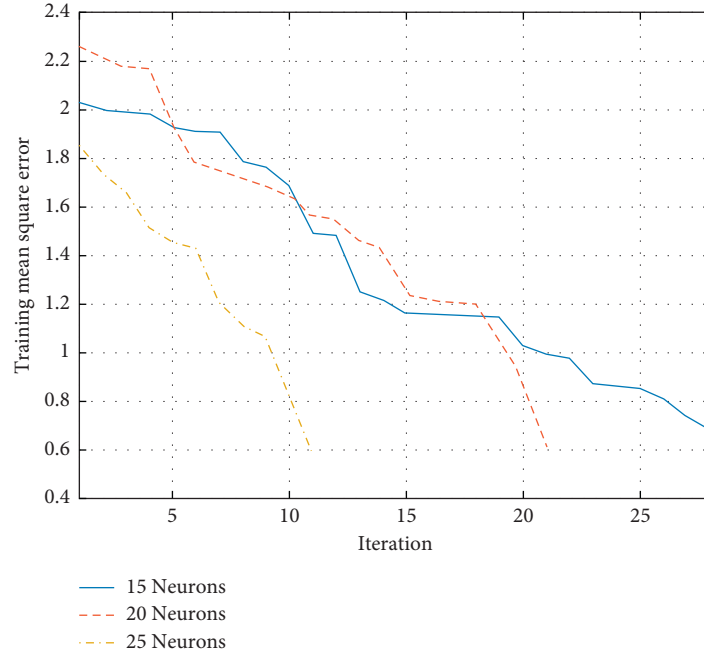


FIGURE 10: ANN training results for Stanford arm with assuming 15, 20, and 25 neurons in the hidden layer.

TABLE 5: Neural network training results for RRR arm.

	25	20	15
Number of neurons	25	20	15
Number of iterations	10	18	24
Number of training samples	700	700	700
Number of validation samples	150	150	150
Number of testing samples	150	150	150
Training mean square error	0.24	0.65	0.48
Validation mean square error	0.069	0.24	0.24
Test mean square error	0.26	0.31	0.22
<i>Total mean square error</i>	<i>0.19</i>	<i>0.47</i>	<i>0.35</i>
Training regression	0.8173	0.702	0.4985
Validation regression	0.4143	0.6003	0.1689
Test regression	0.4905	0.4245	0.473
<i>Total regression</i>	<i>0.6648</i>	<i>0.6129</i>	<i>0.409</i>

TABLE 7: Neural network training results for Stanford arm.

	25	20	15
Number of neurons	25	20	15
Number of iterations	11	21	28
Number of training samples	700	700	700
Number of validation samples	150	150	150
Number of testing samples	150	150	150
Training mean square error	0.59	0.61	0.68
Validation mean square error	0.63	0.18	0.23
Test mean square error	0.39	0.55	0.25
<i>Total mean square error</i>	<i>0.54</i>	<i>0.44</i>	<i>0.46</i>
Training regression	0.7555	0.8012	0.8318
Validation regression	0.7178	0.1051	0.4116
Test regression	0.6074	0.5734	0.4426
<i>Total regression</i>	<i>0.7141</i>	<i>0.3640</i>	<i>0.6491</i>

TABLE 6: Neural network training results for RPR arm.

	25	20	15
Number of neurons	25	20	15
Number of iterations	14	32	37
Number of training samples	700	700	700
Number of validation samples	150	150	150
Number of testing samples	150	150	150
Training mean square error	0.89	0.9	0.61
Validation mean square error	0.95	0.74	0.97
Test mean square error	0.59	0.81	0.51
<i>Total mean square error</i>	<i>0.82</i>	<i>0.84</i>	<i>0.62</i>
Training regression	0.9449	0.9503	0.7899
Validation regression	0.8929	0.9076	0.877
Test regression	0.7317	0.9149	0.7060
<i>Total regression</i>	<i>0.8832</i>	<i>0.9317</i>	<i>0.7762</i>

Generally, following points regarding the training procedure of the proposed ANN for all three robot arms with three different number of neurons in the hidden layer for each case study can be observed from Tables 5–7.

1000 random points (inputs and outputs) have been generated as a feed to ANN. They were generated according to normal distribution in the permissible zone of the joint space of each one of the robots. Moreover, validation and test data samples are each set to 15 percent of the original samples (see Tables 5–7). So, 300 random samples are used for validation and test, and 700 samples are left for training. Although it is correct, by changing this arrangement or using larger data samples and retraining network over and over, different results are faced, but one should note that it would give some marginal improvements. To achieve reliable results, initial conditions are fixed for all three cases (RRR, Stanford, and RPR).

A set of training samples are presented to the network during training and the network is adjusted according to its error. In addition, a set of validation data are used to measure network generalization and to halt training when generalization stops improving. Furthermore, a set of testing samples have no effect on training and provide an

independent measure of network performance during and after training.

Mean square error is the average squared difference between outputs and targets which lower values are better, and zero means there is no error (see Tables 5–7).

Regression R values measure the correlation between outputs and targets. An R value of 1 means a close relationship and 0 means a random relationship. As the data fed into the neural network might be of the scattered type, the discretion and correlation of data values are good measures of those data. This way the regression values help decide on the closeness of the data used for training and the way the ANN is predicting the unknown results.

It can be interpreted from Tables 5–7 that by increasing the number of neurons from 15 to 25, in this special case study, the number of iterations decreases which means that the mean square error decreases to zero. It is important to know this result cannot be used as a pattern for all cases, and there is no guarantee to get better results by increasing the number of neurons and there is a possibility to get worse result by increasing the number of neurons.

The results demonstrate that the increasing number of neurons lead to a decreasing number of iterations which means that the mean square error has been approaching to zero, and the regression data have become closer to one in the case study of this research. So, one may conclude that by increasing the number of neurons, the proposed neural network performance for this research has been increased.

4. Conclusion and Future Work

In this paper, synthesis of three robotic arms such as RRR, RPR, and Stanford with gimbal drive which can be used to achieving the maximum force have been analyzed. Genetic algorithm has been employed to find optimal parameters of the gimbal joints (truncation angles), and then it has been utilized as a model reference for the proposed neural networks. Thousands of randomly generated points have been used as the inputs to the gimbal dynamic model in the GA optimization process. These points have been fed to the neural network to find the relation between inputs and outputs to investigate how well the proposed ANN algorithm can act instead of the GA optimizer of the parameters of the mechanism equipped with gimbal drive.

The results confirm that the proposed ANN optimizer of gimbal drive is a novel and effective technique which can be utilized as an effective optimizer for improving the performance of robots based on their applications. Since robots make a qualitative contribution to productivity, improvement of their performance contributes to sustainability by reducing energy consumption and waste in manufacturing processes.

One of the valuable topics of future works can be defined as measuring the power consumption and material waste reduction rates by utilizing the proposed ANN in real-life industrial implementation which can give a better view to understand how the proposed ANN contributes to sustainability. As another future work, other well-known optimization techniques such as hybrid optimization

techniques, bee colony, and particle swarm can be utilized as a reference model to train the proposed neural networks. Also, different neural network models such as ring probabilistic logic neural networks (RPLNN) and RAM-based neural networks can be utilized instead of the proposed ANN.

Data Availability

No data were used to support this study.

Conflicts of Interest

The authors declare that they have no conflicts of interest.

References

- [1] J. Ogbemhe, K. Mpofu, and N. S. Tlale, "Achieving sustainability in manufacturing using robotic methodologies," *Procedia Manufacturing*, vol. 8, pp. 440–446, 2017.
- [2] L. Wang, C. Wang, W. Du et al., "Parameter optimization of a four-legged robot to improve motion trajectory accuracy using signal-to-noise ratio theory," *Robotics and Computer-Integrated Manufacturing*, vol. 51, pp. 85–96, 2018.
- [3] M. Koopialipour, A. Fallah, D. J. Armaghani, A. Azizi, and E. T. Mohamad, "Three hybrid intelligent models in estimating flyrock distance resulting from blasting," *Engineering with Computers*, vol. 35, no. 1, pp. 243–256, 2018.
- [4] A. Azizi, *Applications of Artificial Intelligence Techniques in Industry 4.0*, Springer, Berlin, Germany, 2019.
- [5] A. Azizi, "Hybrid artificial intelligence optimization technique," in *Applications of Artificial Intelligence Techniques in Industry 4.0*, Springer, Berlin, Germany, 2019.
- [6] A. Azizi, A. Vatankhah Barenji, and M. Hashmipour, "Optimizing radio frequency identification network planning through ring probabilistic logic neurons," *Advances in Mechanical Engineering*, vol. 8, no. 8, 2016.
- [7] E. G. Solberg, *Deep Neural Networks for Object Detection in Agricultural Robotics*, Norwegian University of Life Sciences, Ås, Norway, 2017.
- [8] L. Jin, S. Li, H. M. La, and X. Luo, "Manipulability optimization of redundant manipulators using dynamic neural networks," *IEEE Transactions on Industrial Electronics*, vol. 64, no. 6, pp. 4710–4720, 2017.
- [9] V. T. Yen, W. Y. Nan, P. Van Cuong, N. X. Quynh, and V. H. Thich, "Robust adaptive sliding mode control for industrial robot manipulator using fuzzy wavelet neural networks," *International Journal of Control, Automation and Systems*, vol. 15, no. 6, pp. 2930–2941, 2017.
- [10] V. T. Yen, W. Y. Nan, and P. Van Cuong, "Recurrent fuzzy wavelet neural networks based on robust adaptive sliding mode control for industrial robot manipulators," *Neural Computing and Applications*, vol. 31, no. 11, pp. 6945–6958, 2018.
- [11] F. Mohammadi, I. Hemmatian, and K. G. Osgouie, "Manipulability analysis for Gimbal driven robotic arms," in *Proceedings of the 2009 IEEE International Conference on Robotics and Biomimetics (ROBIO)*, Guilin, China, December 2009.
- [12] A. Ashkzari and A. Azizi, "Introducing genetic algorithm as an intelligent optimization technique," *Applied Mechanics and Materials*, vol. 568–570, pp. 793–797, 2014.

- [13] R. L. Kadri and F. F. Boctor, "An efficient genetic algorithm to solve the resource-constrained project scheduling problem with transfer times: the single mode case," *European Journal of Operational Research*, vol. 265, no. 2, pp. 454–462, 2018.
- [14] B. Yan, C. Yan, F. Long, and X.-C. Tan, "Multi-objective optimization of electronic product goods location assignment in stereoscopic warehouse based on adaptive genetic algorithm," *Journal of Intelligent Manufacturing*, vol. 29, no. 6, pp. 1273–1285, 2018.
- [15] M. Mohammadi, M. Lakestani, and M. H. Mohamed, "Intelligent parameter optimization of savonius rotor using artificial neural network and genetic algorithm," *Energy*, vol. 143, pp. 56–68, 2018.
- [16] F. Mohammadi, I. Hemmatian, and K. G. Osgouie, "Design optimization of gimbal robotic joints based on task space manipulability," in *Proceedings of the ASME 2010 10th Biennial Conference on Engineering Systems Design and Analysis*, vol. 3, Istanbul, Turkey, July 2010.
- [17] J. Salamon and J. P. Bello, "Deep convolutional neural networks and data augmentation for environmental sound classification," *IEEE Signal Processing Letters*, vol. 24, no. 3, pp. 279–283, 2017.
- [18] L. Xiao, Z. Zhang, Z. Zhang, W. Li, and S. Li, "Design, verification and robotic application of a novel recurrent neural network for computing dynamic Sylvester equation," *Neural Networks*, vol. 105, pp. 185–196, 2018.
- [19] A. Azizi, F. Entessari, K. G. Osgouie, and A. R. Rashnoodi, "Introducing neural networks as a computational intelligent technique," *Applied Mechanics and Materials*, vol. 464, pp. 369–374, 2014.
- [20] W. Chan, J. Navdeep, L. Quoc, V. Oriol, and S. Noam, "Speech recognition with attention-based recurrent neural networks," US Patent 9,990,918, 2018.
- [21] J. Liu, M. Gong, Q. Miao, X. Wang, and H. Li, "Structure learning for deep neural networks based on multiobjective optimization," *IEEE Transactions on Neural Networks and Learning Systems*, vol. 29, no. 6, pp. 2450–2463, 2018.
- [22] A. Azizi, "Introducing a novel hybrid artificial intelligence algorithm to optimize network of industrial applications in modern manufacturing," *Complexity*, vol. 2017, Article ID 8728209, 18 pages, 2017.

Research Article

A Case Study on Designing a Sliding Mode Controller to Stabilize the Stochastic Effect of Noise on Mechanical Structures: Residential Buildings Equipped with ATMD

Aydin Azizi 

School of Engineering, Computing and Mathematics, Oxford Brookes University, Wheatley Campus, Oxford OX33 1HX, UK

Correspondence should be addressed to Aydin Azizi; aydin.azizi@brookes.ac.uk

Received 16 April 2019; Accepted 8 October 2019; Published 20 March 2020

Guest Editor: Manuel Zamora

Copyright © 2020 Aydin Azizi. This is an open access article distributed under the Creative Commons Attribution License, which permits unrestricted use, distribution, and reproduction in any medium, provided the original work is properly cited.

This study aims to stabilize the unwanted fluctuation of buildings as mechanical structures subjected to earth excitation as the noise. In this study, the ground motion is considered as a Wiener process, in which the governing stochastic differential equations have been presented in the form of Ito equation. To stabilize the vibration of the system, the ATMD system is considered and located on the upmost story of the building. A sliding mode controller has been utilized to control the ATMD system, which is a robust controller in the presence of uncertainty. For this purpose, the design of a sliding mode controller for the general dynamic system with Lipschitz nonlinearity and considering the Ito relations has been accomplished. The mentioned design has been implemented considering the presence of the Weiner process and existence of uncertainty in the structure and actuator. Then, the obtained general control law has been generalized to control the ATMD system. The results show that the designed controller is effective to reduce the effect of the unwanted imposed vibrations on the building.

1. Introduction

Stochastic factors are one of the inherent aspects of most dynamical systems that occur in different ways such as external force and changes in the inherent parameters of the system. Stochastic Differential Equations (SDE) in financial mathematics and economics have been extensively investigated [1–6]. Also, the effect of stochastic factors in science and mechanical and electronic engineering has been considered [7–20].

Earthquake is an example of a natural phenomenon that influences the dynamics of a structures and building. Dynamic behavior of structures in the presence of earthquakes has been extensively studies in [21–27]. In the mentioned studies, the dynamic behavior of the structures has been investigated under the influence of a particular earthquake. But in this paper, we aim to examine the dynamic behavior of the structure subjected to White Gaussian Noise (WGN) because the density function of its power spectrum is

constant at all frequencies. So, unlike the previous studies, a new formulation should be considered.

For this purpose, Itô formulation is considered to solve governing SDE of the structure [28–30]. The studied structure is an 11-story building equipped with an ATMD system at the upmost story. ATMD has been used to reduce unwanted vibrations. This system has been controlled by means of the sliding mode controller. For this reason, the sliding mode controller has been designed for the general and nonlinear Lipschitz dynamic system in the presence of actuator and system uncertainties and based on the Itô theory. Finally, the designed controller has been generalized to control the ATMD system.

The dynamic behavior of the structure in the active and passive mode and considering the uncertainties has been studied. The effect of various controller parameters on the dynamic behavior of the structure has been also investigated. Moreover, the effect of the controlled system and different parameters of the controller on the basin of attraction was

$$\begin{aligned}
[K] &= \begin{bmatrix} k_1 + k_2 & -k_2 & 0 & 0 & 0 & 0 & 0 & 0 & 0 & 0 & 0 & 0 & 0 \\ -k_2 & k_2 + k_3 & -k_3 & 0 & 0 & 0 & 0 & 0 & 0 & 0 & 0 & 0 & 0 \\ 0 & -k_3 & k_3 + k_4 & -k_4 & 0 & 0 & 0 & 0 & 0 & 0 & 0 & 0 & 0 \\ 0 & 0 & -k_4 & k_4 + k_5 & -k_5 & 0 & 0 & 0 & 0 & 0 & 0 & 0 & 0 \\ 0 & 0 & 0 & -k_5 & k_5 + k_6 & -k_6 & 0 & 0 & 0 & 0 & 0 & 0 & 0 \\ 0 & 0 & 0 & 0 & -k_6 & k_6 + k_7 & -k_7 & 0 & 0 & 0 & 0 & 0 & 0 \\ 0 & 0 & 0 & 0 & 0 & -k_7 & k_7 + k_8 & -k_8 & 0 & 0 & 0 & 0 & 0 \\ 0 & 0 & 0 & 0 & 0 & 0 & -k_8 & k_8 + k_9 & -k_9 & 0 & 0 & 0 & 0 \\ 0 & 0 & 0 & 0 & 0 & 0 & 0 & -k_9 & k_9 + k_{10} & -k_{10} & 0 & 0 & 0 \\ 0 & 0 & 0 & 0 & 0 & 0 & 0 & 0 & -k_{10} & k_{10} + k_{11} & -k_{11} & 0 & 0 \\ 0 & 0 & 0 & 0 & 0 & 0 & 0 & 0 & 0 & -k_{11} & k_{11} + k_{12} & -k_{12} & 0 \\ 0 & 0 & 0 & 0 & 0 & 0 & 0 & 0 & 0 & 0 & -k_{12} & k_{12} & 0 \end{bmatrix}, \\
[C] &= \begin{bmatrix} c_1 + c_2 & -c_2 & 0 & 0 & 0 & 0 & 0 & 0 & 0 & 0 & 0 & 0 & 0 \\ -c_2 & c_2 + c_3 & -c_3 & 0 & 0 & 0 & 0 & 0 & 0 & 0 & 0 & 0 & 0 \\ 0 & -c_3 & c_3 + c_4 & -c_4 & 0 & 0 & 0 & 0 & 0 & 0 & 0 & 0 & 0 \\ 0 & 0 & -c_4 & c_4 + c_5 & -c_5 & 0 & 0 & 0 & 0 & 0 & 0 & 0 & 0 \\ 0 & 0 & 0 & -c_5 & c_5 + c_6 & -c_6 & 0 & 0 & 0 & 0 & 0 & 0 & 0 \\ 0 & 0 & 0 & 0 & -c_6 & c_6 + c_7 & -c_7 & 0 & 0 & 0 & 0 & 0 & 0 \\ 0 & 0 & 0 & 0 & 0 & -c_7 & c_7 + c_8 & -c_8 & 0 & 0 & 0 & 0 & 0 \\ 0 & 0 & 0 & 0 & 0 & 0 & -c_8 & c_8 + c_9 & -c_9 & 0 & 0 & 0 & 0 \\ 0 & 0 & 0 & 0 & 0 & 0 & 0 & -c_9 & c_9 + c_{10} & -c_{10} & 0 & 0 & 0 \\ 0 & 0 & 0 & 0 & 0 & 0 & 0 & 0 & -c_{10} & c_{10} + c_{11} & -c_{11} & 0 & 0 \\ 0 & 0 & 0 & 0 & 0 & 0 & 0 & 0 & 0 & -c_{11} & c_{11} + c_{12} & -c_{12} & 0 \\ 0 & 0 & 0 & 0 & 0 & 0 & 0 & 0 & 0 & 0 & -c_{12} & c_{12} & 0 \end{bmatrix}. \tag{2}
\end{aligned}$$

3. Mathematical Modeling

Without loss of generality, the controller is initially designed for a general system, after which it is applied to the studied structural control.

Consider the mathematical model presented in the following equation:

$$\begin{cases} \dot{x}_1 = x_2, \\ \dot{x}_2 = f(x, t) + b(x, t)u + h(x, t)\dot{v}, \end{cases} \tag{3}$$

where $f(x, t)$, $b(x, t)$, and $h(x, t)$ represent continuous functions satisfying the Lipschitz condition. In this case, u , v , and $\dot{v} = dv/dt$ indicate the control force, standard Wiener process, and white Gaussian noise, respectively. The objective of the controller design is for the x_1 to track x_d . To this end, the dynamic error of $e = x_1 - x_d$ should be defined. However, since x_d is considered zero in structural control, the error is defined as $e = x_1$ and the corresponding dynamic error is defined as follows:

$$\begin{cases} \dot{e}_1 = x_2 - \dot{x}_d, \\ \dot{e}_2 = f(x, t) + b(x, t)u + h(x, t)\dot{v} - \ddot{x}_d. \end{cases} \tag{4}$$

The Lyapunov function is considered as $V = 1/2E(s^2)$. From a mathematical viewpoint and based on Ito's theory,

equation (4) can be reformulated in the form of a differential equation as follows:

$$\begin{cases} de_1 = [x_2 - \dot{x}_d]dt, \\ de_2 = [f(x, t) + b(x, t)u - \ddot{x}_d]dt + h(x, t)dv, \end{cases} \tag{5}$$

$$\ddot{x}_d = 0.$$

Given that $x_d = \dot{x}_d = \ddot{x}_d = 0$, the abovementioned equation is presented as follows for simplification purposes:

$$\begin{cases} de_1 = [x_2]dt, \\ de_2 = [f(x, t) + b(x, t)u]dt + h(x, t)dv. \end{cases} \tag{6}$$

The abovementioned equation represents an Itô SDE used instead of equation (4) and considering the Wiener process. The terms $f(x, t) + b(x, t)u$ and $h(x, t)$ represent the drift function and diffusion, respectively [28, 29].

The sliding surface was considered as $s = e_2 + \lambda e_1$ in the design of the sliding mode controller, from which $\dot{s} = \dot{e}_2 + \lambda \dot{e}_1$ and $ds = de_2 + \lambda e_1 dt$ can be derived. In the final form and according to equation (4), the ds equation can be rewritten to obtain equation (5):

$$ds = [f(x, t) + b(x, t)u + \lambda e_2]dt + h(x, t)dv. \tag{7}$$

Assuming $y = g(x, t)$ and employing Itô's differentiation formula for dy , we have [28, 29]

$$y = g(x, t), \quad (8)$$

$$dy = \frac{\partial g}{\partial t} dt + \frac{\partial g}{\partial x} dx + \frac{1}{2} \frac{\partial^2 g}{\partial x^2} (dx)^2.$$

Based on Ito's formula, differentiating s^2 produces $ds^2 = 2sds + dsds$. Therefore, the dV value emerges as follows:

$$dV = E\left\{s\{[f(x, t) + b(x, t)u + \lambda e_2]dt + h(x, t)dv\} + \frac{1}{2}\{[f(x, t) + b(x, t)u + \lambda e_2]dt + h(x, t)dv\}^2\right\}. \quad (9)$$

By including the following relations proposed by [32, 33] in the calculations,

$$\begin{aligned} dt \cdot dt &= 0, \\ dt \cdot dv &= 0, \\ dv \cdot dv &= dt. \end{aligned} \quad (10)$$

And also considering the properties of the Wiener process [28],

$$\begin{aligned} E[h(x, t)dv] &= 0, \\ E[h(x, t)dv]^2 &= h^2(x, t)dt. \end{aligned} \quad (11)$$

According to equations (10) and (11), the expected value of dV is determined as follows:

$$dV = E\left\{s\{[f(x, t) + b(x, t)u + \lambda e_2]dt\} + \frac{1}{2}h^2(x, t)dt\right\}. \quad (12)$$

Dividing the abovementioned relation by dt , \dot{V} is obtained as follows:

$$\dot{V} = E\{s[f(x, t) + b(x, t)u + \lambda e_2]\} + \frac{1}{2}E\{h^2(x, t)\}. \quad (13)$$

The stability condition for the sliding mode controller is defined as $\dot{V} < 0$ based on the Lyapunov second method for stability [34]. Assuming the systems involve no uncertainty, the controller stability is only guaranteed by considering $f(x, t) + b(x, t)u + \lambda e_2 = -\theta s$, limiting the region of attraction associated with the sliding surface. However, given the presence of uncertainty in most of dynamical systems, the system uncertainties are included in the controller design equations in the following part.

The structural and actuator uncertainties have been considered in the controller model in this study. To this end, some of the inequalities associated with the $f(x, t)$ and $b(x, t)$ functions along with their nominal values should be taken into account.

Assuming $\hat{f}(x, t)$ as the nominal values for $f(x, t)$ and $F(x, t)$ is a positive function expressed as follows:

$$|f(x, t) - \hat{f}(x, t)| \leq F(x, t). \quad (14)$$

As a result, the following equations hold true:

$$\begin{aligned} |sf(x, t) - s\hat{f}(x, t)| &\leq |s|F(x, t), \\ sf(x, t) &\leq s\hat{f}(x, t) + |s|F(x, t). \end{aligned} \quad (15)$$

If $b(x, t)$ is defined as

$$0 < b_0 < b(x, t) < b_M, \quad (16)$$

where b_0 and b_M are positive values representing the upper and lower bounds of the $b(x, t)$ function, the following equations are necessary for the controller design:

$$|s|F(x, t) \leq |s| \frac{b(x, t)}{b_0} F(x, t), \quad (17)$$

$$\begin{aligned} s\lambda e_2 &= s\lambda \frac{b}{b_0} e_2 + s\lambda e_2 \left(1 - \frac{b}{b_0}\right), \\ s\lambda e_2 &\leq s\lambda \frac{b}{b_0} e_2 + |s|\lambda |e_2| b \left(\frac{1}{b_0} - \frac{1}{b}\right), \end{aligned}$$

$$\text{attention to } \longrightarrow |s|\lambda |e_2| b \left(\frac{1}{b_0} - \frac{1}{b}\right) \leq |s|\lambda |e_2| b \left(\frac{1}{b_0} - \frac{1}{b_M}\right),$$

So,

$$s\lambda e_2 \leq s\lambda \frac{b}{b_0} e_2 + |s|\lambda |e_2| b \left(\frac{1}{b_0} - \frac{1}{b_M}\right), \quad (18)$$

$$\begin{aligned} s\hat{f}(x, t) &= s \frac{b}{b_0} \hat{f}(x, t) + s\hat{f}(x, t) \left(1 - \frac{b}{b_0}\right), \\ s\hat{f}(x, t) &\leq s \frac{b}{b_0} \hat{f}(x, t) + |s| |\hat{f}(x, t)| b \left(\frac{1}{b_0} - \frac{1}{b}\right), \end{aligned}$$

$$\begin{aligned} \text{attention to } \longrightarrow |s| |\hat{f}(x, t)| b \left(\frac{1}{b_0} - \frac{1}{b}\right) \\ \leq |s| |\hat{f}(x, t)| b \left(\frac{1}{b_0} - \frac{1}{b_M}\right), \end{aligned} \quad (19)$$

So,

$$s\hat{f}(x, t) \leq s \frac{b}{b_0} \hat{f}(x, t) + |s| |\hat{f}(x, t)| b \left(\frac{1}{b_0} - \frac{1}{b_M}\right).$$

The following inequality holds true considering equations (15), (17), and (19):

$$\begin{aligned} sf(x, t) &\leq s \frac{b}{b_0} \hat{f}(x, t) + |s| |\hat{f}(x, t)| b \left(\frac{1}{b_0} - \frac{1}{b_M}\right) \\ &+ |s| \frac{b(x, t)}{b_0} F(x, t). \end{aligned} \quad (20)$$

Equation (21) also holds true considering equations (18) and (20):

$$\begin{aligned}
\dot{V} &\leq s\lambda \frac{b}{b_0} e_2 + |s|\lambda |e_2| b \left(\frac{1}{b_0} - \frac{1}{b_M} \right) + s \frac{b}{b_0} \hat{f}(x, t) \\
&\quad + |s| |\hat{f}(x, t)| b \left(\frac{1}{b_0} - \frac{1}{b_M} \right) + |s| \frac{b}{b_0} F(x, t) + sb(x, t)u \\
&\quad + \frac{1}{2} h^2(x, t), \\
\dot{V} &\leq s \frac{b}{b_0} [\lambda e_2 + \hat{f}(x, t)] + sb(x, t)u + |s| b \left(\frac{1}{b_0} - \frac{1}{b_M} \right) [\lambda |e_2| \\
&\quad + |\hat{f}(x, t)|] + |s| \frac{b}{b_0} F(x, t) + \frac{1}{2} h^2(x, t).
\end{aligned} \tag{21}$$

By defining u as follows, the relation $\dot{V} \leq -\theta E[s^2] + (1/2)E[h^2(x, t)]$ holds true:

$$u = -\frac{1}{b_0} [\lambda e_2 + \hat{f}(x, t) + \theta \times (s)] - \text{sign}(s) [\eta + \psi], \tag{22}$$

where η represents a positive value and $\psi(x, t) = ((1/b_0) - (1/b_M))[\lambda |e_2| + |\hat{f}(x, t)|] + (1/b_0)F(x, t)$. In fact, $u = u_1 + u_2$, where u_1 and u_2 , which are obtained as follows, cause the nominal and uncertainty terms to be negative definite, respectively:

$$u = u_1 + u_2,$$

$$\lambda \frac{1}{b_0} e_2 + \frac{1}{b_0} \hat{f}(x, t) + u_1 = -\frac{\theta}{b_0} s,$$

$$u_1 = -\frac{1}{b_0} [\lambda e_2 + \hat{f}(x, t) + \theta \times (s)],$$

$$sb(x, t)u_2 + |s|b(x, t) \left\{ \left(\frac{1}{b_0} - \frac{1}{b_M} \right) [\lambda |e_2| + |\hat{f}(x, t)|] + \frac{1}{b_0} F(x, t) \right\} = -\eta b(x, t)|s|,$$

$$su_2 + |s| \left\{ \left(\frac{1}{b_0} - \frac{1}{b_M} \right) [\lambda |e_2| + |\hat{f}(x, t)|] + \frac{1}{b_0} F(x, t) \right\} = -\eta |s|, \tag{23}$$

$$\psi(x, t) = \left(\frac{1}{b_0} - \frac{1}{b_M} \right) [\lambda |e_2| + |\hat{f}(x, t)|] + \frac{1}{b_0} F(x, t),$$

$$su_2 = -\eta |s| - |s| \psi,$$

$$su_2 = -|s|(\eta + \psi),$$

$$u_2 = -\text{sign}(s) [\eta + \psi].$$

Theory. assume Δ as the following set:

$$\Delta = \left\{ s \in R \mid E[s^2] \leq \frac{H^2}{\theta} \right\}, \tag{24}$$

where θ is a positive value. In fact, $\dot{V} \leq -\theta E[s^2] + (1/2)E[h^2(x, t)]$ represents the attraction set for the trajectory $s(t)$. Assuming at $t = 0$, the trajectory $s(t)$ lies outside the attraction set, i.e., $E[s^2(t=0)] > H^2/2\theta$, we obtain

$$\dot{V} \leq -\theta E[s^2(t=0)] + \frac{1}{2} E[h^2(x, t)] < 0, \tag{25}$$

which indicates a declining rate for V as it tends to enter the Δ set and ultimately remains in this region.

If it is located in the domain of s for the moment $t = 0$, it will continue to be in this area.

The designed sliding mode controller is then applied to the system, as shown in Figure 1, based on the above-mentioned equations. The equation governing the dynamic behavior of the 11th story is expressed as follows:

$$\begin{cases} \dot{x}_1 = x_2, \\ \dot{x}_2 = -\frac{1}{M_{11}} [(K_{11} + K_{12})x_{11} + (C_{11} + C_{12})\dot{x}_{11} - K_{11}x_{10} \\ - K_{12}x_{12} - C_{11}\dot{x}_{10} - C_{12}\dot{x}_{12}] - \ddot{x}_g + \frac{b(x, t)}{M_{11}} u. \end{cases} \tag{26}$$

The $f(x, t)$ for this equation is defined as follows:

$$\begin{aligned}
f(x, t) = & -\frac{1}{\widehat{M}_{11} + \Delta M_{11}} \left[(\widehat{K}_{11} + \Delta K_{11} + \widehat{K}_{12} + \Delta K_{12}) x_{11} \right. \\
& + (\widehat{C}_{11} + \Delta C_{11} + \widehat{C}_{12} + \Delta C_{12}) \dot{x}_{11} - (\widehat{K}_{11} + \Delta K_{11}) x_{10} \\
& \left. - (\widehat{K}_{12} + \Delta K_{12}) x_{12} - (\widehat{C}_{11} + \Delta C_{11}) \dot{x}_{10} - (\widehat{C}_{12} + \Delta C_{12}) \dot{x}_{12} \right],
\end{aligned} \tag{27}$$

where \widehat{M}_{11} , \widehat{K}_{11} , \widehat{K}_{12} , \widehat{C}_{11} , and \widehat{C}_{12} denote nominal values and ΔM_{11} , ΔK_{11} , ΔK_{12} , ΔC_{11} , and ΔC_{12} represent the maximum value for the respective uncertainty term.

In this case, $F(x, t)$ is defined as follows:

$$\begin{aligned}
F(x, t) = & \frac{1}{\widehat{M}_{11} - |\Delta \widehat{M}_{11}|} \left[(|\Delta \widehat{K}_{11}| + |\Delta \widehat{K}_{12}|) |x_{11}| + (|\Delta \widehat{C}_{11}| \right. \\
& + |\Delta \widehat{C}_{12}|) |\dot{x}_{11}| + |\Delta \widehat{K}_{11}| |x_{10}| + |\Delta \widehat{K}_{12}| |x_{12}| \\
& \left. + |\Delta \widehat{C}_{11}| |\dot{x}_{10}| + |\Delta \widehat{C}_{12}| |\dot{x}_{12}| \right].
\end{aligned} \tag{28}$$

Moreover, $b(x, t)$ is assumed as $b(x, t) = (1 + \alpha \sin t)/M_{21}$ in this case, meaning that the system's actuator includes the uncertainty $(1 + \alpha \sin t)$. Under these conditions, b_0 and b_M are expressed as follows:

$$\begin{aligned}
b_0 &= \frac{1 - \alpha}{\widehat{M}_{21} + |\Delta \widehat{M}_{21}|}, \\
b_M &= \frac{1 + \alpha}{\widehat{M}_{21} - |\Delta \widehat{M}_{21}|}.
\end{aligned} \tag{29}$$

Finally, the term associated with the control force u is conveniently determined using equation (22).

4. Results and Discussion

In this section, the obtained results will be presented and the control of horizontal displacement of the 11-story building will be discussed. Given that the first vibrational mode of the building is easily excited, the largest displacement in this mode is experienced by the topmost story. Therefore, vibration analysis is conducted on the 11th story. The physical and geometrical specifications of the studied building are given in Table 1. In the first scenario, the uncertainty was assumed as $\Delta M_i = 0.01M_i$, $\Delta K_i = 0.01K_i$, $\Delta C_i = 0.01C_i$, and $\alpha = 0$. The resulting horizontal displacement for story 11 is demonstrated in Figure 2 for both active and passive cases. As shown in this figure, the vibrational amplitude of the controlled system is considerably smaller than that of the uncontrolled system.

The variations of the control force u with respect to time are demonstrated in Figure 3. As shown, the chattering phenomenon is apparent within some time intervals. Chattering is mainly caused by the term $\text{sign}(s)$ in the control force relation. In fact, the discontinuity and undifferentiability of this function at point $s = 0$ is responsible for the chattering phenomenon. The chattering around the zero point is highly harmful, since, in addition to the force magnitude, its sign also changes. However, at

TABLE 1: The physical and geometrical specifications of the studied building.

Properties	Values
M_1, M_2, \dots, M_{11}	255×10^3 kg
M_{12}	77×10^3 kg
K_1, K_2, \dots, K_{11}	25×10^6 N/m
K_{12}	205×10^3 N/m
C_1, C_2, \dots, C_{11}	216×10^3 Ns/m
C_{12}	438×10^3 Ns/m

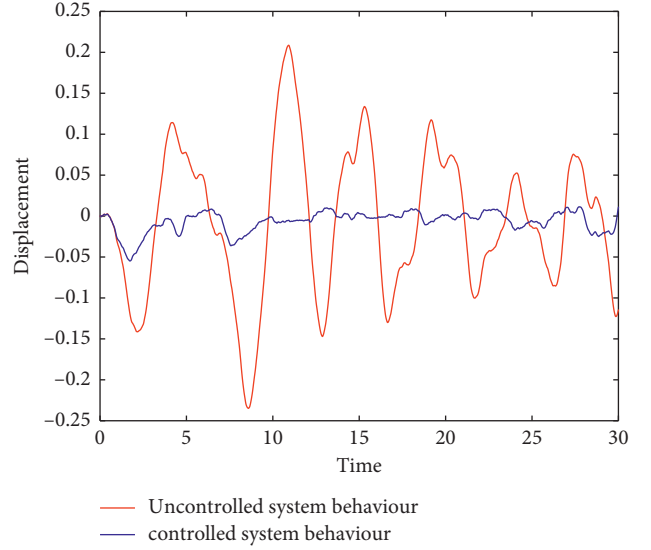


FIGURE 2: The resulting horizontal displacement for 11th story controlled and uncontrolled cases.

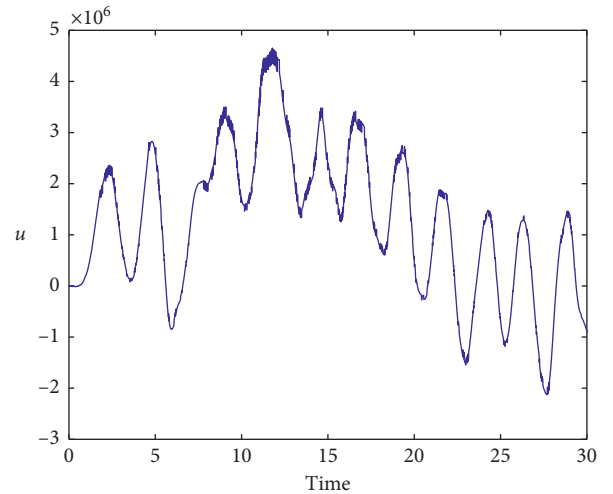


FIGURE 3: Variation of control parameter u for Figure 2.

nonzero points, the chattering only causes a decrease or increase in the force magnitude. In our case, as shown, chattering occurs at nonzero points.

To resolve the chattering problem and satisfy the continuity and Lipschitz condition, the term $\tanh(s)/\epsilon$ was used as an approximation of the $\text{sign}(s)$ function for the function

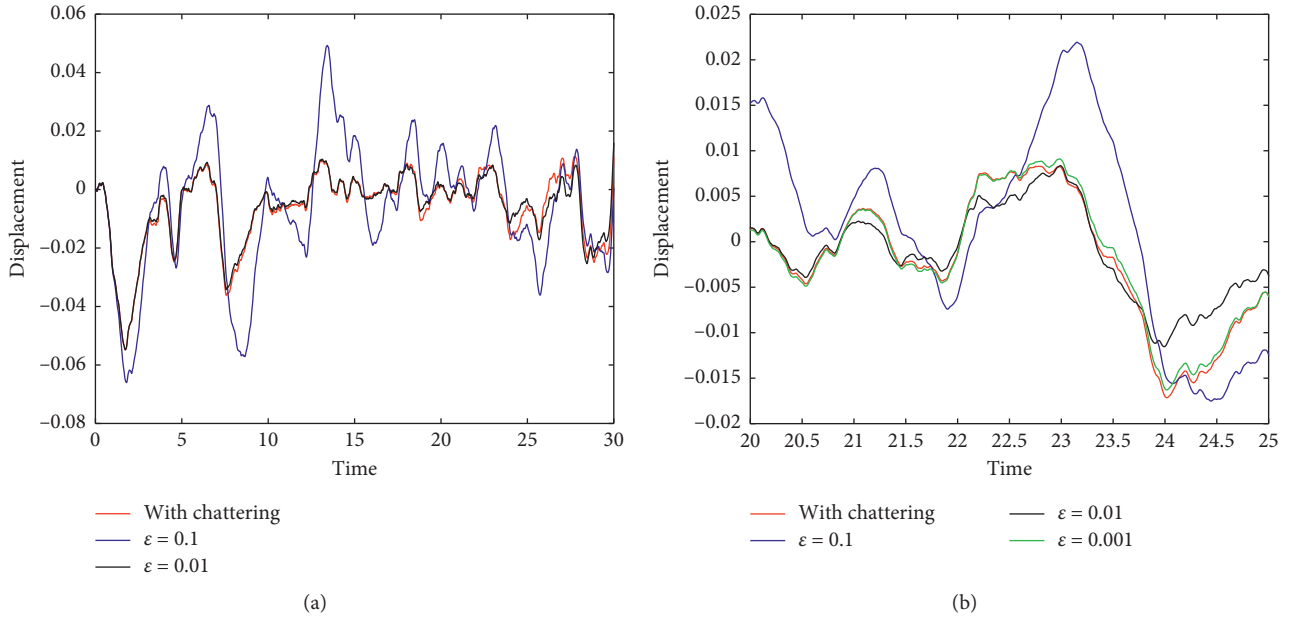


FIGURE 4: (a) Controlled system behavior for different magnitudes of ϵ . (b) Detailed view of Figure 4(a).

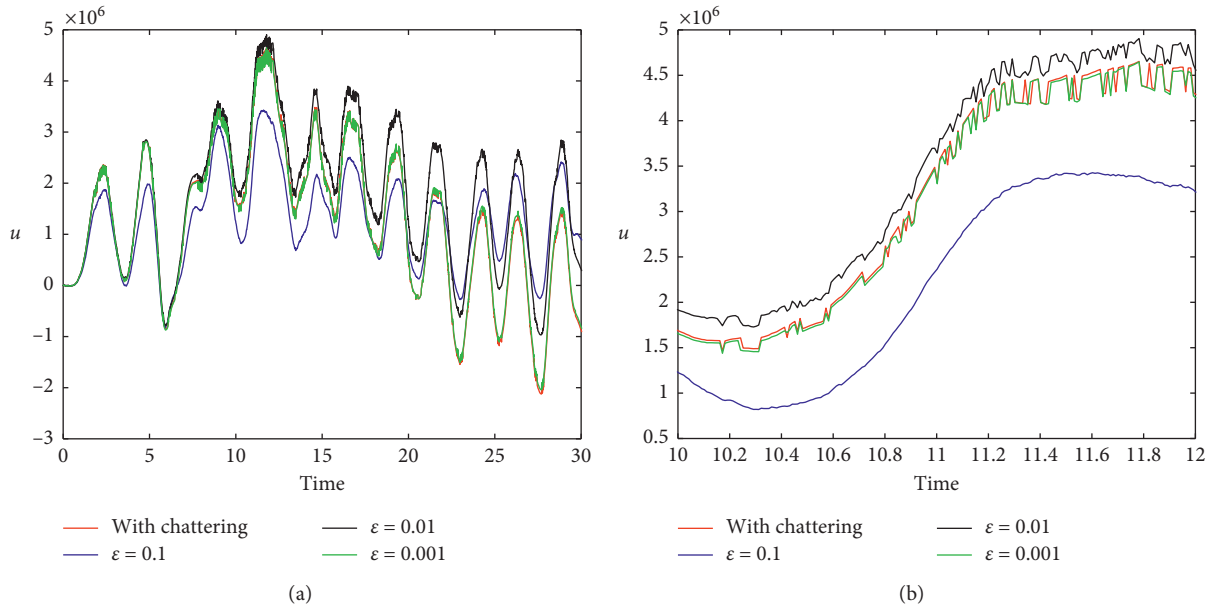


FIGURE 5: (a) The variations of force u corresponding to Figure 4 for different ϵ . (b) Detailed view of Figure 5(a).

$b(x,t)u$, where the continuity and differentiability conditions are satisfied at point $s = 0$. The diagram of horizontal displacements for different ϵ values is demonstrated in Figure 4. As shown, the displacement amplitude is increased by increasing ϵ . However, this increase is negligible compared to the displacement of the uncontrolled system.

The variations of force u corresponding to Figure 4 for different ϵ values are shown in Figure 5. As indicated, the amplitude of force u at $\epsilon = 0.1$ is smaller compared to other ϵ values. Moreover, the chattering phenomenon is also fully resolved in this case, while it is still observed at other cases, for example, $\epsilon = 0.001$. As shown in Figures 4 and 5, the

vibrational amplitudes for both $\text{sign}(s)$ and $\tanh(s/0.001)$ functions are consistent, which is due to the accurate approximation of the $\text{sign}(s)$ function by $\tanh(s/0.001)$.

Moreover, the phase diagram for the 11th story is also demonstrated in Figure 6 for different cases. As shown, by increasing ϵ , the region of attraction is also extended. This region was almost similar for both $\text{sign}(s)$ and $\tanh(s/0.001)$ functions.

The effect of $h(x,t)$ on the dynamic behavior of the structure and the region of attraction is discussed in this part. The vibrational amplitude of the uncontrolled system for different $h(x,t)$ values is shown in Figure 7. As

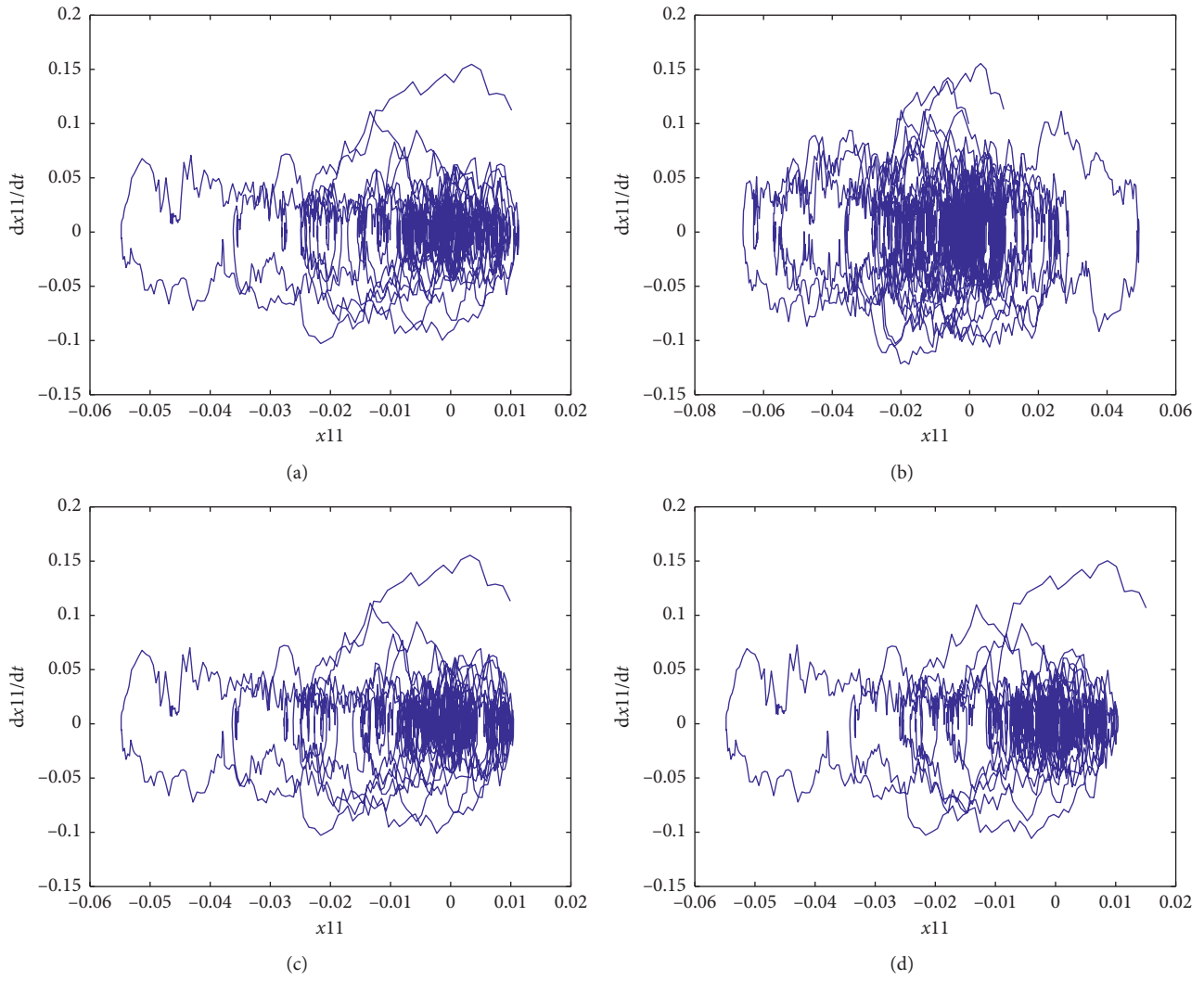


FIGURE 6: Phase portrait of horizontal displacement of 11th story considering functions $\text{sign}(s)$ and $\tanh(s/\varepsilon)$. (a) $\text{sign}(s)$. (b) $\varepsilon = 0.1$. (c) $\varepsilon = 0.01$. (d) $\varepsilon = 0.001$.

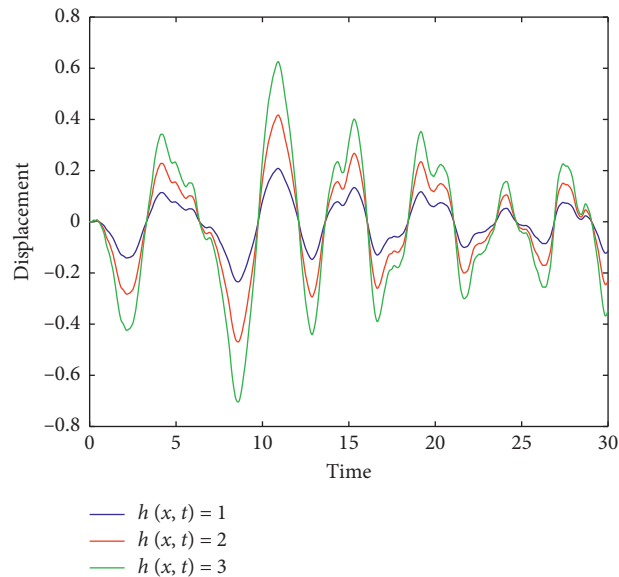


FIGURE 7: Vibrational behavior of 11th story in the passive mode and for different magnitudes of $h(x, t)$.

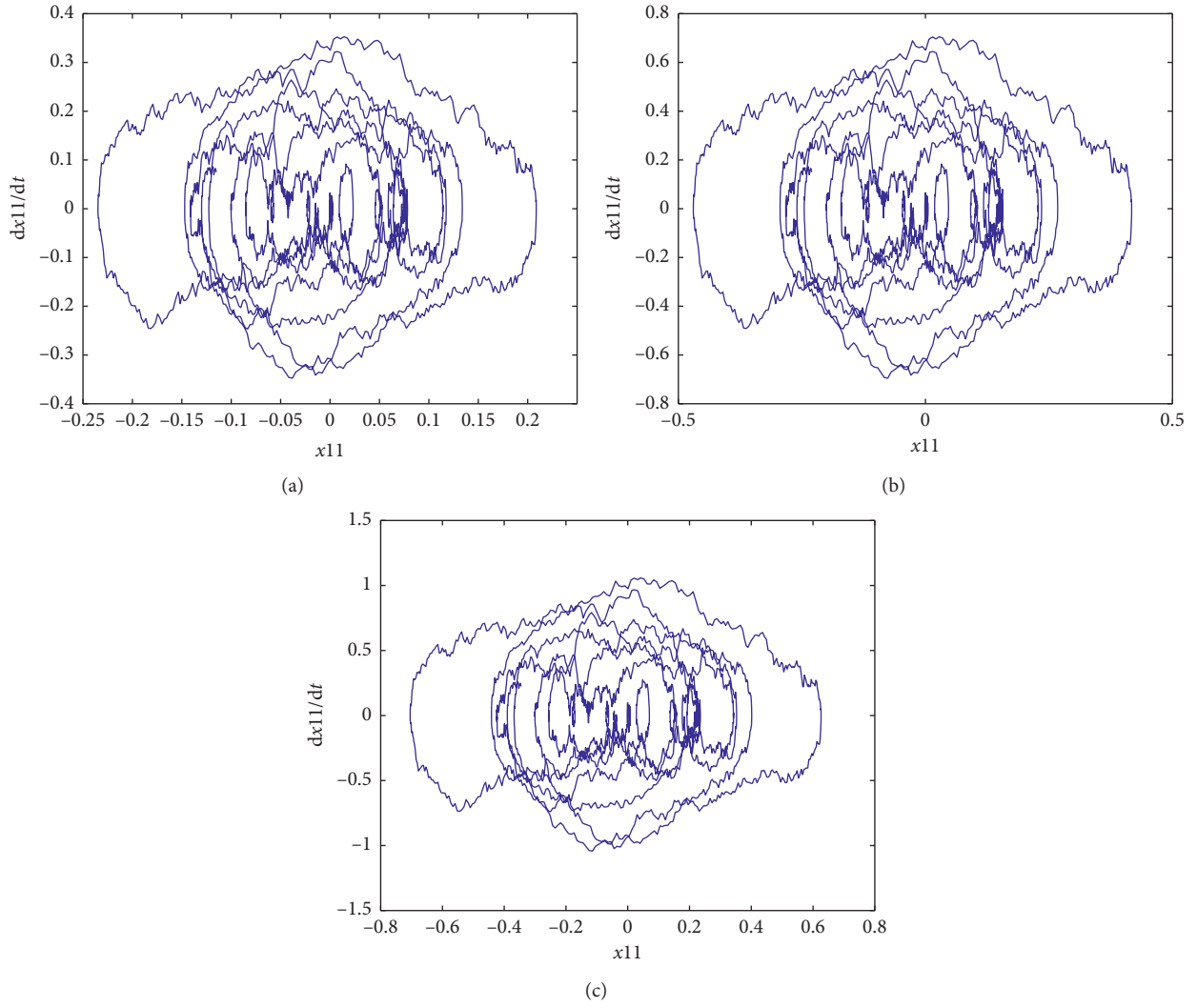


FIGURE 8: Phase portrait of horizontal displacement of 11th story for passive case and different values of $h(x,t)$. (a) $h(x,t) = 1$. (b) $h(x,t) = 2$. (c) $h(x,t) = 3$.

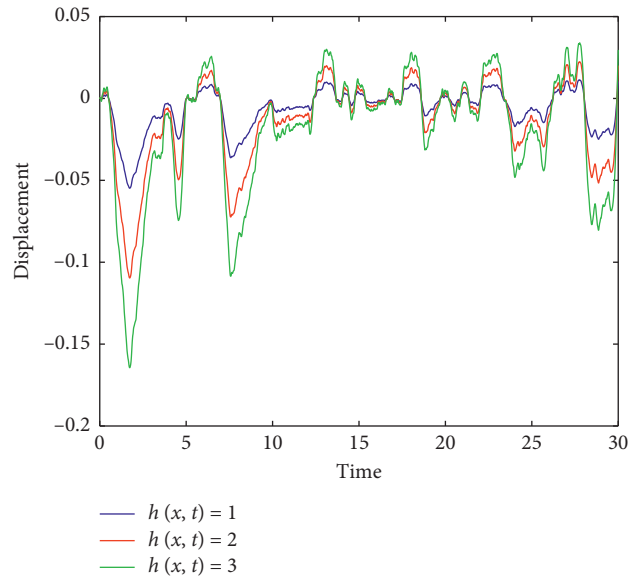


FIGURE 9: The horizontal displacement of 11th story for the controlled case and for different values of $h(x,t)$.

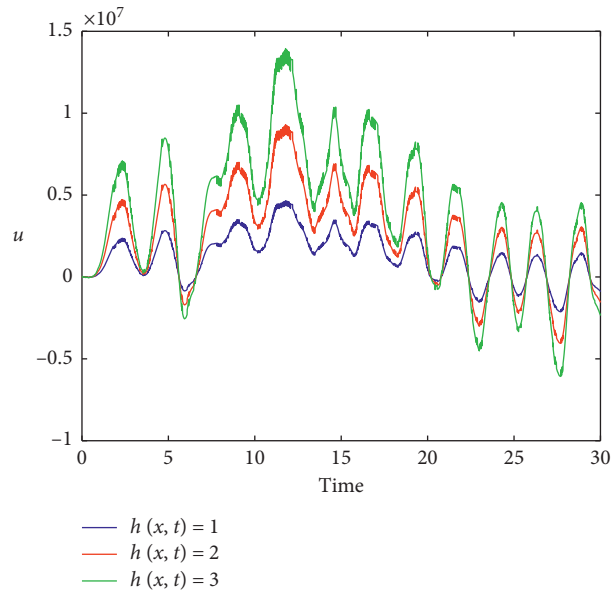


FIGURE 10: The force variations corresponding to Figure 9.

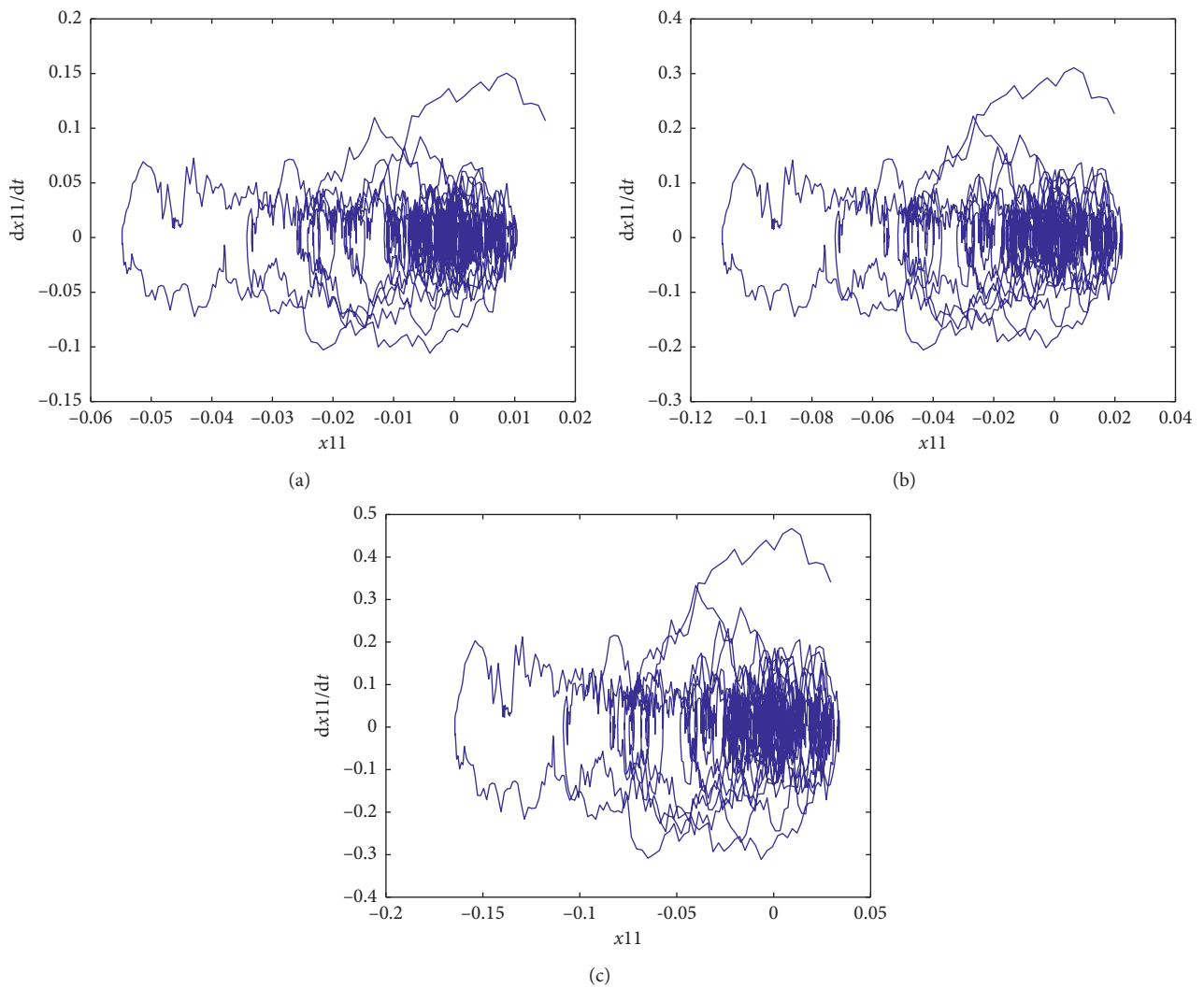


FIGURE 11: Phase portrait of 11th story for the controlled case and different $h(x, t)$. (a) $h(x, t) = 1$. (b) $h(x, t) = 2$. (c) $h(x, t) = 3$.

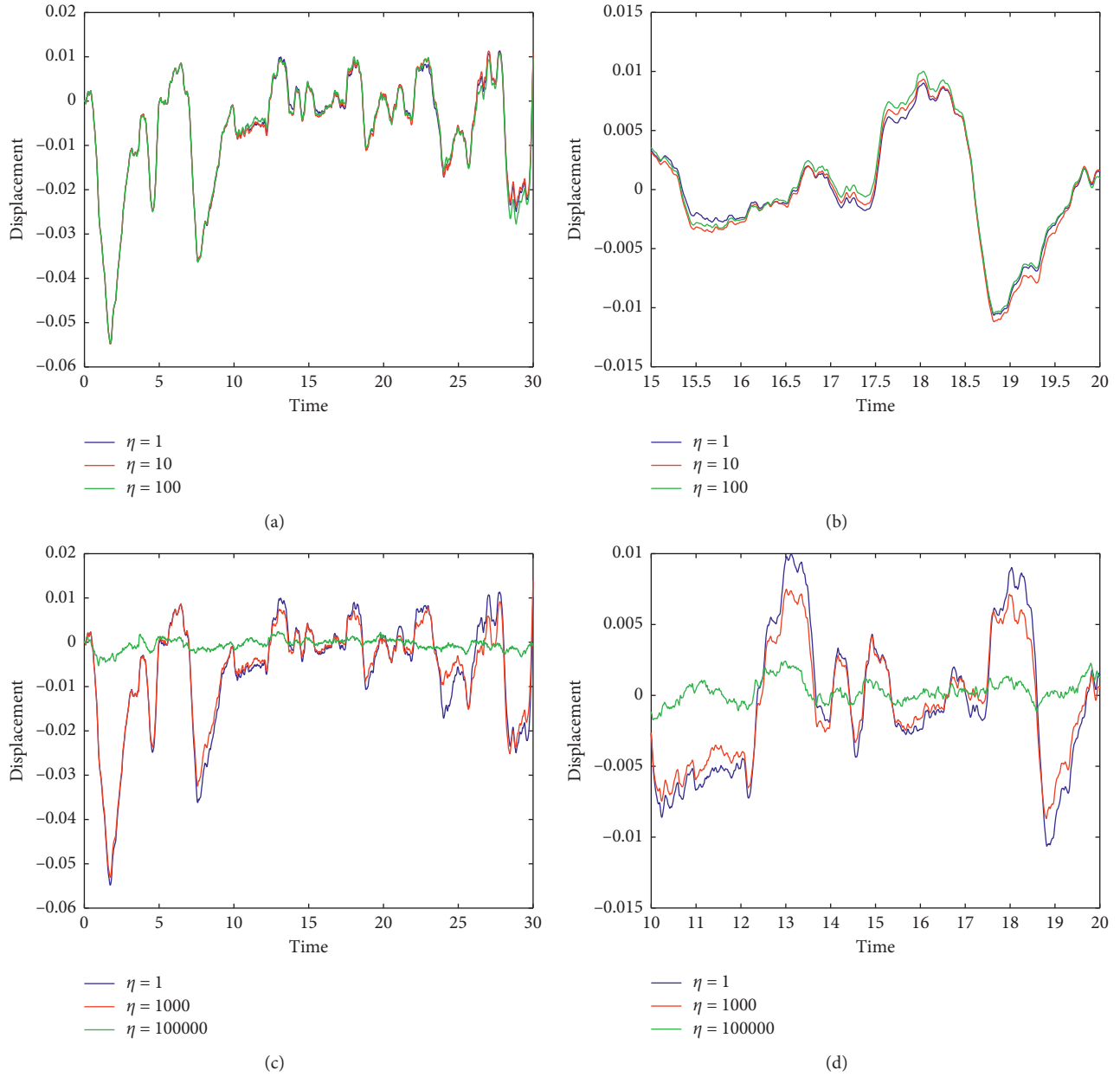


FIGURE 12: The variations in horizontal displacement for different values of η and $\lambda = 1$. (a) The variations in horizontal displacement for $\eta = 1$, $\eta = 10$, and $\eta = 100$ and $\lambda = 1$. (b) Detailed view of Figure 12(a). (c) The variations in horizontal displacement for $\eta = 1$, $\eta = 1000$, and $\eta = 100000$ and $\lambda = 1$. (d) Detailed view of Figure 12(c).

demonstrated, the displacement amplitude is linearly increased by increasing $h(x, t)$.

Also, the attraction domain for the mentioned figure is presented in Figure 8. As is clear from this figure, the domain of attraction set is extended with increasing $h(x, t)$.

The horizontal displacement for the controlled case is demonstrated in Figure 9 with respect to different $h(x, t)$ values. As shown, by increasing $h(x, t)$, the vibrational amplitude is also increased, but its value is substantially smaller compared to the uncontrolled case. The force variations corresponding to Figure 9 is demonstrated in the

diagram of Figure 10. As shown, the amplitude of force variations also experiences an increase as $h(x, t)$ increases.

Moreover, the region of attraction corresponding to Figure 9 is demonstrated in Figure 11. As shown, similar to the uncontrolled case, the region of attraction increases by increasing $h(x, t)$.

The effects of η and λ on the behavior of a controlled system is discussed in this section. The variations in horizontal displacement of the system are demonstrated in Figure 12 for different η values. As shown, for η values lower than 1000, increasing the η values is not significantly effective, but increasing this parameter to 100,000 causes the

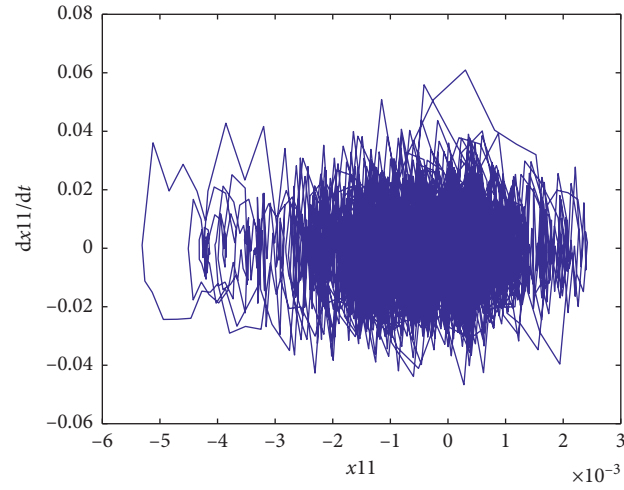


FIGURE 13: Phase portrait and basin of the attraction set for the active case with $\eta = 100000$ and $\lambda = 1$.

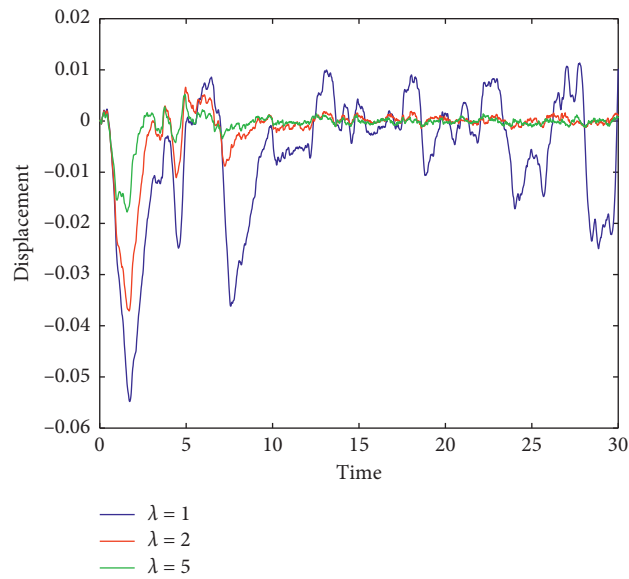


FIGURE 14: The horizontal displacement amplitude of the active system for different λ values and $\eta = 1$.

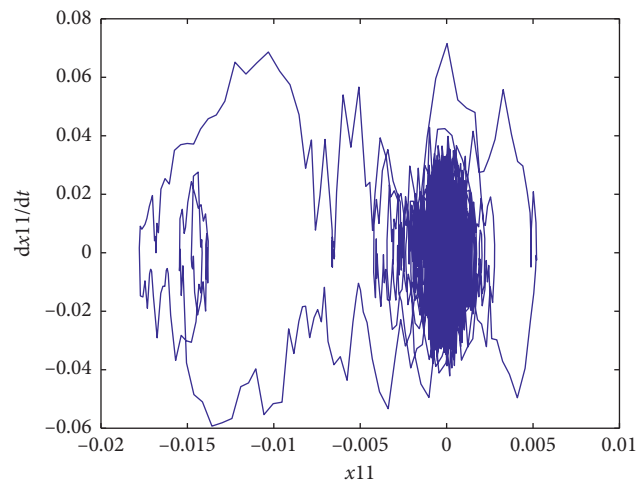


FIGURE 15: The phase portrait of 11th story for the active system considering $\eta = 1$ and $\lambda = 5$.

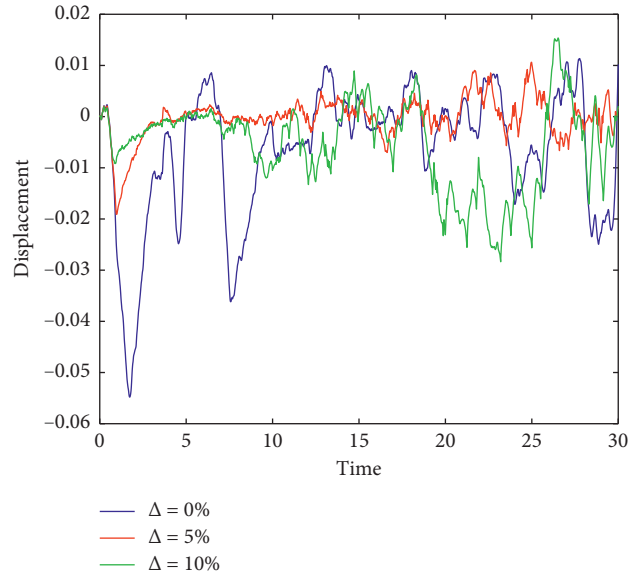


FIGURE 16: The variations of horizontal displacement of 11th story for the active system and different values of Δ .

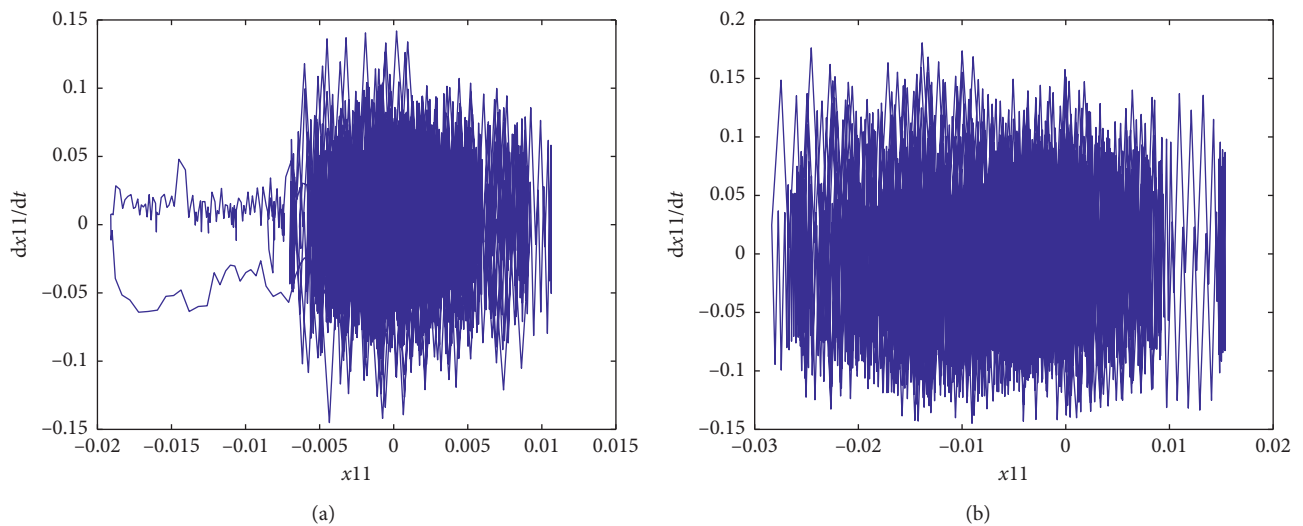


FIGURE 17: The region of the attraction set for Figure 16 and considering different values of $\Delta = 5\%$ and $\Delta = 10\%$. (a) The region of the attraction set for $\Delta = 5\%$. (b) The region of the attraction set for $\Delta = 10\%$.

horizontal displacement of the system to increase substantially.

Additionally, the region of attraction for an η value of 100,000 is shown in Figure 13. As shown, the region of attraction is considerably expanded at this η value.

The displacement amplitude of the system for different λ values and a fixed η value of 1 is demonstrated in Figure 14. As shown, the displacement amplitude is substantially decreased by increasing lambda. The region of attraction for a λ value of 5 is shown in Figure 15. Consider this figure suggests that the region of attraction becomes more limited for a lambda value of 5.

This section discusses the controller robustness to system uncertainty. In the first scenario, only the system uncertainties were considered and the actuator

uncertainties were neglected. The variations of horizontal displacement for different Δ values are demonstrated in Figure 16. As shown, the controller is highly robust to uncertainties and even within some time intervals, and the horizontal displacement of the system is decreased by increasing Δ .

This is due to the fact that $F(x, t)$ is also increased by increasing Δ . However, as expressed in equation (22), presence of $F(x, t)$ in this equation virtually increases the term $\psi(x, t) + \eta$, and as shown in Figure 12, increasing η increases the controller robustness. The regions of attraction for $\Delta = 5\%$ and $\Delta = 10\%$ are plotted in Figure 17. As shown, despite its larger extent for $\Delta = 10\%$ compared to $\Delta = 5\%$, the region of attraction has become more compact.

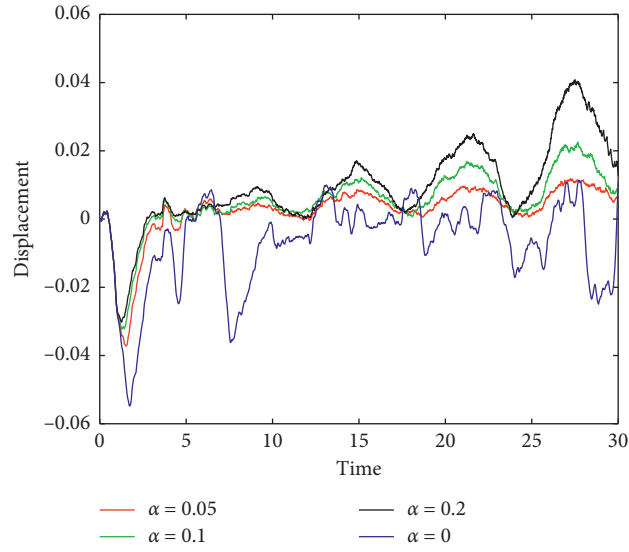


FIGURE 18: The horizontal displacement of 11th story for the active system considering uncertainty with $\Delta = 1\%$ and different values of α .

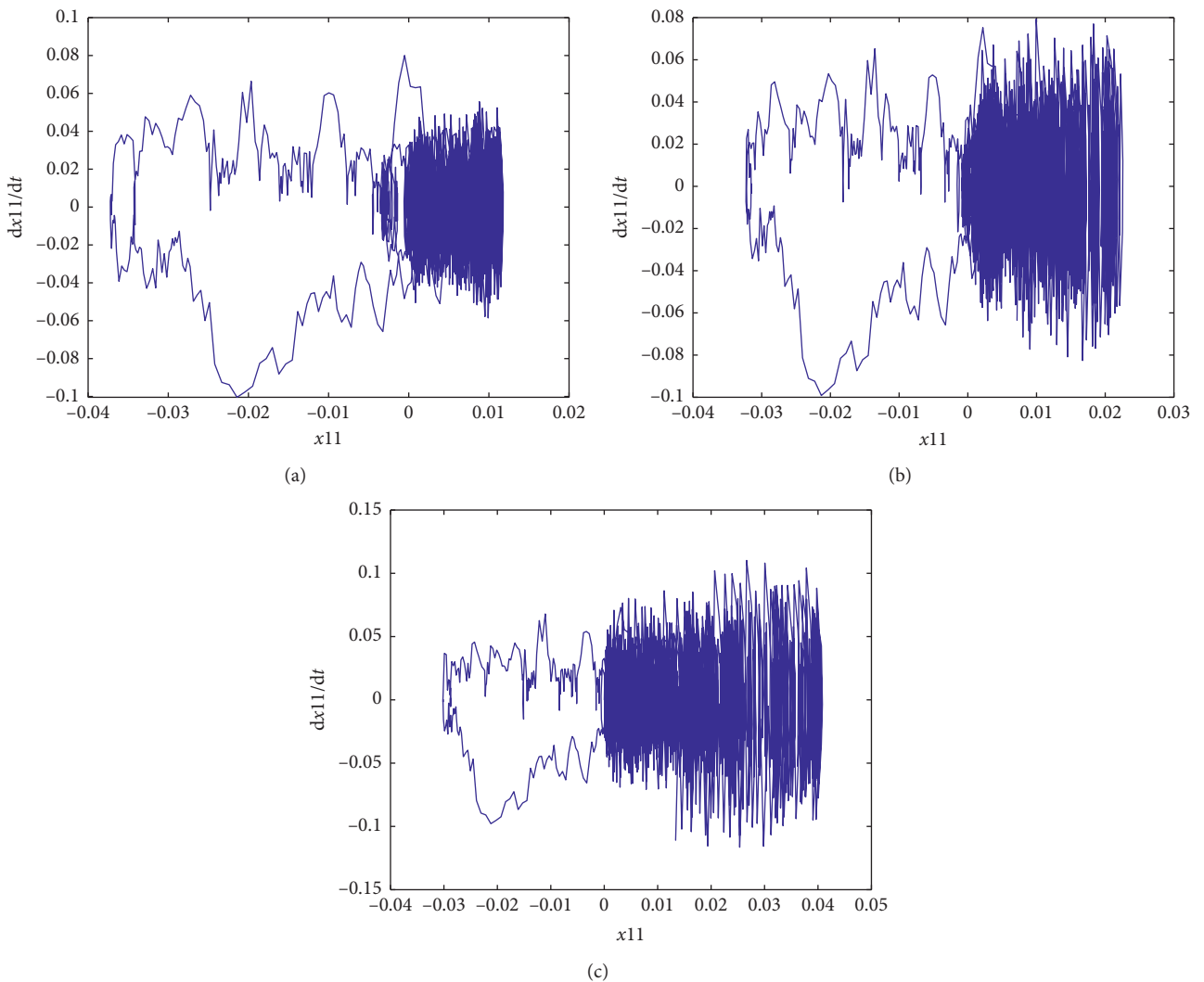


FIGURE 19: Related phase portrait to Figure 18. (a) $\alpha = 0.05$. (b) $\alpha = 0.1$. (c) $\alpha = 0.2$.

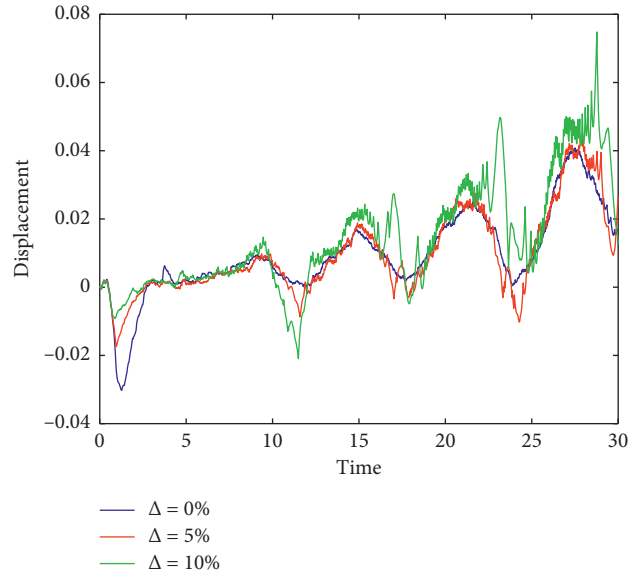


FIGURE 20: The horizontal displacement of 11th story for the active system considering uncertainty with $\alpha = 0.2$ and different values of Δ . (a) $\Delta = 5\%$. (b) $\Delta = 10\%$.

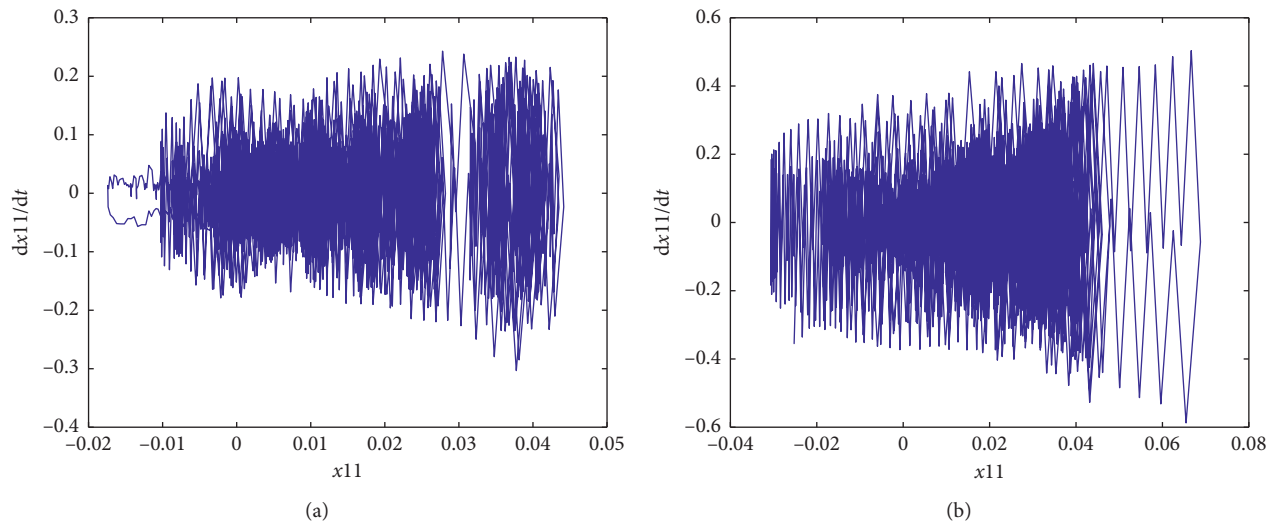


FIGURE 21: Related phase portrait of Figure 20.

The results for the case with actuator uncertainty and $\Delta = 10\%$ were extracted and presented in Figure 18. In this case, $b(x, t) = 1 + \alpha \sin t$. The results for different α values are shown in this figure, which indicates the significant controller robustness in presence of actuator uncertainty.

The region of attraction in this case is depicted in Figure 19. As shown, the extent of region of attraction is increased by increasing α .

The results in presence of actuator and system uncertainties are shown in Figure 20. In this case, α is set to be 0.2. As shown, the controller exhibits a high robustness in presence of actuator and system uncertainties. The region of attraction for this case is demonstrated in Figure 21. As shown, the extent of region of attraction is increased by increasing Δ .

5. Conclusion

This study has examined the dynamic behavior of an 11-story building equipped with an ATMD system. The stimulation force has been applied on the structure in the form of a Wiener process and an earthquake. The sliding mode scheme has been used to control the ATMD system. So, considering Lipschitz nonlinearity and based on the Ito formulation, a sliding mode controller in the presence of the uncertainty for the general dynamical system with the second-order governing stochastic differential equation has been designed.

The designed controller has been further developed to control the ATMD system. The dynamic behaviors of the

structure in the active and passive modes have been simulated. The presented results demonstrate the high ability of the sliding mode controller to reduce unwanted vibrations of buildings under stimulation of the ground. Also, the results show that the designed controller has a good robustness in the presence of structural and actuator uncertainties. In addition, the effects of the controller parameters on system behavior have been studied. The results show that reduction of ε and increase of η reduce the structural vibration amplitude.

Data Availability

No data were used to support this study.

Conflicts of Interest

The author declares that there are no conflicts of interest.

Acknowledgments

This work was supported by The Research Council of Oman with Grant no. ORG/CBS/14/008.

References

- [1] D. Lambertson and B. Lapeyre, *Introduction to Stochastic Calculus Applied to Finance*, Chapman and Hall/CRC, Boca Raton, FL, USA, 2011.
- [2] J. M. Steele, *Stochastic Calculus and Financial Applications*, vol. 45, Springer Science & Business Media, Berlin, Germany, 2012.
- [3] R. Carmona, *Lectures on BSDEs, Stochastic Control, and Stochastic Differential Games with Financial Applications*, vol. 1, SIAM, Philadelphia, PA, USA, 2016.
- [4] B. Remillard, *Statistical Methods for Financial Engineering*, Chapman and Hall/CRC, Boca Raton, FL, USA, 2016.
- [5] M. Di Somma, G. Graditi, E. Heydarian-Forushani, M. Shafiekhah, and P. Siano, "Stochastic optimal scheduling of distributed energy resources with renewables considering economic and environmental aspects," *Renewable Energy*, vol. 116, pp. 272–287, 2018.
- [6] X. Zhao, T. R. Brown, and W. E. Tyner, "Stochastic techno-economic evaluation of cellulosic biofuel pathways," *Bioresource Technology*, vol. 198, pp. 755–763, 2015.
- [7] S. Liu, P. X. Liu, and X. Wang, "Stochastic small-signal stability analysis of grid-connected photovoltaic systems," *IEEE Transactions on Industrial Electronics*, vol. 63, no. 2, pp. 1027–1038, 2015.
- [8] N. Onizawa, D. Katagiri, K. Matsumiya, W. J. Gross, and T. Hanyu, "Gabor filter based on stochastic computation," *IEEE Signal Processing Letters*, vol. 22, no. 9, pp. 1224–1228, 2015.
- [9] P. Pfeffer, F. Hartmann, S. Höfling, M. Kamp, and L. Worschech, "Logical stochastic resonance with a coulomb-coupled quantum-dot rectifier," *Physical Review Applied*, vol. 4, no. 1, Article ID 014011, 2015.
- [10] M. Talha and B. N. Singh, "Stochastic vibration characteristics of finite element modelled functionally gradient plates," *Composite Structures*, vol. 130, pp. 95–106, 2015.
- [11] S. Dey, T. Mukhopadhyay, and S. Adhikari, "Stochastic free vibration analyses of composite shallow doubly curved shells—A Kriging model approach," *Composites Part B: Engineering*, vol. 70, pp. 99–112, 2015.
- [12] C. Vagg, S. Akehurst, C. J. Brace, and L. Ash, "Stochastic dynamic programming in the real-world control of hybrid electric vehicles," *IEEE Transactions on Control Systems Technology*, vol. 24, no. 3, pp. 853–866, 2015.
- [13] J. C. Goodson, B. W. Thomas, and J. W. Ohlmann, "A rollout algorithm framework for heuristic solutions to finite-horizon stochastic dynamic programs," *European Journal of Operational Research*, vol. 258, no. 1, pp. 216–229, 2017.
- [14] W. Chai, A. Naess, and B. J. Leira, "Stochastic dynamic analysis and reliability of a vessel rolling in random beam seas," *Journal of Ship Research*, vol. 59, no. 2, pp. 113–131, 2015.
- [15] A. Azizi, "Computer-based analysis of the stochastic stability of mechanical structures driven by white and colored noise," *Sustainability*, vol. 10, no. 10, p. 3419, 2018.
- [16] A. Azizi and P. G. Yazdi, "Introduction to noise and its applications," in *Computer-Based Analysis of the Stochastic Stability of Mechanical Structures Driven by White and Colored Noise*, Springer, Berlin, Germany, 2019.
- [17] A. Azizi and P. G. Yazdi, "Noise control techniques," in *Computer-Based Analysis of the Stochastic Stability of Mechanical Structures Driven by White and Colored Noise*, Springer, Berlin, Germany, 2019.
- [18] A. Azizi and P. G. Yazdi, "Mechanical structures: mathematical modeling," in *Computer-Based Analysis of the Stochastic Stability of Mechanical Structures Driven by White and Colored Noise*, Springer, Berlin, Germany, 2019.
- [19] A. Azizi and P. G. Yazdi, "White noise: applications and mathematical modeling," in *Computer-Based Analysis of the Stochastic Stability of Mechanical Structures Driven by White and Colored Noise*, Springer, Berlin, Germany, 2019.
- [20] A. Azizi and P. G. Yazdi, "Modeling and control of the effect of the noise on the mechanical structures," in *Computer-Based Analysis of the Stochastic Stability of Mechanical Structures Driven by White and Colored Noise*, Springer, Berlin, Germany, 2019.
- [21] A. Preciado, A. Orduña, G. Bartoli, and H. Budelmann, "Façade seismic failure simulation of an old cathedral in colima, Mexico by 3D limit analysis and nonlinear finite element method," *Engineering Failure Analysis*, vol. 49, pp. 20–30, 2015.
- [22] B. Sołtysik and R. Jankowski, "Building damage due to structural pounding during earthquakes," *Journal of Physics: Conference Series*, vol. 628, 2015.
- [23] A. Kumar, D. Choudhury, and R. Katzenbach, "Effect of earthquake on combined pile–raft foundation," *International Journal of Geomechanics*, vol. 16, no. 5, Article ID 04016013, 2016.
- [24] K.-S. Park and S.-Y. Ok, "Modal-space reference-model-tracking fuzzy control of earthquake excited structures," *Journal of Sound and Vibration*, vol. 334, pp. 136–150, 2015.
- [25] M. Domaneschi and L. Martinelli, "Earthquake-resilience-based control solutions for the extended benchmark cable-stayed bridge," *Journal of Structural Engineering*, vol. 142, no. 8, Article ID C4015009, 2015.
- [26] R. Mitchell, Y.-J. Cha, Y. Kim, and A. A. Mahajan, "Active control of highway bridges subject to a variety of earthquake loads," *Earthquake Engineering and Engineering Vibration*, vol. 14, no. 2, pp. 253–263, 2015.
- [27] A. Y. Grinberger and D. Felsenstein, *A Tale of Two Earthquakes: Dynamic Agent-Based Simulation of Urban Resilience*, The Hebrew University of Jerusalem, Jerusalem, Israel, 2017.

- [28] F. C. Klebaner, *Introduction to Stochastic Calculus with Applications*, World Scientific Publishing Company, Singapore, 2012.
- [29] M. Jeanblanc, M. Yor, and M. Chesney, *Mathematical Methods for Financial Markets*, Springer Science & Business Media, Berlin, Germany, 2009.
- [30] L. C. G. Rogers and D. Williams, *Diffusions, Markov Processes and Martingales: Volume 2, Itô Calculus*, vol. 2, Cambridge University Press, Cambridge, UK, 2000.
- [31] G.-P. Cai, J.-Z. Huang, F. Sun, and C. Wang, “Modified sliding-mode bang-bang control for seismically excited linear structures,” *Earthquake Engineering & Structural Dynamics*, vol. 29, no. 11, pp. 1647–1657, 2000.
- [32] B. Oksendal, *Stochastic Differential Equations: An Introduction with Applications*, Springer Science & Business Media, Berlin, Germany, 2013.
- [33] H. Salarieh and A. Alasty, “Control of stochastic chaos using sliding mode method,” *Journal of Computational and Applied Mathematics*, vol. 225, no. 1, pp. 135–145, 2009.
- [34] W. S. Levine, *The Control Systems Handbook: Control System Advanced Methods*, CRC Press, Boca Raton, FL, USA, 2018.

Research Article

Differential Transform Algorithm for Functional Differential Equations with Time-Dependent Delays

Josef Rebenda ^{1,2} and Zuzana Pátíková³

¹CEITEC BUT, Brno University of Technology, Purkyňova 656/123, 61200 Brno, Czech Republic

²Department of Mathematics, Faculty of Electrical Engineering and Communication, Brno University of Technology, Technická 8, 616 00 Brno, Czech Republic

³Department of Mathematics, Faculty of Applied Informatics, Tomas Bata University in Zlín, Nad Stráněmi 4511, Zlín 76005, Czech Republic

Correspondence should be addressed to Josef Rebenda; josef.rebenda@ceitec.vutbr.cz

Received 23 August 2019; Accepted 31 December 2019; Published 28 February 2020

Guest Editor: Robert Hakl

Copyright © 2020 Josef Rebenda and Zuzana Pátíková. This is an open access article distributed under the Creative Commons Attribution License, which permits unrestricted use, distribution, and reproduction in any medium, provided the original work is properly cited.

An algorithm using the differential transformation which is convenient for finding numerical solutions to initial value problems for functional differential equations is proposed in this paper. We focus on retarded equations with delays which in general are functions of the independent variable. The delayed differential equation is turned into an ordinary differential equation using the method of steps. The ordinary differential equation is transformed into a recurrence relation in one variable using the differential transformation. Approximate solution has the form of a Taylor polynomial whose coefficients are determined by solving the recurrence relation. Practical implementation of the presented algorithm is demonstrated in an example of the initial value problem for a differential equation with nonlinear nonconstant delay. A two-dimensional neutral system of higher complexity with constant, nonconstant, and proportional delays has been chosen to show numerical performance of the algorithm. Results are compared against Matlab function DDENS.

1. Introduction

Functional differential equations (FDEs) are used to model processes and phenomena which depend on past values of the modelled entities. Indicatively, we mention models describing machine tool vibrations [1], predator-prey type models [2], and models used in economics [3]. Further models and details can be found for instance in [4, 5] or [6].

Differential transformation (DT), a semianalytical approach based on Taylor's theorem, has been proved to be efficient in solving a variety of initial value problems (IVPs), ranging from ordinary to functional, partial, and fractional differential equations [7–11]. However, there is no publication about systematic application of DT to IVP for

differential equations with nonconstant delays which are functions of the independent variable.

In this paper, we present an extension of DT to a class of IVPs for delayed differential equations with analytic right-hand side. Albeit the analyticity assumption seems to be quite restrictive, it is reasonable to develop theory for such class of equations [12, 13].

The paper is organised as follows. In Section 2, we define the subject of our study and briefly describe the methods we combine to solve the studied problem, including recalling necessary results of previous studies. Section 3 contains the main results of the paper, including algorithm description, new theorems, examples, and comparison of numerical results. In Section 4, we briefly summarise what has been done in the paper.

2. Methods

2.1. Problem Statement. The problem studied in this paper is to find a solution on a given finite interval $[t_0, T] \subset [0, \infty)$ to an IVP for the following system of p functional differential equations of n -th order with multiple delays $\alpha_1(t), \dots, \alpha_r(t)$:

$$\mathbf{u}^{(n)}(t) = \mathbf{f}(t, \mathbf{u}(t), \mathbf{u}'(t), \dots, \mathbf{u}^{(n-1)}(t), \mathbf{u}_1(\alpha_1(t)), \dots, \mathbf{u}_r(\alpha_r(t))), \quad (1)$$

where $\mathbf{u}^{(n)}(t) = (u_1^{(n)}(t), \dots, u_p^{(n)}(t))^T$, $\mathbf{u}^{(k)}(t) = (u_1^{(k)}(t), \dots, u_p^{(k)}(t))$, $k = 0, 1, \dots, n-1$, and $\mathbf{f} = (f_1, \dots, f_p)^T$ are p -dimensional vector functions, $\mathbf{u}_i(\alpha_i(t)) = (\mathbf{u}(\alpha_i(t)), \mathbf{u}'(\alpha_i(t)), \dots, \mathbf{u}^{(m_i)}(\alpha_i(t)))$ are $(m_i \cdot p)$ -dimensional vector functions, $m_i \leq n$, $i = 1, 2, \dots, r$, $r \in \mathbb{N}$, and $f_j: [t_0, T]$ are real functions for $j = 1, 2, \dots, p$, where $\omega = \sum_{i=1}^r m_i$.

We assume that each $\alpha_i(t) = t - \tau_i(t)$, where $\tau_i(t) \geq \tau_{i0} > 0$ for $t \in [t_0, T]$, $i = 1, 2, \dots, r$, is in general a real function, that is, a time-dependent or time-varying delay. Constant and proportional delays are considered as special cases. In case that some α_i is a proportional delay, we do not require the condition $\tau_i(t) \geq \tau_{i0} > 0$ to be valid at 0 if $t_0 = 0$.

Let $t^* = \min_{1 \leq i \leq r} \{\inf_{t \in [t_0, T]} (\alpha_i(t))\}$ and $m = \max\{m_1, m_2, \dots, m_r\}$; hence, $t^* \leq t_0$ and $m \leq n$. If $m < n$, we have a retarded system (1); otherwise, if $m = n$, we call the system neutral. Furthermore, if $t^* < 0$, initial vector function $\Phi(t) = (\phi_1(t), \dots, \phi_p(t))^T$ must be prescribed on the interval $[t^*, t_0]$.

DT algorithm for the case $t^* = t_0 = 0$ with all delays being proportional is described in [14]. DT algorithm for the case $t^* < t_0$ when all delays are constant is introduced in [15]. In this paper, we develop the algorithm for the case $t^* < t_0$ when at least one delay is nonconstant.

To have a complete IVP, we consider system (1) together with initial conditions:

$$\begin{aligned} \mathbf{u}(t_0) &= \mathbf{v}_0, \\ \mathbf{u}'(t_0) &= \mathbf{v}_1, \dots, \mathbf{u}^{(n-1)}(t_0) = \mathbf{v}_{n-1}, \end{aligned} \quad (2)$$

and, since $t^* < t_0$, also subject to initial vector function $\Phi(t)$ on interval $[t^*, t_0]$ such that

$$\Phi(t_0) = \mathbf{u}(t_0), \dots, \Phi^{(n-1)}(t_0) = \mathbf{u}^{(n-1)}(t_0). \quad (3)$$

We consider the IVPs (1)–(3) under the following hypotheses:

(H1) We assume that all the functions $\phi_j(t)$, $j = 1, \dots, p$, are analytic in $[t^*, t_0]$, the functions $\alpha_i(t)$, $i = 1, \dots, r$, are analytic in $[t_0, T]$ and the functions f_j , $j = 1, \dots, p$, are analytic in an open set containing $[t_0, T] \times [\mathbf{u}(t_0), \mathbf{u}(T)] \times \dots \times [\mathbf{u}_r(\alpha_r(t_0)), \mathbf{u}_r(\alpha_r(T))]$.

(H2) If $\alpha_i(t) = q_i t$ and $m_i = n$ in f_j for some $i \in \{1, \dots, r\}$ and $j \in \{1, \dots, p\}$, that is, j th equation is neutral with respect to the proportional delay α_i , we assume that $u_l^{(n)}(\alpha_i(t)) \equiv 0$ for $l \in \{1, \dots, p\}$, $l \neq j$. This hypothesis is included since if it is not fulfilled, the existence of unique solution of IVP could be violated.

We note that these assumptions imply that the IVP (1)–(3) has a unique solution in the interval $[t_0, T]$.

2.2. Method of Steps. The basic idea of our approach is to combine DT and the general method of steps. The method of steps enables us to replace the terms including delays with initial vector function $\Phi(t)$ and its derivatives. Then, the original IVP for the delayed or neutral system of differential equations is turned into IVP for a system of ordinary differential equations.

For the sake of clarity, we include a simple explanatory example. Suppose that we have a system with three delays, one of each type considered: $\alpha_1(t) = t - \tau_1(t)$, $\alpha_2(t) = t - \tau_2$, and $\alpha_3(t) = q_3 t$. We have to distinguish two cases:

- (a) If $t_0 = 0$, applying the method of steps turns system (1) into

$$\begin{aligned} \mathbf{u}^{(n)}(t) &= \mathbf{f}(t, \mathbf{u}(t), \dots, \mathbf{u}^{(n-1)}(t), \\ &\quad \Phi_1(t - \tau_1(t)), \Phi_2(t - \tau_2), \mathbf{u}_3(q_3 t)), \end{aligned} \quad (4)$$

while

- (b) If $t_0 > 0$, system (1) is simplified to

$$\begin{aligned} \mathbf{u}^{(n)}(t) &= \mathbf{f}(t, \mathbf{u}(t), \dots, \mathbf{u}^{(n-1)}(t), \\ &\quad \Phi_1(t - \tau_1(t)), \Phi_2(t - \tau_2), \Phi_3(q_3 t)), \end{aligned} \quad (5)$$

where

$$\begin{aligned} \Phi_1(t - \tau_1(t)) &= \left(\Phi(t - \tau_1(t)), \Phi'(t - \tau_1(t)), \dots, \right. \\ &\quad \left. \Phi^{(m_1)}(t - \tau_1(t)) \right), \\ \Phi_2(t - \tau_2) &= \left(\Phi(t - \tau_2), \Phi'(t - \tau_2), \dots, \Phi^{(m_2)}(t - \tau_2) \right), \\ \mathbf{u}_3(q_3 t) &= \left(\mathbf{u}(q_3 t), \mathbf{u}'(q_3 t), \dots, \mathbf{u}^{(m_3)}(q_3 t) \right), \\ \Phi_3(q_3 t) &= \left(\Phi(q_3 t), \Phi'(q_3 t), \dots, \Phi^{(m_3)}(q_3 t) \right), \end{aligned} \quad (6)$$

and $m_l \leq n$ for $l = 1, 2, 3, 4$. More details on the general method of steps can be found, for instance, in monographs [4] or [6].

Continuation of the method of steps algorithm for equations with constant delays τ_1, \dots, τ_r is described in [15]. Briefly summarised, the interval $[t_0, T]$ is divided into subintervals $I_l = [t_{l-1}, t_l]$, $l = 1, \dots, K$, where $t_K = T$ and t_l , $l = 1, \dots, K-1$, are the principal discontinuity points which is the set of points $t_{\rho, \sigma}$, such that $t_{0,1} = t_0$ and for $\rho, \sigma \geq 1$, $t_{\rho, \sigma}$ are the minimal roots with odd multiplicity of r equations:

$$t_{\rho, (\sigma-1)r+\mu} - \tau_\mu = t_{\rho-1, \sigma}, \quad \mu = 1, \dots, r. \quad (7)$$

If nonconstant nonproportional delays α_i appear in system (1), the principal set of discontinuity points is defined as follows:

Definition 1. The principal discontinuity points for the solutions of system (1) are given by the set of points $t_{\rho,\sigma}$, such that $t_{0,1} = t_0$ and for $\rho, \sigma \geq 1$, $t_{\rho,\sigma}$ are the minimal roots with odd multiplicity of r equations:

$$\alpha_\mu(t_{\rho,(\sigma-1)r+\mu}) = t_{\rho-1,\sigma} \quad \mu = 1, \dots, r. \quad (8)$$

Similar to the case of constant delays, we break the interval $[t_0, T]$ into subintervals $I_l = [t_{l-1}, t_l]$, $l = 1, \dots, K$. We start with the mesh grid $\{t_0, \dots, t_K\}$ formed by the principal discontinuity points calculated using Definition 1. To improve convergence or performance of the algorithm, there is a possibility to refine the mesh grid by inserting other points into it. For more details on the principal discontinuity points and mesh grid, we refer to the monograph [16].

2.3. Differential Transformation

Definition 2. Differential transformation of a real function $u(t)$ at a point $t_0 \in \mathbb{R}$ is $\mathcal{D}\{u(t)\}[t_0] = \{U(k)[t_0]\}_{k=0}^\infty$, where $U(k)[t_0]$, k -th component of the differential transformation of the function $u(t)$ at t_0 , $k \in \mathbb{N}_0$, is defined as

$$U(k)[t_0] = \frac{1}{k!} \left[\frac{d^k u(t)}{dt^k} \right]_{t=t_0}, \quad (9)$$

provided that the original function $u(t)$ is analytic in a neighbourhood of t_0 .

Definition 3. Inverse differential transformation of $\{U(k)[t_0]\}_{k=0}^\infty$ is defined as

$$u(t) = \mathcal{D}^{-1}\{\{U(k)[t_0]\}_{k=0}^\infty\}[t_0] = \sum_{k=0}^\infty U(k)[t_0] (t - t_0)^k. \quad (10)$$

In applications, the function $u(t)$ is expressed by a finite sum

$$u(t) = \sum_{k=0}^N U(k)[t_0] (t - t_0)^k. \quad (11)$$

As we can observe in (10), DT is based on Taylor series; hence, any theorem about convergence of Taylor series may be used. However, we would like to point out the paper [17] where the finest general explicit *a priori* error estimates are given.

The following formulas are listed, e.g., in [18] and will be used in Section 3.3.

Lemma 1. Assume that $F(k)[t_0]$ and $U(k)[t_0]$ are differential transformations of functions $f(t)$ and $u(t)$, respectively.

$$\text{If } f(t) = \frac{d^n u(t)}{dt^n}, \text{ then } F(k)[t_0] = \frac{(k+n)!}{k!} U(k+n)[t_0].$$

$$\text{If } f(t) = t^n, \text{ then } F(k)[0] = \delta(k-n),$$

where $\delta(k-n) = \delta_{kn}$ is the Kronecker delta.

$$\text{If } f(t) = e^{\lambda t}, \text{ then } F(k)[0] = \frac{\lambda^k}{k!}. \quad (12)$$

Remark 1. Similar formulas can be obtained using numerical approach called Functional Analytical Technique based on Operator Theory [19, 20].

The main disadvantage of many papers about DT is that there are almost no examples of equations with non-polynomial nonlinear terms containing unknown function $u(t)$ like, for instance, $f(u) = \sqrt[3]{1+u^3}$ or $f(u) = e^{\sqrt{\sin u}}$. However, DT of components containing nonlinear terms can be obtained in a consistent way using the algorithm described in [21].

Theorem 1. Let g and f be real functions analytic near t_0 and $g(t_0)$, respectively, and let h be the composition $h(t) = (f \circ g)(t) = f(g(t))$. Denote $\mathcal{D}\{g(t)\}[t_0] = \{G(k)\}_{k=0}^\infty$, $\mathcal{D}\{f(t)\}[g(t_0)] = \{F(k)\}_{k=0}^\infty$, and $\mathcal{D}\{(f \circ g)(t)\}[t_0] = \{H(k)\}_{k=0}^\infty$ as the differential transformations of functions g, f , and h at $t_0, g(t_0)$, and t_0 , respectively. Then, the numbers $H(k)$ in the sequence $\{H(k)\}_{k=0}^\infty$ satisfy the relations $H(0) = F(0)$ and

$$H(k) = \sum_{l=1}^k F(l) \cdot \widehat{B}_{k,l}(G(1), \dots, G(k-l+1)), \quad \text{for } k \geq 1, \quad (13)$$

where $\widehat{B}_{k,l}(\widehat{x}_1, \dots, \widehat{x}_{k-l+1})$ are the partial ordinary Bell polynomials.

The following Lemma proved in [21] is useful when calculating partial ordinary Bell polynomials.

Lemma 2. The partial ordinary Bell polynomials $\widehat{B}_{k,l}(\widehat{x}_1, \dots, \widehat{x}_{k-l+1})$, $l = 1, 2, \dots, k \geq l$, satisfy the recurrence relation

$$\widehat{B}_{k,l}(\widehat{x}_1, \dots, \widehat{x}_{k-l+1}) = \sum_{i=1}^{k-l+1} \frac{i \cdot l}{k} \widehat{x}_i \widehat{B}_{k-i,l-1}(\widehat{x}_1, \dots, \widehat{x}_{k-i-l+2}), \quad (14)$$

where $\widehat{B}_{0,0} = 1$ and $\widehat{B}_{k,0} = 0$ for $k \geq 1$.

3. Results and Discussion

3.1. Algorithm Description. Recall system (1)

$$\mathbf{u}^{(n)}(t) = \mathbf{f}(t, \mathbf{u}(t), \mathbf{u}'(t), \dots, \mathbf{u}^{(n-1)}(t), \mathbf{u}_1(\alpha_1(t)), \dots, \mathbf{u}_r(\alpha_r(t))), \quad (15)$$

with initial conditions

$$\mathbf{u}(t_0) = \mathbf{v}_0, \mathbf{u}'(t_0) = \mathbf{v}_1, \dots, \mathbf{u}^{(n-1)}(t_0) = \mathbf{v}_{n-1}, \quad (16)$$

and initial vector function $\Phi(t)$ on interval $[t^*, t_0]$ satisfying

$$\Phi(t_0) = \mathbf{u}(t_0), \dots, \Phi^{(n-1)}(t_0) = \mathbf{u}^{(n-1)}(t_0). \quad (17)$$

Further recall that in Section 2.2, we broke the interval $[t_0, T]$ into subintervals $I_l = [t_{l-1}, t_l]$, $l = 1, \dots, K$. Define $I_0 = [t^*, t_0]$.

Then, we are looking for a solution $\mathbf{u}(t)$ of the IVP (1)–(3) in the form

$$\mathbf{u}(t) = \begin{cases} \mathbf{u}_{I_1}(t), & t \in I_1, \\ \mathbf{u}_{I_2}(t), & t \in I_2, \\ \vdots \\ \mathbf{u}_{I_K}(t), & t \in I_K, \end{cases} \quad (18)$$

where solution \mathbf{u}_{I_j} in the j th interval I_j is obtained in the following way. We solve the following equation:

$$\begin{aligned} \mathbf{u}_{I_j}^{(n)}(t) &= f\left(t, \mathbf{u}_{I_j}(t), \mathbf{u}'_{I_j}(t), \dots, \mathbf{u}_{I_j}^{(n-1)}(t), \right. \\ &\quad \left. \mathbf{u}_{j,1}(\alpha_1(t)), \dots, \mathbf{u}_{j,r}(\alpha_r(t))\right), \end{aligned} \quad (19)$$

where

$$\mathbf{u}_{j,i}(\alpha_i(t)) = \left(\mathbf{u}_{I_l}(\alpha_i(t)), \mathbf{u}'_{I_l}(\alpha_i(t)), \dots, \mathbf{u}_{I_l}^{(m_i)}(\alpha_i(t)) \right), \quad (20)$$

if $\alpha_i(t) \in I_l$, for $t \in I_j$, $l \in \{1, \dots, j\}$, $j \in \{1, \dots, K\}$.

In case that $\alpha_i(t) \in I_0 = [t^*, t_0]$ for $t \in I_j$, then again

$$\mathbf{u}_{j,i}(\alpha_i(t)) = \left(\phi(\alpha_i(t)), \phi'(\alpha_i(t)), \dots, \phi^{(m_i)}(\alpha_i(t)) \right). \quad (21)$$

Application of DT at t_{j-1} to equation (19) yields a system of recurrence algebraic equations:

$$\mathbf{U}_{I_j}(k+n)[t_{j-1}] = \mathbf{F}\left(k, \mathbf{U}_{I_j}(k), \mathbf{U}_{I_j}(k+1), \dots, \mathbf{U}_{I_j}(k+n-1)\right), \quad (22)$$

where the function \mathbf{F} is the DT of the righthand side of equation (19) and involves application of Theorem 1.

Next, we transform the initial conditions (2). Following Definition 2, we derive

$$\mathbf{U}_{I_j}(k)[t_{j-1}] = \frac{1}{k!} \mathbf{u}_{I_j}^{(k)}(t_{j-1}), \quad \text{for } k = 0, 1, \dots, n-1, j \in \{1, \dots, K\}. \quad (23)$$

Using (22) with (23) and then inverse transformation rule, we obtain approximate solution to (19) in the form of Taylor series:

$$\mathbf{u}_{I_j}(t) = \sum_{k=0}^{\infty} \mathbf{U}_{I_j}(k)[t_{j-1}](t-t_{j-1})^k, \quad t \in I_j, \quad (24)$$

for all $j \in \{1, \dots, K\}$.

To transform (20) correctly, we need the following theorem.

Theorem 2. Let $\alpha_i(t) \in I_l$ for $t \in I_j$, where $l \in \{1, \dots, j-1\}$. Let $p \in \mathbb{N}$. Denote $\mathcal{D}\{\alpha_i(t)\}[t_{j-1}] = \{A_i(k)[t_{j-1}]\}_{k=0}^{\infty}$. Then,

$$\begin{aligned} &\mathcal{D}\{u_{I_l}^{(p)}(\alpha_i(t))\}[t_{j-1}] \\ &= \left\{ \sum_{y=0}^k \frac{(y+p)!}{y!} U_{I_l}(y+p)[\alpha_i(t_{j-1})] \right. \\ &\quad \left. \cdot \widehat{B}_{k,y}(A_i(1)[t_{j-1}], \dots, A_i(k-y+1)[t_{j-1}]) \right\}_{k=0}^{\infty}, \end{aligned} \quad (25)$$

where $\widehat{B}_{0,0} = 1$, $\widehat{B}_{k,0} = 0$ for $k \geq 1$, and

$$\begin{aligned} U_{I_l}(y)[\alpha_i(t_{j-1})] &= \sum_{x=0}^{\infty} \binom{x+y}{x} (\alpha_i(t_{j-1}) - t_{l-1})^x \\ &\quad \cdot U_{I_l}(x+y)[t_{l-1}], \end{aligned} \quad (26)$$

for $y \geq 0$.

Proof. To prove (25) with $p = 0$, we use Theorem 1 with $f(t) = u_{I_l}(t)$, $g(t) = \alpha_i(t)$, and $h(t) = (f \circ g)(t)$. We immediately get

$$\begin{aligned} H(k)[t_{j-1}] &= \sum_{y=1}^k U_{I_l}(y)[\alpha_i(t_{j-1})] \\ &\quad \cdot \widehat{B}_{k,y}(A_i(1)[t_{j-1}], \dots, A_i(k-y+1)[t_{j-1}]), \end{aligned} \quad (27)$$

for $k \geq 1$. For $k = 0$, Theorem 1 yields $H(0)[t_{j-1}] = U_{I_l}(0)[\alpha_i(t_{j-1})] = U_{I_l}(0)[\alpha_i(t_{j-1})] \cdot \widehat{B}_{0,0}(A_i(1)[t_{j-1}])$. Now, (25) for $p > 0$ is a consequence of Lemma 1 and it remains to prove (26). We recall that

$$\mathbf{u}_{I_l}(t) = \sum_{k=0}^{\infty} \mathbf{U}_{I_l}(k)[t_{l-1}](t-t_{l-1})^k, \quad t \in I_l. \quad (28)$$

As the assumption was that $\alpha_i(t_{j-1}) \in I_l$, we may apply Definition 2 to (28) and obtain

$$\begin{aligned} U_{I_l}(y)[\alpha_i(t_{j-1})] &= \frac{1}{y!} \left[\frac{d^y u_{I_l}(t)}{dt^y} \right]_{t=t_0} \frac{1}{z!} \sum_{z=y}^{\infty} \frac{z!}{(z-y)!} U_{I_l}(z)[t_{l-1}] \\ &\quad \cdot (t_0 - t_{l-1})^{z-y}. \end{aligned} \quad (29)$$

Substituting $t_0 = \alpha_i(t_{j-1})$ and $z = x + y$ gives (26). \square

3.2. *New DT Formulas.* In the applications, we also use the following DT formulas.

Theorem 3. Assume that $F(k)[t_0]$ is the differential transformation of the function $f(t)$ and $r \in \mathbb{R}$:

(a) If $f(t) = t^r$, then $F(k)[t_0] = \binom{r}{k} t_0^{r-k}$ for all t such that $|t - t_0| < |t_0|$,

where $\binom{r}{k} = r(r-1)\dots(r-k+1)/k! = (r)_k/k!$ and $(r)_k$ is the Pochhammer symbol.

(b) If $f(t) = \ln(t)$, then $F(k)[t_0] = (-1)^{k-1}/(k \cdot t_0^k)$ for $k \geq 1$.

Proof

(a) Recall the Newton's generalisation of the binomial formula: if x and y are real numbers with $|x| > |y|$, and r is any complex number, one has

$$(x+y)^r = \sum_{k=0}^{\infty} \binom{r}{k} x^{r-k} y^k, \quad (30)$$

where $\binom{r}{k} = r(r-1)\dots(r-k+1)/k!$. Let us rewrite t^r as $t^r = (t - t_0 + t_0)^r = (t_0 + (t - t_0))^r$. Applying (30) yields

$$t^r = \sum_{k=0}^{\infty} \binom{r}{k} t_0^{r-k} (t - t_0)^k. \quad (31)$$

(b) We start by proving the formula

$$(\ln(t))^{(k)} = \frac{(-1)^{k-1} (k-1)!}{t^k}, \quad (32)$$

by induction. For $k = 1$, we have $(\ln(t))' = 1/t$; hence, (32) is valid. Suppose that (32) holds for k . Then,

$$\begin{aligned} (\ln(t))^{(k+1)} &= ((\ln(t))^{(k)})' = \left(\frac{(-1)^{k-1} (k-1)!}{t^k} \right)' \\ &= (-1)^{k-1} (k-1)! (t^{-k})' \\ &= (-1)^{k-1} (k-1)! (-k) t^{-k-1} \\ &= \frac{(-1)^k k!}{t^{k+1}}. \end{aligned} \quad (33)$$

Thus, formula (32) is valid for all $k \in \mathbb{N}$. Now by Definition 2,

$$\begin{aligned} F(k)[t_0] &= \frac{1}{k!} \left[\frac{d^k \ln(t)}{dt^k} \right]_{t=t_0} = \frac{1}{k!} \left[\frac{(-1)^{k-1} (k-1)!}{t^k} \right]_{t=t_0} \\ &= \frac{(-1)^{k-1}}{k \cdot t_0^k}. \end{aligned} \quad (34)$$

□

3.3. *Applications.* In this section, we introduce two test problems and show how the practical implementation of the presented algorithm looks like in concrete examples. Comparison of numerical results is given in Section 3.4.

As the first test problem, we choose an IVP for a scalar equation with one nonconstant delay where the exact solution is known to be the exponential function e^t . The purpose of including this example is to compare results obtained by DT against values of the exact solution and also against results obtained by Matlab function DDENSD which has been designed to approximate solutions to IVP for neutral delayed differential equations.

Example 1. Consider the delayed equation:

$$u'(t) = u(t) - t + u(\ln(t)), \quad (35)$$

with the initial condition

$$u(1) = e, \quad (36)$$

and with the initial function

$$\phi(t) = e^t, \quad t \in [0, 1]. \quad (37)$$

First we find the differential transform of the initial condition (36) which is $U(0)[1] = e$. Further denote $\mathcal{D}\{e^t\}[0] = \{E(k)[0]\}_{k=0}^{\infty}$ as the transformation of the exponential function with the center at 0 and $\mathcal{D}\{\ln(t)\}[1] = \{F(k)[1]\}_{k=0}^{\infty}$ as the transformation of the logarithmic function at 1, respectively. Then, Lemma 1 and Theorem 3 yield

$$E(k)[0] = \frac{1}{k!}, \quad (38)$$

$$F(k)[1] = \frac{(-1)^{k-1}}{k}, \quad \text{for } k \geq 1.$$

For $t \in [1, e]$, equation (35) is transformed into

$$(k+1)U(k+1)[1] = U(k)[1] - \delta(k) - \delta(k-1) + H(k)[1], \quad (39)$$

where

$$H(k)[1] = \sum_{l=1}^k E(l)[0] \widehat{B}_{k,l}(F(1)[1], \dots, F(k-l+1)[1]), \quad \text{for } k \geq 1,$$

$$H(0)[1] = E(0)[0] = 1. \quad (40)$$

We have

$$\begin{aligned}
U(1)[1] &= e - 1 - 0 + 1 = e, \\
H(1)[1] &= E(1)[0] \cdot F(1)[1] = 1 \cdot 1 = 1, \\
U(2)[1] &= \frac{1}{2}(U(1)[1] - 0 - 1 + H(1)[1]) \\
&= \frac{1}{2}(e - 1 + 1) = e \cdot \frac{1}{2}, \\
H(2)[1] &= E(1)[0] \cdot F(2)[1] + E(2)[0] \cdot (F(1)[1])^2 \\
&= 1 \cdot \left(-\frac{1}{2}\right) + \frac{1}{2} \cdot 1 = 0, \\
U(3)[1] &= \frac{1}{3}(U(2)[1] + H(2)[1]) = \frac{1}{3} \cdot e \cdot \frac{1}{2} = e \cdot \frac{1}{3!}, \\
&\vdots
\end{aligned} \tag{41}$$

Using the inverse transformation, we see that for $t \in [1, e]$,

$$u(t) = e \left(1 + (t-1) + \frac{(t-1)^2}{2} + \frac{(t-1)^3}{3!} + \dots \right) = e \cdot e^{t-1} = e^t, \tag{42}$$

which corresponds to the exact solution to the IVPs (35)–(37).

In the second step of the method of steps, i.e., in the interval $t \in [e, e^e]$, we know that $u(t) = e^t$ for $t \in [1, e]$ and equation (35) is transformed into

$$(k+1)U(k+1)[e] = U(k)[e] - e\delta(k) - \delta(k-1) + H(k)[e], \tag{43}$$

where

$$\begin{aligned}
H(0)[e] &= U(0)[1], \\
H(k)[e] &= \sum_{l=1}^k U(l)[1] \widehat{B}_{k,l}(F(1)[e], \dots, F(k-l+1)[e]), \\
&\text{for } k \geq 1.
\end{aligned} \tag{44}$$

Here, $F(k)[e]$, according to Theorem 3, are coefficients of Taylor series of logarithmic function with the center at e :

$$\begin{aligned}
F(0)[e] &= 1, \\
F(k)[e] &= \frac{(-1)^{k-1}}{k \cdot e^k}, \quad \text{for } k \geq 1.
\end{aligned} \tag{45}$$

Taking the values calculated in the first step and substituting them into the recurrence formulas (43) and (44), we obtain

$$\begin{aligned}
U(0)[e] &= u(e) = e^e, \\
U(1)[e] &= U(0)[e] - e\delta(0) - \delta(-1) + H(0)[e] \\
&= e^e - e - 0 + e = e^e, \\
H(1)[e] &= U(1)[1] \cdot F(1)[e] = e \cdot \frac{1}{e} = 1, \\
U(2)[e] &= \frac{1}{2}(U(1)[e] - 0 - 1 + H(1)[e]) \\
&= \frac{1}{2}[e^e - 1 + 1] = \frac{1}{2}e^e, \\
H(2)[e] &= U(1)[1] \cdot \widehat{B}_{2,1}(F(1)[e], F(2)[e]) \\
&\quad + U(2)[1] \cdot \widehat{B}_{2,2}(F(1)[e]) \\
&= e \cdot F(2)[e] + \frac{e}{2} \cdot (F(1)[e])^2 \\
&= e \cdot \frac{1}{2} \left(\frac{-1}{e^2}\right) + \frac{e}{2} \cdot \left(\frac{1}{e}\right)^2 = 0, \\
U(3)[e] &= \frac{1}{3}(U(2)[e] + H(2)[e]) = \frac{1}{3!}e^e, \\
H(3)[e] &= U(1)[1] \cdot \widehat{B}_{3,1}(F(1)[e], F(2)[e], F(3)[e]) \\
&\quad + U(2)[1] \cdot \widehat{B}_{3,2}(F(1)[e], F(2)[e]) + U(3)[1] \\
&\quad \cdot \widehat{B}_{3,3}(F(1)[e]) \\
&= e \cdot F(3)[e] + \frac{e}{2} \cdot 2 \cdot F(1)[e] \cdot F(2)[e] + \frac{e}{3!} (F(1)[e])^3 \\
&= e \cdot \frac{2}{e^3} \frac{1}{3!} + e \cdot \frac{1}{e} \cdot \frac{(-1)}{e^2} \cdot \frac{1}{2} + \frac{e}{6} \cdot \frac{1}{e^3} = \frac{1}{e^2} \left(\frac{1}{3} - \frac{1}{2} + \frac{1}{6}\right) = 0, \\
U(4)[e] &= \frac{1}{4}(U(3)[e] + H(3)[e]) = \frac{1}{4!}e^e.
\end{aligned} \tag{46}$$

Hence, for $t \in [e, e^e]$, we have

$$\begin{aligned}
u(t) &= e^e + e^e(t-e) + \frac{1}{2}e^e(t-e)^2 + \frac{1}{3!}e^e(t-e)^3 \\
&\quad + \frac{1}{4!}e^e(t-e)^4 + \dots \\
&= e^e \left(1 + (t-e) + \frac{(t-e)^2}{2} + \frac{(t-e)^3}{3!} + \frac{(t-e)^4}{4!} + \dots \right) \\
&= e^e \cdot e^{t-e} = e^t,
\end{aligned} \tag{47}$$

which again coincides with the exact solution to problems (35)–(37).

In the second application, we have chosen an IVP for a nonlinear system of neutral delayed differential equations taken from the fully open access paper [18]. There are several reasons to test the proposed algorithm on the particular problem. The first is that the problem involves a nonlinear system of neutral equations of high complexity whose exact solution is unknown. Secondly, the proposed algorithm is a

complete differential transform version of the algorithm presented in [18] where modified Adomian formula has been used. Furthermore, the calculations done in [18] are shown only for the first step of the method of steps up to the first principal discontinuity point, whereas we continue calculations beyond that point in this paper. Last but not least, we want to verify performance and reproduce values obtained by DT and published in [18]. Rebenda et al. [18] has been submitted 4 years ago for the first time, and since that time, the Maple source code has been lost.

Example 2. Consider a nonlinear system of neutral delayed differential equations:

$$\begin{aligned} u_1''' &= u_1'''(t-2)u_1\left(\frac{t}{3}\right) + \sqrt[3]{(u_1(t))^2} + u_2'\left(t - \frac{1}{2}e^{-t}\right), \\ u_2''' &= \frac{1}{2}u_2'''\left(\frac{t}{2}\right) + u_2'(t-1)u_1\left(\frac{t}{3}\right), \end{aligned} \quad (48)$$

with initial functions

$$\begin{aligned} \phi_1(t) &= e^t, \\ \phi_2(t) &= t^2, \end{aligned} \quad (49)$$

for $t \in [-2, 0]$, and initial conditions

$$\begin{aligned} u_1(0) &= 1, \\ u_1'(0) &= 1, \\ u_1''(0) &= 1, \\ u_2(0) &= 0, \\ u_2'(0) &= 0, \\ u_2''(0) &= 2. \end{aligned} \quad (50)$$

For $t \in [0, t_1]$, where $t_1 \approx 0,351734$ is the minimal root of $t - (1/2)e^{-t} = 0$, using the method of steps, we obtain

$$\begin{aligned} u_1''' &= e^{(t-2)}u_1\left(\frac{t}{3}\right) + \sqrt[3]{(u_1(t))^2} + 2t - e^{-t}, \\ u_2''' &= \frac{1}{2}u_2'''\left(\frac{t}{2}\right) + 2(t-1)u_1\left(\frac{t}{3}\right). \end{aligned} \quad (51)$$

We need to find the differential transform of the considered problem. We notice that system (2) contains nonlinear term $h(t) = \sqrt[3]{(u_1(t))^2}$. To get DT of this term, $\mathcal{D}\{h(t)\}[0] = \{H_1(k)[0]\}_{k=0}^{\infty}$, and we apply Theorem 1. First, applying DT to system (2) at $t_0 = 0$, we get the recurrent system:

$$\begin{aligned} (k+1)(k+2)(k+3)U_1(k+3)[0] \\ = e^{-2} \sum_{l=0}^k \frac{1}{l!} \left(\frac{1}{3}\right)^{k-l} U_1(k-l)[0] + H_1(k)[0] + 2\delta(k) - \frac{(-1)^k}{k!}, \end{aligned} \quad (52)$$

$$\begin{aligned} (k+1)(k+2)(k+3) \left(1 - \frac{1}{2^{k+1}}\right) U_2(k+3)[0] \\ = 2 \left(\frac{1}{3}\right)^{k-1} U_1(k-1)[0] - \frac{2}{3^k} U_1(k)[0]. \end{aligned} \quad (53)$$

Denote $g(t) = t^{2/3}$; then, $h(t) = (g \circ u_1)(t)$, and following Theorem 1, we obtain

$$\begin{aligned} H_1(0)[0] &= G_1(0)[1], \\ H_1(k)[0] &= \sum_{l=1}^k G_1(l)[1] \tilde{B}_{k,l}(U_1(1)[0], \dots, U_1(k-l+1)[0]), \end{aligned} \quad (54)$$

for $k \geq 1$, where $\mathcal{D}\{g(t)\}[1] = \{G_1(k)[1]\}_{k=0}^{\infty}$ and, Theorem 3 being applied, $G_1(k)[1] = \binom{2/3}{k}$ for $k \geq 0$. Furthermore, the transformed initial conditions are

$$\begin{aligned} U_1(0)[0] &= 1, \\ U_1(1)[0] &= 1, \\ U_1(2)[0] &= \frac{1}{2}, \\ U_2(0)[0] &= 0, \\ U_2(1)[0] &= 0, \\ U_2(2)[0] &= 1. \end{aligned} \quad (55)$$

Using them, we compute the first three coefficients of the nonlinear term $h(t)$:

$$\begin{aligned} H_1(0)[0] &= G_1(0)[1] = 1, \\ H_1(1)[0] &= G_1(1)[1] \cdot B_{1,1}(U_1(1)[0]) = \frac{2}{3} \cdot 1 = \frac{2}{3}, \\ H_1(2)[0] &= G_1(1)[1] \cdot B_{2,1}(U_1(1)[0], U_1(2)[0]) \\ &\quad + G_1(2)[1] \cdot B_{2,2}(U_1(1)[0]) = \frac{2}{3} \cdot \frac{1}{2} - \frac{1}{9} \cdot 1 = \frac{2}{9}. \end{aligned} \quad (56)$$

Solving recurrent systems (52) and (53), we get

$$\begin{aligned} k=0: U_1(3)[0] &= \frac{1}{6}(e^{-2}U_1(0)[0] + H_1(0)[0] + 1) \\ &= \frac{2+e^{-2}}{6}, \\ U_2(3)[0] &= \frac{1}{3}(-2U_1(0)[0]) = -\frac{2}{3}, \\ k=1: U_1(4)[0] &= \frac{e^{-2}}{24} \left(\frac{1}{3}U_1(1)[0] + U_1(0)[0]\right) \\ &\quad + \frac{1}{24}(H_1(1)[0] + 1) = \frac{4e^{-2} + 5}{72}, \\ U_2(4)[0] &= \frac{1}{18} \left(2U_1(0)[0] - \frac{2}{3}U_1(1)[0]\right) = \frac{2}{27}, \\ k=2: U_1(5)[0] &= \frac{e^{-2}}{60} \left(\frac{1}{9}U_1(2)[0] + \frac{1}{3}U_1(1)[0]\right) \\ &\quad + \frac{1}{2}U_1(0)[0] + \frac{1}{60}(H_1(2)[0] - \frac{1}{2}) \\ &= \frac{16e^{-2} - 5}{1080}, \\ U_2(5)[0] &= \frac{2}{105} \left(\frac{2}{3}U_1(1)[0] - \frac{2}{9}U_1(2)[0]\right) = \frac{2}{189}. \end{aligned} \quad (57)$$

Using the inverse DT (Definition 3), we get approximate solution for the IVPs (48)–(50) on the interval $[0, t_1]$:

$$u_{1,I_1}(t) = 1 + t + \frac{1}{2}t^2 + \frac{2 + e^{-2}}{6}t^3 + \frac{4e^{-2} + 5}{72}t^4 + \frac{16e^{-2} - 5}{1080}t^5 + \dots, \quad (58)$$

$$u_{2,I_1}(t) = t^2 - \frac{2}{3}t^3 + \frac{2}{27}t^4 + \frac{2}{189}t^5 + \dots,$$

which is exactly the same approximate solution which has been obtained in [18].

The second step brings us to solving the given IVP on the interval $[t_1, t_2]$, where t_2 is the minimal root of $t - (1/2)e^{-t} = t_1$, $t_2 \approx 0,620556$. Now taking into account that both proportional delays $q_1 t = (1/3)t$ and $q_2 t = (1/2)t$ and also the time-dependent delay $t - \tau_1(t) = t - (1/2)e^{-t}$ map the interval $[t_1, t_2]$ into the interval $[0, t_1]$, system (2) becomes

$$u_1''' = e^{(t-2)} u_{1,I_1}\left(\frac{t}{3}\right) + \sqrt[3]{(u_1(t))^2} + u_{2,I_1}'\left(t - \frac{1}{2}e^{-t}\right), \quad (59)$$

$$u_2''' = \frac{1}{2}u_{2,I_1}''\left(\frac{t}{2}\right) + 2(t-1)u_{1,I_1}\left(\frac{t}{3}\right).$$

Denote $\mathcal{D}\{h(t)\}[t_1] = \{H_2(k)[t_1]\}_{k=0}^{\infty}$ and $\mathcal{D}\{f(t)\}[t_1] = \{F_2(k)[t_1]\}_{k=0}^{\infty}$, where $f(t) = u_2'(t - (1/2)e^{-t})$. By application of Theorem 2 to corresponding terms, system (2) transformed at $t_0 = t_1$ reads as

$$\begin{aligned} & (k+1)(k+2)(k+3)U_1(k+3)[t_1] \\ &= e^{-2} \sum_{l=0}^k \frac{e^{t_1}}{l!} \left(\frac{1}{3}\right)^{k-l} \sum_{x=0}^{\infty} \binom{x+k-l}{x} U_1(x+k-l)[0] \left(\frac{t_1}{3}\right)^x \\ &+ H_2(k)[t_1] + F_2(k)[t_1], \end{aligned} \quad (60)$$

$$\begin{aligned} & (k+1)(k+2)(k+3)U_2(k+3)[t_1] \\ &= \left(\frac{1}{2}\right)^{k+1} (k+3)(k+2)(k+1) \sum_{x=0}^{\infty} \binom{x+k+3}{x} \\ &\cdot U_2(x+k+3)[0] \left(\frac{t_1}{2}\right)^x + 2 \sum_{l=0}^k [(t_1-1)\delta(l) + \delta(l-1)] \\ &\cdot \left(\frac{1}{3}\right)^{k-l} \sum_{x=0}^{\infty} \binom{x+k-l}{x} U_1(x+k-l)[0] \left(\frac{t_1}{3}\right)^x. \end{aligned} \quad (61)$$

Now denote $\mathcal{D}\{g(t)\}[u_1(t_1)] = \{G_2(k)[u_1(t_1)]\}_{k=0}^{\infty}$; then, according to Theorem 3, $G_2(k)[u_1(t_1)] = \binom{2/3}{k} (u_1(t_1))^{2/3-k}$ for $k \geq 0$ and Theorem 1 implies

$$\begin{aligned} H_2(0)[t_1] &= G_2(0)[u_1(t_1)] = \sqrt[3]{u_1(t_1)^2}, \\ H_2(k)[t_1] &= \sum_{l=1}^k G_2(l)[u_1(t_1)] \cdot \widehat{B}_{k,l}(U_1(1)[t_1], \dots, \\ &U_1(k-l+1)[t_1]), \quad \text{for } k \geq 1. \end{aligned} \quad (62)$$

Further denote $e(t) = t - (1/2)e^{-t}$ and $\mathcal{D}\{e(t)\}[t_1] = \{E_2(k)[t_1]\}_{k=0}^{\infty}$. Then, $f(t) = (u_2' \circ e)(t)$ and, since $e(t_1) = 0$, Theorem 1 in combination with Lemma 1 yields

$$\begin{aligned} E_2(k)[t_1] &= t_1 \cdot \delta(k) + \delta(k-1) - \frac{1}{2} \cdot \frac{e^{-t_1}(-1)^k}{k!}, \quad k \geq 0, \\ F_2(0)[t_1] &= U_2(1)[0] = 0, \\ F_2(k)[t_1] &= \sum_{l=1}^k (l+1)U_2(l+1)[0] \cdot \widehat{B}_{k,l}(E_2(1)[t_1], \dots, \\ &E_2(k-l+1)[t_1]), \quad \text{for } k \geq 1. \end{aligned} \quad (63)$$

To get the initial data $U_1(k)[t_1]$ and $U_2(k)[t_1]$ for $k = 0, 1, 2$, we have to transform

$$u_i(t) = U_i(0)[0] + U_i(1)[0]t + U_i(2)[0]t^2 + U_i(3)[0]t^3 + \dots, \quad (64)$$

at t_1 , $i = 1, 2$. For $k = 0, 1, 2$, we have

$$\begin{aligned} U_i(k)[t_1] &= U_i(0)[0] + U_i(1)[0] \binom{1}{k} t_1^{1-k} \\ &+ U_i(2)[0] \binom{2}{k} t_1^{2-k} + U_i(3)[0] \binom{3}{k} t_1^{3-k} + \dots, \end{aligned} \quad (65)$$

i.e.,

$$\begin{aligned} U_i(0)[t_1] &= \sum_{k=0}^{\infty} U_i(k)[0] t_1^k, \\ U_i(1)[t_1] &= \sum_{k=0}^{\infty} (k+1)U_i(k+1)[0] t_1^k, \\ U_i(2)[t_1] &= \sum_{k=0}^{\infty} \binom{k+2}{2} U_i(k+2)[0] t_1^k. \end{aligned} \quad (66)$$

The initial values at t_1 will be approximated by taking finite sums in computer evaluations of the infinite sums above. Observe that $u_1(t_1) = U_1(0)[t_1]$.

Now let us compute the first few values of $H_2(k)[t_1]$. Denote $\widehat{B}_{k,l} = \widehat{B}_{k,l}(U_1(1)[t_1], \dots, U_1(k-l+1)[t_1])$. Then, the first values of $\widehat{B}_{k,l}$ are

$$\begin{aligned}
\widehat{B}_{0,0} &= 1, \\
\widehat{B}_{1,1} &= U_1(1)[t_1] \cdot \widehat{B}_{0,0} = U_1(1)[t_1], \\
\widehat{B}_{2,1} &= \frac{1}{2}U_1(1)[t_1] \cdot \widehat{B}_{1,0} + U_1(2)[t_1] \cdot \widehat{B}_{0,0} = U_1(2)[t_1], \\
\widehat{B}_{2,2} &= U_1(1)[t_1] \cdot \widehat{B}_{1,1} = (U_1(1)[t_1])^2,
\end{aligned} \tag{67}$$

and the coefficients H_2 for $k = 0, 1, 2$ are

$$\begin{aligned}
H_2(0)[t_1] &= u_1(t_1), \\
H_2(1)[t_1] &= \frac{2}{3}(u_1(t_1))^{-1/3} \cdot \widehat{B}_{1,1} = \frac{2}{3}(u_1(t_1))^{-1/3} \\
&\quad \cdot U_1(1)[t_1], \\
H_2(2)[t_1] &= \frac{2}{3}(u_1(t_1))^{-1/3} \cdot \widehat{B}_{2,1} - \frac{1}{9}(u_1(t_1))^{-4/3} \cdot \widehat{B}_{2,2} \\
&= \frac{2}{3}(u_1(t_1))^{-1/3} \cdot U_1(2)[t_1] - \frac{1}{9}(u_1(t_1))^{-4/3} \\
&\quad \cdot (U_1(1)[t_1])^2.
\end{aligned} \tag{68}$$

Let us turn our attention to the first few values of $F_2(k)[t_1]$. Starting with $E_2(k)[t_1]$,

$$\begin{aligned}
E_2(0)[t_1] &= t_1 - \frac{1}{2}e^{-t_1} = 0, \\
E_2(1)[t_1] &= 1 + \frac{1}{2}e^{-t_1} = 1 + t_1, \\
E_2(2)[t_1] &= -\frac{1}{2} \cdot \frac{e^{-t_1}}{2} = -\frac{t_1}{2}.
\end{aligned} \tag{69}$$

Now, $\widehat{B}_{k,l}$ are $\widehat{B}_{k,l}(E_2(1)[t_1], \dots, E_2(k-l+1)[t_1])$:

$$\begin{aligned}
\widehat{B}_{0,0} &= 1, \\
\widehat{B}_{1,1} &= E_2(1) \cdot \widehat{B}_{0,0} = 1 + t_1, \\
\widehat{B}_{2,1} &= \frac{1}{2}E_2(1) \cdot \widehat{B}_{1,0} + E_2(2) \cdot \widehat{B}_{0,0} = \frac{t_1}{2}, \\
\widehat{B}_{2,2} &= E_2(1) \cdot \widehat{B}_{1,1} = (1 + t_1)^2.
\end{aligned} \tag{70}$$

Finally, coefficients F_2 for $k = 0, 1, 2$ are

$$\begin{aligned}
F_2(0)[t_1] &= U_2(1)[0] = 0, \\
F_2(1)[t_1] &= 2U_2(2)[0] \cdot \widehat{B}_{1,1} = 2(1 + t_1), \\
F_2(2)[t_1] &= 2U_2(2)[0] \cdot \widehat{B}_{2,1} + 3U_2(3)[0] \cdot \widehat{B}_{2,2} \\
&= -t_1 - 2(1 + t_1)^2.
\end{aligned} \tag{71}$$

At this moment, we substitute H_2 and F_2 into systems (60) and (61). The next three coefficients at t_1 for U_1 are

$$\begin{aligned}
k=0: U_1(3)[t_1] &= \frac{1}{6}(e^{-2}e^{t_1} \cdot u_1(\frac{t_1}{3}) + u_1(t_1)), \\
k=1: U_1(4)[t_1] &= \frac{1}{24} \left(e^{-2} \left(e^{t_1} \cdot \frac{1}{3} \cdot \sum_{x=0}^{\infty} (x+1)U_1(x+1)[0] \left(\frac{t_1}{3}\right)^x \right. \right. \\
&\quad \left. \left. + e^{t_1} \cdot u_1\left(\frac{t_1}{3}\right) \right) + \frac{2}{3} \cdot (u_1(t_1))^{-1/3} \cdot U_1(1)[t_1] \right. \\
&\quad \left. + 2(1+t_1) \right), \\
k=2: U_1(5)[t_1] &= \frac{1}{60}e^{-2} \left(e^{t_1} \left(\frac{1}{3}\right)^2 \cdot \sum_{x=0}^{\infty} \binom{x+2}{x} U_1(x+2)[0] \right. \\
&\quad \cdot \left(\frac{t_1}{3}\right)^x + e^{t_1} \cdot \frac{1}{3} \cdot \sum_{x=0}^{\infty} (x+1)U_1(x+1)[0] \left(\frac{t_1}{3}\right)^x \\
&\quad \left. + \frac{e^{t_1}}{2} \cdot u_1\left(\frac{t_1}{3}\right) \right) + \frac{1}{60} \left(\frac{2}{3}(u_1(t_1))^{-1/3} \cdot (U_1(2)[t_1]) \right. \\
&\quad \left. - \frac{1}{9}(u_1(t_1))^{-4/3} \cdot (U_1(1)[t_1])^2 - t_1 - 2(1+t_1)^2 \right),
\end{aligned} \tag{72}$$

and for U_2 , we obtain

$$\begin{aligned}
k=0: U_2(3)[t_1] &= \frac{1}{2} \left(\sum_{x=0}^{\infty} \binom{x+3}{x} U_2(x+3)[0] \left(\frac{t_1}{2}\right)^x \right) \\
&\quad + \frac{1}{3}(t_1-1) \cdot u_1\left(\frac{t_1}{3}\right), \\
k=1: U_2(4)[t_1] &= \frac{1}{4} \left(\sum_{x=0}^{\infty} \binom{x+4}{x} U_2(x+4)[0] \left(\frac{t_1}{2}\right)^x \right) \\
&\quad + \frac{1}{12} \left((t_1-1) \cdot \frac{1}{3} \cdot \sum_{x=0}^{\infty} (x+1)U_1(x+1)[0] \left(\frac{t_1}{3}\right)^x \right. \\
&\quad \left. + u_1\left(\frac{t_1}{3}\right) \right), \\
k=2: U_1(5)[t_1] &= \frac{1}{8} \left(\sum_{x=0}^{\infty} \binom{x+5}{x} U_2(x+5)[0] \left(\frac{t_1}{2}\right)^x \right) \\
&\quad + \frac{1}{30} \left((t_1-1) \cdot \frac{1}{9} \cdot \sum_{x=0}^{\infty} \binom{x+2}{x} U_1(x+2)[0] \left(\frac{t_1}{3}\right)^x \right. \\
&\quad \left. + \frac{1}{3} \sum_{x=0}^{\infty} (x+1)U_1(x+1)[0] \left(\frac{t_1}{3}\right)^x \right).
\end{aligned} \tag{73}$$

Using the inverse DT, again we get approximate solution for the IVPs (48), (49), and (50) on the interval $[t_1, t_2]$:

TABLE 1: Example 1, error analysis of u in $[1, e]$.

	Exact solution	DT 5	DT 10	DT 25	Matlab DDENSD
t	e^t	$ u - e^t $	$ u - e^t $	$ u - e^t $	$ u - e^t $
1	2.7183	0	0	0	0
1.4296	4.1769	0.0000	$6.4890E-12$	$8.8818E-16$	$1.6976E-5$
1.8591	6.4182	0.0017	$1.0381E-8$	$8.8818E-16$	$3.6095E-5$
2.2887	9.8622	0.0211	$1.2409E-6$	$3.5527E-15$	$9.3438E-5$
e	15.1543	0.1273	$3.0578E-5$	$1.2861E-12$	$1.4012E-4$

TABLE 2: Example 1, error analysis of u in $[e, e^e]$.

	Exact solution	DT 5	DT 10	DT 25	Matlab DDENSD
t	e^t	$ u - e^t $	$ u - e^t $	$ u - e^t $	$ u - e^t $
e	15.1543	$3.5527E-15$	$3.5527E-15$	$3.5527E-15$	0
5.8273	339.4331	32.3491	1.333	$2.2737E-13$	0.0743
8.9363	$7.6028E+3$	$4.4755E+3$	397.5509	$2.2638E-5$	3.1741
12.0453	$1.7029E+5$	$1.5373E+5$	$5.6777E+4$	0.9751	112.2467
e^e	$3.8143E+6$	$3.7554E+6$	$2.6576E+6$	$2.0358E+3$	$3.1395E+3$

$$\begin{aligned}
u_{1,I_2}(t) &= U_1(0)[t_1] + U_1(1)[t_1](t - t_1) + U_1(2)[t_1] \\
&\quad \cdot (t - t_1)^2 + U_1(3)[t_1](t - t_1)^3 + \dots, \\
u_{2,I_2}(t) &= U_2(0)[t_1] + U_2(1)[t_1](t - t_1) + U_2(2)[t_1] \\
&\quad \cdot (t - t_1)^2 + U_2(3)[t_1](t - t_1)^3 + \dots
\end{aligned} \tag{74}$$

As the calculations are getting more complicated, all the calculations have been done numerically only.

3.4. Numerical Results and Discussion. Table 1 shows a comparison of results for Example 1 obtained by DT algorithm with the orders of Taylor polynomials of the approximate solution $N = 5, 10, 25$ to results of Matlab function DDENSD in the interval $[1, e]$. Since the exact solution is known, absolute errors illustrate precision of each algorithm setting. All numbers are rounded to four decimal places. We see that DDENSD performs satisfactory well and DT for $N = 10, 25$ does even better, whereas DT for $N = 5$ does not show satisfactory precision.

Table 2 brings the same comparison in the second interval $[e, e^e]$. We can observe a fast growth rate of the function values of the exact solution, which leads to the growth of absolute errors and loss of precision in all settings. It indicates that at the end of the considered interval $[e, e^e]$, the rate of precision would be better seen using relative errors.

Implementation of DT in Matlab in case of Example 2 produces numerical results which are listed in Table 3. The results of DT with order of the Taylor polynomial $N = 10$ are compared to values obtained by DT combined with modified Adomian formula in [18] and to values produced by Matlab function DDENSD.

First, we should say that the function DDENSD had difficulty at 0 where the value of the delayed argument $t/2$

was equal to the argument itself. Hence, to make DDENSD work, we replaced $t/2$ by $t/2 - 10^{-16}$ in the second equation of (2). Our hypothesis is that the reason of the DDENSD failure is a combination of two facts: the second equation is neutral with respect to a proportional delay and the interval where the problem is considered contains 0.

Second, we should mention that the numerical results for DDENSD were obtained by looking for approximate solutions on the whole interval $[0, t_2]$. When trying to follow the method of steps, i.e., using DDENSD on $[0, t_1]$ and then on $[t_1, t_2]$, the results on the second interval $[t_1, t_2]$ did not correspond to reality: there was a discontinuity in u_2 at t_1 .

Furthermore, we recall that the values taken from [18] have been computed using symbolic software Maple and the source code of the computation has been lost.

Now, we can see a very good concordance of all algorithms in numerical values of the second component u_2 , while we observe a growing distance between the values of the first component u_1 computed by presented DT algorithm and values computed by the other two algorithms. As u_1 has exponential characteristics, we interpret the growing distance as growing lack of precision of DT algorithm which is based on approximation by Taylor polynomials. We suppose that dividing the intervals $[0, t_1]$ and $[t_1, t_2]$ into smaller subintervals, i.e., refining the mesh grid, and applying the DT algorithm on those smaller intervals consecutively will improve the performance of the presented algorithm.

Although it seems that the algorithm used in [18] shows better performance than the one presented in this paper, we cannot claim it with certainty as the source code got lost and we are not able to reproduce the data. Moreover, the approach used in [18] involves calculations of symbolic derivatives which makes it difficult to implement in numerical software like Matlab.

TABLE 3: Example 2, comparison of presented DT, DT in [18] and Matlab function DDENSND for u_1 and u_2 in the first step for $t \in [0, t_1]$, and presented DT and DDENSND in the second step for $t \in [t_1, t_2]$.

Method	DT 10	DT 10	Matlab DDENSND	Matlab DDENSND	DT [18]	DT [18]
t	u_1	u_2	u_1	u_2	u_1	u_2
0.00	1.0000	0.0000	1.0000	0.0000	1.0000	0.0000
0.05	1.0513	0.0024	1.0513	0.0024	1.0513	0.0024
0.10	1.1054	0.0093	1.1050	0.0093	1.1051	0.0093
0.15	1.1625	0.0203	1.1614	0.0203	1.1618	0.0203
0.20	1.2230	0.0348	1.2204	0.0348	1.2209	0.0348
0.25	1.2871	0.0524	1.2822	0.0524	1.2832	0.0524
0.30	1.3552	0.0726	1.3469	0.0726	1.3481	0.0726
0.35	1.4277	0.0951	1.4146	0.0951	1.4160	0.0951
0.3520	1.4306	0.0960	1.4174	0.0960	—	—
0.3904	1.4896	0.1146	1.4717	0.1146	—	—
0.4289	1.5514	0.1340	1.5280	0.1340	—	—
0.4673	1.6161	0.1541	1.5864	0.1541	—	—
0.5057	1.6839	0.1747	1.6469	0.1748	—	—
0.5441	1.7548	0.1957	1.7098	0.1957	—	—
0.5826	1.8290	0.2169	1.7750	0.2169	—	—
0.6210	1.9065	0.2380	1.8428	0.2381	—	—

4. Conclusion

In the paper, we presented an algorithm which makes use of the differential transformation to initial value problems for systems of delayed or neutral differential equations with nonconstant delays. Two examples have been chosen to validate and test the algorithm. Numerical comparison of the presented semianalytical approach to Matlab function DDENSND brought interesting and promising results.

Example 1 showed expected and reliable behaviour of the differential transform in the first step of the method of steps and expected deviation in the numerical results from values of the exact solution in the second step. Furthermore, we could observe a good concordance between the presented algorithm and DDENSND.

After facing difficulties with DDENSND in Example 2, we could confirm a very good concordance of both differential transform and DDENSND in values of the component u_2 which has a polynomial character on the considered intervals. On the other hand, we observed a growing discrepancy between the two methods in values of the component u_1 which has an exponential character. Our conclusion is that the disagreement is caused by large lengths of the intervals where the approximate solution is computed using the differential transform and that refining the mesh grid is necessary to obtain better performance.

Further investigation will be focused on experimenting with different densities of mesh grids and studying convergence of the algorithm to find the optimal mesh grid. Numerical experiments will be focused on tuning the performance on problems with high complexity whose exact solutions are known and subsequently on applications to nonartificial real-life problems whose exact solutions are unknown.

Data Availability

The numerical data used to support the findings of this study are included within the article.

Conflicts of Interest

The authors declare that there are no conflicts of interest regarding the publication of this article.

Acknowledgments

The first author was supported by the project CEITEC 2020 (LQ1601) with financial support from the Ministry of Education, Youth and Sports of the Czech Republic under the National Sustainability Programme II, and by the grant FEKT-S-17-4225 of the Faculty of Electrical Engineering and Communication of Brno University of Technology. The Article Processing Charge was funded by Open Access Fund of Brno University of Technology. This support is gratefully acknowledged.

Supplementary Materials

We have included the commented Matlab source code for the first step of the method of steps in Example 1 as supplementary material. (*Supplementary Materials*)

References

- [1] T. Kalmar-Nagy, G. Stepan, and F. C. Moon, "Subcritical Hopf bifurcation in the delay equation model for machine tool vibrations," *Nonlinear Dynamics*, vol. 26, pp. 121–142, 2011.
- [2] D. Adak, N. Bairagi, and R. Hakl, "Chaos in delay-induced Leslie-Gower prey-predator-parasite model and its control through prey harvesting," *Nonlinear Analysis: Real World Applications*, vol. 51, pp. 102998–103020, 2020.
- [3] A. Matsumoto and F. Szidarovszky, "Delay dynamics of a Cournot game with heterogeneous duopolies," *Applied Mathematics and Computation*, vol. 269, pp. 699–713, 2015.
- [4] V. Kolmanovskii and A. Myshkis, *Introduction to the Theory and Applications of Functional Differential Equations*, Kluwer, Dordrecht, Netherlands, 1999.

- [5] I. Györi and G. Ladas, *Oscillation Theory of Delay Differential Equations with Applications*, Clarendon Press, Oxford, UK, 1991.
- [6] J. K. Hale and S. M. Verduyn Lunel, *Introduction to Functional Differential Equations*, Springer, New York, NY, USA, 1993.
- [7] J. Rebenda and Z. Šmarda, “Comparison of differential transformation method with adomian decomposition method for functional differential equations with proportional delays,” in *Proceedings of the 11th International Conference on Numerical Analysis and Applied Mathematics (ICNAAM 2013)*, T. E. Simos, Ed., vol. 1558, pp. 1190–1193, AIP Publishing, Melville, NY, USA, 2013.
- [8] H. Šamajová and T. Li, “Oscillators near Hopf bifurcation,” *Communications-Scientific Letters of the University of Žilina*, vol. 17, pp. 83–87, 2015.
- [9] J. Rebenda, Z. Šmarda, and Y. Khan, “A new semi-analytical approach for numerical solving of Cauchy problem for differential equations with delay,” *Filomat*, vol. 31, no. 15, pp. 4725–4733, 2017.
- [10] H. Šamajová, “Semi-analytical approach to initial problems for systems of nonlinear partial differential equations with constant delay,” in *Proceedings of the EQUADIFF 2017 Conference*, K. Mikula, D. Sevcovic, and J. Urban, Eds., pp. 163–172, Spektrum STU Publishing, Bratislava, Slovakia, 2017.
- [11] J. Rebenda and Z. Šmarda, “A numerical approach for solving of fractional Emden-Fowler type equations,” in *Proceedings of the International Conference of Numerical Analysis and Applied Mathematics (ICNAAM 2017)*, T. E. Simos, Ed., vol. 1978, p. 140006, AIP Publishing, Melville, NY, USA, 2018.
- [12] T. Krisztin, “Analyticity of solutions of differential equations with a threshold delay,” in *Springer Proceedings in Mathematics & Statistics, Recent Advances in Delay Differential and Difference Equations*, F. Hartung and M. Pituk, Eds., vol. 94, pp. 173–180, Springer, Basel, Switzerland, 2014.
- [13] J. Duarte, C. Janeiro, and N. Martins, “Analytical solutions of an economic model by the homotopy analysis method,” *Applied Mathematical Sciences*, vol. 10, no. 49, pp. 2483–2490, 2016.
- [14] Z. Šmarda, J. Diblík, and Y. Khan, “Extension of the differential transformation method to nonlinear differential and integro-differential equations with proportional delays,” *Advances in Difference Equations*, vol. 69, pp. 1–13, 2013.
- [15] J. Rebenda and Z. Šmarda, “A differential transformation approach for solving functional differential equations with multiple delays,” *Communications in Nonlinear Science and Numerical Simulation*, vol. 48, pp. 246–257, 2017.
- [16] A. Bellen and M. Zennaro, *Numerical Methods for Delay Differential Equations*, Oxford University Press, Oxford, UK, 2003.
- [17] P. G. Warne, D. A. P. Warne, J. S. Sochacki, G. E. Parker, and D. C. Carothers, “Explicit *A-Priori* error bounds and adaptive error control for approximation of nonlinear initial value differential systems,” *Computers & Mathematics with Applications*, vol. 52, no. 12, pp. 1695–1710, 2006.
- [18] J. Rebenda and Z. Šmarda, “Numerical algorithm for nonlinear delayed differential systems of n th order,” *Advances in Difference Equations*, vol. 2019, no. 26, pp. 1–13, 2019.
- [19] E. N. Petropoulou, P. D. Sifarakas, and E. E. Tzirtzilakis, “A “discretization” technique for the solution of ODEs,” *Journal of Mathematical Analysis and Applications*, vol. 331, no. 1, pp. 279–296, 2007.
- [20] E. N. Petropoulou, P. D. Sifarakas, and E. E. Tzirtzilakis, “A “discretization” technique for the solution of ODEs II,” *Numerical Functional Analysis and Optimization*, vol. 30, no. 5-6, pp. 613–631, 2009.
- [21] J. Rebenda, “An application of Bell polynomials in numerical solving of nonlinear differential equations,” in *Proceedings of the 17th Conference on Applied Mathematics, APLIMAT 2018*, pp. 891–900, Slovak University of Technology, SPEKTRUM STU, Bratislava, Slovakia, 2018.

Research Article

Multiobjective Optimization Model of Production Planning in Cloud Manufacturing Based on TOPSIS Method with Combined Weights

Zhiru Li, Wei Xu , Huibin Shi, Qingshan Zhang , and Fengyi He

School of Management, Shenyang University of Technology, Shenyang 110870, China

Correspondence should be addressed to Wei Xu; 369252882@qq.com

Received 6 August 2019; Accepted 22 November 2019; Published 18 December 2019

Academic Editor: András Rontó

Copyright © 2019 Zhiru Li et al. This is an open access article distributed under the Creative Commons Attribution License, which permits unrestricted use, distribution, and reproduction in any medium, provided the original work is properly cited.

Combined with the research of mass customization and cloud manufacturing mode, this paper discussed the production planning of mass customization enterprises in the context of cloud manufacturing in detail, analyzed the attribute index of manufacturing resource combination, and given a system considering the characteristics of batch production in mass customization and the decentralization of manufacturing resources in cloud manufacturing environment. Then, a multiobjective optimization model has been constructed according to the product delivery date, product cost, and product quality that customers care most about. The Pareto solution set of production plan has been obtained by using NSGA-II algorithm. This paper established a six-tier attribute index system evaluation model for the optimization of production planning scheme set of mass customization enterprises in cloud manufacturing environment. The weight coefficients of attribute indexes were calculated by combining subjective and objective weights with analytic hierarchy process (AHP) and entropy weight method. Finally, the combined weights calculated were applied to the improved TOPSIS method, and the optimal production planning scheme has been obtained by ranking. This paper validated the effectiveness and feasibility of the multiobjective model and NSGA-II algorithm by the example of company A. The Pareto effective solution has been obtained by solving the model. Then the production plan set has been sorted synthetically according to the comprehensive evaluation model, and the optimal production plan has been obtained.

1. Introduction

With the advent of the big data era and the introduction of the concept of cloud manufacturing, great changes have taken place in the production mode of the manufacturing industry. Cloud manufacturing mode can promote the value added of resources and services, promote the comprehensive sharing of resources, and improve the utilization of resources. Due to the increasing diversity of people's needs and the increasing functional requirements of products, services with a single function cannot meet the needs of customers, but services with multiple functions have diversity and quantity, which makes it possible to have a variety of possibilities and uncertainties to select cloud manufacturing resources. Because the problem of cloud manufacturing production scheme is a multiobjective optimization problem, in order to enable manufacturing enterprises to choose

the optimal production plan, so as to carry out production in an organized manner, it is necessary to design and optimize the production planning.

The concept of cloud manufacturing is put forward by Lee et al. [1] in 2010; he thought the cloud manufacturing is an advanced network manufacturing mode to manage the manufacturing resources and provide the manufacturing services for enterprises through the cloud manufacturing service platform. In view of the cloud manufacturing architecture proposed by Lee, many scholars have carried out relevant theoretical research and proposed different cloud manufacturing architecture models applied in different fields. Du et al. [2] proposed a system architecture of the cloud manufacturing platform based on double-chain architecture to solve the problem of transaction security of the cloud manufacturing platform, aiming at the common problems of information islands and low trust in the cloud

manufacturing platform. In the key technologies of cloud manufacturing, in cloud manufacturing system, it is necessary to virtualize and encapsulate manufacturing resources scattered in different places and connect them into the cloud manufacturing service platform [3]. In this process, the capability and function of manufacturing resources should be considered, so as to establish different granularity description models of manufacturing resources and capabilities. S. Huang and B. Huang [4] analyzed the security requirements of the cloud manufacturing platform in view of the proposed architecture and established a security requirement model of cloud manufacturing platform, which strengthened the security of the cloud manufacturing platform from three aspects: data security, access rights, and network transmission security. In terms of search matching of cloud manufacturing, Yang et al. [5] established an ontology-based cloud service discovery model to realize the search and intelligent matching capabilities of cloud manufacturing. In order to allocate cloud manufacturing resources to manufacturing tasks more effectively, Zhang et al. [6] proposed a dynamic parameter ant colony algorithm in cloud manufacturing combinatorial optimization, which was proved to be effective by an example.

The scholars at home and abroad have also studied mass customization. A domestic scholar named Zhou et al. [7] thinks that mass customization is a kind of mass production mode which meets the market environment and customers' individualized requirements; it can provide customers with products that can meet their individualized needs with mass production costs. Liu et al. [8] described the process of building a product family model based on product family deformation design in product design and combined with family table function in pro/pre to achieve rapid product deformation design. Cariagai et al. [9] analyzed customer needs and indexed customer demand information. On this basis, the change of customer needs was studied through encapsulation and analysis of data. Wu et al. [10] analyzed and demonstrated the mechanism of mass intelligent customization in view of the structure of the black box of personalized demand and the linking of supply and demand paths. It showed that with the help of virtual market and data technology effect, enterprises can meet the personalized demand in the sense of scale. Katzy [11] constructed a conceptual model of agile manufacturing and illustrated the feasibility of the model through an application example of an enterprise.

In this paper, the production planning and optimization of mass customization manufacturing enterprises in the cloud environment are studied, in order to make mass manufacturing enterprises fully and reasonably meet customer requirements and obtain maximum benefits in the cloud manufacturing environment.

2. Formulation of Production Planning in Cloud Manufacturing Environment

Manufacturing enterprises in cloud manufacturing environment can share information at a high level through cloud manufacturing service platform, realize virtualization and

integration of manufacturing resources and manufacturing capabilities, and realize the information exchange and sharing among enterprises.

2.1. Influencing Factors of Production Planning

2.1.1. Production Cost. The cost of production-related products mainly includes production cost, inventory cost, and shortage cost. In the cloud manufacturing environment, enterprises can obtain the services they need at any time through the cloud manufacturing service platform, so the inventory cost is neglected. However, the shortage of goods will affect customer satisfaction and will also lead to the loss of business opportunities and market share, which has a great impact on the competitiveness of enterprises. Therefore, the cost of shortage should be avoided as far as possible. Cost control is particularly important for choosing manufacturers.

2.1.2. Transportation Cost. The distance between each manufacturer and the customer is different, so the transportation cost is different, and the transportation cost accounts for a certain proportion of the total cost. In order to reduce the total product cost of manufacturing enterprises and improve manufacturing efficiency, transportation cost, as one of the product cost, is also a key factor to be considered.

2.1.3. Product Quality. Manufacturers registered and approved in cloud manufacturing service platform need to provide specific information about their manufacturing resources and manufacturing capabilities and provide the qualified rate of a certain product. When selecting manufacturing suppliers, the quality of the products they can supply shall be fully considered. The quality is an important factor in selecting the manufacturing suppliers to complete the manufacturing tasks.

2.1.4. Delivery Time. The delivery time refers to the time between receipt of orders and delivery, which is influenced by factors such as production time, transportation, and information transmission, and has certain uncertainty. Delivery time usually includes the production time of the product and the transportation time. Customers have strict requirements for delivery time, so delivery time has become an important factor affecting production planning and design in cloud manufacturing environment.

2.2. Model Construction

2.2.1. Problem Description. Combined with the actual characteristics of multitask and multimanufacturer selection in cloud manufacturing environment, considering the four factors of production cost, transportation cost, product quality, and delivery time as the key factors in the process of production planning design in cloud manufacturing environment, this paper chooses product cost (C), product

quality (Q), and delivery time (T) as the objective of optimization, in which the product cost includes the sum of production cost and transportation cost. The lower the cost, the higher the profit the manufacturing enterprise can get. Product quality refers to the degree to which the product can meet the needs of customers, expressed by the qualified rate of the product. Delivery time includes the production time of the product and the haulage time of the product, and the delivery time needs to be completed within the customer's time limit. The shorter the delivery time is, the better it is.

To sum up, the problem can be described as follows: at a certain time, a manufacturing enterprise receives the demand of m kinds of products from customers. The enterprise makes production planning on the basis of combining its own manufacturing resources and manufacturing capacities. Through the intelligent search in the cloud manufacturing service platform, it can be seen that there are n manufacturing suppliers that meet the functional requirements of the products, and the index values of different manufacturing suppliers are different. The enterprise can assign some of the products to u manufacturing suppliers, so that the above index values can reach the optimal.

2.2.2. Model Assumptions

- (1) Many kinds of products can be manufactured at each manufacturer, and the products are independent of each other
- (2) Due to the limitation of manufacturing resources and manufacturing capacities of manufacturing enterprises, it is difficult to meet the needs of customers on their own, so it is necessary to find the products that can meet the needs of customers through the cloud manufacturing service platform, so as to allocate the manufacturing tasks
- (3) Mass production and bulk delivery are carried out by each manufacturing supplier, that is, delivery is carried out for every batch of products completed
- (4) There is no idle time between the batches produced by each manufacturer
- (5) Transportation costs are borne by manufacturing enterprises
- (6) Taking into account the volume discount, when the amount purchased meets the corresponding requirements, all purchased products are given the same discount

2.2.3. Symbol Meaning

i : the serial number of the manufacturing supplier that can provide the product ($i=0, 1, 2, \dots, n$) (if $i=0$, the product is provided by the manufacturer who received the customers' order)

n : number of manufacturing suppliers to choose from

j : the serial numbers of different types of products ($j=1, 2, \dots, m$)

m : number of product categories in customer orders received by manufacturing enterprises

x_{ij} : quantity of products j produced by manufacturing supplier i (when $i=0$, it is the cost of the product j produced by the manufacturing enterprise itself)

p_{ij} : undiscounted unit price of product j provided by manufacturing supplier i (when $i=0$, it is the cost of manufacturing enterprises' own products j)

k : serial number of discount phase

r_{ijk} : the discount rate of the k stage given to the manufacturing supplier i when the product j reaches a certain quantity

$y_{ijk} = \begin{cases} 1, & \text{if the periodic discount } k \text{ of product } j \\ & \text{can be obtained from manufacturing supplier } i, \\ 0, & \text{if not;} \end{cases}$

$\lambda_{ij} = \begin{cases} 1, & \text{if the manufacturing supplier } i \text{ produces product } \\ & j, \\ 0, & \text{if not;} \end{cases}$

L_i : the transport batch from manufacturing supplier i to customers

b : the maximum number of products that can be transported per batch

c_i : transportation costs per batch between manufacturer i and customer

t_{ij} : unit production time for manufacturing supplier i to manufacture product j

h_i : transportation time from manufacturing supplier i to customers

q_{ij} : product percent of pass of product j provided by manufacturing supplier i

d_j : demand for product j

Q_j : acceptable minimum product percent of pass of product j

PR_{ij} : maximum production capacity of manufacturer-supplied product j , a constant (when $i=0$, it is the maximum production capacity of manufacturing enterprises themselves)

2.2.4. Constraint Condition

(1) *Supply and Demand Balance Constraints.* Supply-demand balance means that the quantity of products supplied by manufacturing suppliers should be in line with the quantity of products required by customers. If the quantity of products supplied does not reach the quantity of products demanded by customers, it will affect customer satisfaction, thereby reducing the reputation and economic benefits of enterprises. If the quantity of products supplied exceeds the quantity of demand, waste will occur to a certain extent, so the supply-demand balance constraints are as follows:

$$\sum_{i=0}^n \lambda_{ij} x_{ij} = d_j, \quad j = 1, 2, \dots, m. \quad (1)$$

(2) *Production Capacity Constraints of Each Manufacturing Supplier.* Due to the different production capacities and different constraints of each manufacturer, the maximum production capacity that supplier i can provide is PR_{ij} . Therefore, the output of products whether manufactured by the manufacturing enterprise itself or by manufacturing suppliers on the cloud manufacturing platform should not be greater than the manufacturer's maximum production capacity. That is to say:

$$\sum_{j=1}^m \lambda_{ij} x_{ij} \leq PR_{ij}, \quad i = 0, 1, 2, \dots, m. \quad (2)$$

(3) *Discount Constraints on Purchased Products.* Because of the mass customization production model, when the quantity of manufactured products that manufacturers can provide is within a certain range, the discount constraint of manufactured products can be provided for manufacturers. The discount rate of product j purchased from manufacturer i should only fall within one range, that is, only one discount rate or no discount is used, that is,

$$\sum_{k=1}^K y_{ijk} \leq 1. \quad (3)$$

(4) *Quality Constraints.* With the gradual development of customization and individualization, the quality level is one of the most important factors for users. Good product quality can win customer satisfaction, thus gaining the competitiveness of the industry. Suppose Q_j is the minimum quality percent of pass acceptable to product j , q_{ij} is the percent of pass the product j provided by the manufacturing supplier i . The percent of pass of product j provided by all manufacturers should satisfy the following constraints:

$$\sum_{i=0}^n \sum_{j=1}^m \frac{\lambda_{ij} x_{ij} q_{ij}}{D_j} \geq Q_j d_j. \quad (4)$$

(5) *Delivery Time Constraints.* Customers' requirements for punctualization are gradually increasing, and punctual delivery of products can improve customer satisfaction and thus gain industry competitiveness. The time of delivery mainly includes production time and transportation time. The time for the enterprise to produce the product j in factory i is t_{ij} , the time of transportation from factory i to customers is H_i , and the time of delivery required by customers is T' . Then, the time of delivery should meet the following constraints:

$$\sum_{i=0}^n \sum_{j=1}^m \lambda_{ij} x_{ij} t_{ij} + \sum_{i=0}^n H_i \leq T'. \quad (5)$$

2.2.5. Objective Function

(1) *Product Cost.* Product cost is an important factor affecting customer satisfaction. Product cost is mainly

composed of production cost and transportation cost. Considering that manufacturers in cloud manufacturing service platform can offer discounts, the objective function of product cost is as follows:

$$P_1 = \sum_{j=1}^m x_{0j} p_{0j} + \sum_{t=1}^T \sum_{i=1}^n \sum_{j=1}^m \lambda_{ij} x_{ij} p_{ij} r_{ijk} y_{ijk}. \quad (6)$$

Because the location of cloud manufacturing service providers is different from that of customers, the cost of products in the transportation process should also be considered. Because the manufacturing mode of products is mass customization, there are a large number of products. Assuming that the products are transported in batches, the transportation batches from manufacturing suppliers to customers are as follows:

$$L_i = \sum_{j=1}^m \frac{\lambda_{ij} x_{ij}}{b}. \quad (7)$$

The transportation cost of the manufacturing supplier i to the customer is given by

$$P_2 = \sum_{i=0}^n L_i c_i = \sum_{i=0}^n \sum_{j=1}^m \left(\frac{\lambda_{ij} x_{ij}}{b} \right) c_i. \quad (8)$$

From the above, it can be seen that the product cost is composed of production cost and transportation cost; the smaller the cost, the better the attribute. Then

$$\begin{aligned} \text{Min } P = P_1 + P_2 &= \sum_{j=1}^m x_{0j} p_{0j} + \sum_{t=1}^T \sum_{i=1}^n \sum_{j=1}^m \lambda_{ij} x_{ij} p_{ij} r_{ijk} y_{ijk} \\ &+ \sum_{i=0}^n \sum_{j=1}^m \left(\frac{\lambda_{ij} x_{ij}}{b} \right) c_i. \end{aligned} \quad (9)$$

(2) *Product Delivery Time.* The competition in the manufacturing industry is becoming more and more fierce. Enterprise users have more stringent requirements on delivery time. Manufacturing suppliers need to strictly control their delivery time, so as to improve customer satisfaction. In cloud manufacturing environment, due to the geographical location of each manufacturing supplier, transportation time is a factor that must be considered besides production time. On the premise of meeting customer needs, the shorter the delivery time is, the better the objective function of delivery time is as follows:

$$\text{Min } T = \sum_{i=0}^n \sum_{j=1}^m \lambda_{ij} x_{ij} t_{ij} + \sum_{i=0}^n H_i. \quad (10)$$

(3) *Product Quality.* Manufacturing products are gradually developing towards individualization and diversification. Customers' requirements for product quality are getting higher and higher. The quality of products affects customer satisfaction. The higher the quality of the product is, the

better it is. Therefore, the objective function of product quality is as follows:

$$\max Q = \sum_{i=0}^n \sum_{j=1}^m \frac{\lambda_{ij} x_{ij} q_{ij}}{D_j}. \quad (11)$$

From the above description, it can be seen that the production planning problem of manufacturing enterprises in cloud manufacturing environment is a multiobjective optimization problem. The complete mathematical expression of this problem is as follows:

$$\begin{aligned} \min P &= P_1 + P_2 = \sum_{j=1}^m x_{0j} p_{0j} + \sum_{t=1}^T \sum_{i=1}^n \sum_{j=1}^m \lambda_{ij} x_{ij} p_{ij} r_{ijk} y_{ijk} + \sum_{i=0}^n \sum_{j=1}^m \left(\frac{\lambda_{ij} x_{ij}}{b} \right) c_i, \\ \min T &= \sum_{i=0}^n \sum_{j=1}^m \lambda_{ij} x_{ij} t_{ij} + \sum_{i=0}^n H_i, \\ \max Q &= \sum_{i=0}^n \sum_{j=1}^m \frac{\lambda_{ij} x_{ij} q_{ij}}{D_j}, \\ \sum_{i=0}^n \lambda_{ij} x_{ij} &= d_j, \\ \sum_{j=1}^m \lambda_{ij} x_{ij} &\leq PR_{ij}, \\ \sum_{k=1}^K y_{ijk} &\leq 1, \\ \sum_{i=0}^n \sum_{j=1}^m \lambda_{ij} x_{ij} q_{ij} &\geq Q_j d_j, \\ \sum_{i=0}^n \sum_{j=1}^m \lambda_{ij} x_{ij} t_{ij} + \sum_{i=0}^n H_i &\leq T', \end{aligned} \quad (12)$$

$$x_{ij} \geq 0, i = 0, 1, 2, \dots, n, j = 1, 2, \dots, m.$$

2.3. Model Solution

2.3.1. Pareto Optimal Solution. For conventional multi-objective programming problems, if the minimum value is to be calculated, the concept of Pareto optimal solution corresponds to the following: when setting the interval of variables, for the variable group X^* , if there is no other design variable group X , conform to $f_i(X) \leq f_i(X^*)$ without conflict with constraint conditions, then X^* is the Pareto optimal solution.

For multiobjective optimization problems, the solution is not a set of solutions, which constitutes the Pareto optimal solution set to a large extent. There are no more excellent solutions in the feasible solution set, and there are no advantages or disadvantages among the Pareto optimal solutions. Therefore, the decision makers can choose the most ideal solution according to the will and the importance of the goal.

2.3.2. Algorithmic Design. The main process of the elite strategy of NSGA-II is shown in Figure 1. According to the image, the steps taken are as follows:

- (a) Combining P_t and Q_t , the corresponding population R_t is obtained, and its actual size is equal to $2N$.
- (b) Complete the standardized nondominated sorting of R_t , calculate the crowding distance of all individuals, and define the individuals according to the level. When the total number of individuals reaches N , a new paternal population P_{t+1} is formed.
- (c) On this condition, a new generation of variation is formed and the offspring population Q_{t+1} is formed.

According to the analysis above, the calculation flow of using NSGA-II to solve the production planning problem of manufacturing enterprises in cloud manufacturing environment is as follows:

Step 1: the initial population P_t with the total amount equal to N is not oriented in the solution space. After that, all target fitness values are analyzed, and then the hierarchical operation is implemented on it, and the

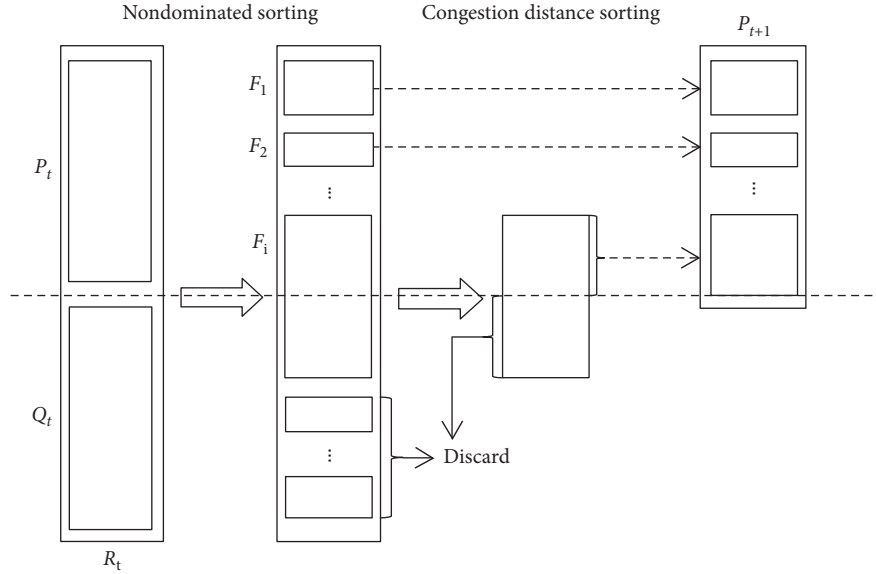


FIGURE 1: Process sketch of NSGA-II elite strategy.

crowding distance corresponding to individuals in various groups is calculated.

Step 2: the binary tournament mechanism is mainly used to make a reasonable selection of the individuals covered by population P_t , and then the genetic operation of variation is completed according to the specification, and then the progeny population Q_t with the total amount equal to N is obtained.

Step 3 (elite strategy): P_t and Q_t are merged effectively, and then population R_t is obtained. After non-dominated sorting, the front segment of the non-dominated solution can be obtained. Then, the crowding degree is calculated and N individuals in the front are selected to form P_{t+1} .

Step 4: let $t = t + 1$, steps 2-3 are completed several times in the set iteration interval to obtain the optimal solution set corresponding to the production planning.

3. Optimization of Production Planning in Cloud Manufacturing Environment

3.1. Problem Description. In order to optimize the existing production planning and select the optimal production planning, it is necessary to establish a set of perfect and reasonable optimization system. Effective evaluation methods are adopted to evaluate the production planning comprehensively. On the basis of a comprehensive evaluation, the optimal selection of production planning of mass customization enterprises in cloud manufacturing environment should be fully combined with the needs of customers and the distinction of importance should be made between competitive targets.

3.2. Construction of Evaluation and Optimization Model. Combining with the three important selected attribute indexes in this paper, this section gives a model of evaluation

and optimization of production planning in cloud manufacturing environment as shown in Figure 2. The following is a detailed description of resource layer, scheme layer, criteria layer, weight layer, and target layer:

Resource layer: according to the request of manufacturing enterprises, the cloud manufacturing service platform searches for manufacturing suppliers who can complete various manufacturing tasks.

Scheme layer: the functional requirements and specific constraints of the manufacturing tasks proposed by the manufacturing enterprises can be met, and the set of manufacturing schemes is formed after being screened by the multiobjective optimization algorithm.

Criteria layer: criteria layer is the evaluation attribute indexes of candidate manufacturing scheme.

Weight layer: the weight layer mainly determines the weight coefficients of each attribute index, which is determined by the users' needs and the value of the attribute index itself.

Evaluation layer: evaluation layer uses a decision method to evaluate and rank all alternative manufacturing schemes comprehensively.

Target layer: target layer is the optimal production planning which is determined by comprehensive evaluation of each production planning through attribute index system. It is the best plan to fully meet needs of customers and management and development of enterprises. It is the ultimate goal to optimize the production planning of manufacturing enterprises in cloud manufacturing environment.

3.3. Model Solution

3.3.1. Pretreatment of Attribute Index Values for Scheme Optimization. According to the characteristics that the decision maker expects to show to the attribute value, the

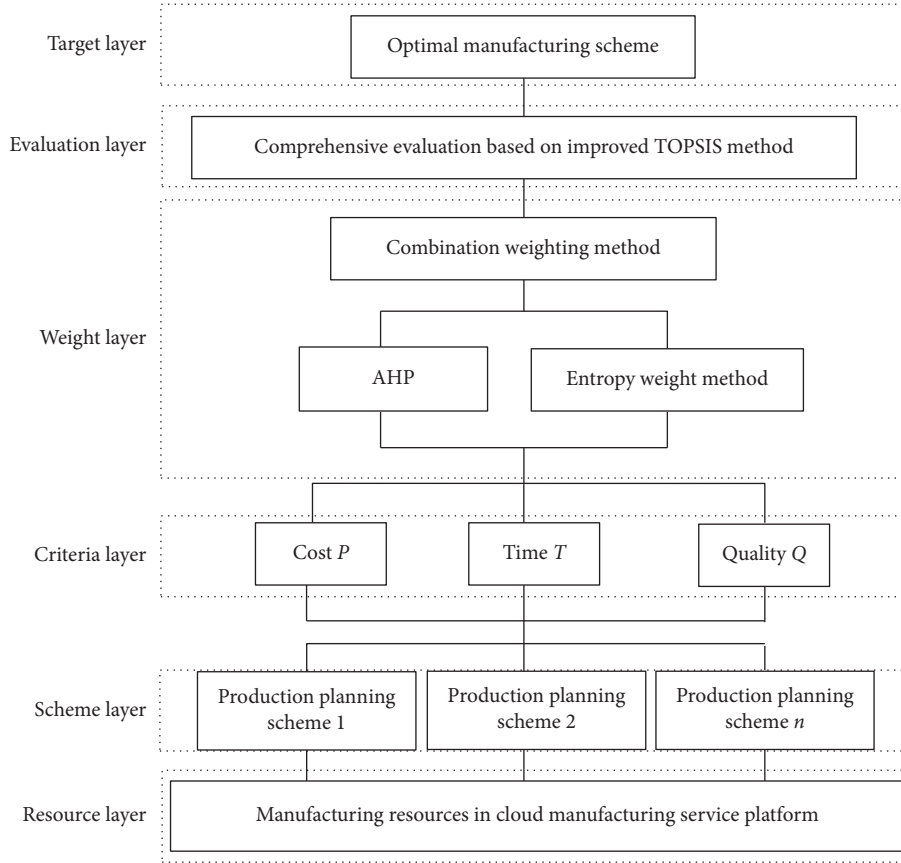


FIGURE 2: A model for evaluating and optimizing production schemes in cloud manufacturing environment.

types of attributes are usually divided into six categories, and their names and characteristics are referred to in Table 1.

In this study, combined with the impact of the attribute index value set by the scheme on the optimal selection, it can be classified as benefit index and cost index. For the traditional three attribute indicators, time and cost are very typical cost indicators, while quality is a representative benefit indicator.

Because there are some deviations in the way of describing the attributes of the production planning, there are great differences in the corresponding range and the unit of quantification is also inconsistent. In order to effectively reduce the negative impact of such factors on the optimization evaluation, so that the consistency check can be completed in the course of the assessment, it is necessary to carry out standardized pretreatment of the attribute index value of the production planning. The representative methods of data preprocessing include normative approach and range transformation.

In the application of the range transformation data preprocessing method, the attribute values measured by each attribute index are mainly changed in $[0, 1]$, and it is convenient to carry out an objective evaluation of other schemes. Therefore, this study mainly chooses the method of range transformation.

Assuming that the total number of production schemes is m , covering n attribute indexes, the original data matrix of

TABLE 1: Six common attribute types.

Attribute type	Characteristic
Benefit	The larger the attribute value, the better the attribute
Cost	The smaller the attribute value, the better the attribute
Fixed	The closer the attribute value is to a fixed value, the better it is
Interval	The closer the attribute value is or belongs to a fixed interval, the better it is
Deviation	The more the attribute value deviates from a fixed value, the better it is
Deviation interval	The more the attribute value deviates from a fixed interval, the better it is

all attribute indexes is $X = (x_{ij})_{m \times n}$, and x_{ij} refers to the value of j attribute indexes at this time; the method of pretreatment that can be used at this time is as follows:

(1) Benefit indexes can be calculated as follows:

$$R_{ij} = \begin{cases} \frac{x_{ij} - \min_j x_{ij}}{\max_j x_{ij} - \min_j x_{ij}}, & \max_j x_{ij} - \min_j x_{ij} \neq 0, \\ 1, & \max_j x_{ij} - \min_j x_{ij} = 0. \end{cases} \quad (13)$$

(2) Cost indexes can be calculated as follows:

$$R_{ij} = \begin{cases} \frac{\max_j x_{ij} - x_{ij}}{\max_j x_{ij} - \min_j x_{ij}}, & \max_j x_{ij} - \min_j x_{ij} \neq 0, \\ 1, & \max_j x_{ij} - \min_j x_{ij} = 0. \end{cases} \quad (14)$$

At this time, $i = 1, 2, \dots, m$; $j = 1, 2, \dots, n$; x_{ij} mainly refers to the attribute index value corresponding to the scheme i ; $\min_j x_{ij}$ refers to the minimum attribute index value corresponding to the group manufacturing resource service composition; $\max_j x_{ij}$ refers to the maximum attribute index value corresponding to the scheme m ; and R_{ij} refers to the attribute index value obtained after normalization.

3.3.2. Combined Weight Method Based on AHP and Entropy Method

(1) *AHP*. Through AHP, the core processes corresponding to weight coefficients are defined:

- (1) Constructing the hierarchy corresponding to the objective problem.
- (2) Constructing decision judgment matrix. Representing specific attributes by a_i ($i = 1, 2, \dots, n$), a_{ij} refers to the importance of a_i over attributes a_j , which can be quantified with the values in Table 2. If a_{ij} is obtained by comparing attribute a_i with attribute a_j , the important level of comparison between a_j and a_i is $a_{ji} = 1/a_{ij}$. The decision judgment matrix B corresponding to the objective problem can be established by using the following formula:

$$B = \begin{bmatrix} a_{11} & a_{12} & \cdots & a_{1n} \\ a_{21} & a_{22} & \cdots & a_{2n} \\ \vdots & \vdots & \vdots & \vdots \\ a_{n1} & a_{n2} & \cdots & a_{nn} \end{bmatrix}. \quad (15)$$

(3) Consistency test:

In some cases, the constructed matrix will show obvious inconsistency. In order to prevent this situation from leading to the lack of scientific results after weight distribution, it must be tested and analyzed according to the following formula:

$$CR = \frac{CI}{RI}. \quad (16)$$

In the above formula, CR mainly refers to the random consistency ratio corresponding to the decision judgment matrix; CI refers to the corresponding consistency index at this time, which can be calculated by using formula (17); and RI refers to the random consistency index corresponding to the matrix, and

the RI value corresponding to the judgment matrix is shown in Table 3:

$$CI = \frac{(\lambda_{\max} - n)}{(n - 1)}. \quad (17)$$

If the consistency ratio of matrix B conforms to $CR < 0.1$, or the maximum eigenvalue conforms to the standard of $\lambda_{\max} = n$, then the consistency of matrix B can be determined to be acceptable. If it does not meet the above criteria, it should be adjusted to reach the criteria of consistency testing.

- (4) The maximum eigenvalues are calculated and the specific eigenvectors are clarified. Matrix B is calculated according to formula (18), so that its maximum eigenvalue is λ_{\max} and corresponding eigenvector $X = (X_1, X_2, \dots, X_n)$. At this time, all the components corresponding to X are positive components:

$$BX = \lambda_{\max} X. \quad (18)$$

- (5) The weight coefficients are calculated. Eigenvector of maximum eigenvalue λ_{\max} is processed according to formula (19), so that the weight vector constructed by weight coefficient can be obtained:

$$t = \frac{X}{\sum_{i=1}^n X_i}. \quad (19)$$

(2) *Entropy Weight Method*. Assuming that there are m sets of data samples and n evaluation indexes, the initial data matrix is $X = (x_{ij})_{m \times n}$; x_{ij} mainly refers to the value of attribute j . The process of defining the weight coefficients is as follows:

- (1) Data standardization: since the corresponding order of magnitudes of each evaluation index is not consistent, in order to effectively eliminate incomparability, the standardized processing of information should be carried out by the method of range normalization, which lays a good foundation for statistical analysis. Assuming that R refers to the matrix obtained after processing, then the operation steps of R_{ij} refer to as formula (13) and formula (14).
- (2) The proportion of attribute index P_{ij} is calculated. At this time, the ratio corresponding to the evaluation value of the object i is as follows:

$$P_{ij} = \frac{R_{ij}}{\sum_{i=1}^m R_{ij}}, \quad (0 \leq P_{ij} \leq 1). \quad (20)$$

- (3) The entropy value e_j of the attribute index is calculated, and then the entropy value corresponding to attribute index j is as follows:

$$e_j = \begin{cases} \frac{1}{\ln(m) \sum_{i=1}^m P_{ij} \ln P_{ij}}, & P_{ij} \neq 0, \\ 0, & P_{ij} = 0. \end{cases} \quad (21)$$

At this time, $0 \leq e_j \leq 1$.

- (4) The diversity factor h_i of attribute index is calculated, and the diversity factor is as follows:

$$h_j = 1 - e_j. \quad (22)$$

- (5) The weight v_j corresponding to the attribute index is calculated, so the weight corresponding to the attribute index of item j is as follows:

$$v_j = \frac{h_j}{\sum_{j=1}^n h_j}. \quad (23)$$

(3) *Combination Weighting Method*. In this part, the subjective weight method and the objective weight method are effectively combined according to the objective needs. The operation method is as follows:

$$w_j = \frac{t_j v_j}{\sum_{j=1}^n t_j v_j}. \quad (24)$$

In the above formula, t_j and v_j refer to the weight coefficient corresponding to the j index obtained by the method of AHP and entropy, and w_j refers to the corresponding combination weight coefficients.

3.3.3. *Multiattribute Decision Method Based on Improved TOPSIS*. At present, assuming that the decision matrix formed by m scheme and n attributes is $X = (x_{ij})_{m \times n}$; at this time, x_{ij} mainly refers to the attribute value of item j , and the operating process of the TOPSIS method after adjustment is as follows:

Step 1: firstly, the decision matrix R is established according to the standard, and the operation method of R_{ij} is referred to as formulas (13) and (14) at this time.

Step 2: the weighted decision matrix V is established by the decision matrix R , and V_{ij} is given by

$$V_{ij} = w_j R_{ij}. \quad (25)$$

At this time, w_j mainly refers to the weight coefficients corresponding to the attribute j ; $\sum_{j=1}^n w_j = 1$, solved by formula (24).

Step 3: the ideal solution V^+ and the negative ideal solution V^- are clarified, which meet the following requirements:

$$V_j^+ = \begin{cases} \max\{V_{1j}, V_{2j}, \dots, V_{mj}\}, & \text{Item } j \text{ is a benefit attribute,} \\ \min\{V_{1j}, V_{2j}, \dots, V_{mj}\}, & \text{Item } j \text{ is a cost attribute,} \end{cases}$$

$$V_j^- = \begin{cases} \min\{V_{1j}, V_{2j}, \dots, V_{mj}\}, & \text{Item } j \text{ is a benefit attribute,} \\ \max\{V_{1j}, V_{2j}, \dots, V_{mj}\}, & \text{Item } j \text{ is a cost attribute.} \end{cases} \quad (26)$$

Step 4: the distance between the two points of all schemes are D^+ , D^- ; at that time, D^+ and D^- are given by

$$D_i^+ = \sqrt{\sum_{j=1}^n (V_{ij} - V_j^+)^2},$$

$$D_i^- = \sqrt{\sum_{j=1}^n (V_{ij} - V_j^-)^2}. \quad (27)$$

Step 5: the approximate horizontal C_i of each scheme i to the ideal solution is calculated using the following equation:

$$C_i = \frac{D_i^+}{D_i^+ + D_i^-}. \quad (28)$$

Step 6: according to the relative degree of approximation C_i in Step 5, all the schemes are ranked reasonably according to the method of descending order, so as to optimize the selection of the schemes and obtain the corresponding optimal production planning.

4. Case Analysis

4.1. *Formulation of Production Planning of Company A in Cloud Manufacturing Environment*. Company A receives an order for automobile production and processing. Because of the limitation of production capacity and the high cost of production, some production tasks need to be handed over to some manufacturers through the cloud manufacturing platform. The enterprise decomposes the automobile processing order according to the modularization theory and concludes that there are three kinds of specific modules that need to be produced and processed, which are recorded as Module 1, Module 2, and Module 3. After that, the enterprise submits specific module requirements to the cloud manufacturing platform. Due to the large difference in the type and functional requirements of the module, some candidate resources can be processed, some cannot be processed, and some candidate resources can be partially processed. Company A needs to work out a production planning for the order according to the specific needs of the customers, combined with the manufacturing resources and manufacturing capabilities of the enterprise and the manufacturers in the cloud manufacturing platform, and the production planning is optimized according to the preferences of the decision makers and the objective situation. The specific process is shown in Figure 3.

As company A still needs to assemble the parts after the processing module to form the product in the order for delivery, according to the requirements of quantity, delivery time, and quality of products required by the project order, company A adjusts the specific requirements of the order according to its own processing conditions as shown in Table 4.

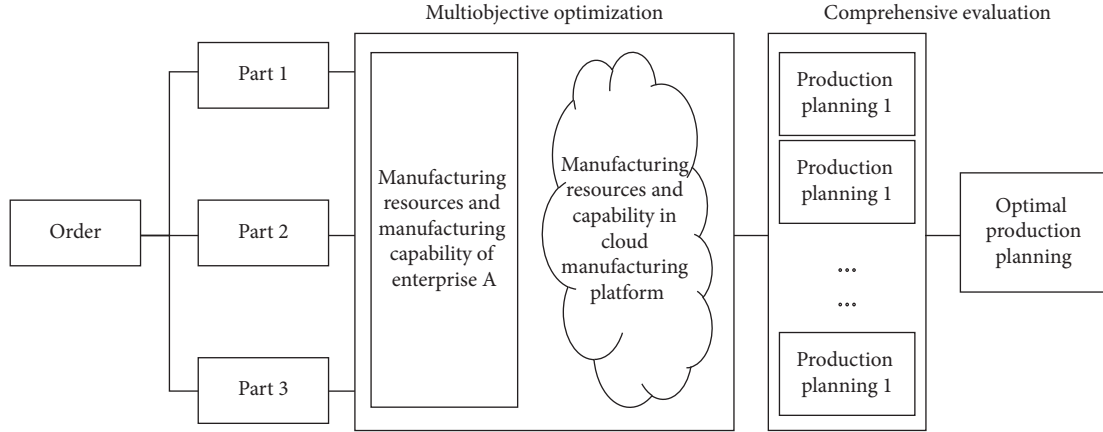


FIGURE 3: Production planning and optimizing process of enterprise A in cloud manufacturing environment.

According to the functional requirements of the parts, company A searches and matches the manufacturing resources using the cloud manufacturing platform and finds out five production suppliers that can meet the requirements of the module tasks. According to the situation of company A, the specific parameters of the manufacturer of its manufacturing module can be obtained from the enterprise and cloud manufacturing platform as shown in Table 5.

In addition, because these enterprises are mass customization production enterprises, when the number of production batches reaches a certain level, there is also a certain discount. The specific discount stage is as follows:

$$\begin{cases} k = 1, & 0 \leq x_{ij} \leq 500, \\ k = 2, & 501 \leq x_{ij} \leq 1000, \\ k = 3, & 1001 \leq x_{ij} \leq 1500, \\ k = 4, & x_{ij} \geq 1501. \end{cases} \quad (29)$$

The corresponding discount rate is given by

$$\begin{cases} r_{ij1} = 0.90, & k = 1, \\ r_{ij2} = 0.85, & k = 2, \\ r_{ij3} = 0.80, & k = 3, \\ r_{ij4} = 0.75, & k = 4. \end{cases} \quad (30)$$

According to the multiobjective optimization model proposed above, this paper uses the operation software of Matlab2017a and the NSGA-II algorithm to solve the model above. The RAM of CPU is 4G, 2.5 GHz. The initial population is $N = 100$, the maximum iteration number is $\text{maxgen} = 200$, the crossover probability is $P_c = 0.90$, and the mutation probability is $P_m = 0.05$. The ratio of the complete dominating set problem is shown in Figure 4, which shows that the proportion of complete

TABLE 2: Scale value of decision judgment matrix.

Order of importance	Value of a_{ij}
Element a_i is as important as element a_j	1
Element a_i is slightly more important than element a_j	3
Element a_i is obviously more important than element a_j	5
Element a_i is mightily more important than element a_j	7
Element a_i is extremely more important than element a_j	9
The intermediate value of the adjacent judgment above	2, 4, 6, 8

TABLE 3: The value of the mean random consistency index RI of n -order decision judgment matrix.

n	1	2	3	4	5	6	7	8
RI	0	0	0.52	0.89	1.12	1.26	1.36	1.41

TABLE 4: The specific needs of the order.

Index	Module 1	Module 2	Module 3
Quantity demanded	3000	3500	4000
Maximum delivery cost		15000	
Latest delivery time		70000	
Minimum qualified rate		80%	

nondominating set problem to population tends to be stable after 60 generations of program operation. The Pareto frontier map obtained by running the program based on three dimensions selected is shown in Figure 5, from which we can obtain the solution set of Pareto. The running time of the program is 33.56 s.

Table 6 is the production planning information set corresponding to all completely nondominating set problem obtained by the algorithm. The results of calculation include 20 groups of noninferior solutions, and each

TABLE 5: A enterprise and manufacturers on cloud platform.

Manufacturer	Type of production module	Productive capacity	Production unit price	Production unit time	Product percent of pass (%)	Delivery time	Delivery cost per batch
Company A	Module 1	1000	10	5	92		
	Module 2	—	—	—	—	—	—
	Module 3	2000	14	10	95		
Cloud manufacturer1	Module 1	3000	13	4	90		
	Module 2	2000	25	12	92	3	23
	Module 3	1000	12	11	85		
Cloud manufacturer 2	Module 1	—	—	—	—		
	Module 2	1000	20	6	85	6	25
	Module 3	2000	14	8	92		
Cloud manufacturer 3	Module 1	3000	11	7	82		
	Module 2	1500	22	5	90	4	23
	Module 3	1500	13	8	85		
Cloud manufacturer 4	Module 1	1000	10	8	80		
	Module 2	1500	21	6	88	6	25
	Module 3	—	—	—	—		
Cloud manufacturer 5	Module 1	2000	12	2	82		
	Module 2	1000	23	8	82	3	23
	Module 3	1000	13	10	80		

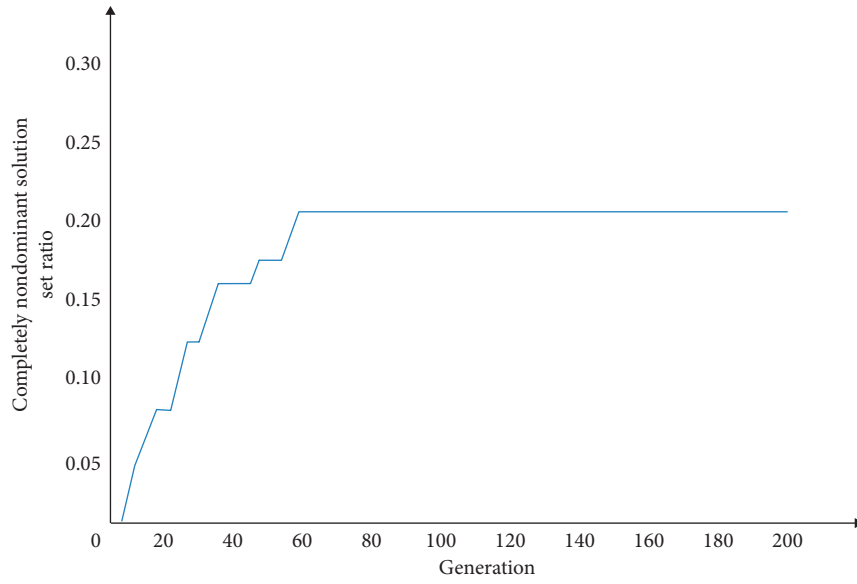


FIGURE 4: Proportion of completely nondominant solution sets.

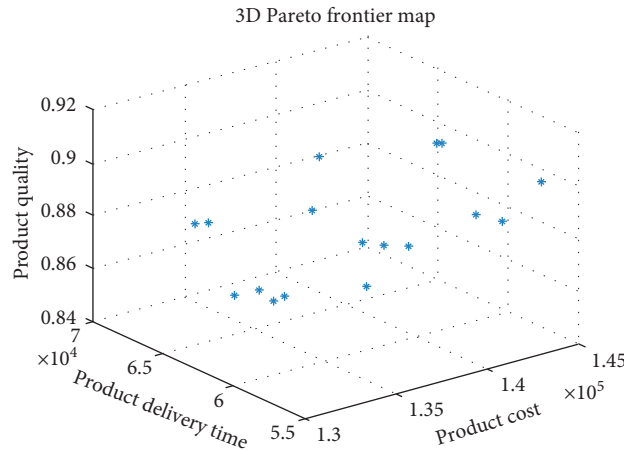


FIGURE 5: Solution set of Pareto.

TABLE 6: Production planning set corresponding to completely nondominating solutions obtained by NSGA-II.

Number	Type of modules	Company A	Cloud manufacturer					Cost	Delivery time	Product quality (%)
			1	2	3	4	5			
Scheme 1	Module 1	251	1570	—	715	256	208	13581	58053	87.14
	Module 2	—	17	926	1150	549	858			
	Module 3	285	908	1892	172	—	773			
Scheme 2	Module 1	254	1571	—	715	255	205	14155	55959	89.06
	Module 2	—	17	926	1453	169	935			
	Module 3	1908	16	1863	174	—	39			
Scheme 3	Module 1	254	21	—	715	2556	1754	13453	62239	85.98
	Module 2	—	17	926	1455	170	932			
	Module 3	285	907	1863	172	—	773			
Scheme 4	Module 1	254	1571	—	715	256	204	14265	61662	90.38
	Module 2	—	1852	258	1150	170	70			
	Module 3	1908	16	1863	175	—	38			
Scheme 5	Module 1	254	1570	—	715	256	205	13915	59417	87.71
	Module 2	—	773	328	1454	169	776			
	Module 3	285	907	1863	172	—	773			
Scheme 6	Module 1	19	21	—	715	735	1510	14038	67404	88.90
	Module 2	—	1852	328	1150	170	—			
	Module 3	1908	16	1863	172	—	41			
Scheme 7	Module 1	251	1570	0	716	256	207	13751	60622	87.88
	Module 2	—	773	928	1453	169	177			
	Module 3	285	907	1863	172	—	773			
Scheme 8	Module 1	19	21	0	715	255	1990	13523	68547	87.10
	Module 2	—	1852	328	1150	170	—			
	Module 3	285	907	1862	174	—	772			
Scheme 9	Module 1	254	1570	—	715	256	205	13846	60305	87.65
	Module 2	—	773	925	1150	169	483			
	Module 3	286	907	1863	173	—	771			
Scheme 10	Module 1	254	1571	—	716	256	203	14246	61801	90.41
	Module 2	—	1852	328	1150	170	—			
	Module 3	1909	18	1863	175	—	35			
Scheme 11	Module 1	254	1570	—	715	256	205	14155	55964	89.06
	Module 2	—	17	926	1453	170	934			
	Module 3	1909	15	1863	174	—	39			
Scheme 12	Module 1	19	21	—	715	735	1510	13312	63953	85.88
	Module 2	—	17	928	1455	549	551			
	Module 3	284	908	1862	172	—	774			
Scheme 13	Module 1	19	21	—	715	256	1989	13431	62712	85.76
	Module 2	—	17	928	1454	170	931			
	Module 3	285	907	1863	172	—	773			
Scheme 14	Module 1	19	21	—	715	735	151	13486	69030	87.01
	Module 2	—	1852	328	1150	170	—			
	Module 3	284	908	1862	172	—	774			
Scheme 15	Module 1	254	21	—	173	256	1753	13371	63004	86.20
	Module 2	—	18	928	1455	549	550			
	Module 3	285	907	1863	716	—	772			
Scheme 16	Module 1	254	1571	—	715	255	205	14494	57565	89.52
	Module 2	—	774	258	1368	169	931			
	Module 3	1909	16	1863	174	—	38			
Scheme 17	Module 1	254	1570	—	715	256	205	13695	63430	88.51
	Module 2	0	1852	328	1150	170	—			
	Module 3	284	907	1863	174	—	772			
Scheme 18	Module 1	253	1571	—	715	255	206	14074	56722	89.28
	Module 2	—	18	926	1453	548	555			
	Module 3	1909	16	1863	174	—	38			

TABLE 6: Continued.

Number	Type of modules	Company A	Cloud manufacturer					Cost	Delivery time	Product quality (%)
			1	2	3	4	5			
Scheme 19	Module 1	19	21	—	715	735	1510	14038	67404	88.91
	Module 2	—	1852	328	1150	170	—			
	Module 3	1908	16	1863	172	—	41			
Scheme 20	Module 1	20	21	—	715	735	1509	13313	63594	85.89
	Module 2	—	18	928	1455	549	550			
	Module 3	285	908	1862	172	—	773			

TABLE 7: Comprehensive ranked list of the production planning scheme.

Number	Product cost	Delivery time	Product quality (%)	Relative proximity	Rank
1	13581	58053	87.14	0.742858	6
2	14155	55959	89.06	0.454256	14
3	13453	62239	85.98	0.789696	1
4	14265	61662	90.38	0.240388	19
5	13915	59417	87.71	0.591227	8
6	14038	67404	88.90	0.303556	17
7	13751	60622	87.88	0.582332	9
8	13523	68547	87.10	0.569427	11
9	13846	60305	87.65	0.598745	7
10	14246	61801	90.41	0.238531	20
11	14155	55964	89.06	0.454184	15
12	13312	36953	85.88	0.759994	5
13	13431	32712	85.76	0.787249	2
14	13486	69030	87.01	0.573461	10
15	13371	63004	86.20	0.765317	4
16	14494	57565	89.52	0.356862	16
17	13695	63430	88.51	0.471384	12
18	14074	56722	89.28	0.434359	13
19	14038	67404	88.91	0.302320	18
20	13313	63594	85.89	0.768361	3

TABLE 8: Final optimum production planning scheme.

Type of production	Company A	Cloud manufacturer					Product cost	Delivery time	Product quality
		1	2	3	4	5			
Module 1	254	21	—	715	2556	1754	13453	62239	85.98
Module 2	—	17	926	1455	170	932			
Module 3	285	907	1863	172	—	773			

group of noninferior solutions corresponds to a production planning.

4.2. Optimization of Production Planning of Company A in Cloud Manufacturing Environment

4.2.1. Weight Determination. According to the comprehensive evaluation model, firstly, the comprehensive weight is determined from subjective and objective aspects by using the AHP and the entropy weight method. According to the preference degree of company A for product cost, product

delivery time, and product quality, the decision judgment matrix is obtained as follows:

$$B = \begin{bmatrix} 1 & 3 & \frac{1}{2} \\ \frac{1}{3} & 1 & 2 \\ 2 & \frac{1}{2} & 1 \end{bmatrix}. \tag{31}$$

By the method of AHP, it can be considered that the weight vector of preference of company A for product cost,

product delivery time, and product quality are $T = [0.369841, 0.297884, 0.332275]$.

Secondly, according to the method of entropy, each group of production planning schemes is weighted objectively. Because there are different quantitative levels and dimensions among different evaluation indicators, it is necessary to standardize the data of product cost, product delivery time, and product quality indicators to obtain the following data preprocessing matrix:

$$\begin{bmatrix} 0.77242 & 0.839798 & 0.296774 \\ 0.286802 & 1 & 0.709677 \\ 0.880711 & 0.519547 & 0.047312 \\ 0.193739 & 0.563691 & 0.993548 \\ 0.489848 & 0.735445 & 0.419355 \\ 0.385787 & 0.124398 & 0.675269 \\ 0.628596 & 0.643256 & 0.455914 \\ 0.821489 & 0.036952 & 0.288172 \\ 0.548223 & 0.667508 & 0.406452 \\ 0.209814 & 0.553056 & 1 \\ 0.286802 & 0.999617 & 0.709677 \\ 1 & 0.388417 & 0.025806 \\ 0.899323 & 0.48336 & 0 \\ 0.852792 & 0 & 0.268817 \\ 0.950085 & 0.461021 & 0.094624 \\ 0 & 0.877133 & 0.808602 \\ 0.675973 & 0.428429 & 0.591396 \\ 0.35533 & 0.941627 & 0.756989 \\ 0.385787 & 0.124398 & 0.677419 \\ 0.999154 & 0.415882 & 0.027957 \end{bmatrix} \quad (32)$$

According to the calculation formula of the entropy weight method, the objective index weight vector $V = [0.246654, 0.303342, 0.450004]$ is obtained by calculating the three indexes of product cost, product delivery time, and product quality.

Then according to the formula of the combination weighting method established in Section 3.3.2, the subjective weight obtained by AHP and objective weight obtained by entropy weight method are synthesized, and the final combination weight vector is $W = [0.275508, 0.272903, 0.451589]$.

4.2.2. Optimal Selection of Production Planning Based on TOPSIS Method. According to the relevant steps of the TOPSIS method, the weight vector values calculated in the previous section are calculated into the model, and the weighted decision matrix V is obtained as follows:

$$\begin{bmatrix} 0.212808 & 0.229184 & 0.13402 \\ 0.079016 & 0.272903 & 0.320483 \\ 0.242643 & 0.141786 & 0.021366 \\ 0.053377 & 0.153833 & 0.448676 \\ 0.134957 & 0.200705 & 0.189376 \\ 0.106287 & 0.033948 & 0.304944 \\ 0.173183 & 0.175547 & 0.205886 \\ 0.226327 & 0.010084 & 0.130135 \\ 0.15104 & 0.182165 & 0.183549 \\ 0.057805 & 0.150931 & 0.451589 \\ 0.079016 & 0.272799 & 0.320483 \\ 0.275508 & 0.106 & 0.011654 \\ 0.247771 & 0.131911 & 0 \\ 0.234951 & 0 & 0.121395 \\ 0.261756 & 0.125814 & 0.042731 \\ 0 & 0.239372 & 0.365156 \\ 0.186236 & 0.11692 & 0.267069 \\ 0.097896 & 0.256973 & 0.341848 \\ 0.106287 & 0.033948 & 0.305915 \\ 0.275275 & 0.113496 & 0.012625 \end{bmatrix} \quad (33)$$

The positive ideal solution V^+ and the negative ideal solution V^- are determined, and the distance from the point corresponding to each production planning scheme to the positive ideal solution and the negative ideal solution is calculated, respectively. Then the relative proximity of each scheme to the ideal solution is calculated, and then each production planning scheme is sorted according to the relative distance, and the comprehensive ranking table is shown in Table 7.

According to the comprehensive ranking calculated by the comprehensive ranking table of production planning schemes, company A can choose the highest comprehensive ranking, that is, production planning Scheme 3 (as shown in Table 8) to arrange production. If there is a change in the actual production, the decision makers can also use the scheme close to the optimal production scheme as the final implementation scheme, in order to improve the flexibility of the production plan.

5. Conclusion

- (1) In this paper, the achievements of domestic and foreign scholars in cloud manufacturing, mass customization, multiobjective optimization, and so on are thoroughly studied and sorted out, the characteristics and attributes of cloud manufacturing system are summarized, and the operation process of cloud manufacturing service platform is systematically introduced.

- (2) The current background is that the manufacturing resources and manufacturing capacity of cloud manufacturing are distributed in different geographical regions. Mass customization enterprises have large manufacturing batches and limited production capacity. Under the premise of meeting the needs of customers, in order to improve the profit of enterprises, the cost, time, and quality that customers are most concerned about are taken as the index, and a multiobjective mathematical model for the production planning of mass customization enterprises in cloud manufacturing environment with the lowest cost, the shortest time, and the highest quality is established. In view of the shortcomings of the traditional multiobjective optimization problem, the algorithm of NSGA-II is used to solve the above multiobjective optimization model.
- (3) The index evaluation model of mass customization enterprise production planning optimization under cloud manufacturing environment is established, and the calculation method of weight coefficient in comprehensive evaluation is improved. The method of combining AHP with entropy weight is used to combine subjective and objective weighting, which is applied to the improved TOPSIS multiattribute decision method, and select the optimal production plan according to the final order.
- (4) Company A is taken as an example to make a case study. According to the needs of customers, combined with the company's own production capacity constraints, the manufacturing resources and manufacturing capacities that meet the manufacturing conditions are searched from the cloud manufacturing platform. According to the multiobjective optimization model proposed above, a set of Pareto solutions satisfying the conditions are solved. According to the comprehensive evaluation model proposed above, the optimal production planning is selected according to the final ranking by using the combined weighting method and TOPSIS, which provides a reference for mass customization enterprises to formulate and optimize the production planning and then verifies the effectiveness of the production planning and optimization method for mass customization enterprises in cloud manufacturing environment.

- [2] L. Du, L. Chen, L. Dai, L. Zhang, and Y. Shen, "Blockchain-based architecture model of cloud manufacturing platform system," *Information Technology and Network Security*, vol. 1, pp. 101–105, 2019.
- [3] E. Qi, T. Li, L. Liang, and Y. Huang, "The review of manufacturing theory, technologies and application states," *Industrial Engineering and Management*, vol. 20, no. 1, pp. 8–14, 2015.
- [4] S. Huang and B. Huang, "Security architecture for cloud manufacturing platform," *Computer Integrated and Manufacturing Systems*, vol. 24, no. 4, pp. 851–861, 2018.
- [5] Y. Chen and W. Zhongjie, "Research on the cloud manufacturing service discovery for industry manufacturing system based on ontology," *Advanced Materials Research*, vol. 712–715, pp. 2639–2643, 2013.
- [6] Y. Zhang, Q. Zhou, and L. Qiang, "Cloud manufacturing service composition based on dynamic parameters ant colony algorithm," *Computer Technology and Development*, vol. 28, no. 1, pp. 127–130, 2018.
- [7] B. Zhou, H. Shi, and J. Cai, "Research on the conceptual model of mass customization production," *Journal of Shanghai University of Engineering Science*, vol. 4, pp. 278–284, 2000.
- [8] L. Liu, D. Xu, and J. Du, "Techniques research for product family variant design under in mass customization," *Aviation Precision Manufacturing Technology*, vol. 51, no. 6, pp. 32–35, 2015.
- [9] I. Cariaga, T. El-Diraby, and H. Osman, "Integrating value analysis and quality function deployment for evaluating design alternatives," *Journal of Construction Engineering and Management*, vol. 133, no. 10, pp. 761–770, 2007.
- [10] Y. Wu, Y. Sheng, and N. Cai, "Mass intelligent customization based on Internet+: a case study of Qingdao red collar clothing and Foshan Weishang furniture," *Chinese Industrial Economy*, vol. 4, pp. 127–143, 2016.
- [11] B. R. Katzy, "Design and implementation of virtual organizations," in *Proceedings of the Hawaii international Conference on System Sciences*, p. 142, IEEE Computer Society, Kohala Coast, HI, USA, January 1998.

Data Availability

The data used to support the findings of this study are available from the corresponding author upon request.

Conflicts of Interest

The authors declare that they have no conflicts of interest.

References

- [1] B. Li, L. Zhang, and S. Wang, "Cloud manufacturing: a new service-oriented networked manufacturing model," *Computer Integrated Manufacturing Systems*, vol. 16, no. 1, pp. 1–7, 2010.

Research Article

Distributed Control and the Lyapunov Characteristic Exponents in the Model of Infectious Diseases

M. Bershadsky,¹ M. Chirkov,² A. Domoshnitsky ,¹ S. Rusakov,² and I. Volinsky ¹

¹Ariel University, Ariel, Israel

²Perm State University, Perm, Russia

Correspondence should be addressed to A. Domoshnitsky; adom@ariel.ac.il

Received 25 May 2019; Revised 22 September 2019; Accepted 14 October 2019; Published 13 November 2019

Academic Editor: Hassan Zargarzadeh

Copyright © 2019 M. Bershadsky et al. This is an open access article distributed under the Creative Commons Attribution License, which permits unrestricted use, distribution, and reproduction in any medium, provided the original work is properly cited.

The Marchuk model of infectious diseases is considered. Distributed control to make convergence to stationary point faster is proposed. Medically, this means that treatment time can be essentially reduced. Decreasing the concentration of antigen, this control facilitates the patient's condition and gives a certain new idea of treating the disease. Our approach involves the analysis of integro-differential equations. The idea of reducing the system of integro-differential equations to a system of ordinary differential equations is used. The final results are given in the form of simple inequalities on the parameters. The results of numerical calculations of simulation models and data comparison in the case of using distributive control and in its absence are given.

1. Introduction

Distributed feedback control system is a challenging problem, but only a few papers were devoted to it (see, for example, [1] and literature therein). A noise in the feedback delay control is one of the main reasons for developing mathematical models with distributed inputs. The second one is resulted from the fact that the dynamics of the processes rather depends on the average value of the process than on the value at a corresponding moment.

We propose a method reducing the stability analysis of the system with memory to the analysis of a corresponding finite-dimensional system. This idea was proposed, as well as we know, in [2] and realized, in finite spectrum assignment (see, for example, [3–6]). Our realization of this idea is different. We propose a simple method that allows to reduce the analysis of systems with memory to one of a higher order but finite-dimensional systems. Questions of stability and estimates of solutions can be considered on this base.

The model of infectious diseases, constructed by Marchuk in his well-known book [7], reflects the most significant patterns of the immune system acting during these diseases. This model was studied in many works; note, for example, the recent papers [8–12] and the bibliography

therein. The adding control was proposed, for example, in [11–14]. In [10, 15], the basic mathematical model that takes into account the concentrated control of the immune response was proposed. It can be noted that the use of information about behavior of a disease and the immune system for a long time (defined by distributed control, for example, in the form of an integral term) looks very natural in choosing strategy of a possible treatment. Optimal control in the basic model of the infectious diseases was considered in the work [15], where the control function characterizing the realization of an immunotherapy which consists in administration of ready immunoglobulins or donor antibodies is proposed. In [16], the model of influence of an immunotherapy on dynamics of an immune response which represents a generalization of basic model was considered. On the basis of the proposed model, the problem of determination of coefficients on the basis of laboratory data was considered and also the management was proposed in [13, 14, 17]. Such task is called control in uncertain conditions [11]. The control algorithm in the case of uncertain conditions was proposed in the work ([15], see pages 71–73).

The Lyapunov exponents characterize the rate at which solutions approach each other with increasing time. In our case, one of these solutions is a certain stationary state of the system.

The stationary state determines the conditions of recovery of the body after exposure to infection. The speed of approaching this state has a very important role. It allows us to estimate the duration of treatment. In some cases, this can determine the choice of treatment strategy. It is enough to imagine a situation when the patients' body is weakened by some chronic diseases and is not able to endure too long treatment.

Our approach to treatment modeling can be described as follows. We introduce a distributed feedback control in the form of an integral term. This management is based on long-term monitoring of the patient's condition and comparing the patients' condition with a certain stationary state over a long period of time. Thus, a closed controlled system, the purpose of which is to improve the patient's condition, is created. Intuitively, such a treatment strategy is understandable. Further, the scheme of reducing the integro-differential system to a system of ordinary differential equations is proposed. This ordinary differential system is studied. The technique based on properties of the Cauchy matrices is used to estimate possible deviations of solutions in the case of various modifications of this model, such as nonlinear models or delay models, from the solution of this system ordinary differential equation. Note the papers [1, 18–21] where the distributed control was also considered for various problems.

In this paper, we consider the Marchuk model of infectious diseases [7]:

$$\begin{cases} \frac{dV}{dt} = \beta V(t) - \gamma F(t)V(t), \\ \frac{dC}{dt} = \zeta(m)\alpha F(t)V(t) - \mu_c(C(t) - C^*), \\ \frac{dF}{dt} = \rho C(t) - \eta\gamma F(t)V(t) - \mu_f F(t), \\ \frac{dm}{dt} = \sigma V(t) - \mu_m m(t), \end{cases} \quad (1)$$

where $V(t)$ is the antigen concentration rate, $C(t)$ is the plasma cell concentration rate, $F(t)$ is the antibody concentration rate, and $m(t)$ is the relative features of the body. Denote $\alpha, \beta, \gamma, \rho, \sigma, \eta, \mu_c, \mu_f$, and μ_m as corresponding coefficients described in [7]. $\zeta(m)$ takes into account the destruction of the normal functioning immune system, $\zeta(0) = 1$. Denote C^* as the plasma rate concentration of the healthy body and F^* the antibody concentration that we wish to achieve after the treatment.

Let us discuss every equation in the model (1) in more detail. The first equation $dV/dt = \beta V(t) - \gamma F(t)V(t)$ presents the block of the virus dynamics. It describes the change in the antigen concentration rate and includes the amount of antigen in the blood. Antigen concentration decreases as a result of interaction with antibodies. The immune process is characterized by the number of antibodies, whose concentration is described by the equation $dF/dt = \rho C(t) - \eta\gamma F(t)V(t) - \mu_f F(t)$. The value of $F(t)$ decreases as a result of the interaction and mutual destruction with antigens. The amount of the antibody cells also decreases as a result of

natural destruction. However, the plasma restores antibodies and therefore the plasma state plays an important role in the immune process. Thus, the change in the plasma cell concentration rate is included in several equations of the system. Taking into account the healthy body level of plasma cells and their natural aging, the term $\mu_c(C(t) - C^*)$ is included in the second equation of system (1). It is assumed that the plasma is restored as a result of the interaction of the antigen and the antibody cells. The second and third equations present the block of the humoral immune response dynamics.

Concerning the last equation $dm/dt = \sigma V(t) - \mu_m m(t)$ of system (1), we can note the following. The value of m increases with the antigen's concentration rate $V(t)$. The maximum value of m is 1 in the case of 100% organ damage and is equal to 0 for a fully healthy organ. The coefficient μ_m describes the rate of degeneration of the target organ.

The main goal of this paper is to demonstrate new ideas in the use of distributed control in the model of infectious diseases [7]. Our goal is to make convergence to a stationary point faster. This allows us to decrease the duration of disease's treatment. We add a distributed control in the equation describing antibody concentration rate. Numerical simulations demonstrate that this approach could open some new possibilities for a treatment.

2. Modeling Distributed Control

Let us consider the following system:

$$\begin{cases} \frac{dV}{dt} = \beta V(t) - \gamma F(t)V(t), \\ \frac{dC}{dt} = \zeta(m)\alpha F(t)V(t) - \mu_c(C(t) - C^*), \\ \frac{dF}{dt} = \rho C(t) - \eta\gamma F(t)V(t) - \mu_f F(t) - bu(t), \\ \frac{dm}{dt} = \sigma V(t) - \mu_m m(t). \end{cases} \quad (2)$$

Comparing this system with the model of Marchuk (1), we see the control $u(t)$ added in the third equation describing the antibody concentration rate. Note that this control is a reasonable one from the medical point of view [10, 15].

We choose the control $u(t)$ in the following form:

$$u(t) = \int_0^t (F(s) - F^*)e^{-k(t-s)} ds. \quad (3)$$

It can be noted that influence of a corresponding average value instead of $F(t) - F^*$ at the point t looks reasonable since the control $u(t)$ is rather dependent on an "average" value of the difference $F(s) - F^*$ on a corresponding time-interval than on this difference at the moment t only. The integral term in (3) increases the influence of the previous moments which are closer to the current moment t .

Following [15], we can pass to the dimensionless case, substituting $V(t) = v(t)V_m, C(t) = s(t)C^*, F(t) = f(t)F^*$, and $u(t) = \tilde{u}(t)F^*$ in (2). In the dimensionless case, system (2) is of the following form:

$$\left\{ \begin{array}{l} \frac{dv}{dt} = \beta v(t) - \gamma F^* f(t)v(t), \\ \frac{ds}{dt} = \alpha V_m \frac{F^*}{C^*} \zeta(m) f(t)v(t) - \mu_c(s(t) - 1), \\ \frac{df}{dt} = \frac{\rho C^*}{F^*} s(t) - \eta \gamma V_m f(t)v(t) - \mu_f f(t) \\ \quad - b \int_0^t (f(s) - 1)e^{-k(t-s)} ds, \\ \frac{dm}{dt} = \sigma V_m v(t) - \mu_m m(t). \end{array} \right. \quad (4)$$

Consider the system

$$\left\{ \begin{array}{l} \frac{dv}{dt} = \beta v(t) - \gamma F^* f(t)v(t), \\ \frac{ds}{dt} = \alpha V_m \frac{F^*}{C^*} \zeta(m) f(t)v(t) - \mu_c(s(t) - 1), \\ \frac{df}{dt} = \frac{\rho C^*}{F^*} s(t) - \eta \gamma V_m f(t)v(t) - \mu_f f(t) - b\bar{u}(t), \\ \frac{dm}{dt} = \sigma V_m v(t) - \mu_m m(t), \\ \frac{d\bar{u}}{dt} = f(t) - 1 - k\bar{u}(t). \end{array} \right. \quad (5)$$

Denoting in (5)

$$\begin{aligned} \alpha_1 &= \beta, \\ \alpha_2 &= \gamma F^*, \\ \alpha_3 &= \alpha V_m \frac{F^*}{C^*}, \\ \alpha_4 &= \mu_f = \frac{\rho C^*}{F^*}, \\ \alpha_5 &= \mu_c, \\ \alpha_6 &= \sigma V_m, \\ \alpha_7 &= \mu_m, \\ \alpha_8 &= \eta \gamma V_m, \end{aligned} \quad (6)$$

we obtain

$$\left\{ \begin{array}{l} \frac{dv}{dt} = \alpha_1 v(t) - \alpha_2 f(t)v(t), \\ \frac{ds}{dt} = \alpha_3 \zeta(m) f(t)v(t) - \alpha_5 (s(t) - 1), \\ \frac{df}{dt} = \alpha_4 (s(t) - f(t)) - \alpha_8 f(t)v(t) - b\bar{u}(t), \\ \frac{dm}{dt} = \alpha_6 v(t) - \alpha_7 m(t), \\ \frac{d\bar{u}}{dt} = f(t) - 1 - k\bar{u}(t). \end{array} \right. \quad (7)$$

Let us find possible stationary points of system (7). Their coordinates v, s, f, m , and \bar{u} satisfy the following algebraic system:

$$\left\{ \begin{array}{l} \alpha_1 v - \alpha_2 f v = 0, \\ \alpha_3 \zeta(m) f v - \alpha_5 (s - 1) = 0, \\ \alpha_4 (s - f) - \alpha_8 f v - b\bar{u} = 0, \\ \alpha_6 v - \alpha_7 m = 0, \\ f - 1 - k\bar{u} = 0. \end{array} \right. \quad (8)$$

Only in two cases, the first equation is satisfied: $v = 0$ or $f = \alpha_1/\alpha_2$. Let us start with the first case. If $v = 0$, then $s = 1$ from the second equation and $m = 0$ from the fourth one. We have the system for f and \bar{u} :

$$\left\{ \begin{array}{l} \alpha_4 - \alpha_4 f - b\bar{u} = 0, \\ f - k\bar{u} = 1. \end{array} \right. \quad (9)$$

From the last equation, we have $\bar{u} = (f - 1)/k$, and substituting this into the first one, we obtain $f = 1$, and then $\bar{u} = 0$. Thus, starting with $v = 0$, we can come only to the stationary point $v = m = \bar{u} = 0, s = f = 1$. In the second case of $f = \alpha_1/\alpha_2$, we consider only the case of $v \neq 0$, since in the case of $v = 0$, we come to the same stationary point. From the fourth equation $\alpha_6 v = \alpha_7 m$, we obtain that $m \neq 0$. This means that there is no possibility to completely disinfect the affected organ. That is why we study below the behavior of solutions only in the neighborhood of the noted above stationary point $v = m = \bar{u} = 0, s = f = 1$.

Remark 1. It was obtained in [15] on the basis of the laboratory data that $\alpha_1 = 0.25; \alpha_2 = 8.5000332; \alpha_3 = 1792175675; \alpha_4 = 1.95992344 \cdot 10^{-7}; \alpha_5 = 0.5; \alpha_6 = 10; \alpha_7 = 0.4; \alpha_8 = 1.7 \cdot 10^{-3}$.

It was noted above that $\zeta(0) = 1$. Linearizing systems (7) and (4) in the neighborhood of the stationary point, we obtain the corresponding linear systems:

$$\left\{ \begin{array}{l} \frac{dx_1}{dt} = (\alpha_1 - \alpha_2)x_1, \\ \frac{dx_2}{dt} = \alpha_3 x_1 - \alpha_5 x_2, \\ \frac{dx_3}{dt} = -\alpha_8 x_1 + \alpha_4 x_2 - \alpha_4 x_3 - b x_5, \\ \frac{dx_4}{dt} = \alpha_6 x_1 - \alpha_7 x_4, \\ \frac{dx_5}{dt} = x_3 - k x_5, \end{array} \right. \quad (10)$$

$$\left\{ \begin{array}{l} \frac{dx_1}{dt} = (\alpha_1 - \alpha_2)x_1, \\ \frac{dx_2}{dt} = \alpha_3 x_1 - \alpha_5 x_2, \\ \frac{dx_3}{dt} = -\alpha_8 x_1 + \alpha_4 x_2 - \alpha_4 x_3 - b \int_0^t x_3(s) e^{-k(t-s)} ds, \\ \frac{dx_4}{dt} = \alpha_6 x_1 - \alpha_7 x_4, \end{array} \right. \quad (11)$$

where $x_1 = v, x_2 = s - 1, x_3 = f - 1, x_4 = m, x_5 = \bar{u}$, respectively. Denote the matrix of the coefficients of system (10):

$$A = \begin{pmatrix} \alpha_1 - \alpha_2 & 0 & 0 & 0 & 0 \\ \alpha_3 & -\alpha_5 & 0 & 0 & 0 \\ -\alpha_8 & \alpha_4 & -\alpha_4 & 0 & -b \\ \alpha_6 & 0 & 0 & -\alpha_7 & 0 \\ 0 & 0 & 1 & 0 & -k \end{pmatrix}. \quad (12)$$

Note that a corresponding linear system for the Marchuk model of infectious diseases without control (see system (1)) can be written in the form:

$$\begin{cases} \frac{dx_1}{dt} = (\alpha_1 - \alpha_2)x_1, \\ \frac{dx_2}{dt} = \alpha_3x_1 - \alpha_5x_2, \\ \frac{dx_3}{dt} = -\alpha_8x_1 + \alpha_4x_2 - \alpha_4x_3, \\ \frac{dx_4}{dt} = \alpha_6x_1 - \alpha_7x_4. \end{cases} \quad (13)$$

3. About Comparison of the Lyapunov Exponents

Our approach is based on the following auxiliary assertion.

Lemma 1. *The solution-vector $col(v(t), s(t), f(t), m(t))$ of system (4) and 4 first components of the solution-vector $col(v(t), s(t), f(t), m(t), \bar{u}(t))$ of system (5) satisfying the condition $\bar{u}(0) = 0$ coincide.*

Proof of Lemma 1. Let us consider the last equation of system (5). Using the representation of solution of the first-order scalar equation, we can write $\bar{u}(t) = \int_0^t e^{-k(t-s)} (f(s) - 1) ds + \bar{u}(0)e^{-kt}$. Note that system (5) is considered with the condition $\bar{u}(0) = 0$. Substituting now this representation of $\bar{u}(t)$ into the third equation of system (5), we obtain the third equation of system (4). Thus in systems (4) and (5), the first, second, and fourth equations coincide and the third equation of (4) is equivalent to the last equation of system (5) with the initial condition $\bar{u}(0) = 0$.

This completes the proof of Lemma 1. \square

Remark 2. It is clear that Lemma 1 can be used also for integro-differential system (11) and system of ordinary differential equations (10). Every solution-vector $(x_1(t), x_2(t), x_3(t), x_4(t))$ of integro-differential system (11) coincides with the first 4 components of the solution-vector.

Take $(x_1(t), x_2(t), x_3(t), x_4(t), x_5(t))$ of system (10) with the initial condition $x_5(0) = 0$. Thus, if we take a part of the space of solutions of ordinary differential system (10),

satisfying the initial condition $x_5(0) = 0$ and delete then the fifth component of solution-vectors, we come to the 4-space of solutions of integro-differential equation (11). Now, it is clear that the exponential stability of the 5-dimensional ordinary differential system (10) implies the exponential stability of 4-dimensional integro-differential system (11). The roots of the characteristic equation for ordinary differential system (10) can be used in the representation of vector-solution in the space of solutions of integro-differential system (11). Negativity of real parts of the roots of the characteristic equation of system (10) with constant coefficients allows to make the conclusion about the exponential stability of the integro-differential system (11). The root with maximal real part of the characteristic equation for (11) cannot be greater than the one of the characteristic equations for (10).

The characteristic polynomial of system (10) of ordinary differential equations,

$$P_5(\lambda^*) = (\lambda^* - \alpha_1 + \alpha_2)(\lambda^* + \alpha_5)(\lambda^* + \alpha_7) \cdot [\lambda^{*2} + (\alpha_4 + k)\lambda^* + k\alpha_4 + b], \quad (14)$$

has 5 roots $\lambda_1^*, \lambda_2^*, \lambda_3^*, \lambda_4^*$, and λ_5^* .

Denote $\lambda_i, i = \overline{1, 4}$ as the roots of the characteristic polynomial of systems (13), and $\tilde{\lambda} = \max_{1 \leq i \leq 4} \lambda_i, \lambda^* = \max_{1 \leq j \leq 5} \text{Re}(\lambda_j^*)$.

Theorem 1. *If $\beta < \gamma F^*$, $b > 0$ and $k > 0$, then integro-differential system (11) is exponentially stable, and if in addition, the inequality $k > \alpha_4$ is fulfilled then $\tilde{\lambda} \geq \lambda^*$.*

The proof is based on the following assertion.

Lemma 2. *For the roots of the characteristic polynomials of systems (11) and (13), the following facts are true:*

$$\lambda_1 = \lambda_1^*, \lambda_2 = \lambda_2^*, \lambda_3 = \lambda_3^*, \quad (15)$$

and if $k > \alpha_4, b > 0$, then

$$\begin{aligned} \lambda_4 &> \text{Re}(\lambda_4^*), \\ \lambda_4 &> \text{Re}(\lambda_5^*). \end{aligned} \quad (16)$$

Proof of Lemma 2. The characteristic polynomial of systems (13) is

$$P_4(\lambda) = (\lambda - \alpha_1 + \alpha_2)(\lambda + \alpha_4)(\lambda + \alpha_5)(\lambda + \alpha_7), \quad (17)$$

and the characteristic polynomial of system (10) is (14).

It is clear from the definition of the coefficients α_j (6) that

$$\lambda_2 = \lambda_2^* = -\alpha_5 < 0, \lambda_3 = \lambda_3^* = -\alpha_7 < 0, \lambda_4 = -\alpha_4 < 0. \quad (18)$$

The inequality $\beta < \gamma F^*$ in the conditions of Theorem 1 implies that $\alpha_1 - \alpha_2 < 0$ and consequently $\lambda_1 = \lambda_1^* = \alpha_1 - \alpha_2 < 0$. It is clear that

$$\lambda_4^* = \frac{-(\alpha_4 + k) - \sqrt{(\alpha_4 - k)^2 - 4b}}{2}, \quad (19)$$

$$\lambda_5^* = \frac{-(\alpha_4 + k) + \sqrt{(\alpha_4 - k)^2 - 4b}}{2}.$$

In the case of complex roots λ_4^* and λ_5^* , we have $\operatorname{Re}\lambda_4^* = \operatorname{Re}\lambda_5^* < 0$ if $k > 0$. In the case of real roots λ_4^* and λ_5^* , we have $\lambda_4^* \leq \lambda_5^* < 0$. Thus we obtain the exponential stability of system (10). According to Remark 2 mentioned above, system (11) is exponentially stable.

Comparing the values of the roots of the characteristic polynomials (17) and (14) we have to verify only the inequality

$$\operatorname{Re}(\lambda_5^*) < \lambda_4, \quad (20)$$

in (16). Substituting the values of λ_5^* and λ_4 to (20), we have to obtain the inequalities:

$$\frac{-(\alpha_4 + k) + \sqrt{(\alpha_4 - k)^2 - 4b}}{2} < -\alpha_4, \quad (21)$$

for the case of real roots λ_4^* and λ_5^* , and

$$\frac{-(\alpha_4 + k)}{2} < -\alpha_4, \quad (22)$$

for the case of the complex roots λ_4^* and λ_5^* .

The inequalities (21) and (22) are fulfilled if $k > \alpha_4$ and $b > 0$.

Substituting the values of α_i in Remark 1, we see that $\lambda_4 > \max_{1 \leq i \leq 3} \lambda_i$. If the inequalities $k > \alpha_4$ and $b > 0$ are fulfilled, then (16) is true.

Note the assertion following from Theorem 1. \square

Corollary 1. *Let the coefficients α_i be defined by the formulas in Remark 1, and $k > 1.95992344 \cdot 10^{-7}$, $b > 0$, then the Lyapunov exponents of system (11) are less than the ones of system (13).*

4. Numerical Simulations and Comments

The mathematical model can be represented in the following form:

$$\frac{dx}{dt} = \Phi(x(t)), \quad x(t) = \operatorname{col}\{v(t), s(t), f(t), m(t), \tilde{u}(t)\}, \quad (23)$$

where $\Phi(x(t))$ is the right-hand side of (7). Values of the parameters are defined in Remark 1, $k = 4$ and $b = 1$ and the initial conditions are $v(0) = 10^{-6}$, $f(0) = 1$, $s(0) = 1$, $m(0) = 0$ and $u(0) = 0$. We use the second-order Runge–Kutta's scheme with a constant step h .

In Figures 1–4, the solution of model with the natural flow of data without the control of disease is presented by curves of red color and disease in the case of considered distributed control by curves of green color.

Figure 1 demonstrates the dynamics in antigen concentration during the course of the disease. The insert

detailing the process in the first two days was performed on a different scale and demonstrates the fact that the management transfers the disease from the acute form to the subclinical one (the antigen concentration only decreases after injection). Figure 2 demonstrates the dynamics in plasma cell concentration during the disease process. It can be seen from the figure that control leads to a faster increase in the concentration of plasma cells, which in this case ensures a transition to the subclinical form of the disease. In addition, it is necessary to note a fourfold increase in the maximum concentration of plasma cells in the case of control, compared with the option without control. Figure 3 demonstrates the dynamics in antibody concentration during the disease process. The graph shows that the concentration of antibodies in the solution with control practically does not change, because in this case, they are replaced by donor antibodies, which is what the control actually consists of. The dynamics in the proportion of target organ cells destroyed by antigen during the disease process is presented in Figure 4. The values for the variant with control are given with an increase of 10^4 times. Thus, control allows to reduce the maximum proportion of affected cells of the target organ by more than 2.5×10^4 times. The dynamics of the control (concentration of donor antibodies) during the disease process is presented in Figure 5.

Remark 3. The integral term can accumulate small mistakes made in the process of numerical integration. This explains difficulties in the use of numerical methods for solving integro-differential equations. The idea to reduce a system of integro-differential equations to a corresponding system of ordinary differential ones and the use of the well-developed technique for their solution could be one of the possible ways to develop numerical methods for integro-differential equations.

5. System with Delay in Equation of Plasma Concentration

It was explained in [7] why the delay $\tau(t)$ can appear in the second equation of system (1) in the model of infectious diseases:

$$\begin{cases} \frac{dV}{dt} = \beta V(t) - \gamma F(t)V(t), \\ \frac{dC}{dt} = \zeta(m)\alpha F(t - \tau(t))V(t - \tau(t)) - \mu_c(C(t) - C^*), \\ \frac{dF}{dt} = \rho C(t) - \eta\gamma F(t)V(t) - \mu_f F(t), \\ \frac{dm}{dt} = \sigma V(t) - \mu_m m(t). \end{cases} \quad (24)$$

We have to define what should be set instead of $V(t - \tau(t))$ and $F(t - \tau(t))$ when $t - \tau(t) < 0$. We consider all delay systems with the initial function $V(\zeta) = 0$ for $\zeta < 0$. Let us consider the following system with the control in antibody concentration:

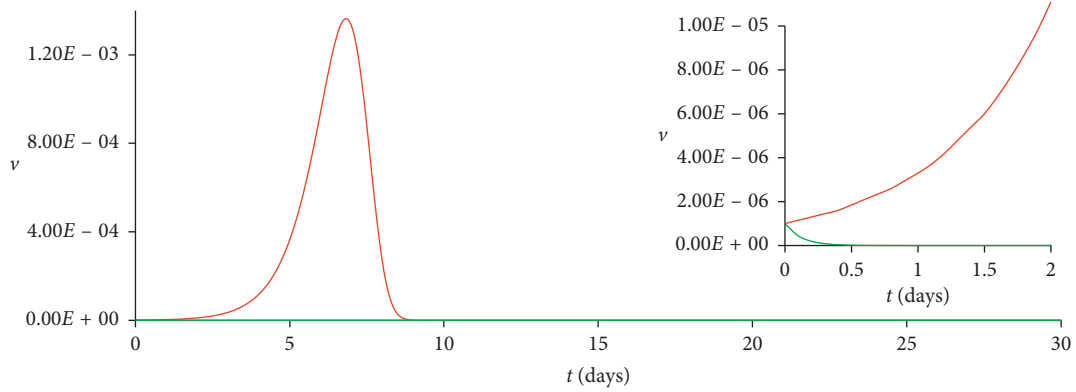


FIGURE 1: Dynamics of the immune response: antigen.

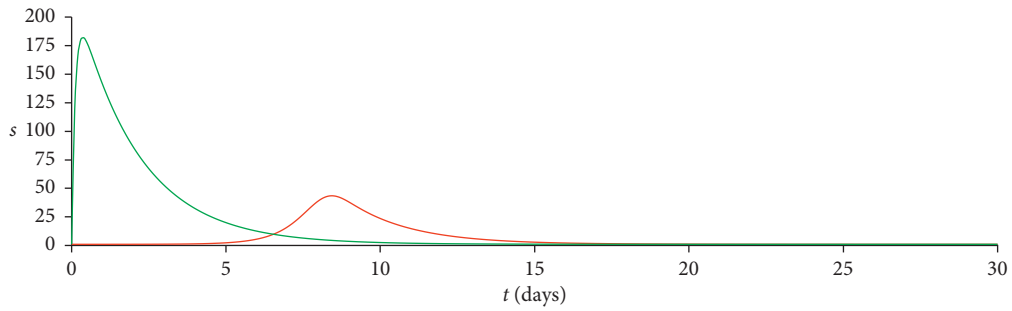


FIGURE 2: Dynamics of the immune response: plasma.

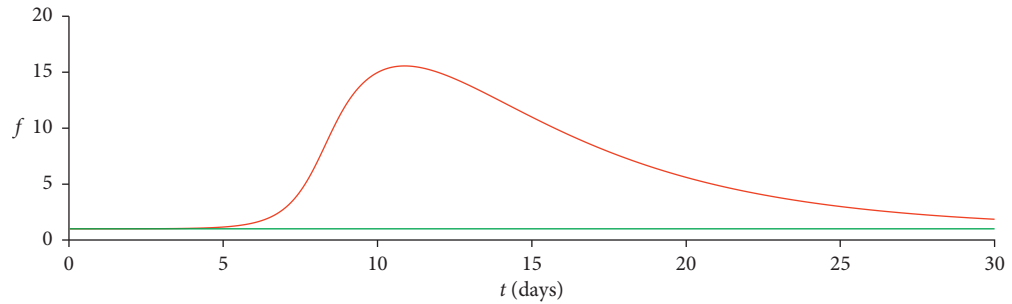


FIGURE 3: Dynamics of the immune response: antibodies.

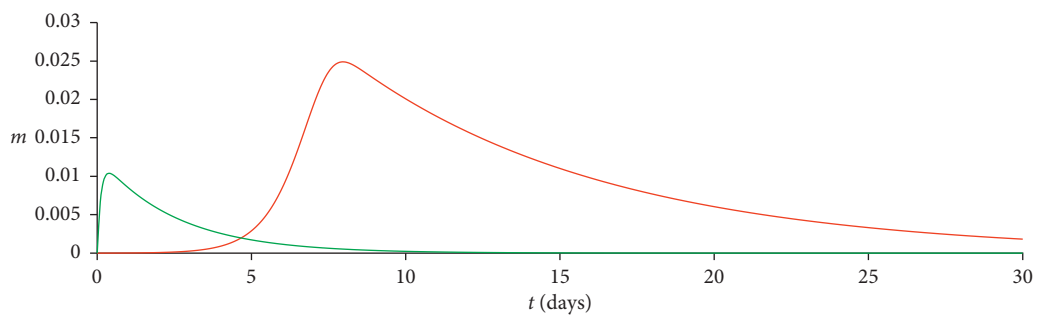


FIGURE 4: Dynamics of the immune response: rate of the destroyed cells.

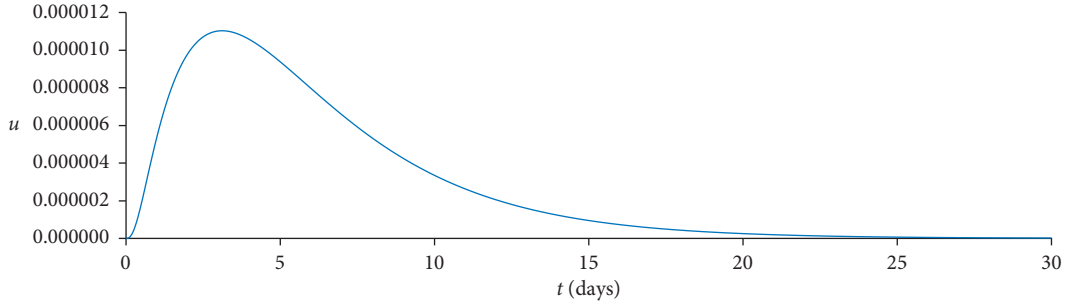


FIGURE 5: Control function.

$$\begin{cases} \frac{dV}{dt} = \beta V(t) - \gamma F(t)V(t), \\ \frac{dC}{dt} = \zeta(m)\alpha F(t - \tau(t))V(t - \tau(t)) - \mu_c(C(t) - C^*), \\ \frac{dF}{dt} = \rho C(t) - \eta\gamma F(t)V(t) - \mu_f F(t) - bu(t), \\ \frac{dm}{dt} = \sigma V(t) - \mu_m m(t), \end{cases} \quad (25)$$

where $u(t) = \int_0^t (F(s) - F^*)e^{-k(t-s)} ds$.

We can pass to dimensionless case

$$\begin{cases} \frac{dv}{dt} = \beta v(t) - \gamma F^* f(t)v(t), \\ \frac{ds}{dt} = \alpha V_m \frac{F^*}{C^*} \zeta(m) f(t - \tau(t))v(t - \tau(t)) - \mu_c(s(t) - 1), \\ \frac{df}{dt} = \frac{\rho C^*}{F^*} s(t) - \eta\gamma V_m f(t)v(t) - \mu_f f(t) - b\bar{u}(t), \\ \frac{dm}{dt} = \sigma V_m V(t) - \mu_m m(t), \\ \frac{d\bar{u}}{dt} = f(t) - 1 - k\bar{u}(t). \end{cases} \quad (26)$$

Denoting α_i ($i = 1, \dots, 8$), according to (6), we obtain

$$\begin{cases} \frac{dv}{dt} = \alpha_1 v(t) - \alpha_2 f(t)v(t), \\ \frac{ds}{dt} = \alpha_3 \zeta(m) f(t - \tau(t))v(t - \tau(t)) - \alpha_5 (s(t) - 1), \\ \frac{df}{dt} = \alpha_4 (s(t) - f(t)) - \alpha_8 f(t)v(t) - \mu_f f(t) - b\bar{u}(t), \\ \frac{dm}{dt} = \alpha_6 V(t) - \alpha_7 m(t), \\ \frac{d\bar{u}}{dt} = f(t) - 1 - k\bar{u}(t). \end{cases} \quad (27)$$

For stability studies, only behavior of solutions for sufficiently large t is considered. Below, we assume that $t - \tau(t) \geq 0$. We can write the second equation in the following form:

$$\begin{aligned} \frac{ds}{dt} &= \alpha_3 \zeta(m) \left[f(t)v(t) - \int_{t-\tau(t)}^t [f(\varphi)v(\varphi)]' d\varphi \right] \\ &\quad - \alpha_5 (s(t) - 1), \\ \frac{df}{dt} &= \alpha_3 \zeta(m) \left[f(t)v(t) - \int_{t-\tau(t)}^t [f'(\varphi)v(\varphi) + f(\varphi)v'(\varphi)] d\varphi \right] \\ &\quad - \alpha_5 (s(t) - 1). \end{aligned} \quad (28)$$

We can write the expression under the integral in the following form:

$$\begin{aligned} f'(\varphi)v(\varphi) + f(\varphi)v'(\varphi) &= v(\varphi) [\alpha_4 (s(\varphi) - f(\varphi)) \\ &\quad - \alpha_8 f(\varphi)v(\varphi) - \mu_f f(\varphi) - b\bar{u}(\varphi)] \\ &\quad + f(\varphi) [\alpha_1 v(\varphi) - \alpha_2 f(\varphi)v(\varphi)] \\ &= \alpha_4 [(s(\varphi) - 1 + 1) - (f(\varphi) - 1 + 1)]v(\varphi) \\ &\quad - \alpha_8 f(\varphi)v^2(\varphi) - \mu_f f(\varphi)v(\varphi) \\ &\quad - b\bar{u}(\varphi)v(\varphi) + \alpha_1 v(\varphi)(f(\varphi) - 1 + 1) \\ &\quad - \alpha_2 f^2(\varphi)v(\varphi)\alpha_1 v(\varphi). \end{aligned} \quad (29)$$

Linearizing system (27) in the neighborhood of the stationary point

$$\begin{aligned} v = m = \bar{u} &= 0, \\ s = f &= 1, \end{aligned} \quad (30)$$

we obtain

$$\begin{cases} \frac{dx_1}{dt} = (\alpha_1 - \alpha_2)x_1, \\ \frac{dx_2}{dt} = \alpha_3 x_1 - \alpha_5 x_2 - \alpha_3 \int_{t-\tau(t)}^t \alpha_1 x_1(\varphi) d\varphi, \\ \frac{dx_3}{dt} = -\alpha_8 x_1 + \alpha_4 x_2 - \alpha_4 x_3 - bx_5, \\ \frac{dx_4}{dt} = \alpha_6 x_1 - \alpha_7 x_4, \\ \frac{dx_5}{dt} = x_3 - kx_5. \end{cases} \quad (31)$$

Consider the system

$$X'(t) = P(t)X(t) + G(t), \quad (32)$$

where $P(t)$ is a $(n \times n)$ -matrix and $G(t)$ is n -vector. The general solution $X(t) = \text{col}\{x_1(t), \dots, x_n(t)\}$ can be represented in the following form:

$$X(t) = \int_0^t C(t,s)G(s)ds + C(t,0)X(0), \quad (33)$$

where $n \times n$ -matrix $C(t,s) = \{C_{ij}(t,s)\}_{i,j=1}^n$ is called the Cauchy matrix. Its j -th column ($j = 1, \dots, n$) for every fixed s as a function of t is a solution of the corresponding homogeneous system:

$$X'(t) = P(t)X(t), \quad (34)$$

satisfying the initial conditions $x_i(s) = \delta_{ij}$, where

$$\delta_{ij} = \begin{cases} 1, & i = j, \\ 0, & i \neq j, \end{cases} \quad i = 1, \dots, n. \quad (35)$$

Construction of the Cauchy matrix of system with ordinary differential equations can be found, for example, in [22].

Let us denote $\tau^* = \text{ess sup}_{t \geq 0} \tau(t)$.

Theorem 2. *If $\beta < \gamma F^*$, $k > 0$, $b > 0$ and*

$$\tau^* \max_{1 \leq j \leq 5} \sup_{t \geq 0} \int_0^t |C_{2j}(t,s)| ds < \frac{1}{\alpha_3 \alpha_1}, \quad (36)$$

where $C(t,s) = \{C_{ij}(t,s)\}_{i,j=1}^5$ is the Cauchy matrix of system (10), then system (31) is exponentially stable.

Proof of Theorem 2. Consider the nonhomogeneous system corresponding to homogeneous system (31):

$$\begin{cases} \frac{dx_1}{dt} = (\alpha_1 - \alpha_2)x_1 + g_1(t), \\ \frac{dx_2}{dt} = \alpha_3 x_1 - \alpha_5 x_2 - \alpha_3 \int_{t-\tau(t)}^t \alpha_1 x_1(\varphi) d\varphi + g_2(t), \\ \frac{dx_3}{dt} = -\alpha_8 x_1 + \alpha_4 x_2 - \alpha_4 x_3 - b x_5 + g_3(t), \\ \frac{dx_4}{dt} = \alpha_6 x_1 - \alpha_7 x_4 + g_4(t), \\ \frac{dx_5}{dt} = x_3 - k x_5 + g_5(t), \end{cases} \quad (37)$$

where $g_1(t), \dots, g_5(t)$ are measurable essentially bounded functions on the semiaxis (i.e., they are from the space L_∞).

We can write system (37) in the following form:

$$x'(t) = Ax(t) + (Fx)(t) + G(t), \quad (38)$$

where

$$\begin{aligned} x(t) &= \text{col}\{x_1(t), x_2(t), x_3(t), x_4(t), x_5(t)\}, \\ (Fx)(t) &= \text{col}\left\{0, -\alpha_3 \int_{t-\tau(t)}^t \alpha_1 x_1(\varphi) d\varphi, 0, 0, 0\right\}, \end{aligned} \quad (39)$$

$$G(t) = \text{col}\{g_1(t), g_2(t), g_3(t), g_4(t), g_5(t)\},$$

and A is defined by (12). It is clear that the use of the standard formula of solutions' representation leads to the following system:

$$x(t) = \int_0^t C(t,s)(Fx)(s)ds + \int_0^t C(t,s)G(s)ds + C(t,0)x(0). \quad (40)$$

It follows from Theorem 1 that the Cauchy matrix $C(t,s)$ satisfies the exponential estimate, i.e., there exist such positive γ and N , then all elements $C_{ij}(t,s)$ of the Cauchy matrix $C(t,s)$ satisfy the following estimate:

$$\begin{aligned} |C_{ij}(t,s)| &\leq N e^{-\gamma(t-s)}, \\ 0 &\leq s \leq t < \infty, \\ i, j &= 1, \dots, 5. \end{aligned} \quad (41)$$

Now it is clear that the vector-function $\tilde{G}(t) \equiv \int_0^t C(t,s)G(s)ds + C(t,0)X(0)$ is bounded for $t \in [0, \infty)$.

Define the operator $K : C^5 \rightarrow C^5$ (C^5 is the space of 5-dimensional vector-functions $x : [0, \infty)$ with continuous components) by the following formula:

$$(Kx)(t) = \int_0^t C(t,s)(Fx)(s)ds. \quad (42)$$

System (40) can be rewritten in the form

$$x(t) = (Kx)(t) + \tilde{G}(t), \quad (43)$$

where

$$\tilde{G}(t) = \int_0^t C(t,s)G(s)ds + C(t,0)x(0). \quad (44)$$

The inequality (36) implies that the norm of the operator $K : C^5 \rightarrow C^5$ is less than one, then there exists the operator $(I - K)^{-1} : C^5 \rightarrow C^5$ and it is bounded. Thus, the solution-vector $x(t)$ is bounded for $t \in [0, \infty)$, for every bounded on the semiaxis right-hand side $G(t)$. Now the exponential estimate of the solution $x(t)$ of the homogeneous system (31) follows the Bohl-Perron theorem [23, 24]. We have proven the exponential stability of system (31). \square

Remark 4. It is clear that system (31) is exponentially stable if $\beta < \gamma F^*$, $k > 0$, $b > 0$ for sufficiently small delay $\tau(t)$.

Remark 5. Let us compare the difference of solution $x(t) = \text{col}\{x_1(t), \dots, x_5(t)\}$ of system (10) and solution $y(t) = \text{col}\{y_1(t), \dots, y_5(t)\}$ of system (31) with the same initial conditions $x(0) = y(0)$. It is clear that

$$y'(t) - x'(t) = A(y(t) - x(t)) + (Fy)(t). \quad (45)$$

Denote $z(t) = y(t) - x(t)$. $z(t)$ satisfies the following equation:

$$z'(t) = Az(t) + (Fy)(t). \quad (46)$$

The solution $z(t)$ can be represented in the following form:

$$z(t) = \int_0^t C(t,s)(Fy)(s)ds. \quad (47)$$

It follows from the exponential estimates of $C(t,s)$ and $y(t)$ that $z(t)$ tends to zero exponentially, when $t \rightarrow \infty$.

In order to estimate $z(t)$, we can use the results of the paper [25], where the elements of the Cauchy matrix $C(t,s)$ were constructed.

6. Construction of the Cauchy Matrix and Stability of Model with Delay

In order to use Theorem 2, we have to obtain the estimates of $\max_{1 \leq j \leq 5} \sup_{t \geq 0} \int_0^t |C_{2j}(t,s)|ds$. In this section, we present these estimates.

Let us denote $c = (a_1^2 - 2a_1a_2 + a_1a_4 + a_1k + a_2^2 - a_2a_4 - a_2k + a_4k + b)/(a_1a_8 - a_2a_8 - a_3a_4 + a_5a_8)$,

$$\begin{aligned} \vec{C}_2(t,s) &= \frac{\alpha_{32} - \alpha_{34}}{\alpha_{24}(\alpha_{31} - \alpha_{32})} \begin{pmatrix} 0 \\ 0 \\ \frac{2b}{a_4 - k + \sqrt{(a_4 - k)^2 - 4b}} \\ 0 \\ 1 \end{pmatrix} e^{((-a_4 - k + \sqrt{(a_4 - k)^2 - 4b})/2)(t-s)} - \frac{\alpha_{31} - \alpha_{34}}{\alpha_{24}(\alpha_{31} - \alpha_{32})} \\ &\cdot \begin{pmatrix} 0 \\ 0 \\ \frac{2b}{a_4 - k - \sqrt{(a_4 - k)^2 - 4b}} \\ 0 \\ 1 \end{pmatrix} e^{((-a_4 - k - \sqrt{(a_4 - k)^2 - 4b})/2)(t-s)} + \frac{1}{\alpha_{24}} \begin{pmatrix} 0 \\ \frac{a_4a_5 - a_4k - a_5^2 + a_5k - b}{a_4} \\ -a_5 + k \\ 0 \\ 1 \end{pmatrix} e^{-a_5(t-s)}. \end{aligned} \quad (48)$$

Let us denote $\beta_{31} = -2b/a_4 - k$, $\beta_{52} = 2/a_4 - k$, $\beta_{24} = -a_4a_5 - a_4k - a_5^2 + a_5k - b/a_4$, $\beta_{34} = -a_5 + k$, $\beta_{15} = -c(a_5 + a_1 - a_2)$, $\beta_{25} = -ca_3$, $\beta_{35} = a_1 - a_2 + k$, $\beta_{45} = -(a_5 + a_1 - a_2)a_6c/a_1 - a_2 + a_7$.

$$\begin{aligned} \alpha_{31} &= \frac{2b}{\left(a_4 - k + \sqrt{(a_4 - k)^2 - 4b}\right)}, \\ \alpha_{32} &= \frac{2b}{\left(a_4 - k - \sqrt{(a_4 - k)^2 - 4b}\right)}, \\ \alpha_{24} &= \frac{(a_4a_5 - a_4k - a_5^2 + a_5k - b)}{a_4}, \\ \alpha_{34} &= -a_5 + k, \\ \alpha_{15} &= -c(a_5 + a_1 - a_2), \\ \alpha_{25} &= -ca_3, \\ \alpha_{35} &= a_1 - a_2 + k, \\ \alpha_{45} &= \frac{(a_5 + a_1 - a_2)a_6c}{a_1 - a_2 + a_7}. \end{aligned} \quad (48)$$

Lemma 3 (see [25]). *If $(a_4 - k)^2 > 4b$, then the second column of the Cauchy matrix of (10) is as follows:*

Lemma 4 (see [25]). *If $(a_4 - k)^2 = 4b$, then the second column of the Cauchy matrix of (10) is as follows:*

$$\vec{C}_2(t, s) = \left[\frac{\beta_{34}}{\beta_{24}\beta_{31}} \begin{pmatrix} 0 \\ 0 \\ 2b \\ 0 \\ 1 \end{pmatrix} - \frac{\beta_{31} - \beta_{34}}{\beta_{31}\beta_{24}\beta_{52}} \begin{pmatrix} 0 \\ 0 \\ 0 \\ 0 \\ \frac{2}{a_4 - k} \end{pmatrix} + (t-s) \begin{pmatrix} 0 \\ 0 \\ -\frac{2b}{a_4 - k} \\ 0 \\ 1 \end{pmatrix} \right] e^{-(a_4+k)/2(t-s)} + \frac{1}{\beta_{24}} \begin{pmatrix} 0 \\ \frac{a_4 a_5 - a_4 k - a_5^2 + a_5 k - b}{a_4} \\ -a_5 + k \\ 0 \\ 1 \end{pmatrix} e^{-a_5(t-s)}. \quad (50)$$

Let us denote $\gamma_{32} = \sqrt{4b - (a_4 - k)^2}/2$, $\gamma_{24} = -a_4 a_5 - a_4 k - a_5^2 + a_5 k - b/a_4$, $\gamma_{15} = -c(a_5 + a_1 - a_2)$, $\gamma_{25} = -ca_3$, $\gamma_{35} = a_1 - a_2 + k$, $\gamma_{45} = -(a_5 + a_1 - a_2)a_6 c/a_1 - a_2 + a_7$.

Lemma 5 (see [25]). *If $(a_4 - k)^2 < 4b$, then the second column of the Cauchy matrix of (10) is as follows:*

$$\begin{aligned} \vec{C}_2(t, s) = & \frac{1}{\gamma_{24}} \cdot \left[\begin{pmatrix} 0 \\ 0 \\ \frac{k - a_4}{2} \\ 0 \\ 1 \end{pmatrix} \cdot e^{-(a_4+k)/2(t-s)} \cdot \cos\left(\frac{\sqrt{4b - (a_4 - k)^2}}{2}(t-s)\right) \right. \\ & + \left. \begin{pmatrix} 0 \\ 0 \\ -\frac{\sqrt{4b - (a_4 - k)^2}}{2} \\ 0 \\ 0 \end{pmatrix} \cdot e^{-(a_4+k)/2(t-s)} \cdot \sin\left(\frac{\sqrt{4b - (a_4 - k)^2}}{2}(t-s)\right) \right] \frac{1}{2} \frac{a_4 - 3k + 2a_5}{\gamma_{24}\gamma_{32}} \\ & \cdot \left[\begin{pmatrix} 0 \\ 0 \\ \frac{\sqrt{4b - (a_4 - k)^2}}{2} \\ 0 \\ 0 \end{pmatrix} \cdot e^{-(a_4+k)/2(t-s)} \cdot \cos\left(\frac{\sqrt{4b - (a_4 - k)^2}}{2}(t-s)\right) + \begin{pmatrix} 0 \\ 0 \\ \frac{a_4 - k}{2} \\ 0 \\ 1 \end{pmatrix} \right. \\ & \left. \cdot e^{-a_4+k/2(t-s)} \cdot \sin\left(\frac{\sqrt{4b - (a_4 - k)^2}}{2}(t-s)\right) \right] \frac{1}{\gamma_{24}} \cdot \begin{pmatrix} 0 \\ \frac{a_4 a_5 - a_4 k - a_5^2 + a_5 k - b}{a_4} \\ a_5 - k \\ 0 \\ 1 \end{pmatrix} \cdot e^{-a_5(t-s)}. \quad (51) \end{aligned}$$

The following assertions are results of substitutions of $C_{2j}(t, s)$ presented in Lemmas 3–5 into inequality (36) in Theorem 2.

Theorem 3. If $(\alpha_4 - k)^2 > 4b$, $\beta < \gamma F^*$, $k > 0$, $b > 0$, and

$$\tau^* \max \left\{ \begin{array}{l} \frac{|\alpha_{32} - \alpha_{34}|}{|\alpha_{24}(\alpha_{31} - \alpha_{32})|} \frac{2b}{|a_4 - k + \sqrt{(a_4 - k)^2 - 4b}|} \frac{2}{|-a_4 - k + \sqrt{(a_4 - k)^2 - 4b}|} + \frac{|\alpha_{31} - \alpha_{34}|}{|\alpha_{24}(\alpha_{31} - \alpha_{32})|} \\ \frac{2b}{|a_4 - k - \sqrt{(a_4 - k)^2 - 4b}|} \frac{2}{|-a_4 - k - \sqrt{(a_4 - k)^2 - 4b}|} + \frac{1}{|\alpha_{24}|} \frac{|a_4 a_5 - a_4 k - a_5^2 + a_5 k - b|}{a_4} \frac{1}{a_5} \\ \frac{|\alpha_{32} - \alpha_{34}|}{|\alpha_{24}(\alpha_{31} - \alpha_{32})|} \frac{2}{|-a_4 - k + \sqrt{(a_4 - k)^2 - 4b}|} + \frac{|\alpha_{31} - \alpha_{34}|}{|\alpha_{24}(\alpha_{31} - \alpha_{32})|} \frac{2}{|-a_4 - k + \sqrt{(a_4 - k)^2 - 4b}|} + \frac{1}{|\alpha_{24}|} \frac{1}{a_5} \\ \frac{1}{|\alpha_{24}|} \frac{|a_5 + k|}{a_5} \end{array} \right\} < \frac{1}{\alpha_3 \alpha_1}, \quad (52)$$

then system (31) is exponentially stable.

Theorem 4. If $(\alpha_4 - k)^2 = 4b$, $\beta < \gamma F^*$, $k > 0$, $b > 0$, and

$$\tau^* \max \left\{ \begin{array}{l} \frac{1}{|\beta_{24}|} \frac{|a_4 a_5 - a_4 k - a_5^2 + a_5 k - b|}{a_4} \frac{1}{a_5} \\ \frac{|\beta_{34}|}{|\beta_{24} \beta_{31}|} \frac{4b}{|a_4^2 - k^2|} + \frac{|\beta_{31} - \beta_{34}|}{|\beta_{31} \beta_{24} \beta_{52}|} \frac{2b}{|a_4 - k|} \frac{4}{(a_4 + k)^2} + \frac{1}{|\beta_{24}|} \frac{a_5 + k}{a_5} \\ \frac{|\beta_{34}|}{|\beta_{24} \beta_{31}|} \frac{2}{a_4 + k} + \frac{|\beta_{31} - \beta_{34}|}{|\beta_{31} \beta_{24} \beta_{52}|} \frac{4}{|a_4^2 - k^2|} + \frac{|\beta_{31} - \beta_{34}|}{|\beta_{31} \beta_{24} \beta_{52}|} \frac{4}{(a_4 + k)^2} + \frac{1}{|\beta_{24}|} \frac{1}{a_5} \end{array} \right\} < \frac{1}{\alpha_3 \alpha_1}, \quad (53)$$

then system (31) is exponentially stable.

Theorem 5. If $(\alpha_4 - k)^2 < 4b$, $\beta < \gamma F^*$, $k > 0$, $b > 0$, and

$$\tau^* \max \left\{ \begin{array}{l} \frac{1}{|\gamma_{24}| a_5} \frac{|a_4 a_5 - a_4 k - a_5^2 + a_5 k - b|}{a_4} \\ \frac{1}{|\gamma_{24}|} \frac{|a_4 - k|}{a_4 + k} + \frac{1}{|\gamma_{24}|} \frac{\sqrt{4b - (a_4 - k)^2}}{a_4 + k} + \frac{1}{2} \frac{|a_4 - 3k + 2a_5|}{|\gamma_{24} \gamma_{32}|} \frac{\sqrt{4b - (a_4 - k)^2}}{a_4 + k} \\ + \frac{1}{2} \frac{|a_4 - 3k + 2a_5|}{|\gamma_{24} \gamma_{32}|} \frac{|a_4 - k|}{a_4 + k} + \frac{1}{|\gamma_{24}|} \frac{|a_5 - k|}{a_5} \\ \frac{1}{|\gamma_{24}|} \frac{2}{a_4 + k} + \frac{|a_4 - 3k + 2a_5|}{|\gamma_{24} \gamma_{32}|} \frac{1}{a_4 + k} + \frac{1}{|\gamma_{24}|} \frac{1}{a_5} \end{array} \right\} < \frac{1}{\alpha_3 \alpha_1}, \quad (54)$$

then system (31) is exponentially stable.

Data Availability

The data used to support the findings of this study are available within the article.

Disclosure

This paper is part of the first author's Ph.D. thesis which is being carried out in the Department of Mathematics at Ariel University.

Conflicts of Interest

The authors declare that there are no conflicts of interest regarding the publication of this article.

References

- [1] F. Mazenc, S. I. Niculescu, and M. Bekaik, "Stabilization of time-varying nonlinear systems with distributed input delay by feedback of plant's state," *IEEE Transactions on Automatic Control*, vol. 58, no. 1, pp. 264–269, 2013.
- [2] Z. Artstein, "Linear systems with delayed controls: a reduction," *IEEE Transactions on Automatic Control*, vol. 27, no. 4, pp. 869–879, 1982.
- [3] B. Zhou, Q. Liu, and F. Mazenc, "Stabilization of linear systems with both input and state delays by observer-predictors," *Automatica*, vol. 83, pp. 368–377, 2017.
- [4] B. Zhou and Q. Liu, "Input delay compensation for neutral type time-delay systems," *Automatica*, vol. 78, pp. 309–319, 2017.
- [5] B. Zhou, "Input delay compensation of linear systems with both state and input delays by nested prediction," *Automatica*, vol. 50, no. 5, pp. 1434–1443, 2014.
- [6] V. L. Kharitonov, "An extension of the predictor scheme to the case of systems with both input and state delay," *Automatica*, vol. 50, pp. 211–217, 2014, in Press.
- [7] G. I. Marchuk, "Mathematical modelling of immune response in infection diseases," in *Mathematics and its Applications*, Springer, Dordrecht, The Netherlands, 1997.
- [8] V. P. Martsenyuk, "On stability of immune protection model with regard for damage of target organ: the degenerate Liapunov functionals method," *Cybernetics and Systems Analysis*, vol. 40, no. 1, pp. 126–136, 2004.
- [9] V. P. Martsenyuk, I. Y. Andrushchak, and I. S. Gvozdetska, "Qualitative analysis of the antineoplastic immunity system on the basis of a decision tree," *Cybernetics and Systems Analysis*, vol. 51, no. 3, pp. 461–470, 2015.
- [10] S. V. Rusakov and M. V. Chirkov, "Mathematical model of influence of immuno-therapy on dynamics of immune response," *Problems of Control*, vol. 6, pp. 45–50, 2012.
- [11] S. V. Rusakov and M. V. Chirkov, "Identification of parameters and control in mathematical models of immune response," *Russian Journal of Biomechanics*, vol. 18, no. 2, pp. 259–269, 2014.
- [12] M. Skvortsova, "Asymptotic properties of solutions in Marchuk's basic model of disease," *Functional Differential Equations*, vol. 24, no. 3-4, pp. 127–135, 2017.
- [13] L. N. Belih, "On the numerical solution of models of diseases," in *Mathematical models in Immunology and Medicine*, G. I. Marchuk and L. N. Belih, Eds., pp. 291–297, Mountain View, CA, USA, 1986, in Russian.
- [14] I. P. Bolodurina and Y. P. Lugovskova, "Mathematical model of management immune system," *Review of Applied and Industrial Mathematics*, vol. 15, no. 6, pp. 1043–1044, 2008, in Russian.
- [15] M. V. Chirkov, *Parameter identification and control in mathematical models of the immune response*, Ph.D. thesis, Perm State University, Perm, Russia, 2014, in Russian.
- [16] A. L. Asachenkov and G. I. Marchuk, "The specified mathematical model of an infectious disease," in *Mathematical Modeling in Immunology and Medicine*, E. G. I. Marchuk, Ed., pp. 44–59, Novosibirsk, Russia, 1982, in Russian.
- [17] Y. Bard, *Nonlinear Estimation of Parameters*, Academic Press, New York, NY, USA, 1974, in Russian.
- [18] N. Bekiaris-Liberis and M. Krstic, "Lyapunov stability of linear predictor feedback for distributed input delays," *IEEE Transactions on Automatic Control*, vol. 56, no. 3, pp. 655–660, 2011.
- [19] A. Domoshnitsky, I. Volinsky, A. Polonsky, and A. Sitkin, "Stabilization by delay distributed feedback control," *Mathematical Modelling of Natural Phenomena*, vol. 12, no. 6, pp. 91–105, 2017.
- [20] A. Domoshnitsky, I. Volinsky, and A. Polonsky, "Stabilization of third order differential equation by delay distributed feedback control with unbounded memory," *Mathematica Slovaca*, vol. 69, no. 5, pp. 1165–1176, 2019.
- [21] G. Goebel, U. Munz, and F. Allgower, "Stabilization of linear systems with distributed input delay," in *Proceedings of the 2010 American Control Conference*, pp. 5800–5805, IEEE, Baltimore, MD, USA, July 2010.
- [22] A. Domoshnitsky, I. Volinsky, A. Polonsky, and A. Sitkin, "Practical constructing the Cauchy function of integro-differential equation," *Functional Differential Equations*, vol. 23, no. 3-4, pp. 109–118, 2016.
- [23] R. P. Agarwal, L. Berezansky, E. Braverman, and A. Domoshnitsky, *Nonoscillation Theory of Functional Differential Equations with Applications*, Springer, New York, NY, USA, 2012.
- [24] N. V. Azbelev, V. P. Maksimov, and L. F. Rahmatullina, "Introduction to theory of linear functional-differential equations," in *Advances Series in Mathematical Science and Engineering*, vol. 3, World Federation Publishers Company, Atlanta, GA, USA, 1995.
- [25] A. Domoshnitsky, I. Volinsky, and M. Bershadsky, "Around the model of infection disease: the Cauchy matrix and its properties," *Symmetry*, vol. 11, no. 8, p. 1016, 2019.

Research Article

Nonlocal Symmetry and Bäcklund Transformation of a Negative-Order Korteweg–de Vries Equation

Jinxi Fei,¹ Weiping Cao ,¹ and Zhengyi Ma ^{2,3}

¹Institute of Optoelectronic Technology, Lishui University, Lishui 323000, China

²Institute of Nonlinear Analysis and Department of Mathematics, Lishui University, Lishui 323000, China

³Department of Mathematics, Zhejiang Sci-Tech University, Hangzhou 310018, China

Correspondence should be addressed to Weiping Cao; phycao@lsu.edu.cn

Received 18 July 2019; Revised 15 September 2019; Accepted 17 September 2019; Published 29 October 2019

Guest Editor: Robert Hakl

Copyright © 2019 Jinxi Fei et al. This is an open access article distributed under the Creative Commons Attribution License, which permits unrestricted use, distribution, and reproduction in any medium, provided the original work is properly cited.

The residual symmetry of a negative-order Korteweg–de Vries (nKdV) equation is derived through its Lax pair. Such residual symmetry can be localized, and the original nKdV equation is extended into an enlarged system by introducing four new variables. By using Lie's first theorem, we obtain the finite transformation for the localized residual symmetry. Furthermore, we localize the linear superposition of multiple residual symmetries and construct n -th Bäcklund transformation for this nKdV equation in the form of the determinants.

1. Introduction

It is well known that infinitely many symmetries or flows appear for finding evolution equations, and a general method was proposed by Olver, which was applied to the Korteweg–de Vries (KdV), modified Korteweg–de Vries (mKdV), Burgers, and sine-Gordon equations [1, 2]. Then, Olver's concept of a recursion operator for symmetries of an evolution equation was extended to negative powers of the operator, and some negative-order Korteweg–de Vries (nKdV) equations were derived, including the following nKdV equation [3–12]:

$$\begin{aligned} u_x - v_t &= 0, \\ u_{xxx} + 4u_x v + 2uv_x &= 0. \end{aligned} \quad (1)$$

Several years later, Lou reobtained the negative KdV hierarchy from the conformal invariance of its Schwartz form [13]. This new method used for the KdV equation can be extended to get more symmetries from known ones for arbitrary partial differential equations without using a recursion operator. Also, the theory can be used as a new criterion to verify whether a model is integrable or not. Based on the regular KdV system, Qiao originally studied nKdV equations, particularly their Hamiltonian structures, Lax pairs, conservation laws, and explicit multisoliton and

multikink wave solutions through bilinear Bäcklund transformations [14–17]. By using the simplified form of Hirota's direct method, Wazwaz developed the nKdV equation and negative-order Kadomtsev–Petvishvili (nKP) equation in $2+1$ dimensions and found multiple soliton solutions with free coefficients [18]. However, Kudryashov showed that existence of multisoliton solutions for the nonlinear evolution equation is the consequence of complete integrability [19, 20]. According to Theorem 1 in Reference [14], the nKdV equation (1) admits a Lax pair with the parameter λ as follows:

$$\begin{aligned} L\psi &\equiv \psi_{xx} + v\psi = \lambda\psi, \\ \psi_t &= -\frac{1}{2\lambda}u\psi_x + \frac{1}{4\lambda}u_x\psi, \end{aligned} \quad (2)$$

and also possesses a Lax pair without the parameter as follows:

$$\begin{aligned} L\psi &= (\partial_x^2 + v)\psi = 0, \\ M\psi &= (4\partial_x^2\partial_t + 4v\partial_t + 2u\partial_x + 3u_x)\psi = 0. \end{aligned} \quad (3)$$

This paper is organized as follows: In Section 2, with the aid of the Lax pair, the residual symmetry of the nKdV equation (1) is derived, and this nonlocal symmetry is localized by introducing four auxiliary variables. Subsequently,

we can obtain the finite symmetry transformation by solving the initial value problem. In Section 3, through localizing the linear superposition of multiple residual symmetries and constructing the infinite transformation for the nKdV equation, multiple residual symmetries and n -th Bäcklund transformation are obtained. A direct result shows that one can derive special soliton solutions from some seed solutions. A brief summary is given in Section 4.

2. Nonlocal Symmetry and Finite Transformation of the nKdV Equation

First, under the infinitesimal transformations $u \rightarrow u + \varepsilon\sigma_1$ and $v \rightarrow v + \varepsilon\sigma_2$ with the infinitesimal parameter ε , the symmetries σ_1 and σ_2 of the nKdV equation (1) can be expressed as a solution of their linear equations:

$$\sigma_{1,x} - \sigma_{2,t} = 0, \quad (4a)$$

$$\sigma_{1,xxx} + 4v\sigma_{1,x} + 2v_x\sigma_1 + 4u_x\sigma_2 + 2u\sigma_{2,x} = 0, \quad (4b)$$

which means that equation (1) is form invariant. At the same time, we can obtain the linear form of equation (2) under the infinitesimal transformation as follows:

$$\psi \rightarrow \psi + \varepsilon\sigma_3. \quad (5)$$

That is, the symmetric equations of the Lax pair (2) are

$$\sigma_{3,xx} - \lambda\sigma_3 + v\sigma_3 + \psi\sigma_2 = 0, \quad (6a)$$

$$\sigma_{3,t} + \frac{1}{2\lambda}(u\sigma_{3,x} + \psi_x\sigma_1) - \frac{1}{4\lambda}(u_x\sigma_3 + \psi\sigma_{1,x}) = 0. \quad (6b)$$

Second, supposing the symmetries σ_1 and σ_2 with the auxiliary variable ψ as

$$\begin{aligned} \sigma_1 &= \psi\psi_t, \\ \sigma_2 &= \psi\psi_x, \end{aligned} \quad (7)$$

the symmetry σ_3 can be derived from equations (1), (6a)-(6b), and (7) as follows:

$$\sigma_3 = -\frac{f\psi}{4}, \quad (8)$$

where the auxiliary variable ψ satisfies $\psi^2 = f_x$, and the corresponding symmetric equation is $2\psi\sigma_3 - \sigma_{4,x} = 0$, where f is a auxiliary function and its infinitesimal transformation is $f \rightarrow f + \varepsilon\sigma_4$. The direct result is

$$\sigma_4 = -\frac{f^2}{4}. \quad (9)$$

So, equation (1) can be expressed by the auxiliary variable ψ through equation (2) as

$$u = -\frac{1}{2\psi\psi_x}(\psi\psi_{xxt} - \psi_{xx}\psi_t + 4\lambda\psi\psi_t), \quad (10a)$$

$$v = \frac{\lambda\psi - \psi_{xx}}{\psi}. \quad (10b)$$

The consistent condition of the auxiliary function f is derived from equation (10) as

$$f_t = \frac{1}{4\lambda\psi_x}(\psi^2\psi_{xxt} - \psi\psi_{xx}\psi_t + 4\lambda\psi^2\psi_t + 4\psi_x^2\psi_t - 4\psi\psi_x\psi_{xt}). \quad (11)$$

Indeed, equation (11) has a typical Schwarzian form of the nKdV equation defined as follows:

$$S_t + 4\lambda C_x = 0,$$

$$C = \frac{f_t}{f_x}, \quad (12)$$

$$S = \frac{f_{xxx}}{f_x} - \frac{3f_{xx}^2}{2f_x^2},$$

which is invariant under the Möbius transformation

$$f \rightarrow \frac{a+bf}{c+df}, \quad (ad-bc \neq 0). \quad (13)$$

The corresponding symmetric equation of equation (11) is

$$\begin{aligned} &(\psi_{xx}\psi_t + 4\psi_x\psi_{xt} - 2\psi\psi_{xxt} - 8\lambda\psi\psi_t)\sigma_3 \\ &+ 4(\lambda f_t + \psi\psi_{xt} - 2\psi_x\psi_t)\sigma_{3,x} \\ &+ (\psi\psi_{xx} - 4\psi_x^2 - 4\lambda\psi^2)\sigma_{3,t} + \psi\psi_t\sigma_{3,xx} \\ &+ 4\psi\psi_x\sigma_{3,xt} - \psi^2\sigma_{3,xxt} + 4\lambda\psi_x\sigma_{4,t} = 0. \end{aligned} \quad (14)$$

Since the nonlocal symmetry could not be used to construct the explicit solutions of a partial differential equation (PDE) directly, we need to transform these components to local ones. In this part, we will seek an enlarged system which possesses a Lie point symmetry for the nonlocal symmetry. For this purpose, we further introduce four auxiliary variables $g, h, p,$ and $q,$ which need to obey the rule

$$\begin{aligned} \psi_t &= g, \\ \psi_x &= h, \\ f_t &= p, \\ h_t &= q. \end{aligned} \quad (15)$$

The related symmetries are

$$\begin{aligned} \sigma_{3,t} - \sigma_5 &= 0, \\ \sigma_{3,x} - \sigma_6 &= 0, \\ \sigma_{4,t} - \sigma_7 &= 0, \\ \sigma_{6,t} - \sigma_8 &= 0, \end{aligned} \quad (16)$$

under the infinitesimal transformations $g \rightarrow g + \varepsilon\sigma_5,$ $h \rightarrow h + \varepsilon\sigma_6,$ $p \rightarrow p + \varepsilon\sigma_7,$ and $q \rightarrow q + \varepsilon\sigma_8.$

It can be verified that equations (7)-(9), (14), and (16) have the following solution:

$$\begin{aligned} \sigma &\equiv \{\sigma_1, \sigma_2, \sigma_3, \sigma_4, \sigma_5, \sigma_6, \sigma_7, \sigma_8\} \\ &= \left\{ g\psi, h\psi, -\frac{f\psi}{4}, -\frac{f^2}{4}, -\frac{1}{4}(p\psi + fg), -\frac{1}{4}(\psi^3 + fh), \right. \\ &\quad \left. -\frac{fP}{2}, -\frac{1}{4}(3g\psi^2 + ph + fq) \right\}. \end{aligned} \quad (17)$$

This is a local Lie point symmetry of the prolonged equations (1), (2), and (15) with $\psi^2 = f_x$.

Correspondingly, the initial value problem can be written as follows:

$$\frac{dU(\varepsilon)}{d\varepsilon} = G(\varepsilon)\Psi(\varepsilon), \quad U(0) = u, \quad (18a)$$

$$\frac{dV(\varepsilon)}{d\varepsilon} = H(\varepsilon)\Psi(\varepsilon), \quad V(0) = v,$$

$$\begin{aligned} \frac{d\Psi(\varepsilon)}{d\varepsilon} &= -\frac{1}{4}F(\varepsilon)\Psi(\varepsilon), \quad \Psi(0) = \psi, \\ \frac{dF(\varepsilon)}{d\varepsilon} &= -\frac{1}{4}F^2(\varepsilon), \quad F(0) = f, \end{aligned} \quad (18b)$$

$$\begin{aligned} \frac{dG(\varepsilon)}{d\varepsilon} &= -\frac{1}{4}[P(\varepsilon)\Psi(\varepsilon) + F(\varepsilon)G(\varepsilon)], \quad G(0) = g, \\ \frac{dH(\varepsilon)}{d\varepsilon} &= -\frac{1}{4}[\Psi^3(\varepsilon) + F(\varepsilon)H(\varepsilon)], \quad H(0) = h, \end{aligned} \quad (18c)$$

$$\begin{aligned} \frac{dP(\varepsilon)}{d\varepsilon} &= -\frac{1}{2}F(\varepsilon)P(\varepsilon), \quad P(0) = p, \\ \frac{dQ(\varepsilon)}{d\varepsilon} &= -\frac{1}{4}[3G(\varepsilon)\Psi^2(\varepsilon) + P(\varepsilon)H(\varepsilon) + F(\varepsilon)Q(\varepsilon)], \quad Q(0) = q. \end{aligned} \quad (18d)$$

By solving this initial value problem, one can obtain the following finite transformation theorem.

Theorem 1. *If $\{u, v, \psi, f, g, h, p, q\}$ is a solution of the extended system (1), (2), and (15), so is*

$$U(\varepsilon) = u + \frac{4g\psi\varepsilon}{4+f\varepsilon} - \frac{2p\psi^2\varepsilon^2}{(4+f\varepsilon)^2}, \quad (19a)$$

$$V(\varepsilon) = v + \frac{4h\psi\varepsilon}{4+f\varepsilon} - \frac{2\psi^4\varepsilon^2}{(4+f\varepsilon)^2},$$

$$\begin{aligned} \Psi(\varepsilon) &= \frac{4\psi}{4+f\varepsilon}, \\ F(\varepsilon) &= \frac{4f}{4+f\varepsilon}, \end{aligned} \quad (19b)$$

$$\begin{aligned} G(\varepsilon) &= \frac{4g}{4+f\varepsilon} - \frac{4p\psi\varepsilon}{(4+f\varepsilon)^2}, \\ H(\varepsilon) &= \frac{h}{4+f\varepsilon} - \frac{\psi^3\varepsilon}{(4+f\varepsilon)^2}, \end{aligned} \quad (19c)$$

$$\begin{aligned} P(\varepsilon) &= \frac{16p}{(4+f\varepsilon)^2}, \\ Q(\varepsilon) &= \frac{4q}{4+f\varepsilon} - \frac{4(ph+3g\psi^2)\varepsilon}{(4+f\varepsilon)^2} + \frac{8p\psi^3\varepsilon^2}{(4+f\varepsilon)^3}, \end{aligned} \quad (19d)$$

where ε is an arbitrary group parameter.

3. Bäcklund Transformation Related to Multiple Residual Symmetries

Considering the intrusion of the spectral parameter λ in the nonlocal symmetry of equation (7), we can derive infinitely many residual symmetries of the fields u and v , that is,

$$\begin{aligned} \sigma_1 &= \sum_{i=1}^n c_i \Psi_i \Psi_{i,t}, \\ \sigma_2 &= \sum_{i=1}^n c_i \Psi_i \Psi_{i,x}, \end{aligned} \quad (20)$$

where ψ_i ($i = 1, 2, \dots, n$) are spectral functions of the Lax pair in equation (2) with different spectral parameters $\lambda_i \neq \lambda_j$ ($i \neq j$).

Just as the case of $n = 1$, to find the finite transformation of equation (20), we have to introduce a suitable prolonged system such that the symmetry can be localized to a Lie point symmetry. The corresponding finite transformation can be summarized as the following theorem.

Theorem 2. *If $\{u, v, \psi_i, f_i, g_i, h_i, p_i, q_i, i = 1, 2, \dots, n\}$ is a solution of the enlarged system*

$$u_x - v_t = 0, \quad (21a)$$

$$u_{xxx} + 4u_x v + 2uv_x = 0,$$

$$\psi_{i,xx} + v\psi_i - \lambda_i\psi_i = 0, \quad (21b)$$

$$\psi_{i,t} + \frac{1}{2\lambda_i}u\psi_{i,x} - \frac{1}{4\lambda_i}u_x\psi_i = 0, \quad (21c)$$

$$\psi_i^2 - f_{i,x} = 0,$$

$$4\lambda_i f_{i,t}\psi_{i,x} - \psi_i^2\psi_{i,xtt} + \psi_i\psi_{i,xx}\psi_{i,t} - 4\lambda_i\psi_i^2\psi_{i,t} \quad (21d)$$

$$- 4\psi_{i,x}^2\psi_{i,t} + 4\psi_i\psi_{i,x}\psi_{i,xt} = 0,$$

$$\psi_{i,t} - g_i = 0,$$

$$\psi_{i,x} - h_i = 0,$$

$$f_{i,t} - p_i = 0,$$

$$h_{i,t} - q_i = 0, \quad (21e)$$

then the symmetry (20) is localized to a Lie point symmetry as follows:

$$\sigma_1 = \sum_{i=1}^n c_i g_i \psi_i, \quad (22a)$$

$$\sigma_2 = \sum_{i=1}^n c_i h_i \psi_i,$$

$$\sigma_3 = -\frac{1}{4}c_i f_i \psi_i - \frac{1}{4} \sum_{j \neq i} c_j \psi_j \frac{(h_i \psi_j - h_j \psi_i)}{\lambda_i - \lambda_j}, \quad (22b)$$

$$\sigma_4 = -\frac{1}{4}c_i f_i^2 - \frac{1}{4} \sum_{j \neq i} c_j \frac{(h_i \psi_j - h_j \psi_i)^2}{(\lambda_i - \lambda_j)^2},$$

$$\sigma_5 = -\frac{1}{4}c_i (p_i \psi_i - f_i g_i) - \frac{1}{4} \sum_{j \neq i} c_j \frac{[g_j (h_i \psi_j - h_j \psi_i) + \psi_j (q_i \psi_j - q_j \psi_i) + \psi_j (g_j h_i - g_i h_j)]}{\lambda_i - \lambda_j}, \quad (22c)$$

$$\sigma_6 = -\frac{1}{4}c_i (\psi_i^3 + f_i h_i) - \frac{1}{4} \sum_{j \neq i} c_j \left[\frac{h_j (h_i \psi_j - h_j \psi_i)}{\lambda_i - \lambda_j} + \psi_i \psi_j^2 \right], \quad (22d)$$

$$\sigma_7 = -\frac{1}{2}c_i f_i p_i - \frac{1}{2} \sum_{j \neq i} c_j \frac{(h_i \psi_j - h_j \psi_i)(q_i \psi_j - q_j \psi_i + g_j h_i - g_i h_j)}{(\lambda_i - \lambda_j)^2}, \quad (22e)$$

$$\sigma_8 = -\frac{1}{4}c_i (3g_i \psi_i^2 + p_i h_i + f_i q_i) - \frac{1}{4} \sum_{j \neq i} c_j \left[\frac{q_j (h_i \psi_j - h_j \psi_i) + h_j (g_j h_i - g_i h_j) + h_j (q_i \psi_j - q_j \psi_i)}{\lambda_i - \lambda_j} + \psi_j^2 g_i + 2\psi_j \psi_i g_j \right]. \quad (22f)$$

Proof. The enlarged system (21a)–(21e) has the following linearized form:

$$\sigma_{1,x} - \sigma_{2,t} = 0, \quad (23a)$$

$$\sigma_{1,xxx} + 4v\sigma_{1,x} + 2v_x\sigma_1 + 4u_x\sigma_2 + 2u\sigma_{2,x} = 0,$$

$$\sigma_{3,xx} - \lambda_i\sigma_3 + v\sigma_3 + \psi_i\sigma_2 = 0, \quad (23b)$$

$$\sigma_{3,t} + \frac{1}{2\lambda_i}(u\sigma_{3,x} + \psi_{i,x}\sigma_1) - \frac{1}{4\lambda_i}(u_x\sigma_3 + \psi_i\sigma_{1,x}) = 0, \quad (23c)$$

$$\begin{aligned} & (\psi_{i,xx}\psi_{i,t} + 4\psi_{i,x}\psi_{i,xt} - 2\psi_i\psi_{i,xtt} - 8\lambda_i\psi_i\psi_{i,t})\sigma_3 \\ & + 4(\lambda_i f_{i,t} + \psi_i\psi_{i,xt} - 2\psi_{i,x}\psi_{i,t})\sigma_{3,x} \\ & + (\psi_i\psi_{i,xx} - 4\psi_{i,x}^2 - 4\lambda_i\psi_i^2)\sigma_{3,t} + \psi_i\psi_{i,t}\sigma_{3,xx} \\ & + 4\psi_i\psi_{i,x}\sigma_{3,xt} - \psi_i^2\sigma_{3,xtt} + 4\lambda_i\psi_{i,x}\sigma_{4,t} = 0, \end{aligned} \quad (23d)$$

$$\begin{aligned}
2\psi_i\sigma_{3_i} - \sigma_{4_i,x} &= 0, \\
\sigma_{3_i,t} - \sigma_{5_i} &= 0, \\
\sigma_{3_i,x} - \sigma_{6_i} &= 0, \\
\sigma_{4_i,t} - \sigma_{7_i} &= 0, \\
\sigma_{6_i,t} - \sigma_{8_i} &= 0, \\
i &= 1, 2, \dots, n.
\end{aligned} \tag{23e}$$

We first consider the special case, i.e., for any fixed $i = k, c_k \neq 0$ while $c_j = 0 (j \neq k)$ in equations (22a)–(22f). In this case, we obtain the localized symmetry for $u, v, \psi_k, f_k, g_k, h_k, p_k,$ and q_k from equation (17) as follows:

$$\begin{aligned}
\sigma &\equiv \{\sigma_1, \sigma_2, \sigma_{3_k}, \sigma_{4_k}, \sigma_{5_k}, \sigma_{6_k}, \sigma_{7_k}, \sigma_{8_k}\} \\
&= \left\{ c_k g_k \psi_k, c_k h_k \psi_k, -\frac{c_k f_k \psi_k}{4}, -\frac{c_k f_k^2}{4}, -\frac{c_k}{4} (p_k \psi_k + f_k g_k), -\frac{c_k}{4} (\psi_k^3 + f_k h_k), -\frac{c_k f_k p_k}{2}, -\frac{c_k}{4} (3g_k \psi_k^2 + p_k h_k + f_k q_k) \right\}.
\end{aligned} \tag{24}$$

For $j \neq k$, we eliminate v through equation (21b) by taking $i = k$ and $i = j$, respectively. Then, we have

$$\psi_{j,xx} = \frac{\psi_j \psi_{k,xx}}{\psi_k} - (\lambda_k - \lambda_j) \psi_j. \tag{25}$$

Substituting $\sigma_2 = c_k h_k \psi_k$, into equation (23b) with $i = j$ and vanishing $\psi_{j,xx}$ through equation (25), we have

$$\left(\lambda_k - \lambda_j + \frac{\psi_{j,xx}}{\psi_j} \right) \sigma_{3_j} - \sigma_{3_j,xx} - c_j \psi_k \psi_j \psi_{j,x} = 0. \tag{26}$$

It can be easily verified that equation (26) has the following solution:

$$\sigma_{3_j} = -\frac{c_j \psi_j (h_k \psi_j - h_j \psi_k)}{4(\lambda_k - \lambda_j)}. \tag{27}$$

The symmetry for $\sigma_{4_j}, \sigma_{5_j}, \sigma_{6_j}, \sigma_{7_j},$ and σ_{8_j} can be easily obtained from equation (23e) with $i = j$:

$$\sigma_{4_j} = -\frac{c_j (h_j \psi_k - h_k \psi_j)^2}{4(\lambda_k - \lambda_j)^2}, \tag{28a}$$

$$\sigma_{5_j} = -\frac{c_j [g_j (h_k \psi_j - h_j \psi_k) + \psi_j (q_k \psi_j - q_j \psi_k) + \psi_j (g_j h_k - g_k h_j)]}{4(\lambda_k - \lambda_j)},$$

$$\sigma_{6_j} = -\frac{1}{4} c_j \left[\frac{h_j (h_k \psi_j - h_j \psi_k)}{\lambda_k - \lambda_j} + \psi_k \psi_j^2 \right], \tag{28b}$$

$$\sigma_{7_j} = -\frac{1}{2} \frac{c_j (h_k \psi_j - h_j \psi_k) (q_k \psi_j - q_j \psi_k + g_j h_k - g_k h_j)}{(\lambda_k - \lambda_j)^2},$$

$$\sigma_{8_j} = -\frac{1}{4} c_j \left[\frac{q_j (h_k \psi_j - h_j \psi_k) + h_j (g_j h_k - g_k h_j) + h_j (q_k \psi_j - q_j \psi_k)}{\lambda_k - \lambda_j} + \psi_j^2 g_k + 2\psi_j \psi_k g_j \right]. \tag{28c}$$

After taking the linear combination of the above results for all $k = 1, 2, \dots, n$, Theorem 2 is proved.

When a nonlocal symmetry is localized to a Lie point symmetry, searching for its finite transformation is inevitable according to Lie's first principle. For the Lie point symmetry (22a)–(22f), its initial value problem has

$$\frac{dU(\varepsilon)}{d\varepsilon} = \sum_{i=1}^n c_i G_i(\varepsilon) \Psi_i(\varepsilon), \quad U(0) = u, \quad (29a)$$

$$\frac{dV(\varepsilon)}{d\varepsilon} = \sum_{i=1}^n c_i H_i(\varepsilon) \Psi_i(\varepsilon), \quad V(0) = v,$$

$$\begin{aligned} \frac{d\Psi_i(\varepsilon)}{d\varepsilon} &= -\frac{1}{4} c_i F_i(\varepsilon) \Psi_i(\varepsilon) \\ &\quad - \frac{1}{4} \sum_{j \neq i} c_j \Psi_j(\varepsilon) \frac{[H_i(\varepsilon) \Psi_j(\varepsilon) - H_j(\varepsilon) \Psi_i(\varepsilon)]}{\lambda_i - \lambda_j}, \\ \Psi_i(0) &= \psi_i, \end{aligned} \quad (29b)$$

$$\begin{aligned} \frac{dF_i(\varepsilon)}{d\varepsilon} &= -\frac{1}{4} c_i F_i^2(\varepsilon) \\ &\quad - \frac{1}{4} \sum_{j \neq i} c_j \frac{[H_i(\varepsilon) \Psi_j(\varepsilon) - H_j(\varepsilon) \Psi_i(\varepsilon)]^2}{(\lambda_i - \lambda_j)^2}, \\ F_i(0) &= f_i, \end{aligned} \quad (29c)$$

$$\begin{aligned} \frac{dG_i(\varepsilon)}{d\varepsilon} &= -\frac{1}{4} c_i [P_i(\varepsilon) \Psi_i(\varepsilon) - F_i(\varepsilon) G_i(\varepsilon)] \\ &\quad - \frac{1}{4} \sum_{j \neq i} \frac{c_j}{\lambda_i - \lambda_j} \left\{ G_j(\varepsilon) [H_i(\varepsilon) \Psi_j(\varepsilon) - H_j(\varepsilon) \Psi_i(\varepsilon)] \right. \\ &\quad + \Psi_j(\varepsilon) [Q_i(\varepsilon) \Psi_j(\varepsilon) - Q_j(\varepsilon) \Psi_i(\varepsilon)] \\ &\quad \left. + \Psi_j(\varepsilon) [G_j(\varepsilon) H_i(\varepsilon) - G_i(\varepsilon) H_j(\varepsilon)] \right\}, \\ G_i(0) &= g_i, \end{aligned} \quad (29d)$$

$$\begin{aligned} \frac{dH_i(\varepsilon)}{d\varepsilon} &= -\frac{1}{4} c_i [\Psi_i^3(\varepsilon) + F_i(\varepsilon) H_i(\varepsilon)] \\ &\quad - \frac{1}{4} \sum_{j \neq i} c_j \left\{ \frac{H_j(\varepsilon) [H_i(\varepsilon) \Psi_j(\varepsilon) - H_j(\varepsilon) \Psi_i(\varepsilon)]}{\lambda_i - \lambda_j} \right. \\ &\quad \left. + \Psi_i(\varepsilon) \Psi_j^2(\varepsilon) \right\}, \quad H_i(0) = h_i, \end{aligned} \quad (29e)$$

$$\begin{aligned} \frac{dP_i(\varepsilon)}{d\varepsilon} &= -\frac{1}{2} c_i F_i(\varepsilon) P_i(\varepsilon) - \frac{1}{2} \sum_{j \neq i} \frac{c_j}{(\lambda_i - \lambda_j)^2} \\ &\quad \cdot [H_i(\varepsilon) \Psi_j(\varepsilon) - H_j(\varepsilon) \Psi_i(\varepsilon)] \% [Q_i(\varepsilon) \Psi_j(\varepsilon) \\ &\quad - Q_j(\varepsilon) \Psi_i(\varepsilon) + G_j(\varepsilon) H_i(\varepsilon) - G_i(\varepsilon) H_j(\varepsilon)], \\ P_i(0) &= p_i, \end{aligned} \quad (29f)$$

$$\begin{aligned} \frac{dQ_i(\varepsilon)}{d\varepsilon} &= -\frac{1}{4} c_i [3G_i(\varepsilon) \Psi_i^2(\varepsilon) + P_i(\varepsilon) H_i(\varepsilon) + F_i(\varepsilon) Q_i(\varepsilon)] \\ &\quad - \frac{1}{4} \sum_{j \neq i} c_j \left[\frac{1}{\lambda_i - \lambda_j} \% (Q_j(\varepsilon) (H_i(\varepsilon) \Psi_j(\varepsilon) \right. \\ &\quad - H_j(\varepsilon) \Psi_i(\varepsilon)) + H_j(\varepsilon) (G_j(\varepsilon) H_i(\varepsilon) - G_i(\varepsilon) H_j(\varepsilon)) \\ &\quad \left. + H_j(\varepsilon) (Q_i(\varepsilon) \Psi_j(\varepsilon) - Q_j(\varepsilon) \Psi_i(\varepsilon)) \% \right], \\ \frac{dQ_i(\varepsilon)}{d\varepsilon} &= -\frac{1}{4} c_i [3G_i(\varepsilon) \Psi_i^2(\varepsilon) + P_i(\varepsilon) H_i(\varepsilon) + F_i(\varepsilon) Q_i(\varepsilon)] \\ &\quad - \frac{1}{4} \sum_{j \neq i} c_j \left\{ \frac{Q_j(\varepsilon) [H_i(\varepsilon) \Psi_j(\varepsilon) - H_j(\varepsilon) \Psi_i(\varepsilon)]}{\lambda_i - \lambda_j} \right. \\ &\quad + \frac{H_j(\varepsilon) [G_j(\varepsilon) H_i(\varepsilon) - G_i(\varepsilon) H_j(\varepsilon)]}{\lambda_i - \lambda_j} \\ &\quad + \frac{H_j(\varepsilon) [Q_i(\varepsilon) \Psi_j(\varepsilon) - Q_j(\varepsilon) \Psi_i(\varepsilon)]}{\lambda_i - \lambda_j} \\ &\quad \left. + \Psi_j^2(\varepsilon) G_i(\varepsilon) + 2\Psi_j(\varepsilon) \Psi_i(\varepsilon) G_j(\varepsilon) \right\}, \quad Q_i(0) = q_i. \end{aligned} \quad (29g)$$

Then, one can get the following n -th Bäcklund theorem for the enlarged system (21a)–(21e) by solving (29a)–(29g). \square

Theorem 3. If $\{u, v, \psi_i, f_i, g_i, h_i, p_i, q_i, i = 1, 2, \dots, n\}$ is a solution of the prolonged nKdV equations (21a)–(21e), so is $\{U(\varepsilon), V(\varepsilon), \Psi_i(\varepsilon), F_i(\varepsilon), G_i(\varepsilon), H_i(\varepsilon), P_i(\varepsilon), Q_i(\varepsilon), i = 1, 2, \dots, n\}$, where

$$U(\varepsilon) = u + 2(\ln \Delta)_{xt}, \quad (30a)$$

$$V(\varepsilon) = v + 2(\ln \Delta)_{xx},$$

$$\Psi_i(\varepsilon) = \frac{2\Gamma_i}{\Delta}, \quad (30b)$$

$$F_i(\varepsilon) = \frac{2\Delta_i}{\Delta},$$

$$G_i(\varepsilon) = \Psi_{i,t}(\varepsilon),$$

$$\begin{aligned}
H_i(\varepsilon) &= \Psi_{i,x}(\varepsilon), \\
P_i(\varepsilon) &= F_{i,x}(\varepsilon), \\
Q_i(\varepsilon) &= \Psi_{i,xt}(\varepsilon),
\end{aligned} \tag{30c}$$

where Δ , Δ_i , and Γ_i are three determinants of the matrices D , D_i , and E_i , respectively, which are defined as follows:

$$\begin{aligned}
D &= \begin{pmatrix} c_1 \varepsilon f_1 + 4 & c_1 \varepsilon \mu_{1,2} & \cdots & c_1 \varepsilon \mu_{1,j} & \cdots & c_1 \varepsilon \mu_{1,n} \\ c_2 \varepsilon \mu_{1,2} & c_2 \varepsilon f_2 + 4 & \cdots & c_2 \varepsilon \mu_{2,j} & \cdots & c_2 \varepsilon \mu_{2,n} \\ \cdots & \cdots & \cdots & \cdots & \cdots & \cdots \\ c_j \varepsilon \mu_{1,j} & c_j \varepsilon \mu_{2,j} & \cdots & c_j \varepsilon f_j + 4 & \cdots & c_j \varepsilon \mu_{j,n} \\ \cdots & \cdots & \cdots & \cdots & \cdots & \cdots \\ c_n \varepsilon \mu_{1,n} & c_n \varepsilon \mu_{2,n} & \cdots & c_n \varepsilon \mu_{j,n} & \cdots & c_n \varepsilon f_n + 4 \end{pmatrix}, \quad \mu_{i,j} = \frac{h_j \psi_i - h_i \psi_j}{\lambda_i - \lambda_j}, \\
D_i &= \begin{pmatrix} c_1 \varepsilon f_1 + 4 & c_1 \varepsilon \mu_{1,2} & \cdots & c_1 \varepsilon \mu_{1,i-1} & c_1 \varepsilon \mu_{1,i} & c_1 \varepsilon \mu_{1,i+1} & \cdots & c_1 \varepsilon \mu_{1,n} \\ c_2 \varepsilon \mu_{1,2} & c_2 \varepsilon f_2 + 4 & \cdots & c_2 \varepsilon \mu_{2,i-1} & c_2 \varepsilon \mu_{2,i} & c_2 \varepsilon \mu_{2,i+1} & \cdots & c_2 \varepsilon \mu_{2,n} \\ \cdots & \cdots & \cdots & \cdots & \cdots & \cdots & \cdots & \cdots \\ c_{i-1} \varepsilon \mu_{1,i-1} & c_{i-1} \varepsilon \mu_{2,i-1} & \cdots & c_{i-1} \varepsilon f_{i-1} + 4 & c_{i-1} \varepsilon \mu_{i-1,i} & c_{i-1} \varepsilon \mu_{i-1,i+1} & \cdots & c_{i-1} \varepsilon \mu_{i-1,n} \\ \mu_{1,i} & \mu_{2,i} & \cdots & \mu_{i,i-1} & f_i & \mu_{i,i+1} & \cdots & \mu_{i,n} \\ c_{i+1} \varepsilon \mu_{1,i+1} & c_{i+1} \varepsilon \mu_{2,i+1} & \cdots & c_{i+1} \varepsilon \mu_{i-1,i+1} & c_{i+1} \varepsilon \mu_{i,i+1} & c_{i+1} \varepsilon f_{i+1} + 4 & \cdots & c_{i+1} \varepsilon \mu_{i+1,n} \\ \cdots & \cdots & \cdots & \cdots & \cdots & \cdots & \cdots & \cdots \\ c_n \varepsilon \mu_{1,n} & c_n \varepsilon \mu_{2,n} & \cdots & c_n \varepsilon \mu_{i-1,n} & c_n \varepsilon \mu_{i,n} & c_n \varepsilon \mu_{i+1,n} & \cdots & c_n \varepsilon f_n + 4 \end{pmatrix}, \\
E_i &= \begin{pmatrix} c_1 \varepsilon f_1 + 4 & c_1 \varepsilon \mu_{1,2} & \cdots & c_1 \varepsilon \mu_{1,i-1} & c_1 \varepsilon \mu_{1,i} & c_1 \varepsilon \mu_{1,i+1} & \cdots & c_1 \varepsilon \mu_{1,n} \\ c_2 \varepsilon \mu_{1,2} & c_2 \varepsilon f_2 + 4 & \cdots & c_2 \varepsilon \mu_{2,i-1} & c_2 \varepsilon \mu_{2,i} & c_2 \varepsilon \mu_{2,i+1} & \cdots & c_2 \varepsilon \mu_{2,n} \\ \cdots & \cdots & \cdots & \cdots & \cdots & \cdots & \cdots & \cdots \\ c_{i-1} \varepsilon \mu_{1,i-1} & c_{i-1} \varepsilon \mu_{2,i-1} & \cdots & c_{i-1} \varepsilon f_{i-1} + 4 & c_{i-1} \varepsilon \mu_{i-1,i} & c_{i-1} \varepsilon \mu_{i-1,i+1} & \cdots & c_{i-1} \varepsilon \mu_{i-1,n} \\ \psi_1 & \psi_2 & \cdots & \psi_{i-1} & \psi_i & \psi_{i+1} & \cdots & \psi_n \\ c_{i+1} \varepsilon \mu_{1,i+1} & c_{i+1} \varepsilon \mu_{2,i+1} & \cdots & c_{i+1} \varepsilon \mu_{i-1,i+1} & c_{i+1} \varepsilon \mu_{i,i+1} & c_{i+1} \varepsilon f_{i+1} + 4 & \cdots & c_{i+1} \varepsilon \mu_{i+1,n} \\ \cdots & \cdots & \cdots & \cdots & \cdots & \cdots & \cdots & \cdots \\ c_n \varepsilon \mu_{1,n} & c_n \varepsilon \mu_{2,n} & \cdots & c_n \varepsilon \mu_{i-1,n} & c_n \varepsilon \mu_{i,n} & c_n \varepsilon \mu_{i+1,n} & \cdots & c_n \varepsilon f_n + 4 \end{pmatrix}.
\end{aligned} \tag{31}$$

From Theorem 3, we can obtain an infinite number of new solutions from a suitable seed solution of the nKdV equation (1). Especially, one can obtain recursive soliton solutions of this system from the known one. For example, taking the seed solution $u = \alpha$ and $v = \beta$ for equation (1), it is not difficult to verify that equations (21a)–(21e) possess the following solution:

$$\begin{aligned}
\psi_i &= \exp\left(\frac{\xi_i}{2}\right), \\
f_i &= \frac{1}{2k_i} \exp(\xi_i), \\
\lambda_i &= k_i^2 + \beta, \\
\mu_{i,j} &= \frac{\exp((\xi_i + \xi_j)/2)}{k_i + k_j}, \\
\xi_i &= 2k_i x - \frac{\alpha k_i t}{k_i^2 + \beta},
\end{aligned} \tag{32}$$

$$i, j = 1, 2, \dots, n.$$

The corresponding first three multiple wave solutions for equation (1) are

$$\Delta_1 \equiv \Delta = c_1 \varepsilon f_1 + 4, \tag{33}$$

$$u = \alpha + 2(\ln \Delta_1)_{xt} = \alpha - \frac{32c_1 k_1^3 \alpha \varepsilon \exp(\xi_1)}{(k_1^2 + \beta)[8k_1 + c_1 \varepsilon \exp(\xi_1)]^2}, \tag{34a}$$

$$v = \beta + 2(\ln \Delta_1)_{xx} = \beta + \frac{64c_1 k_1^3 \varepsilon \exp(\xi_1)}{[8k_1 + c_1 \varepsilon \exp(\xi_1)]^2}, \tag{34b}$$

for the line soliton solution:

$$\begin{aligned}
\Delta_2 \equiv \Delta &= (c_1 \varepsilon f_1 + 4)(c_2 \varepsilon f_2 + 4) - c_1 c_2 \varepsilon^2 \mu_{1,2}^2 \\
&= 16 + 4c_1 \varepsilon f_1 + 4c_2 \varepsilon f_2 + \frac{c_1 c_2 \varepsilon^2 (k_1 - k_2)^2 f_1 f_2}{(k_1 + k_2)^2},
\end{aligned} \tag{35}$$

$$\begin{aligned}
u &= \alpha + 2(\ln \Delta_2)_{xt}, \\
v &= \beta + 2(\ln \Delta_2)_{xx},
\end{aligned} \tag{36}$$

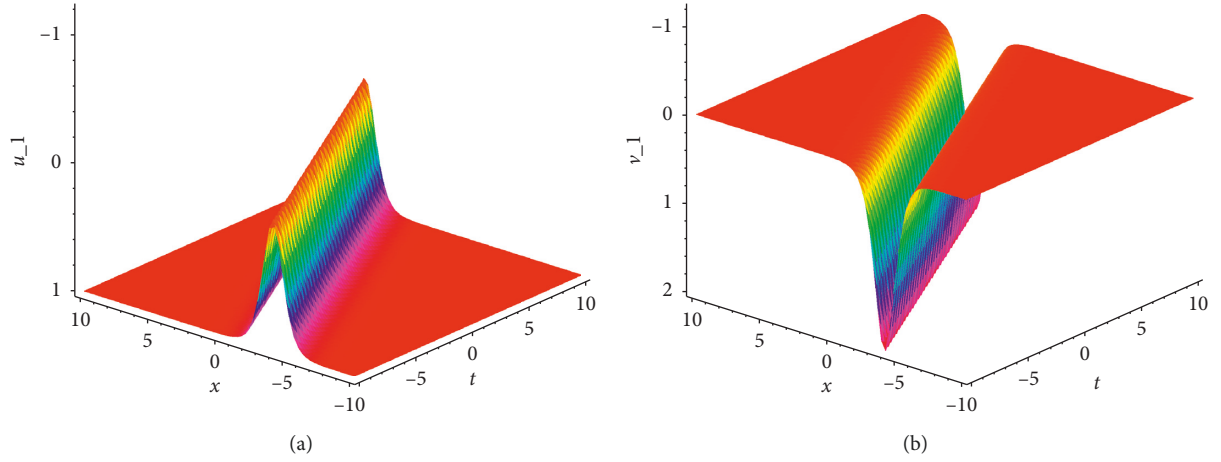


FIGURE 1: Plots of two line solitons expressed by equations (34a)–(34b) for solution of the nKdV equation (1) with the parameters $a = \varepsilon = c_1 = k_1 = 1$.

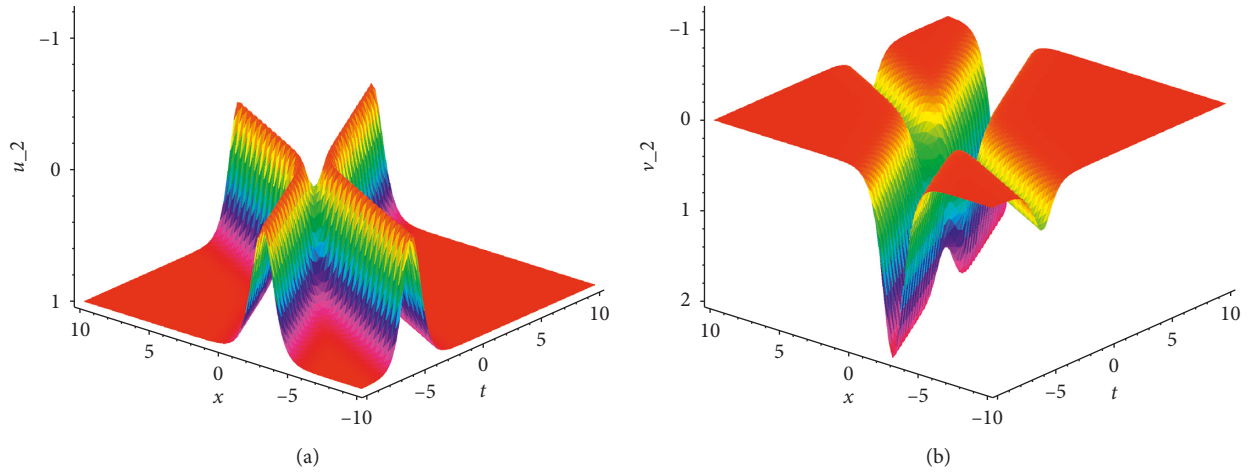


FIGURE 2: Interactions of two-resonant solitons expressed by equation (36) for solution of the nKdV equation (1) with the parameters $a = \varepsilon = c_1 = c_2 = k_1 = 1$ and $k_2 = 1/2$.

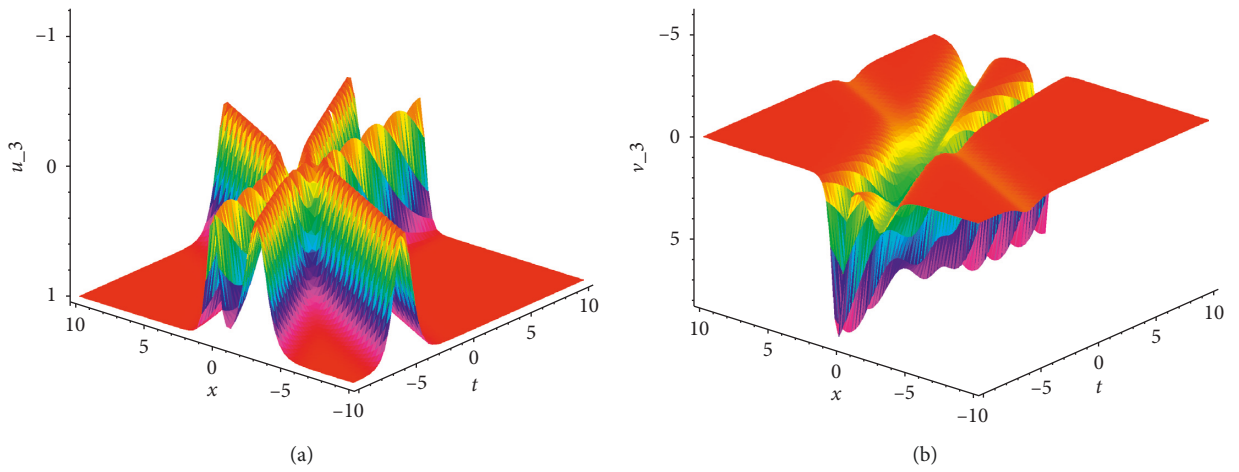


FIGURE 3: Interactions of three-resonant solitons expressed by equation (37) for solution of the nKdV equation (1) with the parameters $a = \varepsilon = c_1 = c_2 = c_3 = k_1 = 1$, $k_2 = 1/2$, and $k_3 = 2$.

$$\begin{aligned} u &= \alpha + 2(\ln \Delta_3)_{xt}, \\ v_3 &= \beta + 2(\ln \Delta_3)_{xx}, \end{aligned} \quad (37)$$

$$\begin{aligned} \Delta_3 &= \begin{vmatrix} c_1 \varepsilon f_1 + 4 & c_1 \varepsilon \mu_{1,2} & c_1 \varepsilon \mu_{1,3} \\ c_2 \varepsilon \mu_{1,2} & c_2 \varepsilon f_2 + 4 & c_2 \varepsilon \mu_{2,3} \\ c_3 \varepsilon \mu_{1,3} & c_3 \varepsilon \mu_{2,3} & c_3 \varepsilon f_3 + 4 \end{vmatrix} \\ &= 64 + 16c_1 \varepsilon f_1 + 16c_2 \varepsilon f_2 + 16c_3 \varepsilon f_3 \\ &\quad + \frac{4c_1 c_2 \varepsilon^2 (k_1 - k_2)^2 f_1 f_2}{(k_1 + k_2)^2} + \frac{4c_1 c_3 \varepsilon^2 (k_1 - k_3)^2 f_1 f_3}{(k_1 + k_3)^2} \\ &\quad + \frac{4c_2 c_3 \varepsilon^2 (k_2 - k_3)^2 f_2 f_3}{(k_2 + k_3)^2} \\ &\quad + \frac{c_1 c_2 c_3 \varepsilon^3 (k_1 - k_2)^2 (k_1 - k_3)^2 (k_2 - k_3)^2 f_1 f_2 f_3}{(k_1 + k_2)^2 (k_1 + k_3)^2 (k_2 + k_3)^2}. \end{aligned} \quad (38)$$

For illustrating more details, the parameters are set as follows: $a = \varepsilon = c_1 = c_2 = c_3 = k_1 = 1, k_2 = 1/2$, and $k_3 = 2$. Figure 1 displays the bell-like bright and dark solitons for the above condition of equations (34a)–(34b). Figure 1(a) shows a line dark soliton for u_1 with the amplitude 1, while Figure 1(b) shows a bright one for v_1 with the amplitude 2. Similarly, Figure 2 shows the collision of two-resonant solitons in equation (36), and Figure 3 shows interactions of three-resonant solitons expressed in equation (37).

4. Summary

The nonlocal symmetry of the nKdV equation is obtained with the aid of its Lax pair. After introducing four auxiliary variables g, h, p , and q , an enlarged system which possesses a Lie point symmetry for the nonlocal symmetry is taken. By applying Lie's first theorem for the localized point symmetries, we obtain the corresponding finite transformation. Furthermore, we can localize the linear superposition of multiple residual symmetries and construct the infinite transformation for the nKdV equation. From Theorem 3, the n -th Bäcklund transformation can be expressed in a compact way of determinants. According to this conclusion, one can derive special soliton solutions from some seed solutions.

Data Availability

The data used to support the findings of this study are included within the article.

Conflicts of Interest

The authors declare that there are no conflicts of interest regarding the publication of this paper.

Acknowledgments

This work was supported by the National Natural Science Foundation of China (Grant no. 11775104). WC thanks the

financial support from the High Level Talents Projects of Lishui City (Grant no. 2017RC16).

References

- [1] D. J. Korteweg and G. de Vries, "On the change of form of long waves advancing in a rectangular canal, and on a new type of long stationary waves," *Philosophical Magazine*, vol. 39, no. 240, pp. 422–443, 1895.
- [2] P. J. Olver, "Evolution equations possessing infinitely many symmetries," *Journal of Mathematical Physics*, vol. 18, no. 6, pp. 1212–1215, 1977.
- [3] J. M. Verosky, "Negative powers of Olver recursion operators," *Journal of Mathematical Physics*, vol. 32, no. 7, pp. 1733–1736, 1991.
- [4] J. Chen and S. Zhu, "Residual symmetries and soliton-cnoidal wave interaction solutions for the negative-order Korteweg–de Vries equation," *Applied Mathematics Letters*, vol. 73, pp. 136–142, 2017.
- [5] Z.-Y. Ma, J.-X. Fei, and J.-C. Chen, "The residual symmetry and consistent tanh expansion for the Benney system," *Zeitschrift für Naturforschung A*, vol. 72, no. 9, pp. 863–871, 2017.
- [6] S.-y. Lou, "Symmetries of the KdV equation and four hierarchies of the integrodifferential KdV equations," *Journal of Mathematical Physics*, vol. 35, no. 5, pp. 2390–2396, 1994.
- [7] Z. Qiao and J. Li, "Negative-order KdV equation with both solitons and kink wave solutions," *Europhysics Letters*, vol. 94, no. 5, p. 50003, 2011.
- [8] B. Fuchssteiner, "Some tricks from the symmetry-toolbox for nonlinear equations: generalizations of the Camassa-Holm equation," *Physica D: Nonlinear Phenomena*, vol. 95, no. 3–4, pp. 229–243, 1996.
- [9] R. G. Zhou, "Mixed hierarchy of soliton equations," *Journal of Mathematical Physics*, vol. 50, no. 12, Article ID 123502, 2009.
- [10] A.-M. Wazwaz and G.-Q. Xu, "Negative-order modified KdV equations: multiple soliton and multiple singular soliton solutions," *Mathematical Methods in the Applied Sciences*, vol. 39, no. 4, pp. 661–667, 2015.
- [11] H. Leblond and D. Mihalache, "Few-optical-cycle solitons: modified Korteweg–de Vries sine-Gordon equation versus other non-slowly-varying-envelope-approximation models," *Physical Review A*, vol. 79, no. 6, Article ID 063835, 2009.
- [12] A.-M. Wazwaz, "A new integrable equation combining the modified KdV equation with the negative-order modified KdV equation: multiple soliton solutions and a variety of solitonic solutions," *Waves Random Complex Media*, vol. 28, no. 3, pp. 533–543, 2018.
- [13] S.-y. Lou, "Negative kadmomtsev-petviashvili hierarchy," *Physica Scripta*, vol. 57, no. 4, pp. 481–485, 1998.
- [14] Z. Qiao and E. Fan, "Negative-order Korteweg–de Vries equations," *Physical Review E*, vol. 86, no. 1, Article ID 016601, 2012.
- [15] Z. J. Qiao, "A general approach for getting the commutator representations of the hierarchies of nonlinear evolution equations," *Physics Letters A*, vol. 212, no. 6, p. 350, 1994.
- [16] Z. J. Qiao, C. W. Cao, and W. Strampp, "Category of nonlinear evolution equations, algebraic structure, and r-matrix," *Journal of Mathematical Physics*, vol. 44, no. 2, p. 701, 2003.
- [17] Z. J. Qiao, *Finite-dimensional Integrable System and Nonlinear Evolution Equations*, Higher Education Press, Beijing, China, 2002.

- [18] A.-M. Wazwaz, "Negative-order KdV and negative-order KP equations: multiple soliton solutions," *Proceedings of the National Academy of Sciences, India Section A: Physical Sciences*, vol. 87, no. 2, pp. 291–296, 2017.
- [19] N. A. Kudryashov, "On completely integrability systems of differential equations," 2010, <http://arxiv.org/abs/1011.3936v1>.
- [20] N. A. Kudryashov, "Unnecessary exact solutions of nonlinear ordinary differential equations," 2010, <http://arxiv.org/abs/1011.1623v1>.

Research Article

Oscillation Criteria for Third-Order Emden–Fowler Differential Equations with Unbounded Neutral Coefficients

George E. Chatzarakis,¹ Said R. Grace ,² Irena Jadlovská,³
Tongxing Li ,⁴ and Ercan Tunç ⁵

¹Department of Electrical and Electronic Engineering Educators, School of Pedagogical and Technological Education (ASPETE), 14121 N. Heraklio, Athens, Greece

²Department of Engineering Mathematics, Faculty of Engineering, Cairo University, Orman, Giza 12221, Egypt

³Department of Mathematics and Theoretical Informatics, Faculty of Electrical Engineering and Informatics, Technical University of Košice, B. Němcovej 32, 042 00, Košice, Slovakia

⁴School of Control Science and Engineering, Shandong University, Jinan, Shandong 250061, China

⁵Department of Mathematics, Faculty of Arts and Sciences, Gaziosmanpasa University, 60240 Tokat, Turkey

Correspondence should be addressed to Tongxing Li; litongx2007@163.com

Received 10 May 2019; Accepted 22 July 2019; Published 28 August 2019

Academic Editor: András Rontó

Copyright © 2019 George E. Chatzarakis et al. This is an open access article distributed under the Creative Commons Attribution License, which permits unrestricted use, distribution, and reproduction in any medium, provided the original work is properly cited.

New sufficient conditions for the oscillation of all solutions to a class of third-order Emden–Fowler differential equations with unbounded neutral coefficients are established. The criteria obtained essentially improve related results in the literature. In particular, as opposed to known results, new criteria can distinguish solutions of third-order differential equations with different behaviors. Examples are also provided to illustrate the results.

1. Introduction

This paper is concerned with the oscillation of solutions of the third-order Emden–Fowler neutral differential equation

$$z'''(t) + q(t)x^\lambda(g(t)) = 0, \quad t \geq t_0 > 0, \quad (1)$$

where $z(t) := x(t) + p(t)x(\eta(t))$, $\lambda > 0$ is the ratio of odd positive integers. Throughout, the following conditions are assumed to hold:

(C1) $p, q : [t_0, \infty) \rightarrow \mathbb{R}$ are continuous functions, $p(t) \geq 1$, $p(t) \neq 1$ for large t , $q(t) \geq 0$, and $q(t)$ is not identically zero for large t ;

(C2) $\eta, g : [t_0, \infty) \rightarrow \mathbb{R}$ are continuous functions, $\eta(t) \leq t$, η is strictly increasing, and $\lim_{t \rightarrow \infty} \eta(t) = \lim_{t \rightarrow \infty} g(t) = \infty$.

The study of (1) is important due to the further development of the oscillation theory and its practical reasons.

Emden–Fowler differential equations have numerous applications in physics (mathematical, theoretical, and chemical physics) and engineering; see, e.g., the papers by Agarwal et al. [1], Li and Rogovchenko [2–5], and Wong [6].

By a solution of (1) we mean a continuous function $x : [t_x, \infty) \rightarrow \mathbb{R}$, $t_x \geq t_0$, such that $z \in C^3([t_x, \infty), \mathbb{R})$ and $x(t)$ satisfies (1) on $[t_x, \infty)$. We consider only proper solutions $x(t)$ of (1) that satisfy $\sup\{|x(t)| : t \geq T\} > 0$ for all $T \geq t_x$. Furthermore, we tacitly suppose that (1) possesses such solutions. Such a solution $x(t)$ of (1) is said to be oscillatory if it has arbitrarily large zeros on $[t_x, \infty)$; i.e., for any $t_1 \in [t_x, \infty)$, there exists a $t_2 \geq t_1$ such that $x(t_2) = 0$; otherwise, it is called nonoscillatory, i.e., if it is either eventually positive or eventually negative. Equation (1) is said to be oscillatory if all its proper solutions oscillate.

In recent years, there has been much research activity concerning the oscillation and asymptotic behavior of solutions to various classes of third-order neutral differential equations. We refer the reader to the papers [2, 7–17] and

the references contained therein as examples of recent results on this topic. However, the sufficient conditions established in these papers except [10, 13] ensure that every solution $x(t)$ of equations either oscillates or converges to zero as $t \rightarrow \infty$. This means that these results cannot distinguish solutions with different behaviors. On the other hand, the papers [2, 7–17] were concerned with the case where p is bounded, i.e., the cases where $-1 < p_0 \leq p(t) \leq 0$, $0 \leq p(t) \leq p_0 < 1$, and $0 \leq p(t) \leq p_0 < \infty$ were considered. In view of the observations above, we wish to develop new sufficient conditions which not only ensure oscillation of (1) but also can be applied to the case where p is unbounded. We would like to point out that only a few results are known regarding oscillatory and asymptotic behavior of third-order neutral differential equations for unbounded p ; see, e.g., the papers [18–20], where the Riccati transformation technique and comparison method were used to obtain the results. A similar observation as above is valid for these papers as well, i.e., the sufficient conditions established in these papers cannot distinguish solutions with different behaviors too.

Consequently, our work is of significance because of the above-mentioned reasons. Moreover, the results obtained in this paper can easily be extended to more general third-order differential equations with unbounded neutral coefficients to derive more general oscillation results. It is our belief that the present paper will contribute significantly to the study of oscillatory behavior of solutions of third-order neutral differential equations. In the sequel, all functional inequalities are supposed to hold eventually.

2. Main Results

We begin with the following lemmas that will play an important role in establishing our main results. For notational purposes, we let

$$\begin{aligned} \varphi(t) &:= \frac{1}{p(\eta^{-1}(t))} \left(1 - \frac{1}{p(\eta^{-1}(\eta^{-1}(t)))} \right) \geq 0, \\ \psi(t) &:= \frac{1}{p(\eta^{-1}(t))} \left(1 - \frac{1}{p(\eta^{-1}(\eta^{-1}(t)))} \right) \\ &\quad - \frac{1}{p(\eta^{-1}(\eta^{-1}(t)))} \frac{(\eta^{-1}(\eta^{-1}(t)))^{2/l_1}}{(\eta^{-1}(t))^{2/l_1}} \geq 0, \end{aligned} \quad (2)$$

where $l_1 \in (0, 1)$ is a constant and η^{-1} is the inverse function of η .

Lemma 1 (see [21]). *Let the function h satisfy $h^{(i)}(t) > 0$, $i = 0, 1, \dots, m$ and $h^{(m+1)}(t) \leq 0$ eventually. Then, for every $l \in (0, 1)$, $h(t)/h'(t) \geq lt/m$ eventually.*

Lemma 2. *Let conditions (C1) and (C2) be satisfied and assume that x is an eventually positive solution of (1). Then for sufficiently large t , either*

$$(I) \ z(t) > 0, \ z'(t) > 0, \ z''(t) > 0, \ \text{and} \ z'''(t) \leq 0; \ \text{or}$$

$$(II) \ z(t) > 0, \ z'(t) < 0, \ z''(t) > 0, \ \text{and} \ z'''(t) \leq 0.$$

Proof. The proof is not difficult and so is omitted. \square

Theorem 3. *In addition to conditions (C1) and (C2), assume that there exists a function $\sigma \in C([t_0, \infty), \mathbb{R})$ such that $g(t) \leq \sigma(t) < \eta(t)$ for $t \geq t_0$. If for some constants $l_1, l_2 \in (0, 1)$, the two first-order delay differential equations*

$$\begin{aligned} Y'(t) + \frac{(l_1 l_2)^\lambda}{2^\lambda} q(t) \psi^\lambda(g(t)) (\eta^{-1}(g(t)))^{2\lambda} \\ \cdot Y^\lambda(\eta^{-1}(g(t))) = 0 \end{aligned} \quad (3)$$

and

$$\begin{aligned} W'(t) + \frac{1}{2^\lambda} q(t) \varphi^\lambda(g(t)) (\eta^{-1}(\sigma(t)) - \eta^{-1}(g(t)))^{2\lambda} \\ \cdot W^\lambda(\eta^{-1}(\sigma(t))) = 0 \end{aligned} \quad (4)$$

oscillate, then (1) oscillates.

Proof. Let x be a nonoscillatory solution of (1). Since $-x$ is also a solution of (1), without loss of generality, we may suppose that there exists a $t_1 \in [t_0, \infty)$ such that, for $t \geq t_1$, $x(t) > 0$, $x(\eta(t)) > 0$, and $x(g(t)) > 0$. It follows from Lemma 2 that z satisfies either case (I) or case (II).

Assume first that case (I) holds. By virtue of the definition of z , we conclude that

$$\begin{aligned} x(t) &= \frac{1}{p(\eta^{-1}(t))} (z(\eta^{-1}(t)) - x(\eta^{-1}(t))) \\ &= \frac{z(\eta^{-1}(t))}{p(\eta^{-1}(t))} \\ &\quad - \frac{z(\eta^{-1}(\eta^{-1}(t))) - x(\eta^{-1}(\eta^{-1}(t)))}{p(\eta^{-1}(t)) p(\eta^{-1}(\eta^{-1}(t)))} \\ &\geq \frac{z(\eta^{-1}(t))}{p(\eta^{-1}(t))} - \frac{z(\eta^{-1}(\eta^{-1}(t)))}{p(\eta^{-1}(t)) p(\eta^{-1}(\eta^{-1}(t)))}. \end{aligned} \quad (5)$$

Taking into account (I) and Lemma 1 with $m = 2$, we deduce that, for every $l_1 \in (0, 1)$,

$$\frac{z(t)}{z'(t)} \geq l_1 \frac{t}{2}, \quad (6)$$

which yields

$$\left(\frac{z(t)}{t^{2/l_1}} \right)' = \frac{tz'(t) - (2/l_1)z(t)}{t^{(2/l_1)+1}} \leq 0. \quad (7)$$

Hence, $z(t)/t^{2/l_1}$ is nonincreasing for sufficiently large t . It follows from $\eta(t) \leq t$ and the monotonicities of $\eta(t)$ and $z(t)/t^{2/l_1}$ that

$$z(\eta^{-1}(\eta^{-1}(t))) \leq \frac{(\eta^{-1}(\eta^{-1}(t)))^{2/l_1}}{(\eta^{-1}(t))^{2/l_1}} z(\eta^{-1}(t)). \quad (8)$$

Using (8) in (5), we arrive at

$$x(t) \geq \psi(t) z(\eta^{-1}(t)), \quad (9)$$

and thus

$$x(g(t)) \geq \psi(g(t)) z(\eta^{-1}(g(t))). \quad (10)$$

Combining (1) and (10), we obtain

$$z'''(t) + q(t) \psi^\lambda(g(t)) z^\lambda(\eta^{-1}(g(t))) \leq 0. \quad (11)$$

It follows now from (6) and (11) that

$$\begin{aligned} & z'''(t) \\ & + \frac{l_1^\lambda}{2^\lambda} q(t) \psi^\lambda(g(t)) (\eta^{-1}(g(t)))^\lambda (z'(\eta^{-1}(g(t))))^\lambda \\ & \leq 0. \end{aligned} \quad (12)$$

Letting $w(t) := z'(t)$, we have

$$\begin{aligned} & w(t) > 0, \\ & w'(t) > 0, \\ & w''(t) \leq 0, \end{aligned} \quad (13)$$

and inequality (12) can be written as

$$\begin{aligned} & w''(t) \\ & + \frac{l_1^\lambda}{2^\lambda} q(t) \psi^\lambda(g(t)) (\eta^{-1}(g(t)))^\lambda w^\lambda(\eta^{-1}(g(t))) \\ & \leq 0. \end{aligned} \quad (14)$$

Combining (13) and Lemma 1 with $m = 1$, we get, for every $l_2 \in (0, 1)$,

$$\frac{w(t)}{w'(t)} \geq l_2 t, \quad (15)$$

and so

$$w(\eta^{-1}(g(t))) \geq l_2 \eta^{-1}(g(t)) w'(\eta^{-1}(g(t))). \quad (16)$$

Using (16) in (14), we deduce that

$$\begin{aligned} & w''(t) + \frac{(l_1 l_2)^\lambda}{2^\lambda} q(t) \psi^\lambda(g(t)) (\eta^{-1}(g(t)))^{2\lambda} \\ & \cdot (w'(\eta^{-1}(g(t))))^\lambda \leq 0. \end{aligned} \quad (17)$$

Letting $Y(t) := w'(t)$, we see that Y is a positive solution of the first-order delay differential inequality

$$\begin{aligned} & Y'(t) + \frac{(l_1 l_2)^\lambda}{2^\lambda} q(t) \psi^\lambda(g(t)) (\eta^{-1}(g(t)))^{2\lambda} \\ & \cdot Y^\lambda(\eta^{-1}(g(t))) \leq 0. \end{aligned} \quad (18)$$

Therefore, by [22, Theorem 1], we conclude that, for every $l_1, l_2 \in (0, 1)$, (3) has a positive solution, which contradicts the fact that (3) oscillates.

Next, suppose that case (II) holds. Since z is strictly decreasing and $\eta(t) \leq t$, we have

$$z(\eta^{-1}(t)) \geq z(\eta^{-1}(\eta^{-1}(t))). \quad (19)$$

Using (19) in (5), we conclude that

$$x(t) \geq \varphi(t) z(\eta^{-1}(t)), \quad (20)$$

and thus

$$x(g(t)) \geq \varphi(g(t)) z(\eta^{-1}(g(t))). \quad (21)$$

Substitution of (21) into (1) implies that

$$z'''(t) + q(t) \varphi^\lambda(g(t)) z^\lambda(\eta^{-1}(g(t))) \leq 0. \quad (22)$$

Since $z(t) > 0$, $z'(t) < 0$, $z''(t) > 0$, and $z'''(t) \leq 0$, for $v \geq u \geq t_2$, one can easily arrive at

$$z(u) \geq \frac{(v-u)^2}{2} z''(v). \quad (23)$$

By virtue of $g(t) \leq \sigma(t)$ and the fact that η is strictly increasing, we deduce that $\eta^{-1}(g(t)) \leq \eta^{-1}(\sigma(t))$. Substitute $u = \eta^{-1}(g(t))$ and $v = \eta^{-1}(\sigma(t))$ into (23) to obtain

$$\begin{aligned} & z(\eta^{-1}(g(t))) \\ & \geq \frac{(\eta^{-1}(\sigma(t)) - \eta^{-1}(g(t)))^2}{2} z''(\eta^{-1}(\sigma(t))). \end{aligned} \quad (24)$$

Using (24) in (22), we get

$$\begin{aligned} & z'''(t) + \frac{1}{2^\lambda} q(t) \varphi^\lambda(g(t)) (\eta^{-1}(\sigma(t)) - \eta^{-1}(g(t)))^{2\lambda} \\ & \cdot (z''(\eta^{-1}(\sigma(t))))^\lambda \leq 0. \end{aligned} \quad (25)$$

Letting $W(t) := z''(t)$, we see that W is a positive solution of the first-order delay differential inequality

$$\begin{aligned} & W'(t) + \frac{1}{2^\lambda} q(t) \varphi^\lambda(g(t)) (\eta^{-1}(\sigma(t)) - \eta^{-1}(g(t)))^{2\lambda} \\ & \cdot W^\lambda(\eta^{-1}(\sigma(t))) \leq 0. \end{aligned} \quad (26)$$

The rest of the proof is similar to that of case (I) and hence is omitted. This completes the proof. \square

From [23], it is well known that if

$$\liminf_{t \rightarrow \infty} \int_{\tau(t)}^t R(s) ds > \frac{1}{e}, \quad (27)$$

then the first-order delay differential equation

$$x'(t) + R(t) x(\tau(t)) = 0 \quad (28)$$

oscillates, where $R, \tau \in C([t_0, \infty), \mathbb{R})$, $R(t) \geq 0$, $\tau(t) < t$, and $\lim_{t \rightarrow \infty} \tau(t) = \infty$. Therefore, by virtue of Theorem 3, we have the following result.

Corollary 4. *Let conditions (C1) and (C2) be satisfied and $\lambda = 1$. Assume that there exists a function $\sigma \in C([t_0, \infty), \mathbb{R})$ such that $g(t) \leq \sigma(t) < \eta(t)$ for $t \geq t_0$. If for some constant $l_1 \in (0, 1)$,*

$$\liminf_{t \rightarrow \infty} \int_{\eta^{-1}(g(t))}^t q(s) \psi(g(s)) (\eta^{-1}(g(s)))^2 ds > \frac{2}{l_1 e} \quad (29)$$

and

$$\liminf_{t \rightarrow \infty} \int_{\eta^{-1}(\sigma(t))}^t q(s) \varphi(g(s)) \cdot (\eta^{-1}(\sigma(s)) - \eta^{-1}(g(s)))^2 ds > \frac{2}{e}, \quad (30)$$

then (1) oscillates.

Corollary 5. *Let conditions (C1) and (C2) be satisfied and $\lambda < 1$. Assume that there exists a function $\sigma \in C([t_0, \infty), \mathbb{R})$ such that $g(t) \leq \sigma(t) < \eta(t)$ for $t \geq t_0$. If for some constant $l_1 \in (0, 1)$,*

$$\int_{t_0}^{\infty} q(t) \psi^\lambda(g(t)) (\eta^{-1}(g(t)))^{2\lambda} dt = \infty \quad (31)$$

and

$$\int_{t_0}^{\infty} q(t) \varphi^\lambda(g(t)) (\eta^{-1}(\sigma(t)) - \eta^{-1}(g(t)))^{2\lambda} dt = \infty, \quad (32)$$

then (1) oscillates.

Proof. Applications of (31), (32), and [24, Theorem 2] imply that (3) and (4) oscillate. Hence, by Theorem 3, (1) oscillates. \square

Next, we present the following interesting result for which we need to assume that the function g in condition (C2) is nondecreasing.

Theorem 6. *In addition to conditions (C1) and (C2), assume that the function g with $g(t) < \eta(t)$ is nondecreasing on $[t_0, \infty)$. If for some constant $l_1 \in (0, 1)$,*

$$\limsup_{t \rightarrow \infty} (\eta^{-1}(g(t)))^{2\lambda} \cdot \int_t^{\infty} q(s) \psi^\lambda(g(s)) ds \begin{cases} > \frac{2}{l_1}, & \text{if } \lambda = 1, \\ = \infty, & \text{if } \lambda < 1, \end{cases} \quad (33)$$

and

$$\limsup_{t \rightarrow \infty} \int_{\eta^{-1}(g(t))}^t q(s) \varphi^\lambda(g(s)) (\eta^{-1}(g(t)) - \eta^{-1}(g(s)))^{2\lambda} ds \begin{cases} > 2, & \text{if } \lambda = 1, \\ = \infty, & \text{if } \lambda < 1, \end{cases} \quad (34)$$

then (1) oscillates.

Proof. Let x be a nonoscillatory solution of (1). Without loss of generality, we may suppose that there exists a $t_1 \in [t_0, \infty)$

such that, for $t \geq t_1$, $x(t) > 0$, $x(\eta(t)) > 0$, and $x(g(t)) > 0$. It follows from Lemma 2 that z satisfies either case (I) or case (II).

Assume that case (I) holds. Proceeding as in the proof of Theorem 3, we deduce that (13), (14), and (16) hold for every $l_1, l_2 \in (0, 1)$. Integrating (14) from t to u , $u \geq t$ and letting $u \rightarrow \infty$, we obtain

$$\begin{aligned} w'(t) &\geq \int_t^{\infty} \frac{l_1^\lambda}{2^\lambda} q(s) \psi^\lambda(g(s)) (\eta^{-1}(g(s)))^\lambda \\ &\quad \cdot w^\lambda(\eta^{-1}(g(s))) ds \\ &\geq \left(\int_t^{\infty} \frac{l_1^\lambda}{2^\lambda} q(s) \psi^\lambda(g(s)) (\eta^{-1}(g(s)))^\lambda ds \right) \\ &\quad \cdot w^\lambda(\eta^{-1}(g(t))). \end{aligned} \quad (35)$$

Using (16) in (35), we conclude that

$$\begin{aligned} w'(t) &\geq \left(\int_t^{\infty} \frac{(l_1 l_2)^\lambda}{2^\lambda} q(s) \psi^\lambda(g(s)) (\eta^{-1}(g(s)))^\lambda ds \right) \\ &\quad \cdot (\eta^{-1}(g(t)))^\lambda (w'(\eta^{-1}(g(t))))^\lambda, \end{aligned} \quad (36)$$

which yields

$$\begin{aligned} w'(t) &\geq \left(\int_t^{\infty} \frac{(l_1 l_2)^\lambda}{2^\lambda} q(s) \psi^\lambda(g(s)) ds \right) \\ &\quad \cdot (\eta^{-1}(g(t)))^{2\lambda} (w'(\eta^{-1}(g(t))))^\lambda. \end{aligned} \quad (37)$$

Using (13) and the fact that $\eta^{-1}(g(t)) \leq t$, we have

$$w'(\eta^{-1}(g(t))) \geq w'(t), \quad (38)$$

and so inequality (37) implies that

$$\begin{aligned} w'(t) &\geq \left(\int_t^{\infty} \frac{(l_1 l_2)^\lambda}{2^\lambda} q(s) \psi^\lambda(g(s)) ds \right) \\ &\quad \cdot (\eta^{-1}(g(t)))^{2\lambda} (w'(t))^\lambda, \end{aligned} \quad (39)$$

i.e.,

$$\begin{aligned} (w'(t))^{1-\lambda} &\geq \left(\int_t^{\infty} \frac{(l_1 l_2)^\lambda}{2^\lambda} q(s) \psi^\lambda(g(s)) ds \right) (\eta^{-1}(g(t)))^{2\lambda}. \end{aligned} \quad (40)$$

Taking lim sup as $t \rightarrow \infty$ in (40), we obtain a contradiction to (33).

Next, let case (II) hold. Then, we arrive at (22) and (23). For $t \geq s \geq t_2$, we see that $\eta^{-1}(g(t)) \geq \eta^{-1}(g(s))$. Putting $u = \eta^{-1}(g(s))$ and $v = \eta^{-1}(g(t))$ into (23), we get

$$\begin{aligned} z(\eta^{-1}(g(s))) &\geq \frac{(\eta^{-1}(g(t)) - \eta^{-1}(g(s)))^2}{2} z''(\eta^{-1}(g(t))). \end{aligned} \quad (41)$$

Integrating (22) from $\eta^{-1}(g(t))$ to t and using (41), we obtain

$$\begin{aligned} z''(\eta^{-1}(g(t))) &\geq \left(\int_{\eta^{-1}(g(t))}^t \frac{1}{2^\lambda} q(s) \varphi^\lambda(g(s)) \right. \\ &\quad \cdot (\eta^{-1}(g(t)) - \eta^{-1}(g(s)))^{2\lambda} ds \Big) \\ &\quad \cdot (z''(\eta^{-1}(g(t))))^\lambda, \end{aligned} \quad (42)$$

which can be written as

$$\begin{aligned} (z''(\eta^{-1}(g(t))))^{1-\lambda} &\geq \int_{\eta^{-1}(g(t))}^t \frac{1}{2^\lambda} q(s) \varphi^\lambda(g(s)) \\ &\quad \cdot (\eta^{-1}(g(t)) - \eta^{-1}(g(s)))^{2\lambda} ds. \end{aligned} \quad (43)$$

Taking lim sup as $t \rightarrow \infty$ in (43), we obtain a contradiction to (34). The proof is complete. \square

We conclude this paper with the following examples and remarks to illustrate the main results. The first example is concerned with the case where $p(t) \rightarrow \infty$ as $t \rightarrow \infty$, whereas the second example is concerned with the case where p is a bounded function.

Example 7. Consider the sublinear Emden–Fowler neutral differential equation

$$\left(x(t) + tx \left(\frac{t}{2} \right) \right)''' + \frac{k}{t^\alpha} x^{1/3} \left(\frac{t}{4} \right) = 0, \quad t \geq 17, \quad (44)$$

where $k > 0$ and $0 < \alpha < 1$ are constants. Here $\lambda = 1/3$, $p(t) = t$, $\eta(t) = t/2$, $g(t) = t/4$, $q(t) = k/t^\alpha$, $\eta^{-1}(g(t)) = t/2$, and $\varphi(g(t)) = 2(1 - 1/t)/t$. Let $l_1 = 1/2$. Then $\psi(g(t)) = 2(1 - 16/t)/t$ and condition (31) becomes

$$\begin{aligned} &\int_{17}^{\infty} \frac{k}{t^\alpha} \left(\frac{2t - 32}{t^2} \right)^{1/3} \left(\frac{t}{2} \right)^{2/3} dt \\ &= \frac{1}{2^{2/3}} \int_{17}^{\infty} \frac{k}{t^\alpha} (2t - 32)^{1/3} dt \geq \frac{1}{2^{1/3}} \int_{17}^{\infty} \frac{k}{t^\alpha} dt \\ &= \infty. \end{aligned} \quad (45)$$

Letting $\sigma(t) = t/3$, then $\eta^{-1}(\sigma(t)) = 2t/3$ and condition (32) reduces to

$$\begin{aligned} &\int_{17}^{\infty} \frac{k}{t^\alpha} \left(\frac{2t - 2}{t^2} \right)^{1/3} \left(\frac{t}{6} \right)^{2/3} dt \\ &= \frac{1}{6^{2/3}} \int_{17}^{\infty} \frac{k}{t^\alpha} (2t - 2)^{1/3} dt \geq \frac{2^{5/3}}{6^{2/3}} \int_{17}^{\infty} \frac{k}{t^\alpha} dt \\ &= \infty. \end{aligned} \quad (46)$$

Therefore, by Corollary 5, (44) oscillates.

Example 8. Consider the linear differential equation

$$\left(x(t) + \frac{6t + 9}{t + 1} x \left(\frac{t}{2} \right) \right)''' + \frac{k}{t^3} x \left(\frac{t}{3} \right) = 0, \quad t \geq 1. \quad (47)$$

Here $\lambda = 1$, $p(t) = (6t + 9)/(t + 1)$, $\eta(t) = t/2$, $g(t) = t/3$, $q(t) = k/t^3$, and $k > 1390$ is a constant. It is easy to deduce that $6 \leq p(t) \leq 15/2$, $\eta^{-1}(g(t)) = 2t/3$, $\varphi(g(t)) \geq 1/9$, and $\psi(g(t)) \geq 1/25$ for some constant $l_1 \in (1/2, 1)$. Using $\lambda = 1$ in (33), we have

$$\begin{aligned} &(\eta^{-1}(g(t)))^{2\lambda} \int_t^{\infty} q(s) \psi^\lambda(g(s)) ds \\ &\geq \frac{1}{25} \left(\frac{2t}{3} \right)^2 \int_t^{\infty} \frac{k}{s^3} ds = \frac{2k}{225}. \end{aligned} \quad (48)$$

That is, condition (33) with $\lambda = 1$ holds.

Next, using $\lambda = 1$ in (34), we obtain

$$\begin{aligned} &\int_{\eta^{-1}(g(t))}^t q(s) \varphi^\lambda(g(s)) \\ &\quad \cdot (\eta^{-1}(g(t)) - \eta^{-1}(g(s)))^{2\lambda} ds \geq \frac{1}{9} \\ &\quad \cdot \int_{2t/3}^t \frac{k}{s^3} \left(\frac{2t - 2s}{3} \right)^2 ds = \frac{k}{81} \\ &\quad \cdot \int_{2t/3}^t \left(\frac{4t^2}{s^3} - \frac{8t}{s^2} + \frac{4}{s} \right) ds = \frac{k}{81} \left(4 \ln \frac{3}{2} - \frac{3}{2} \right). \end{aligned} \quad (49)$$

That is, condition (34) with $\lambda = 1$ holds. Therefore, by Theorem 6, (47) oscillates.

Remark 9. For a class of third-order Emden–Fowler delay differential equations with unbounded neutral coefficients (1), we established new oscillation criteria which complement and improve results in the cited papers because these criteria apply also in the case where p is unbounded and ensure that all solutions of (1) are oscillatory (that is, these results can distinguish solutions with different behaviors).

Remark 10. Using different methods, we improve results of Li and Rogovchenko [2] by removing restrictive condition $\eta \circ g = g \circ \eta$, which, in a certain sense, is a significant improvement compared to the results reported in the cited papers.

Remark 11. Combining Theorem 3 and the results obtained in [25], one can derive various oscillation criteria for (1) in the linear case. To study the oscillation of (1) in the superlinear case, it would be of interest to establish oscillation criteria for (3) and (4) assuming that $\lambda > 1$.

Remark 12. In the conclusion of Lemma 1, the existence of the constant $l \in (0, 1)$ is necessary in some cases. For instance, for $t \geq 2$, if $y(t) = t - 1/t$, then $y'(t) > 0$, $y''(t) < 0$, and $y(t) < ty'(t)$, and so the function y does not satisfy the conclusion of Lemma 1 provided that there is no $l \in (0, 1)$. On the basis of Lemma 1, one can easily revisit the results reported in [26–28].

Data Availability

No data were used to support this study.

Conflicts of Interest

The authors declare that they have no conflicts of interest.

Authors' Contributions

All five authors contributed equally to this work and are listed in alphabetical order. They all read and approved the final version of the manuscript.

Acknowledgments

This research is supported by NNSF of P. R. China (Grant No. 61503171), CPSF (Grant No. 2015M582091), and NSF of Shandong Province (Grant No. ZR2016JL021). The research of the third author is supported by the grant project KEGA 035TUKE-4/2017.

References

- [1] R. P. Agarwal, M. Bohner, T. Li, and C. Zhang, "Oscillation of second-order Emden-Fowler neutral delay differential equations," *Annali di Matematica Pura ed Applicata (1923 -)*, vol. 193, no. 6, pp. 1861–1875, 2014.
- [2] T. Li and Yu. V. Rogovchenko, "Asymptotic behavior of higher-order quasilinear neutral differential equations," *Abstract and Applied Analysis*, vol. 2014, Article ID 395368, 11 pages, 2014.
- [3] T. Li and Yu. V. Rogovchenko, "Oscillation of second-order neutral differential equations," *Mathematische Nachrichten*, vol. 288, no. 10, pp. 1150–1162, 2015.
- [4] T. Li and Yu. V. Rogovchenko, "On asymptotic behavior of solutions to higher-order sublinear Emden-Fowler delay differential equations," *Applied Mathematics Letters*, vol. 67, pp. 53–59, 2017.
- [5] T. Li and Yu. V. Rogovchenko, "Oscillation criteria for second-order superlinear Emden-Fowler neutral differential equations," *Monatshefte für Mathematik*, vol. 184, no. 3, pp. 489–500, 2017.
- [6] J. S. W. Wong, "On the generalized Emden-Fowler equation," *SIAM Review*, vol. 17, no. 2, pp. 339–360, 1975.
- [7] B. Baculiková and J. Džurina, "Oscillation of third-order neutral differential equations," *Mathematical and Computer Modelling*, vol. 52, no. 1-2, pp. 215–226, 2010.
- [8] B. Baculiková, B. Rani, S. Selvarangam, and E. Thandapani, "Properties of Kneser's solution for half-linear third order neutral differential equations," *Acta Mathematica Hungarica*, vol. 152, no. 2, pp. 525–533, 2017.
- [9] Z. Došlá and P. Liška, "Oscillation of third-order nonlinear neutral differential equations," *Applied Mathematics Letters*, vol. 56, pp. 42–48, 2016.
- [10] J. Džurina, S. R. Grace, and I. Jadlovská, "On nonexistence of Kneser solutions of third-order neutral delay differential equations," *Applied Mathematics Letters*, vol. 88, pp. 193–200, 2019.
- [11] S. R. Grace, J. R. Graef, and M. A. El-Beltagy, "On the oscillation of third order neutral delay dynamic equations on time scales," *Computers & Mathematics with Applications*, vol. 63, no. 4, pp. 775–782, 2012.
- [12] S. R. Grace, J. R. Graef, and E. Tunç, "Oscillatory behavior of a third-order neutral dynamic equation with distributed delays," in *Proceedings of the 10th Colloquium on the Qualitative Theory of Differential Equations*, pp. 1–14, Szeged, Hungary, 2016.
- [13] S. R. Grace and I. Jadlovská, "Oscillatory behavior of odd-order nonlinear differential equations with a nonpositive neutral term," *Dynamic Systems and Applications*, vol. 27, no. 1, pp. 125–136, 2018.
- [14] T. S. Hassan and S. R. Grace, "Oscillation criteria for third order neutral nonlinear dynamic equations with distributed deviating arguments on time scales," *Tatra Mountains Mathematical Publications*, vol. 61, no. 1, pp. 141–161, 2014.
- [15] Y. Jiang, C. Jiang, and T. Li, "Oscillatory behavior of third-order nonlinear neutral delay differential equations," *Advances in Difference Equations*, vol. 2016, Article ID 171, 12 pages, 2016.
- [16] T. Li and E. Thandapani, "Oscillation of solutions to odd-order nonlinear neutral functional differential equations," *Electronic Journal of Differential Equations*, vol. 2011, Article ID 23, 12 pages, 2011.
- [17] B. Mihalíková and E. Kostiková, "Boundedness and oscillation of third order neutral differential equations," *Tatra Mountains Mathematical Publications*, vol. 43, no. 1, pp. 137–144, 2009.
- [18] J. R. Graef, E. Tunç, and S. R. Grace, "Oscillatory and asymptotic behavior of a third-order nonlinear neutral differential equation," *Opuscula Mathematica*, vol. 37, no. 6, pp. 839–852, 2017.
- [19] T. Li and C. Zhang, "Properties of third-order half-linear dynamic equations with an unbounded neutral coefficient," *Advances in Difference Equations*, vol. 2013, Article ID 333, 8 pages, 2013.
- [20] E. Tunç, "Oscillatory and asymptotic behavior of third-order neutral differential equations with distributed deviating arguments," *Electronic Journal of Differential Equations*, vol. 2017, Article ID 16, 12 pages, 2017.
- [21] I. T. Kiguradze and T. A. Chanturia, *Asymptotic Properties of Solutions of Nonautonomous Ordinary Differential Equations*, Kluwer Academic, Dordrecht, The Netherlands, 1993, Translated from the 1985 Russian original.
- [22] Ch. G. Philos, "On the existence of nonoscillatory solutions tending to zero at ∞ for differential equations with positive delays," *Archiv der Mathematik*, vol. 36, no. 1, pp. 168–178, 1981, <https://link.springer.com/article/10.1007/BF01223686>.
- [23] R. G. Koplatadze and T. A. Chanturiya, "Oscillating and monotone solutions of first-order differential equations with deviating argument," *Differentsial'nye Uravneniya*, vol. 18, no. 8, pp. 1463–1465, 1472, 1982 (Russian).
- [24] Y. Kitamura and T. Kusano, "Oscillation of first-order nonlinear differential equations with deviating arguments," *Proceedings of the American Mathematical Society*, vol. 78, no. 1, pp. 64–68, 1980.
- [25] G. E. Chatzarakis and T. Li, "Oscillation criteria for delay and advanced differential equations with nonmonotone arguments," *Complexity*, vol. 2018, Article ID 8237634, 18 pages, 2018.
- [26] R. P. Agarwal, M. Bohner, T. Li, and C. Zhang, "A new approach in the study of oscillatory behavior of even-order neutral delay differential equations," *Applied Mathematics and Computation*, vol. 225, pp. 787–794, 2013.
- [27] T. Li and Yu. V. Rogovchenko, "Oscillation criteria for even-order neutral differential equations," *Applied Mathematics Letters*, vol. 61, pp. 35–41, 2016.

- [28] E. Tu and A. Kaymaz, "On oscillation of second-order linear neutral differential equations with damping term," *Dynamic Systems and Applications*, vol. 28, no. 2, pp. 289–301, 2019.

Research Article

An Application of (3+1)-Dimensional Time-Space Fractional ZK Model to Analyze the Complex Dust Acoustic Waves

Lei Fu and Hongwei Yang 

Shandong University of Science and Technology, Qingdao, Shandong 266590, China

Correspondence should be addressed to Hongwei Yang; hwyang1979@163.com

Received 25 April 2019; Revised 26 June 2019; Accepted 22 July 2019; Published 5 August 2019

Guest Editor: Robert Hakl

Copyright © 2019 Lei Fu and Hongwei Yang. This is an open access article distributed under the Creative Commons Attribution License, which permits unrestricted use, distribution, and reproduction in any medium, provided the original work is properly cited.

Dust plasma is a new field of physics which has developed rapidly in recent decades. The study of dust plasma has received much attention due to its importance in the environment of space and the Earth. Dust acoustic waves are generated because of the inertia of dust mass while the restoring force is provided by the thermal pressure of electrons and ions. Since dust acoustic waves were first reported theoretically in unmagnetized dust plasma by Rao et al., they have become a research hot spot. In this paper, the excitation of dust acoustic waves by a gravity field in a dust plasma is analyzed. According to the control equations of dust plasma motion and employing multiscale analysis and perturbation method, we have obtained a (3+1)-dimensional ZK model. Because of the space property of dust plasma, (3+1)-dimensional ZK equation is more suitable than KdV equation and (2+1)-dimensional ZK equation to describe the real dust acoustic waves. Then, the (3+1)-dimensional time-space fractional ZK (TSF-ZK) equation describing the fractal process of nonlinear dust acoustic waves is given for the first time. To further explore how dust acoustic waves change energy as they travel, we discuss the conservation laws of the new model. Moreover, we study the exact solution of (3+1)-dimensional TSF-ZK equation by using extended Kudryashov method. Finally, based on the exact solution, we further investigate the effect of the parameter k , the charge properties of dust particle Z_{d0} , the fractional order values α , β , γ , and θ , the temperature T_d , the gravity g , and the collision frequency β_0 and β_1 on the properties of dust acoustic waves by a gravity field in dust plasma.

1. Introduction

Plasma is a macroscopic system composed of a large number of charged particles, and it is the fourth state in which matter exists. The characteristics of motion of plasma are more complex than those of other substances. In many cases, the production and maintenance of plasma are difficult. Therefore, plasma physics is a branch with research value, which is closely related to the generation of new technology. In recent years, plasma physics has become an important basis for human understanding of the universe and an important guarantee for understanding and controlling the changes of the Earth's environment. It is hoped that mankind will finally solve the energy problem in the future. As a result, plasmas are getting more attention.

In recent years, the study of nonlinear structures in various kinds of plasmas has been the emphasis of the researchers [1, 2]. Dust plasma is a new field of physics

research which has developed rapidly in recent decades. In addition to electrons, ions, and neutral gases, dust plasma also contains dust particles of any shape and size ranging from tens of nm to a few microns. Charged dust grains exist widely in space, plasma equipment in laboratory as well as plasma processing. It is widely believed that dust plasma plays a very important role in the formation of galaxies, such as planetary rings, cometary surroundings, interstellar clouds, and the Earth's ionosphere. Dust plasma is also important in the laboratory. And the main reason is that dust plasma mode is formed due to the existence of mixtures, which greatly affects the state or behavior of plasma. The dust acoustic waves are generated due to the inertia of dust mass while the restoring force is provided by the thermal pressure of electrons and ions. Low frequency dust acoustic waves were first predicted by Rao [3] in a dust plasma in 1990. Later, in 1992, Shukla-Silin [4] obtained the high frequency dust ion-acoustic waves. Merlino [5] has experimentally confirmed the

existence of dust acoustic waves and dust ion-acoustic waves in 1998. Since then, more and more attention has been paid to the study of dust acoustic waves.

At the beginning of the investigations, the (1+1)-dimensional model was used to study the dust acoustic waves. Using the reductive perturbation method, a KdV equation has been derived by Bharuthram [6] to study the large amplitude ion-acoustic solitons in a dust plasma, and Duan [7] got a KdV equation to describe the effect of dust size distribution for two ion temperature dusty plasma. Later, Kadomstev and Petviashvili [8] made an attempt to describe the solitons in (2+1)-dimensional systems by applying Kadomstev-Petviashvili (KP) equation. Singh and Honzawa [9] studied the effects of ion temperature and relativistic factor on the width and amplitude of ion-acoustic solitons in an unmagnetized two-dimensional weakly relativistic collisionless plasma with finite ion temperature by using the KP equation. Lin [10] derived the KP equation which is considered as two-dimensional extension of KdV equation to study dust acoustic waves in hot dusty plasma. Employing multiscale analysis and perturbation method, a KP equation was obtained for the stability of dust acoustic waves for host dust plasma by Duan [11]. Gill [12] proved the existence of compressive and rarefactive dust acoustic solitons under the solution of KP equation in two-dimensional dusty plasma with two-temperature ions. However, in the real environment, dust plasma moves in space, so we must study the higher dimensions of dust acoustic waves. Thus, in this paper, we will be working on the (3+1)-dimensional model.

For a long time, people have been committed to the study of integral calculus. Therefore, researchers conduct scientific research based on integer order models [13–18]. However, with the continuous development of calculus theory, the appearance and development of fractional order have become a major trend of integral science [19–21]. As we know, Leibniz was the first to study the theory of fractional derivatives. So far, the development of fractional derivatives has been very mature, and fractional calculus and the corresponding fractional partial differential equations have attracted wide attention in many subjects [22–28]. Compared with integer order models, fractional models can better explain nonlinear physical processes and propagation characteristics in real environment [29–33]. However, fractional models were rarely used to study the dust plasma in the past. Therefore, it is of great research value to construct the (3+1)-dimensional TSF-ZK equation to discuss the influence of fractional order for the dust acoustic waves in gravity field for dust plasma.

The solution of the nonlinear partial differential equation is an important research topic in nonlinear physical phenomena. Similarly, the solutions of fractional differential equations have attracted the attention of researchers in many fields. Thus, many methods have been proposed one after another, such as the first integral method [34, 35], (G'/G)-expansion method [36, 37], the Hirota method [38, 39], the trial function method [40], the subequation method [41], and others [42–46]. In this paper, using extended Kudryashov method [47], the exact solution of (3+1)-dimensional TSF-ZK equation is obtained.

The rest of the paper is organized as follows. In Section 2, based on the control equations of motion, a (3+1)-dimensional integer order ZK equation is derived by employing multiscale analysis and perturbation method [48, 49]. Applying the semi-inverse method and the fractional variational principle [50], the integer order ZK equation is transformed into a time-space fractional ZK (TSF-ZK) equation. Next, we study the exact solution of (3+1)-dimensional TSF-ZK equation by using extended Kudryashov method. Then, the conservation law of (3+1)-dimensional TSF-ZK equation is got by applying Lie symmetry analysis method. In the end, on the basis of the exact solution of (3+1)-dimensional TSF-ZK equation, we further investigate the property of dust acoustic waves. The influence of the parameter k , the charge properties of dust particle Z_{d0} , fractional order values α , β , γ , θ , temperature T_d , gravity g , and collision frequency β_0 , β_1 on the properties of dust acoustic waves by a gravity field in dust plasma are studied.

2. Derivation of the (3+1)-Dimensional ZK Equation

For low frequency dust acoustic wave, the control equations are composed of mass conservation equation, momentum conservation equation, and Poisson equation [51, 52] following

$$\begin{aligned} \frac{\partial n_d}{\partial t} + \nabla \cdot (n_d \vec{u}_d) &= 0, \\ n_d m_d \frac{\partial \vec{u}_d}{\partial t} + n_d m_d \vec{u}_d \cdot \nabla \vec{u}_d + T_d \nabla \vec{u}_d - n_d e Z_d \nabla \phi & \quad (1) \\ &= -\beta' n_d m_d \vec{u}_d + n_d m_d \vec{g}, \\ \Delta \phi &= 4\pi e (Z_d n_d + n_e - n_i), \end{aligned}$$

where $\Delta = \nabla^2 = \partial^2/\partial x^2 + \partial^2/\partial y^2 + \partial^2/\partial z^2$ is three-dimensional Laplace operator, \vec{u}_d is the velocity of dust particles, ϕ is the electrostatic potential, n_d , n_e , and n_i are the number densities of the dust particles, electrons, and ions in the dusty plasma, respectively, T_d is the temperature of dust particles, Z_d is the basic unit electric quantity of dust particles, and its positive and negative represent the electrical properties of dust particles. \vec{u}_d is expressed by $\vec{u}_d = u_d \vec{i} + v_d \vec{j} + w_d \vec{k}$, where \vec{i} , \vec{j} , and \vec{k} are the unit vectors in the x , y , and z directions, respectively. $n_e = \nu e^{s\delta\phi}$ and $n_i = \mu e^{-s\phi}$, where $s = 1/(\mu + \nu\delta)$, $\delta = T_e/T_i$, $T_{eff} = T_e T_i / (\mu T_e + \nu T_i)$ is the effective temperature, where T_e and T_i are the temperatures of electrons and ions, respectively, $\mu = n_{i0}/n_{d0} Z_{d0}$, and $\nu = n_{e0}/n_{d0} Z_{d0}$. In a state of complete constant temperature, the ions and electrons will obey the Boltzmann condition. The equilibrium state satisfies the neutral condition $n_{i0} = Z_{d0} n_{d0} + n_{e0}$, where n_{d0} , n_{i0} , n_{e0} , and Z_{d0} are the unperturbed number densities of dust particles, ions, electrons, and the numbers of electrons residing on the dust particles, respectively. n_d is normalized by n_{d0} , and Z_d is normalized by Z_{d0} . The space coordinates (x, y, z) , time t , velocity (u_d, v_d, w_d) , electrostatic potential ϕ , collision frequency β' , and gravity g are normalized by

Debye length $\lambda_{Dd} = (T_{eff}/4\pi Z_{d0} n_{d0} e^2)^{1/2}$, the characteristic dust period $\omega_{pd}^{-1} = (m_d/4\pi Z_{d0} n_{d0} e^2)^{1/2}$, the dust acoustic speed $C_d = (Z_{d0} T_{eff}/m_d)^{1/2}$, and T_{eff}/e , respectively, and the collision frequency β' refers to the number of collisions between one plasma and another over a period of time. The detailed description is given in [45].

We assume that the charge of dust particles is constant; that is, $Z_d = Z_{d0}$, Z_{d0} is constant. Then the dimensionless forms of the control equations are as follows:

$$\begin{aligned} \frac{\partial n_d}{\partial t} + \frac{\partial}{\partial x}(n_d u_d) + \frac{\partial}{\partial y}(n_d v_d) + \frac{\partial}{\partial z}(n_d w_d) &= 0, \\ \frac{\partial u_d}{\partial t} + u_d \frac{\partial u_d}{\partial x} + v_d \frac{\partial u_d}{\partial y} + w_d \frac{\partial u_d}{\partial z} + \frac{T_d}{Z_d} \frac{1}{n_d} \frac{\partial n_d}{\partial x} - \frac{\partial \phi}{\partial x} \\ &= -\beta_x u_d + g, \\ \frac{\partial v_d}{\partial t} + u_d \frac{\partial v_d}{\partial x} + v_d \frac{\partial v_d}{\partial y} + w_d \frac{\partial v_d}{\partial z} + \frac{T_d}{Z_d} \frac{1}{n_d} \frac{\partial n_d}{\partial y} - \frac{\partial \phi}{\partial y} \\ &= -\beta_y v_d, \\ \frac{\partial w_d}{\partial t} + u_d \frac{\partial w_d}{\partial x} + v_d \frac{\partial w_d}{\partial y} + w_d \frac{\partial w_d}{\partial z} + \frac{T_d}{Z_d} \frac{1}{n_d} \frac{\partial n_d}{\partial z} - \frac{\partial \phi}{\partial z} \\ &= -\beta_z w_d, \\ \frac{\partial^2 \phi}{\partial x^2} + \frac{\partial^2 \phi}{\partial y^2} + \frac{\partial^2 \phi}{\partial z^2} &= n_d + n_e - n_i. \end{aligned} \quad (2)$$

We introduce the following slow space-time variables:

$$\begin{aligned} \xi &= \epsilon^{1/2} (x - v_0 t), \\ \eta &= \epsilon^{1/2} y, \\ \zeta &= \epsilon^{1/2} z, \\ \tau &= \epsilon^{3/2} t. \end{aligned} \quad (3)$$

Then we have

$$\begin{aligned} \frac{\partial}{\partial t} &= \epsilon^{3/2} \frac{\partial}{\partial \tau} - \epsilon^{1/2} v_0 \frac{\partial}{\partial \xi}, \\ \frac{\partial}{\partial x} &= \epsilon^{1/2} \frac{\partial}{\partial \xi}, \\ \frac{\partial}{\partial y} &= \epsilon^{1/2} \frac{\partial}{\partial \eta}, \\ \frac{\partial}{\partial z} &= \epsilon^{1/2} \frac{\partial}{\partial \zeta}. \end{aligned} \quad (4)$$

The dependent variables n_d , u_d , v_d , w_d , and ϕ are expanded as follows:

$$\begin{aligned} n_d &= 1 + \epsilon n_{d1} + \epsilon^2 n_{d2} + \epsilon^3 n_{d3} + \dots, \\ u_d &= u_{d0} + \epsilon u_{d1} + \epsilon^2 u_{d2} + \epsilon^3 u_{d3} + \dots, \end{aligned}$$

$$\begin{aligned} v_d &= \epsilon^{3/2} v_{d1} + \epsilon^{5/2} v_{d2} + \epsilon^{7/2} v_{d3} + \dots, \\ w_d &= \epsilon^{3/2} w_{d1} + \epsilon^{5/2} w_{d2} + \epsilon^{7/2} w_{d3} + \dots, \\ \phi &= \epsilon \phi_1 + \epsilon^2 \phi_2 + \epsilon^3 \phi_3 + \dots, \\ \beta_x &= \beta_0 + \epsilon \beta_1, \\ \beta_y &= \epsilon \beta_1, \\ \beta_z &= \epsilon \beta_1. \end{aligned} \quad (5)$$

Substituting (4) and (5) into (3), the following equations can be got:

$$\begin{aligned} &\left(\epsilon^{3/2} \frac{\partial}{\partial \tau} - \epsilon^{1/2} v_0 \frac{\partial}{\partial \xi} \right) (1 + \epsilon n_{d1} + \epsilon^2 n_{d2} + \epsilon^3 n_{d3}) \\ &+ \left(\epsilon^{1/2} \frac{\partial}{\partial \xi} \right) [(1 + \epsilon n_{d1} + \epsilon^2 n_{d2} + \epsilon^3 n_{d3}) \\ &\cdot (u_{d0} + \epsilon u_{d1} + \epsilon^2 u_{d2} + \epsilon^3 u_{d3})] + \left(\epsilon^{1/2} \frac{\partial}{\partial \eta} \right) \\ &\cdot [(1 + \epsilon n_{d1} + \epsilon^2 n_{d2} + \epsilon^3 n_{d3}) \\ &\cdot (\epsilon^{3/2} v_{d1} + \epsilon^{5/2} v_{d2} + \epsilon^{7/2} v_{d3})] + \left(\epsilon^{1/2} \frac{\partial}{\partial \zeta} \right) \\ &\cdot [(1 + \epsilon n_{d1} + \epsilon^2 n_{d2} + \epsilon^3 n_{d3}) \\ &\cdot (\epsilon^{3/2} w_{d1} + \epsilon^{5/2} w_{d2} + \epsilon^{7/2} w_{d3})] = 0, \\ &\left(\epsilon^{3/2} \frac{\partial}{\partial \tau} - \epsilon^{1/2} v_0 \frac{\partial}{\partial \xi} \right) (u_{d0} + \epsilon u_{d1} + \epsilon^2 u_{d2} + \epsilon^3 u_{d3}) \\ &+ (u_{d0} + \epsilon u_{d1} + \epsilon^2 u_{d2} + \epsilon^3 u_{d3}) \cdot \left(\epsilon^{1/2} \frac{\partial}{\partial \xi} \right) (u_{d0} \\ &+ \epsilon u_{d1} + \epsilon^2 u_{d2} + \epsilon^3 u_{d3}) + (\epsilon^{3/2} v_{d1} + \epsilon^{5/2} v_{d2} \\ &+ \epsilon^{7/2} v_{d3}) \left(\epsilon^{1/2} \frac{\partial}{\partial \eta} \right) (u_{d0} + \epsilon u_{d1} + \epsilon^2 u_{d2} + \epsilon^3 u_{d3}) \\ &+ (\epsilon^{3/2} w_{d1} + \epsilon^{5/2} w_{d2} + \epsilon^{7/2} w_{d3}) \left(\epsilon^{1/2} \frac{\partial}{\partial \zeta} \right) (u_{d0} \\ &+ \epsilon u_{d1} + \epsilon^2 u_{d2} + \epsilon^3 u_{d3}) + \frac{T_d}{Z_{d0}} \\ &\cdot \frac{1}{1 + \epsilon n_{d1} + \epsilon^2 n_{d2} + \epsilon^3 n_{d3}} \left(\epsilon^{1/2} \frac{\partial}{\partial \xi} \right) (1 + \epsilon n_{d1} \\ &+ \epsilon^2 n_{d2} + \epsilon^3 n_{d3}) - \left(\epsilon^{1/2} \frac{\partial}{\partial \xi} \right) (\epsilon \phi_1 + \epsilon^2 \phi_2 + \epsilon^3 \phi_3) \\ &= -(\beta_0 + \epsilon \beta_1) (u_{d0} + \epsilon u_{d1} + \epsilon^2 u_{d2} + \epsilon^3 u_{d3}) + g, \\ &\left(\epsilon^{3/2} \frac{\partial}{\partial \tau} - \epsilon^{1/2} v_0 \frac{\partial}{\partial \xi} \right) (\epsilon^{3/2} v_{d1} + \epsilon^{5/2} v_{d2} + \epsilon^{7/2} v_{d3}) \end{aligned}$$

$$\begin{aligned}
& + (u_{d0} + \epsilon u_{d1} + \epsilon^2 u_{d2} + \epsilon^3 u_{d3}) \left(\epsilon^{1/2} \frac{\partial}{\partial \xi} \right) \cdot (\epsilon^{3/2} v_{d1} \\
& + \epsilon^{5/2} v_{d2} + \epsilon^{7/2} v_{d3}) + (\epsilon^{3/2} v_{d1} + \epsilon^{5/2} v_{d2} + \epsilon^{7/2} v_{d3}) \\
& \cdot \left(\epsilon^{1/2} \frac{\partial}{\partial \eta} \right) (\epsilon^{3/2} v_{d1} + \epsilon^{5/2} v_{d2} + \epsilon^{7/2} v_{d3}) + (\epsilon^{3/2} w_{d1} \\
& + \epsilon^{5/2} w_{d2} + \epsilon^{7/2} w_{d3}) \left(\epsilon^{1/2} \frac{\partial}{\partial \zeta} \right) (\epsilon^{3/2} v_{d1} + \epsilon^{5/2} v_{d2} \\
& + \epsilon^{7/2} v_{d3}) + \frac{T_d}{Z_{d0}} \\
& \cdot \frac{1}{1 + \epsilon n_{d1} + \epsilon^2 n_{d2} + \epsilon^3 n_{d3}} \left(\epsilon^{1/2} \frac{\partial}{\partial \eta} \right) (1 + \epsilon n_{d1} \\
& + \epsilon^2 n_{d2} + \epsilon^3 n_{d3}) - \left(\epsilon^{1/2} \frac{\partial}{\partial \eta} \right) (\epsilon \phi_1 + \epsilon^2 \phi_2 + \epsilon^3 \phi_3) \\
& = -(\epsilon \beta_1) (\epsilon^{3/2} v_{d1} + \epsilon^{5/2} v_{d2} + \epsilon^{7/2} v_{d3}), \\
& \left(\epsilon^{3/2} \frac{\partial}{\partial \tau} - \epsilon^{1/2} v_0 \frac{\partial}{\partial \xi} \right) (\epsilon^{3/2} w_{d1} + \epsilon^{5/2} w_{d2} + \epsilon^{7/2} w_{d3}) \\
& + (u_{d0} + \epsilon u_{d1} + \epsilon^2 u_{d2} + \epsilon^3 u_{d3}) \left(\epsilon^{1/2} \frac{\partial}{\partial \xi} \right) \cdot (\epsilon^{3/2} w_{d1} \\
& + \epsilon^{5/2} w_{d2} + \epsilon^{7/2} w_{d3}) + (\epsilon^{3/2} v_{d1} + \epsilon^{5/2} v_{d2} \\
& + \epsilon^{7/2} v_{d3}) \left(\epsilon^{1/2} \frac{\partial}{\partial \eta} \right) (\epsilon^{3/2} w_{d1} + \epsilon^{5/2} w_{d2} + \epsilon^{7/2} w_{d3}) \\
& + (\epsilon^{3/2} w_{d1} + \epsilon^{5/2} w_{d2} + \epsilon^{7/2} w_{d3}) \left(\epsilon^{1/2} \frac{\partial}{\partial \zeta} \right) (\epsilon^{3/2} w_{d1} \\
& + \epsilon^{5/2} w_{d2} + \epsilon^{7/2} w_{d3}) + \frac{T_d}{Z_{d0}} \\
& \cdot \frac{1}{1 + \epsilon n_{d1} + \epsilon^2 n_{d2} + \epsilon^3 n_{d3}} \left(\epsilon^{1/2} \frac{\partial}{\partial \zeta} \right) (1 + \epsilon n_{d1} \\
& + \epsilon^2 n_{d2} + \epsilon^3 n_{d3}) - \left(\epsilon^{1/2} \frac{\partial}{\partial \zeta} \right) (\epsilon \phi_1 + \epsilon^2 \phi_2 + \epsilon^3 \phi_3) \\
& = -(\epsilon \beta_1) (\epsilon^{3/2} w_{d1} + \epsilon^{5/2} w_{d2} + \epsilon^{7/2} w_{d3}), \\
& \left(\epsilon \frac{\partial^2}{\partial \xi^2} \right) (\epsilon \phi_1 + \epsilon^2 \phi_2 + \epsilon^3 \phi_3) + \left(\epsilon \frac{\partial^2}{\partial \eta^2} \right) (\epsilon \phi_1 + \epsilon^2 \phi_2 \\
& + \epsilon^3 \phi_3) + \left(\epsilon \frac{\partial^2}{\partial \zeta^2} \right) (\epsilon \phi_1 + \epsilon^2 \phi_2 + \epsilon^3 \phi_3) = (1 + \epsilon n_{d1} \\
& + \epsilon^2 n_{d2} + \epsilon^3 n_{d3}) + (\epsilon \phi_1 + \epsilon^2 \phi_2 + \epsilon^3 \phi_3).
\end{aligned} \tag{6}$$

In (6), letting

$$T = \frac{T_d}{Z_{d0}} \frac{1}{1 + \epsilon n_{d1} + \epsilon^2 n_{d2} + \epsilon^3 n_{d3}} \left(\epsilon^{1/2} \frac{\partial}{\partial \xi} \right)$$

$$\begin{aligned}
& \cdot (1 + \epsilon n_{d1} + \epsilon^2 n_{d2} + \epsilon^3 n_{d3}) = \frac{T_d}{Z_{d0}} \left(\epsilon^{1/2} \frac{\partial}{\partial \xi} \right) \\
& \cdot \left[\ln (1 + \epsilon n_{d1} + \epsilon^2 n_{d2} + \epsilon^3 n_{d3}) \right],
\end{aligned} \tag{7}$$

and using the Taylor's series, T can be approximately rewritten as

$$T = \frac{T_d}{Z_{d0}} \left(\epsilon^{1/2} \frac{\partial}{\partial \xi} \right) (\epsilon n_{d1} + \epsilon^2 n_{d2} + \epsilon^3 n_{d3} + \dots). \tag{8}$$

A series of approximate equations for ϵ in the following form can be obtained

$$\epsilon^0 : -\beta_0 u_{d0} = g; \tag{9}$$

$$\epsilon^1 : \beta_1 u_{d0} + \beta_0 u_{d1} = 0; \tag{10}$$

$$\epsilon^{3/2} : \begin{cases} (u_{d0} - v_0) \frac{\partial n_{d1}}{\partial \xi} + \frac{\partial u_{d1}}{\partial \xi} = 0, \\ (u_{d0} - v_0) \frac{\partial u_{d1}}{\partial \xi} + \frac{T_d}{Z_d} \frac{\partial n_{d1}}{\partial \xi} - \frac{\partial \phi_1}{\partial \xi} = 0; \end{cases} \tag{11}$$

$$\epsilon^2 : \begin{cases} \beta_0 u_{d2} + \beta_1 u_{d1} = 0, \\ \frac{\partial^2 \phi_1}{\partial \xi^2} + \frac{\partial^2 \phi_1}{\partial \eta^2} + \frac{\partial^2 \phi_1}{\partial \zeta^2} = n_{d2} + \phi_2; \end{cases} \tag{12}$$

$$\epsilon^{5/2} : \begin{cases} (u_{d0} - v_0) \frac{\partial n_{d2}}{\partial \xi} + \frac{\partial u_{d2}}{\partial \xi} = -\frac{\partial n_{d1}}{\partial \tau} - n_{d1} \frac{\partial u_{d1}}{\partial \xi} - u_{d1} \frac{\partial n_{d1}}{\partial \xi}, \\ (u_{d0} - v_0) \frac{\partial u_{d2}}{\partial \xi} - \frac{\partial \phi_2}{\partial \xi} + \frac{T_d}{Z_d} \frac{\partial n_{d2}}{\partial \xi} = -\frac{\partial u_{d1}}{\partial \tau} - u_{d1} \frac{\partial u_{d1}}{\partial \xi}. \end{cases} \tag{13}$$

Based on (9) and (10), we get the following relations

$$\begin{aligned}
\beta_0 &= \frac{g}{u_{d0}}, \\
\beta_1 &= \frac{-\beta_0 (u_{d0} - v_0)}{u_{d0}} \phi_1 = \frac{-\beta_0^2 (u_{d0} - v_0)}{g} \phi_1.
\end{aligned} \tag{14}$$

According to (11), the following relationship can be given as

$$\left[(u_{d0} - v_0)^2 - \frac{T_d}{Z_d} \right] \frac{\partial n_{d1}}{\partial \xi} + \frac{\partial \phi_{d1}}{\partial \xi} = 0. \tag{15}$$

Assuming that

$$n_{d1} = -\phi_1, \tag{16}$$

we get

$$\begin{aligned}
u_{d1} &= (u_{d0} - v_0) \phi_1, \\
\frac{Z_{d0}}{Z_{d0} (u_{d0} - v_0)^2 - T_d} &= 1.
\end{aligned} \tag{17}$$

Combining (12), (13), (16), and (17) and letting $\phi_1 = \phi$, we can obtain the following model:

$$\frac{\partial \phi}{\partial \tau} + a_1 \phi \frac{\partial \phi}{\partial \xi} + a_2 \frac{\partial^3 \phi}{\partial \xi^3} + a_3 \frac{\partial^3 \phi}{\partial \xi \partial \eta^2} + a_4 \frac{\partial^3 \phi}{\partial \xi \partial \zeta^2} = 0, \tag{18}$$

where

$$\begin{aligned} a_1 &= \frac{3(g - \beta_0 v_0)}{2\beta_0} = \frac{3}{2} \sqrt{\frac{Z_{d0} + T_d}{Z_{d0}}}, \\ a_2 = a_3 = a_4 &= -\frac{\beta_0}{2(g - \beta_0 v_0)} = -\frac{1}{2} \sqrt{\frac{Z_{d0}}{Z_{d0} + T_d}}. \end{aligned} \quad (19)$$

When $a_3 = a_4 = 0$, (18) is the KdV equation. When $a_4 = 0$, (18) is the ZK equation. On the basis of $a_3(\partial^3 \phi / \partial \xi \partial \eta^2)$ and $a_4(\partial^3 \phi / \partial \xi \partial \zeta^2)$, (18) is a (3+1)-dimensional ZK equation. It is well known that the KdV equation reflects the propagation of dust acoustic waves along a line, and the ZK equation can describe the propagation of dust acoustic waves on one surface. Dust acoustic waves in dust plasma move around in space. Therefore, the (3+1)-dimensional ZK equation is more

suitable to describe the dust acoustic waves in the real dust plasma.

3. Derivation of the (3+1)-Dimensional Time-Space Fractional ZK (TSF-ZK) Equation

Based on the above section, we get a (3+1)-dimensional ZK equation. In this section, the (3+1)-dimensional TSF-ZK equation is obtained by using the semi-inverse method and the fractional variational principle.

Firstly, let us introduce some basic fractional definitions.

Definition 1 (see [50]). The Riemann-Liouville fractional derivative operator is defined as

$$D_t^\alpha u = \begin{cases} \frac{\partial_m u}{\partial t^m}, & \alpha = m \in N, \\ \frac{1}{\Gamma(m - \alpha)} \frac{\partial_m}{\partial t^m} \int_0^t \frac{u(\tau, x)}{(t - \tau)^{\alpha + 1 - m}} d\tau, & m - 1 < \alpha < m, m \in N. \end{cases} \quad (20)$$

Definition 2 (see [50]). The modified Riemann-Liouville fractional derivative operator is defined as

$$D_t^\alpha f(t) = \frac{1}{\Gamma(1 - \alpha)} \frac{d}{dt} \left[\int_a^t \frac{f(\tau) - f(a)}{(t - \tau)^\alpha} d\tau \right], \quad (21)$$

$0 \leq \alpha < 1.$

Letting $\phi = Q_\xi$, where $Q(\tau, \xi, \eta, \zeta)$ is a potential function, then the (18) can be written as

$$Q_{\xi\tau} + a_1 Q_\xi Q_{\xi\xi} + a_2 Q_{\xi\xi\xi} + a_3 Q_{\xi\xi\eta\eta} + a_4 Q_{\xi\xi\zeta\zeta} = 0. \quad (22)$$

The functional of the above potential equation can be given as

$$J(Q) = \int_R d\xi \int_R d\eta \int_R d\zeta \int_T d\tau \left[Q(\tau, \xi, \eta, \zeta) \left(b_1 Q_{\xi\tau} + b_2 a_1 Q_\xi Q_{\xi\xi} + b_3 a_2 Q_{\xi\xi\xi} + b_4 a_3 Q_{\xi\xi\eta\eta} + b_5 a_4 Q_{\xi\xi\zeta\zeta} \right) \right], \quad (23)$$

where d_i ($i = 1, 2, 3, 4, 5$) are Lagrangian multipliers, which can be obtained later, and $\xi \in R$. Integrating (23) by parts and letting $Q_\tau|_T = Q_\xi|_R = Q_\eta|_R = Q_\zeta|_R = Q_\xi|_T = Q_{\xi\xi}|_R = Q_{\xi\eta\eta}|_R = Q_{\xi\zeta\zeta}|_R = 0$, we can get

$$\begin{aligned} J(Q) &= \iiint_V d\xi d\eta d\zeta \int_R \left(-b_1 Q_\tau Q_\xi - \frac{1}{2} b_2 a_1 Q_\xi^3 \right. \\ &\quad \left. + b_3 a_2 Q_{\xi\xi}^2 + b_4 a_3 Q_{\xi\eta}^2 + b_5 a_4 Q_{\xi\zeta}^2 \right) d\tau, \end{aligned} \quad (24)$$

where $V = [R \times R \times R]$. Using the variation of (24) and integrating each term by parts, we get

$$\begin{aligned} F(\tau, \xi, \eta, \zeta, Q, Q_\tau, Q_\xi, Q_{\xi\xi}, Q_{\xi\eta}, Q_{\xi\zeta}) \\ = -\frac{\partial}{\partial \tau} \left(\frac{\partial F}{\partial Q_\tau} \right) - \frac{\partial}{\partial \xi} \left(\frac{\partial F}{\partial Q_\xi} \right) + \frac{\partial^2}{\partial \xi^2} \left(\frac{\partial F}{\partial Q_{\xi\xi}} \right) \end{aligned}$$

$$\begin{aligned} &+ \frac{\partial^2}{\partial \xi \eta} \left(\frac{\partial F}{\partial Q_{\xi\eta}} \right) + \frac{\partial^2}{\partial \xi \zeta} \left(\frac{\partial F}{\partial Q_{\xi\zeta}} \right) \\ &= b_1 Q_{\xi\tau} + 3b_2 a_1 Q_\xi Q_{\xi\xi} + 2b_3 a_2 Q_{\xi\xi\xi} + 2b_4 a_3 Q_{\xi\xi\eta\eta} \\ &\quad + 2b_5 a_4 Q_{\xi\xi\zeta\zeta}. \end{aligned} \quad (25)$$

Thus, the following comparison expression is given as

$$\begin{aligned} b_1 Q_{\xi\tau} + 3b_2 a_1 Q_\xi Q_{\xi\xi} + 2b_3 a_2 Q_{\xi\xi\xi} + 2b_4 a_3 Q_{\xi\xi\eta\eta} \\ + 2b_5 a_4 Q_{\xi\xi\zeta\zeta} = 0. \end{aligned} \quad (26)$$

At this point, (26) is equivalent to (22), so the Lagrangian multipliers are as follows:

$$b_1 = \frac{1}{2},$$

$$\begin{aligned}
b_2 &= \frac{1}{3}, \\
b_3 &= b_4 = b_5 = \frac{1}{2}.
\end{aligned} \tag{27}$$

The Lagrangian form of the (3+1)-dimensional ZK equation can be written as follows:

$$\begin{aligned}
L(Q_\tau, Q_\xi, Q_{\xi\xi}, Q_{\xi\eta}, Q_{\xi\zeta}) \\
= -\frac{1}{2}Q_\tau Q_\xi - \frac{1}{6}a_1 Q_\xi^3 + \frac{1}{2}Q_{\xi\xi}^2 + \frac{1}{2}Q_{\xi\eta}^2 + \frac{1}{2}Q_{\xi\zeta}^2.
\end{aligned} \tag{28}$$

Similarly, the following Lagrangian form of the (3+1)-dimensional TSF-ZK equation can be obtained

$$\begin{aligned}
F(D_\tau^\alpha Q, D_\xi^\beta Q, D_{\xi\xi}^{\beta\beta} Q, D_\xi^\beta D_\eta^\gamma Q, D_\xi^\beta D_\zeta^\theta Q) \\
= -\frac{1}{2}D_\tau^\alpha Q D_\xi^\beta Q - \frac{1}{6}a_1 (D_\xi^\beta Q)^3 + \frac{1}{2}(D_{\xi\xi}^{\beta\beta} Q)^3 \\
+ \frac{1}{2}(D_\xi^\beta D_\eta^\gamma Q)^2 + \frac{1}{2}D_\xi^\beta D_\zeta^\theta Q,
\end{aligned} \tag{29}$$

where α , β , β , and θ are fractional order values. Thereby the functional of (3+1)-dimensional TSF-ZK equation is given as follows:

$$\begin{aligned}
J_F(Q) &= \iiint_V (d\xi)^\beta (d\eta)^\gamma (d\zeta)^\theta \\
&\cdot \int_T F(D_\tau^\alpha Q, D_\xi^\beta Q, D_{\xi\xi}^{\beta\beta} Q, D_\xi^\beta D_\eta^\gamma Q, D_\xi^\beta D_\zeta^\theta Q) \\
&\cdot (d\tau)^\alpha,
\end{aligned} \tag{30}$$

where

$$\int_a^t f(\tau) (d\tau)^\alpha = \alpha \int_a^t f(\tau) (t-\tau)^{\alpha-1} d\tau. \tag{31}$$

Using the fractional integration by parts

$$\begin{aligned}
\int_a^b f(t) D_t^\alpha g(t) (dt)^\alpha \\
= \Gamma(1+\alpha) \left[g(t) f(t) \Big|_a^b - \int_a^b g(t) D_t^\alpha f(t) (dt)^\alpha \right],
\end{aligned} \tag{32}$$

$f(t), g(t) \in [a, b],$

optimizing the above functional (30), and letting $\delta J_F(Q) = 0$, we can get the following Euler-Lagrange equation of (3+1)-dimensional TSF-ZK equation

$$\begin{aligned}
-D_\tau^\alpha \left(\frac{\partial F}{\partial D_\tau^\alpha Q} \right) - D_\xi^\beta \left(\frac{\partial F}{\partial D_\xi^\beta Q} \right) + D_{\xi\xi}^{\beta\beta} \left(\frac{\partial F}{\partial D_{\xi\xi}^{\beta\beta} Q} \right) \\
+ D_\xi^\beta D_\eta^\gamma \left(\frac{\partial F}{\partial D_\xi^\beta D_\eta^\gamma Q} \right) + D_\xi^\beta D_\zeta^\theta \left(\frac{\partial F}{\partial D_\xi^\beta D_\zeta^\theta Q} \right) \\
= 0.
\end{aligned} \tag{33}$$

According to (29), (33) can be rewritten as

$$\begin{aligned}
D_\tau^\alpha (D_\xi^\beta Q) + a_1 D_\xi^\beta Q D_\xi^\beta Q + a_2 D_{\xi\xi}^{\beta\beta} Q \\
+ a_3 D_\xi^\beta D_\eta^\gamma Q + a_4 D_\xi^\beta D_\eta^\theta Q = 0.
\end{aligned} \tag{34}$$

Letting $D_\xi^\beta Q = \phi(\xi, \eta, \zeta, \tau)$, we get

$$\begin{aligned}
D_\tau^\alpha \phi + a_1 \phi D_\xi^\beta \phi + a_2 D_{\xi\xi}^{\beta\beta} \phi + a_3 D_\xi^\beta D_\eta^\gamma \phi + a_4 D_\xi^\beta D_\eta^\theta \phi \\
= 0.
\end{aligned} \tag{35}$$

Equation (35) is a new model, namely, the (3+1)-dimensional TSF-ZK equation. When $\alpha = \beta = \gamma = \theta = 1$, (35) is the integer order (3+1)-dimensional ZK equation. This shows that the integer order model is the special type of fractional model. The fractional derivatives of the (3+1)-dimensional TSF-ZK equation are related to the dust acoustic waves propagation with fractal properties. Equation (35) can describe fractal processes of the dust acoustic waves. The fractional order model could simulate various real plasma environments more adequately than the integer order model and provide an excellent tool for the description of dynamical processes. Therefore, (3+1)-dimensional TSF-ZK equation can better describe the dust acoustic waves in the real dust plasma.

4. Conservation Law of the (3+1)-Dimensional TSF-ZK Equation

In the last section, we extend the integral order equations describing dust acoustic waves to the fractional order of time-space and obtain some new properties of dust acoustic waves propagation. In this section, in order to research the energy changes during the propagation of dust acoustic waves, we use the Lie symmetry method to obtain multiple conservation law of the (3+1)-dimensional TSF-ZK equation.

Considering that, under one-parameter Lie group of point transformations, (35) is invariant with the dependent and independent variables, the transformations are given by

$$\begin{aligned}
\bar{\xi} &\longrightarrow \xi + \varepsilon l(\xi, \eta, \zeta, \tau) + O(\varepsilon^2), \\
\bar{\eta} &\longrightarrow \eta + \varepsilon \kappa(\xi, \eta, \zeta, \tau) + O(\varepsilon^2), \\
\bar{\zeta} &\longrightarrow \zeta + \varepsilon v(\xi, \eta, \zeta, \tau) + O(\varepsilon^2), \\
\bar{\tau} &\longrightarrow \tau + \varepsilon \sigma(\xi, \eta, \zeta, \tau) + O(\varepsilon^2), \\
\bar{\phi} &\longrightarrow \phi + \varepsilon \Phi(\xi, \eta, \zeta, \tau) + O(\varepsilon^2),
\end{aligned}$$

$$\begin{aligned}
D_\tau^\alpha \bar{\phi} &\longrightarrow D_\tau^\alpha \phi + \varepsilon \Phi_\alpha^\tau + O(\varepsilon^2), & -\phi_{\xi\eta\zeta} D_\xi^\beta (v) - \phi_{\xi\eta\tau} D_\xi^\beta (\sigma), \\
D_\xi^\beta \bar{\phi} &\longrightarrow D_\xi^\beta \phi + \varepsilon \Phi_\beta^\xi + O(\varepsilon^2), & \Phi_{\alpha,\zeta}^{\tau\theta\theta} = D_\xi^\beta \left(\Phi_\beta^{\zeta\zeta} \right) - \phi_{\xi\zeta\tau} D_\xi^\beta (\iota) - \phi_{\xi\zeta\eta} D_\xi^\beta (\kappa) \\
D_\xi^{\beta\beta} \bar{\phi} &\longrightarrow D_\xi^{\beta\beta} \phi + \varepsilon \Phi_\beta^{\xi\xi\xi} + O(\varepsilon^2), & -\phi_{\xi\zeta\zeta} D_\xi^\beta (v) - \phi_{\xi\zeta\tau} D_\xi^\beta (\sigma), \\
D_\tau^\alpha D_\xi^{\beta\beta} \bar{\phi} &\longrightarrow D_\tau^\alpha D_\xi^{\beta\beta} \phi + \varepsilon \Phi_{\alpha,\beta}^{\tau\xi\xi} + O(\varepsilon^2), \\
D_\tau^\alpha D_\zeta^{\theta\theta} \bar{\phi} &\longrightarrow D_\tau^\alpha D_\zeta^{\theta\theta} \phi + \varepsilon \Phi_{\alpha,\zeta}^{\tau\theta\theta} + O(\varepsilon^2),
\end{aligned} \tag{36}$$

where ι, κ, v, σ are infinitesimal function of the transformations, $\varepsilon \ll 1$ is the group parameter, and $\Phi_\alpha^\tau, \Phi_\beta^\xi, \Phi_\beta^{\xi\xi\xi}, \Phi_{\alpha,\beta}^{\tau\xi\xi}, \Phi_{\alpha,\zeta}^{\tau\theta\theta}$ are extended infinitesimal functions in the following explicit expression:

$$\begin{aligned}
\Phi_\alpha^\tau &= D_\tau^\alpha (\Phi) + \iota D_\tau^\alpha (\phi_\xi) - D_\tau^\alpha (\iota \phi_\xi) + \kappa D_\tau^\alpha (\phi_\eta) \\
&\quad - D_\tau^\alpha (\kappa \phi_\eta) + \nu D_\tau^\alpha (\phi_\zeta) - D_\tau^\alpha (\nu \phi_\zeta) \\
&\quad + D_\tau^\alpha (D_\tau (\sigma) \phi) - D_\tau^{\alpha+1} (\sigma \phi) \\
&\quad + \sigma D_\tau^{\alpha+1} (\phi), \\
\Phi_\beta^\xi &= D_\xi^\beta (\Phi) + D_\xi^\beta (\phi) D_\xi (\iota) - D_\eta^\nu (\phi) D_\xi (\kappa) \\
&\quad - D_\zeta^\theta (\phi) D_\xi (v), \\
\Phi_\beta^{\xi\xi\xi} &= D_\xi^\beta \left(\Phi_\beta^{\xi\xi\xi} \right) - \phi_{\xi\xi\xi} D_\xi^\beta (\iota) - \phi_{\xi\xi\eta} D_\xi^\beta (\kappa) \\
&\quad - \phi_{\xi\xi\zeta} D_\xi^\beta (v) - \phi_{\xi\xi\tau} D_\xi^\beta (\sigma), \\
\Phi_{\alpha,\beta}^{\tau\xi\xi} &= D_\xi^\beta \left(\Phi_\beta^{\eta\eta} \right) - \phi_{\xi\eta\xi} D_\xi^\beta (\iota) - \phi_{\xi\eta\eta} D_\xi^\beta (\kappa)
\end{aligned}$$

where D_τ and D_ξ are the total derivative operators as follows:

$$\begin{aligned}
D_\tau &= \frac{\partial}{\partial \tau} + \phi_\tau \frac{\partial}{\partial \tau} + \phi_{\tau\tau} \frac{\partial}{\partial \phi_\tau} + \phi_{\xi\tau} \frac{\partial}{\partial \phi_\xi} + \phi_{\eta\tau} \frac{\partial}{\partial \phi_\eta} \\
&\quad + \phi_{\zeta\tau} \frac{\partial}{\partial \phi_\zeta} + \dots, \\
D_\xi &= \frac{\partial}{\partial \xi} + \phi_\xi \frac{\partial}{\partial \xi} + \phi_{\xi\xi} \frac{\partial}{\partial \phi_\xi} + \phi_{\tau\xi} \frac{\partial}{\partial \phi_\tau} + \phi_{\eta\xi} \frac{\partial}{\partial \phi_\eta} \\
&\quad + \phi_{\zeta\xi} \frac{\partial}{\partial \phi_\zeta} + \dots.
\end{aligned} \tag{38}$$

Applying the generalized Leibnitz rule and the chain rule, the extended symmetry operator Φ can be introduced in the following form:

$$\begin{aligned}
\Phi_\alpha^\tau &= \frac{\partial^\alpha \Phi}{\partial \tau^\alpha} + (\Phi_\phi - \alpha D_\tau^\sigma) \frac{\partial^\alpha \phi}{\partial \tau^\alpha} - \phi \frac{\partial^\alpha \Phi_\phi}{\partial \tau^\alpha} \\
&\quad + \sum_{n=1}^{\infty} \left[\binom{\alpha}{n} \frac{\partial^\alpha \Phi_\phi}{\partial \tau^\alpha} - \binom{\alpha}{n+1} D_\tau^{n+1} (\sigma) \right] D_\tau^{\alpha-n} \\
&\quad - \sum_{n=1}^{\infty} \binom{\alpha}{n} \left[D_\tau^n (\iota) D_\tau^{\alpha-n} (\phi_\xi) + D_\tau^n (\kappa) D_\tau^{\alpha-n} (\phi_\eta) \right. \\
&\quad \left. + D_\tau^n (v) D_\tau^{\alpha-n} (\phi_\zeta) \right] + R_\tau,
\end{aligned} \tag{39}$$

where

$$R_\tau = \sum_{n=2}^{\infty} \sum_{m=2}^n \sum_{k=2}^m \sum_{r=0}^{k-1} \left[\binom{\alpha}{n} \binom{n}{m} \binom{k}{r} \frac{1}{k!} \frac{\tau^{n-\alpha}}{\Gamma(n+1-\alpha)} (-\phi)^r \frac{\partial^\phi}{\partial \tau^\phi} (\phi)^{k-r} \frac{\partial^{n-m+k} \Phi}{\partial \tau^{n-m} \partial \phi^k} \right]. \tag{40}$$

Similarly, we also have the following equation:

$$\begin{aligned}
\Phi_\beta^\xi &= \frac{\partial^\beta \Phi}{\partial \xi^\beta} + (\Phi_\phi - \beta D_\xi^\iota) \frac{\partial^\beta \phi}{\partial \xi^\beta} - \phi \frac{\partial^\beta \Phi_\phi}{\partial \xi^\beta} \\
&\quad + \sum_{n=1}^{\infty} \left[\binom{\beta}{n} \frac{\partial^\beta \Phi_\phi}{\partial \xi^\beta} - \binom{\beta}{n+1} D_\xi^{n+1} (\iota) \right] D_\xi^{\beta-n}
\end{aligned}$$

$$\begin{aligned}
&\quad - \sum_{n=1}^{\infty} \binom{\beta}{n} \left[D_\xi^n (\sigma) D_\xi^{\beta-n} (\phi_\tau) + D_\xi^n (\kappa) D_\xi^{\beta-n} (\phi_\eta) \right. \\
&\quad \left. + D_\xi^n (v) D_\xi^{\beta-n} (\phi_\zeta) \right] + R_\xi,
\end{aligned} \tag{41}$$

where

$$R_\xi = \sum_{n=2}^{\infty} \sum_{m=2}^n \sum_{k=2}^m \sum_{r=0}^{k-1} \left[\binom{\beta}{n} \binom{n}{m} \binom{k}{r} \frac{1}{k!} \frac{\xi^{n-\beta}}{\Gamma(n+1-\beta)} (-\phi)^r \frac{\partial^\phi}{\partial \xi^\phi} (\phi)^{k-r} \frac{\partial^{n-m+k} \Phi}{\partial \xi^{n-m} \partial \phi^k} \right]. \tag{42}$$

Introducing the Lie algebra N associated with (35) is composed of the following infinitesimal generator

$$N = \iota \frac{\partial}{\partial \xi} + \kappa \frac{\partial}{\partial \eta} + \nu \frac{\partial}{\partial \zeta} + \Phi \frac{\partial}{\partial \phi}. \quad (43)$$

Applying the infinitesimal transformations, the (35) is invariable that results in the invariance conditions given as

$$Pr^{(\alpha, \beta, \gamma, \theta, 4)} N(\Delta) \Big|_{\Delta=0} = 0, \quad (44)$$

where Δ represents the (3+1)-dimensional TSF-ZK equation.

We get following symmetry determining equation by using the third prolongation to (35)

$$\begin{aligned} \Phi_\alpha^\tau + a_1 \Phi D_\xi^\beta \phi + a_1 \Phi_\beta^\xi + a_2 \Phi_\beta^{\xi\xi} + a_3 \Phi_{\beta, \gamma}^{\xi\eta} + a_4 \Phi_{\beta, \theta}^{\xi\zeta} \\ = 0. \end{aligned} \quad (45)$$

Substituting (37), (38), (39), and (41) into this equation, letting the same coefficients of derivatives to zero, and then solving the series of determining equations, we can obtain the following infinitesimal functions

$$\begin{aligned} \sigma &= \frac{b_1 \tau}{\alpha} + b_2, \\ \iota &= \frac{b_1 \xi}{\beta} + b_3, \\ \kappa &= \frac{b_1 \eta}{2\gamma} + b_4, \\ \nu &= \frac{b_1 \zeta}{2\theta} + b_5, \\ \Phi &= b_1 \left(\frac{3 - \beta - \alpha}{\beta + \alpha} \right) \phi, \end{aligned} \quad (46)$$

where $b_i, i = 1 \dots 5$, are arbitrary constants, since the corresponding infinitesimal generators can be expressed as

$$\begin{aligned} N_1 &= \frac{\partial}{\partial \xi}, \\ N_2 &= \frac{\partial}{\partial \eta}, \\ N_3 &= \frac{\partial}{\partial \zeta}, \\ N_4 &= \frac{\partial}{\partial \tau}, \\ N_5 &= \frac{\tau}{\alpha} \frac{\partial}{\partial \tau} + \frac{\xi}{\beta} \frac{\partial}{\partial \xi} + \frac{\eta}{2\gamma} \frac{\partial}{\partial \eta} + \frac{\zeta}{2\theta} \frac{\partial}{\partial \zeta} \\ &\quad + \left(\frac{3 - \beta - \alpha}{\beta + \alpha} \right) \phi \frac{\partial}{\partial \phi}. \end{aligned} \quad (47)$$

The conserved vector of (35) is $C = (C^\tau, C^\xi, C^\eta, C^\zeta)$ which satisfies the conservation equation

$$D_\tau(C^\tau) + D_\xi(C^\xi) + D_\eta(C^\eta) + D_\zeta(C^\zeta) = 0. \quad (48)$$

A formal Lagrangian for the (3+1)-dimensional TSF-ZK equation is given as

$$\begin{aligned} L_a = \rho(\xi, \eta, \zeta, \tau) \left(D_\tau^\alpha \phi + a_1 \phi D_\xi^\beta \phi + a_2 D_\xi^{\beta\beta\beta} \phi \right. \\ \left. + a_3 D_\xi^\beta D_\eta^{\gamma\gamma} \phi + a_4 D_\xi^\beta D_\eta^{\theta\theta} \phi \right), \end{aligned} \quad (49)$$

where $\rho(\xi, \eta, \zeta, \tau)$ is the new dependent variable.

In the considered linear case, the adjoint equation to (35) as the Euler-Lagrange equation is represented as

$$F^* = \frac{\delta L_a}{\delta \phi} = 0. \quad (50)$$

Here $\delta/\delta\phi$ is the Euler-Lagrange operator which is defined as

$$\begin{aligned} \frac{\delta}{\delta \phi} &= \frac{\partial}{\partial \phi} + (D_\tau^\alpha)^* \frac{\partial}{\partial D_\tau^\alpha} + (D_\xi^\beta)^* \frac{\partial}{\partial D_\xi^\beta} \\ &\quad - (D_\xi^{\beta\beta\beta})^* \frac{\partial}{\partial D_\xi^{\beta\beta\beta} \phi} - (D_\xi^\beta D_\eta^{\gamma\gamma})^* \frac{\partial}{\partial D_\xi^\beta D_\eta^{\gamma\gamma} \phi} \\ &\quad - (D_\xi^\beta D_\zeta^{\theta\theta})^* \frac{\partial}{\partial D_\xi^\beta D_\zeta^{\theta\theta} \phi}, \end{aligned} \quad (51)$$

where $(D_\tau^\alpha)^*, (D_\xi^{\beta\beta\beta})^*, (D_\xi^\beta D_\eta^{\gamma\gamma})^*$, and $(D_\xi^\beta D_\zeta^{\theta\theta})^*$ are the adjoint operators.

Hence, the adjoint equation (50) can be rewritten as

$$\begin{aligned} F^* &= (D_\tau^\alpha)^* \rho + a_1 \phi (D_\xi^\beta)^* \rho - a_2 (D_\xi^{\beta\beta\beta})^* \rho \\ &\quad - a_3 (D_\xi^\beta D_\eta^{\gamma\gamma})^* \rho - a_4 (D_\xi^\beta D_\eta^{\theta\theta})^* \rho = 0. \end{aligned} \quad (52)$$

We introduce the Lie characteristic function W for generator N as follows:

$$W = \Phi - \iota \phi_\xi - \kappa \phi_\eta - \nu \phi_\zeta - \sigma \phi_\tau. \quad (53)$$

The fractional Noether operator for the variables τ, ξ, η , and ζ are given by

$$\begin{aligned} C^\tau &= \sum_{k=0}^{n-1} (-1)^k D_\tau^{\alpha-1-k} (W) D_\tau^k \left(\frac{\partial L_a}{\partial (D_\tau^\alpha \phi)} \right) - (-1)^n \\ &\quad \cdot J \left(W, D_\tau^n \left(\frac{\partial L_a}{\partial (D_\tau^\alpha \phi)} \right) \right), \\ C^\xi &= \sum_{k=0}^{m-1} (-1)^k D_\xi^{\beta-1-k} (W) D_\xi^k \left(\frac{\partial L_a}{\partial D_\xi^\beta \phi} + D_\xi^{\beta\beta} \frac{\partial L_a}{\partial D_\xi^{\beta\beta\beta} \phi} \right. \\ &\quad \left. + D_\eta^{\gamma\gamma} \frac{\partial L_a}{\partial D_\xi^\beta D_\eta^{\gamma\gamma} \phi} + D_\zeta^{\theta\theta} \frac{\partial L_a}{\partial D_\xi^\beta D_\zeta^{\theta\theta} \phi} \right) - (-1)^m \end{aligned}$$

$$\begin{aligned}
& \cdot J \left(W, D_\xi^m \left(\frac{\partial L_a}{\partial D_\xi^\beta \phi} + D_\xi^{\beta\beta} \frac{\partial L_a}{\partial D_\xi^{\beta\beta\beta} \phi} \right. \right. \\
& \left. \left. + D_\eta^{\gamma\gamma} \frac{\partial L_a}{\partial D_\xi^\beta D_\eta^{\gamma\gamma} \phi} + D_\zeta^{\theta\theta} \frac{\partial L_a}{\partial D_\xi^\beta D_\zeta^{\theta\theta} \phi} \right) \right), \\
C^\eta &= \sum_{k=0}^{l-1} (-1)^k D_\eta^{\gamma-1-k} (W) D_\eta^k \left(D_\xi^\beta \frac{\partial L_a}{\partial D_\eta^{\gamma\gamma} \phi} \right) - (-1)^l \\
& \cdot J \left(W, D_\eta^l \left(D_\xi^\beta \frac{\partial L_a}{\partial D_\eta^{\gamma\gamma} \phi} \right) \right), \\
C^\zeta &= \sum_{k=0}^{s-1} (-1)^k D_\zeta^{\theta-1-k} (W) D_\zeta^k \left(D_\xi^\beta \frac{\partial L_a}{\partial D_\zeta^{\theta\theta} \phi} \right) - (-1)^s \\
& \cdot J \left(W, D_\zeta^s \left(D_\xi^\beta \frac{\partial L_a}{\partial D_\zeta^{\theta\theta} \phi} \right) \right),
\end{aligned} \tag{54}$$

where

$$\begin{aligned}
n &= [\alpha] + 1, \\
m &= [\beta] + 1, \\
l &= [\gamma] + 1, \\
s &= [\theta] + 1,
\end{aligned} \tag{55}$$

and J is an integral equation.

Consequently, the conservation law of the (3+1)-dimensional TSF-ZK equation is obtained. This indicates that the dust acoustic wave described by this new model is conserved in energy during its propagation, no matter in the fractal process or in the interaction.

5. The Solution of the (3+1)-Dimensional TSF-ZK Equation

In this section, we seek the exact solution of (3+1)-dimensional TSF-ZK equation by using the extended Kudryashov method. Firstly, for a given nonlinear partial differential equation

$$\begin{aligned}
F(\phi, \phi_\tau, \phi_\xi, \phi_\eta, \phi_\zeta, \dots, D_\tau^\alpha \phi, D_\xi^\beta \phi, D_\eta^\gamma \phi, D_\zeta^\theta \phi, \dots) \\
= 0,
\end{aligned} \tag{56}$$

we present the main solving process by using the extended Kudryashov method [47].

Step 1. We introduce the traveling wave solutions of the given nonlinear partial differential equation by making the following transformations:

$$\begin{aligned}
\phi(\xi, \eta, \zeta, \dots, \tau) &= \phi(E), \\
E &= \frac{k_1 \tau^\alpha}{\Gamma(1+\alpha)} + \frac{k_2 \xi^\beta}{\Gamma(1+\beta)} + \frac{k_3 \eta^\gamma}{\Gamma(1+\gamma)} + \frac{k_4 \zeta^\theta}{\Gamma(1+\theta)} + \dots,
\end{aligned} \tag{57}$$

where k_i ($i = 1, 2, 3, \dots$) are arbitrary constants. Thus, the nonlinear partial differential equation reduces to a nonlinear ordinary differential equation as follows:

$$G(\phi, \phi_E, \phi_{EE}, \phi_{EEE}, \dots) = 0. \tag{58}$$

Step 2. We let the new nonlinear ordinary differential equation have the following solution:

$$\phi(E) = \sum_{i=0}^N c_i P^i(E), \quad c_N \neq 0, \tag{59}$$

where $\phi(E) = \pm 1/\sqrt{1 \pm e^{2E}}$ and the function P satisfies the following equation:

$$P_E(E) = P^3(E) - P(E). \tag{60}$$

Step 3. We assume that the solution of (58) can be given in the following form:

$$\phi = c_N P^N + c_{N-1} P^{N-1} + \dots. \tag{61}$$

In order to determine the value of the pole order N , we balance the highest order nonlinear terms $\phi^l(E)\phi^{(s)}(E)$ and the highest order linear terms $(\phi^{(p)}(E))^r$ analogously. In the traditional method [53], we assume that the value of the pole order of $\phi(E)$ is $o(\phi(E)) = N$, so the values of the pole order of the other terms are as follows:

$$\begin{aligned}
o(\phi^l(E)\phi^{(s)}(E)) &= (l+1)N + s, \\
o((\phi^{(p)}(E))^r) &= (N+p)r.
\end{aligned} \tag{62}$$

Letting $o(\phi^l(E)\phi^{(s)}(E)) = o((\phi^{(p)}(E))^r)$, we get N . However, there are some differences in the extended Kudryashov method. The value of the pole order N is defined as

$$N = \frac{2(s-rp)}{r-l-1}. \tag{63}$$

Step 4. Substituting (59), (60), (61), and (63) into (58) and equating the coefficients of P^i to zero, we can get a series of algebraic equations. The exact solution of (56) can be gained by solving those algebraic equations.

For the (3+1)-dimensional TSF-ZK equation, we introduce the traveling wave solutions by making the following transformations

$$\begin{aligned}
\phi(\xi, \eta, \zeta, \tau) &= \phi(E), \\
E &= \frac{k_1 \tau^\alpha}{\Gamma(1+\alpha)} + \frac{k_2 \xi^\beta}{\Gamma(1+\beta)} + \frac{k_3 \eta^\gamma}{\Gamma(1+\gamma)} + \frac{k_4 \zeta^\theta}{\Gamma(1+\theta)},
\end{aligned} \tag{64}$$

where k_i ($i = 1, 2, 3, 4$) are arbitrary constants. Thus, the (3+1)-dimensional TSF-ZK equation reduces to a nonlinear ordinary differential equation as follows:

$$k_1 \phi_\xi + a_1 k_2 \phi \phi_\xi + (a_2 k_2^3 + a_3 k_2 k_3^2 + a_4 k_2 k_4^2) \phi_{\xi\xi\xi} = 0. \tag{65}$$

Next, $\phi(E)$ is expanded to the following power series of the Jacobian elliptic function:

$$\phi(E) = c_0 + c_1 P + \cdots + c_{N-1} P^{N-1} + c_N P^N, \quad c_N \neq 0, \quad (66)$$

where $\phi(E) = \pm 1/\sqrt{1 \pm e^{2E}}$ and the function P is the solution of $P_E(E) = P^3(E) - P(E)$. In (65), balancing the highest order nonlinear terms $\phi(E)\phi_\xi(E)$ and the highest order linear terms $\phi_{\xi\xi\xi}(E)$, we acquire $N = 4$. Thus, the $\phi_{\xi\xi\xi}(E)$ can be expanded as follows:

$$\phi(E) = c_0 + c_1 P + c_2 P^2 + c_3 P^3 + c_4 P^4, \quad c_4 \neq 0. \quad (67)$$

Based on (67), we obtain

$$\begin{aligned} \phi_\xi &= 4c_4 P^6 + 3c_3 P^5 + (2c_2 - 4c_4) P^4 + (c_1 - 3c_3) P^3 \\ &\quad - 2c_2 P^2 - c_1 P, \end{aligned}$$

$$\begin{aligned} \phi_{\xi\xi} &= 24c_4 P^8 + 15c_3 P^7 + (8c_2 - 40c_4) P^6 \\ &\quad + (3c_1 - 24c_3) P^5 + (16c_4 - 12c_2) P^4 \\ &\quad + (9c_3 - 4c_1) P^3 + 4c_2 P^2 + c_1 P, \end{aligned} \quad (68)$$

$$\begin{aligned} \phi_{\xi\xi\xi} &= 192c_4 P^{10} + 105c_3 P^9 + (48c_2 - 432c_4) P^8 \\ &\quad + (15c_1 - 225c_3) P^7 + (304c_4 - 96c_2) P^6 \\ &\quad + (147c_3 - 27c_1) P^5 + (56c_2 - 64c_4) P^4 \\ &\quad + (13c_1 - 27c_3) P^3 - 8c_2 P^2 - c_1 P. \end{aligned}$$

Substituting (67) and (68) into (65) and collecting the coefficient of each power of P^i ($i = 12, 3, \dots$), we can present a system of algebraic equations in the following form:

$$P^{10} : 4a_1 k_2 c_4^2 + 192c_4 (a_2 k_2^3 + a_3 k_2 k_3^2 + a_4 k_2 k_4^2) = 0,$$

$$P^9 : 7a_1 k_2 c_3 c_4 + 105c_3 (a_2 k_2^3 + a_3 k_2 k_3^2 + a_4 k_2 k_4^2) = 0,$$

$$\begin{aligned} P^8 : & a_1 k_2 (6c_2 c_4 + 3c_3^2 - 4c_4^2) \\ & + (48c_2 - 432c_4) (a_2 k_2^3 + a_3 k_2 k_3^2 + a_4 k_2 k_4^2), \end{aligned}$$

$$\begin{aligned} P^7 : & a_1 k_2 (5c_1 c_4 + 4c_2 c_3 - 4c_3 c_4) \\ & + (15c_1 - 225c_3) (a_2 k_2^3 + a_3 k_2 k_3^2 + a_4 k_2 k_4^2) = 0, \end{aligned}$$

$$\begin{aligned} P^6 : & 4k_1 c_4 + a_1 k_2 (4c_0 c_4 + 4c_1 c_3 + 2c_2^2 - 6c_2 c_4 + 3c_3^2) \\ & + (304c_4 - 96c_2) (a_2 k_2^3 + a_3 k_2 k_3^2 + a_4 k_2 k_4^2) = 0, \end{aligned}$$

$$\begin{aligned} P^5 : & 3c_3 k_1 + a_1 k_2 (3c_0 c_3 + 3c_1 c_2 - 5c_1 c_4 - 5c_2 c_3) \\ & + (147c_3 - 27c_1) (a_2 k_2^3 + a_3 k_2 k_3^2 + a_4 k_2 k_4^2) = 0, \end{aligned}$$

$$\begin{aligned} P^4 : & (2c_2 - 4c_4) k_1 \\ & + a_1 k_2 (2c_0 c_2 - 4c_0 c_4 + c_1^2 - 4c_1 c_3 - 2c_2^2) \\ & + (56c_2 - 64c_4) (a_2 k_2^3 + a_3 k_2 k_3^2 + a_4 k_2 k_4^2) = 0, \end{aligned}$$

$$\begin{aligned} P^3 : & (c_1 - 3c_3) k_1 + a_1 k_2 (c_0 c_1 - 3c_0 c_3 - 3c_1 c_2) \\ & + (13c_1 - 27c_3) (a_2 k_2^3 + a_3 k_2 k_3^2 + a_4 k_2 k_4^2) = 0, \end{aligned}$$

$$\begin{aligned} P^2 : & -2c_2 k_1 - a_1 k_2 (c_0 c_2 + c_1^2) \\ & - 8c_2 (a_2 k_2^3 + a_3 k_2 k_3^2 + a_4 k_2 k_4^2) = 0, \end{aligned}$$

$$\begin{aligned} P : & -c_1 k_1 - a_1 k_2 c_0 c_1 \\ & - c_1 (a_2 k_2^3 + a_3 k_2 k_3^2 + a_4 k_2 k_4^2) = 0. \end{aligned} \quad (69)$$

Solving the above algebraic equations, the coefficients can be written as

$$\begin{aligned} c_0 &= \frac{2}{a_1} k (\sqrt[3]{12a_2} - \sqrt{12a_2}), \\ c_1 &= c_3 = 0, \\ c_2 &= \frac{12k\sqrt{12a_2}}{a_1}, \\ c_4 &= -\frac{12k\sqrt{12a_2}}{a_1}, \\ k_1 &= k, \\ k_2 &= k_3 = k_4 = -\sqrt[3]{\frac{k}{12a_2}}. \end{aligned} \quad (70)$$

Thus, we get the solution of (3+1)-dimensional TSF-ZK equation in the following form:

$$\begin{aligned} \phi &= \frac{2}{a_1} k (\sqrt[3]{12a_2} - \sqrt{12a_2}) + \frac{3k\sqrt{12a_2}}{a_1} \\ &\cdot \operatorname{sech}^2 \left[2\sqrt[3]{\frac{k}{12a_2}} \left(\frac{\xi^\beta}{\Gamma(1+\beta)} + \frac{\eta^\gamma}{\Gamma(1+\gamma)} \right. \right. \\ &\quad \left. \left. + \frac{\eta^\theta}{\Gamma(1+\theta)} \right) - 2k \frac{\tau^\alpha}{\Gamma(1+\alpha)} \right]. \end{aligned} \quad (71)$$

6. The Property of the Dust Acoustic Waves by a Gravity Field in Collisional Dust Plasma

According to the above section, we can obtain the exact solution of (3+1)-dimensional TSF-ZK equation. Assuming that $\alpha = \beta = \gamma = \theta$, (71) can be rewritten as

$$\phi = \frac{2}{a_1} k (\sqrt[3]{12a_2} - \sqrt{12a_2}) + \frac{3k\sqrt{12a_2}}{a_1}$$

$$\cdot \operatorname{sech}^2 \left[\frac{2}{\Gamma(1+\alpha)} \cdot \sqrt[3]{\frac{k}{12a_2}} \left(\xi^\beta + \eta^\gamma + \eta^\theta - k \sqrt[3]{\frac{12a_2}{k}} \tau^\alpha \right) \right]. \quad (72)$$

Letting ϕ_m and ω be amplitude and width of solitary waves, respectively, we gain the following definitions:

$$\phi_m = \frac{3k\sqrt{12a_2}}{a_1}, \quad (73)$$

$$\omega = \frac{\Gamma(1+\alpha)}{2} \sqrt[3]{\frac{12a_2}{k}}.$$

When $\alpha = \beta = \gamma = \theta = 1$, the motion velocity of the solitary wave is

$$v = \frac{k}{\sqrt{3}} \sqrt[3]{\frac{12a_2}{k}}. \quad (74)$$

Furthermore, according to (17), the phase velocity of solitary waves is in the following form:

$$v_0 = \frac{g}{\beta_0} \pm \sqrt{1 + \frac{T_d}{Z_d}}. \quad (75)$$

6.1. Study of the Charge Properties of Dust Particle Z_{d0} in Dust Acoustic Waves. According to ϕ_m , we know that when $a_1 a_2 > 0$, the TSF-ZK equation has the bright soliton solution, and when $a_1 a_2 < 0$, the (3+1)-dimensional TSF-ZK equation has the dark soliton solution.

Case 1. We assume that the dust particles are negatively charged; that is, $Z_{d0} > 0$. Based on the coefficient equation (19) of (3+1)-dimensional TSF-ZK equation, we know that a_1 and a_2 are real numbers and $a_1 a_2 < 0$. Therefore, in a dust plasma system, the solution (72) of an solitary wave in the case of negative dust charge is a dark soliton. These results are consistent with those obtained by the Sagdeev potential method used by Ma [54].

Case 2. We assume that the dust particles are positively charged; that is, $Z_{d0} < 0$. Based on (19), when $T_d < -Z_{d0}$, we also get that a_1 and a_2 are real numbers and $a_1 a_2 < 0$. At this time, the solution (72) is dark soliton in the dust plasma system. When $T_d > -Z_{d0}$, a_1 and a_2 are complex numbers; that is, solitary waves show a trend of decay, so there are no solitary waves in dust plasma system.

6.2. Study of the Parameter k in Dust Acoustic Waves. Based on the extended Kudryashov method, the exact solution (72) of (3+1)-dimensional TSF-ZK equation is obtained. For the (3+1)-dimensional TSF-ZK equation and its solution, we know that the positive and negative of k are the same as the positive and negative of a_2 , indicating the direction of propagation of dust acoustic waves. $a_2 > 0$ represents the

right traveling waves, and $a_2 < 0$ represents the left traveling waves. As long as there are dust acoustic waves in the system, where a_1 and a_2 are real numbers, there is always $a_2 < 0$. This indicates that the left traveling waves exist in the dust plasma system.

Furthermore, we know that polynomial coefficients and parameters are in the same equivalence class with the solution which is obtained by using classical method. However, according to the solution by using extended Kudryashov method, as the value of k changes, the amplitude, wavelength, and velocity of the dust acoustic waves could change accordingly. From Figure 1, we find that when k increases, so do the amplitude and wavelength of the solitary waves. When $k \rightarrow \infty$, the amplitude, wavelength, and velocity of the dust acoustic waves reach their maximum values. At a physical level, dust acoustic waves are driven by electron thermal pressure and the ion pressure T_i . The increase of k can be regarded as the increase of electron thermal pressure, which increases the amplitude, wavelength, and velocity of the solitary waves with small amplitude.

6.3. Study of the Fractional Order Values α , β , γ , and θ in Dust Acoustic Waves. In this section, we study the effect of the variation of fractional order values α , β , γ , and θ in the dust acoustic waves. Based on the soliton solution (74), we obtain Figure 2. Figure 2(a) shows that the time fractional order value α of differentiation has a small effect only on the position of the wave peak. It does not change the amplitude and wavelength of dust acoustic waves. As the value of α increases, the wave peak moves to the left. Figure 2(b) shows that the space fractional order values β , γ , and θ of differentiation have a small effect only on the position of the wave peak. They also do not change the amplitude and wavelength of dust acoustic waves. And as the values of β , γ , and θ increase, the wave peak moves to the left.

6.4. Study of the Temperature T_d in Dust Acoustic Waves. At this point, the effect of dust temperature on dust acoustic waveforms is considered. When the dust ion temperature increases, the nonlinear term coefficient a_1 and dispersion coefficient a_2 of (3+1)-dimensional TSF-ZK equation both decrease. According to the exact solution of (3+1)-dimensional TSF-ZK equation, we obtain three pictures of the dust acoustic waves. Based on Figure 3, we know that the dust acoustic waveforms are constantly changing with the temperature of dust ions. Furthermore, with the increase in temperature, the motion velocity and the phase velocity of the dust acoustic waves also increase. In [55], the effect of temperature ratio between ions and electrons $\sigma = T_i/T_e$ on classical solitons is studied. The amplitude of the classical isolator increases and the characteristic width decreases with the decrease of σ , which is consistent with the waveform change of the dust acoustic waves in Figure 3.

6.5. Study of the Gravity g and the Collision Frequency β_0, β_1 in Dust Acoustic Waves. According to the (3+1)-dimensional TSF-ZK equation and its exact solution, we can study the effect of gravity g and collision frequency β_0 on the dust

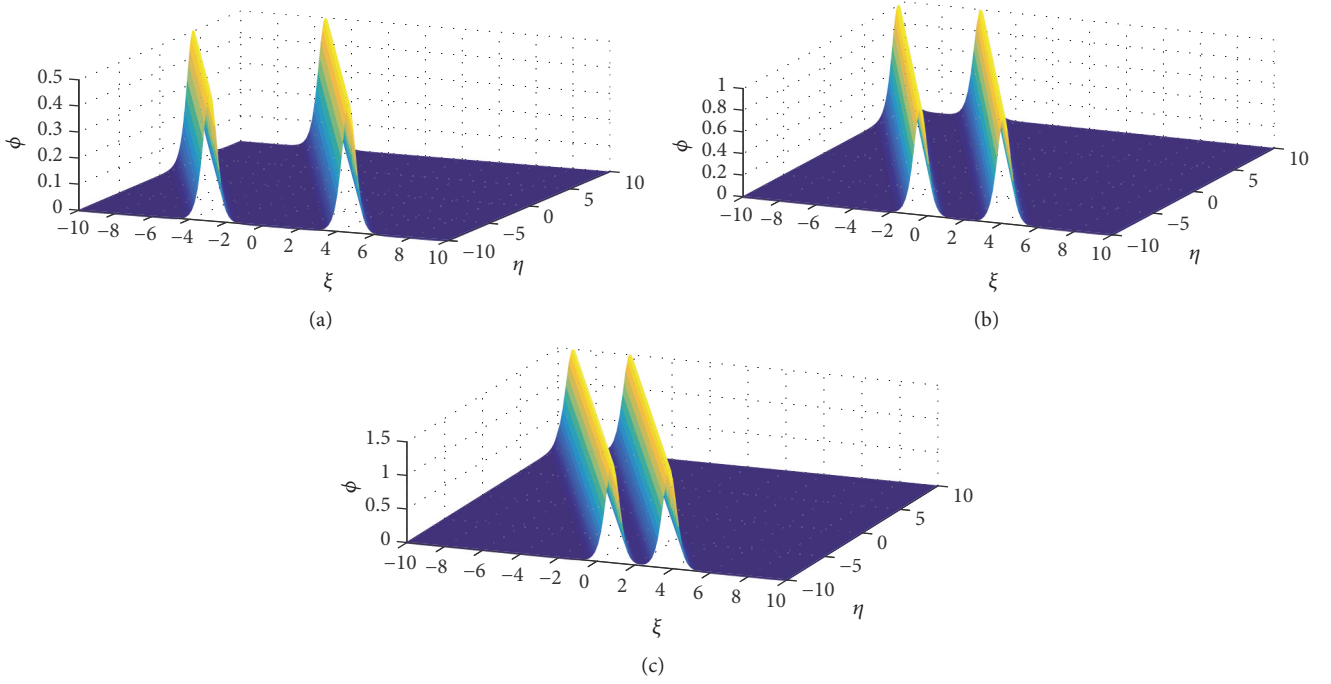


FIGURE 1: Plots for the evolution of the exact solution of dust acoustic solitary waves with (a) $k = 0.5$, $t = 2$, $a_1 = 1.67$, $a_2 = a_3 = a_4 = 1.29$, $\alpha = 0.5$, $\beta = \gamma = \theta = 1$, and $k_2 = k_3 = k_4 = 0.26$; (b) $k = 1$, $t = 2$, $a_1 = 1.67$, $a_2 = a_3 = a_4 = 1.29$, $\alpha = 0.5$, $\beta = \gamma = \theta = 1$, and $k_2 = k_3 = k_4 = 0.26$; (c) $k = 1.5$, $t = 2$, $a_1 = 1.67$, $a_2 = a_3 = a_4 = 1.29$, $\alpha = 0.5$, $\beta = \gamma = \theta = 1$, and $k_2 = k_3 = k_4 = 0.26$.

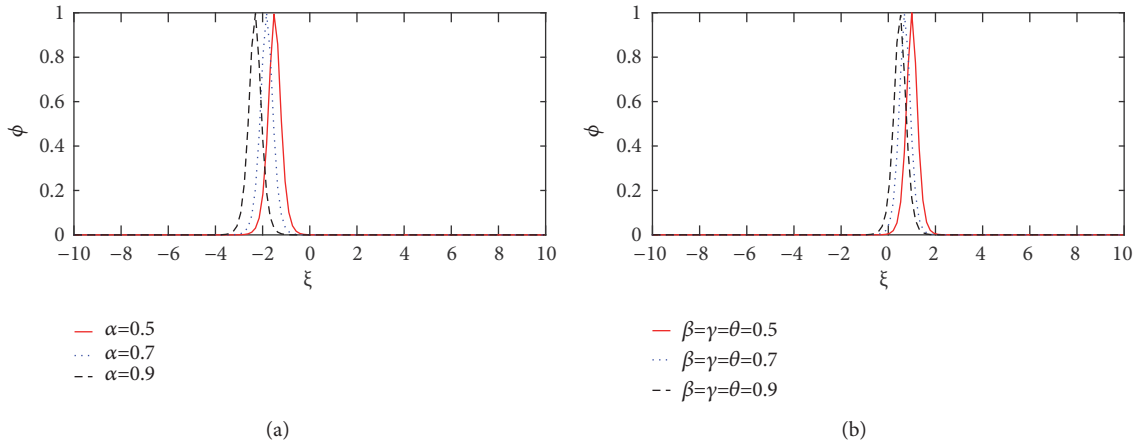


FIGURE 2: The dust acoustic waves with position at different values of (a) α for $k = 2$, $t = 2$, $a_2 = a_3 = a_4 = 1.29$, $\beta = \gamma = \theta = 1$, and $k_2 = k_3 = k_4 = 0.38$; (b) β, γ, θ for $k = 2$, $t = 2$, $a_2 = a_3 = a_4 = 1.29$, $\alpha = 0.5$, and $k_2 = k_3 = k_4 = 0.38$.

acoustic waves. Assuming that there are no collisions and no gravity in the neutral gas and using the same reduced perturbation method, we can get the following coefficients and phase velocity

$$\begin{aligned}
 a_1 &= -\frac{3v_0}{2}, \\
 a_2 &= \frac{1}{2v_0}, \\
 v_0 &= \pm \sqrt{1 + \frac{T_d}{Z_{d0}}}.
 \end{aligned} \tag{76}$$

The result shows that, in the presence of gravity and collision frequency, that is, taking g and β_0 into account, the phase velocity of the dust acoustic waves is increasing. Because $g > 0$ and $\beta_0 > 0$, their ratio g/β_0 is always positive. There is no significant influence on the amplitude of the dust acoustic waves. However, using reduction perturbation analysis, we find that the collision disturbance β_1 of neutral gas contributes to the nonlinear term; thus the soliton solution appears in the colliding plasma. In [52], we can know that if there are unstable dust acoustic waves, that is, there is an imaginary part in the dispersion relationship, the solitary wave will not exist. The difference between our study and

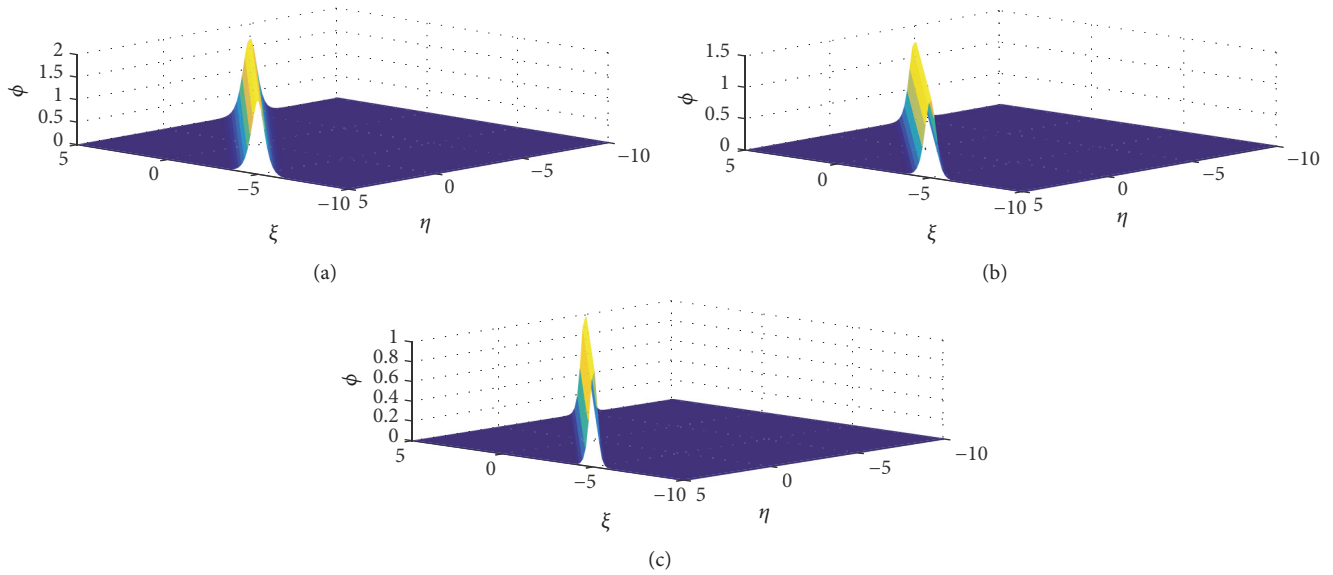


FIGURE 3: Plots for the evolution of the exact solution (72) of dust acoustic solitary waves with (a) $T = 2$, $t = 2$, $a_1 = 1.67$, $a_2 = a_3 = a_4 = 1.29$, $\alpha = 0.5$, $\beta = \gamma = \theta = 1$, and $k_2 = k_3 = k_4 = 0.38$; (b) $T = 3$, $t = 2$, $a_1 = 1.67$, $a_2 = a_3 = a_4 = 1.29$, $\alpha = 0.5$, $\beta = \gamma = \theta = 1$, and $k_2 = k_3 = k_4 = 0.38$; (c) $T = 4$, $t = 2$, $a_1 = 1.67$, $a_2 = a_3 = a_4 = 1.29$, $\alpha = 0.5$, $\beta = \gamma = \theta = 1$, and $k_2 = k_3 = k_4 = 0.38$.

[52] is that we consider the collision of neutral gases as the perturbation term. From the actual physical background, this view is more reasonable.

7. Conclusion

In this paper, according to the control equations of motion, we obtain a (3+1)-dimensional ZK equation describing the propagation of nonlinear dust acoustic waves in space. Then, we extend this equation to the fractional order for the first time and have a completely new model which is the (3+1)-dimensional TSF-ZK equation. The fractional equation that can describe fractal processes of the dust acoustic waves is related to the dust acoustic waves propagation with fractal properties. In the following, we study the conservation law of the (3+1)-dimensional TSF-ZK equation. This indicates that the dust acoustic wave described by this new model is conserved in energy during its propagation, no matter in the fractal process or in the interaction. In addition, according to the extended Kudryashov method, we get the exact solution of (3+1)-dimensional TSF-ZK equation. Then we draw on the exact solution to study the effect of the parameter k , the charge properties of dust particle Z_{d0} , the fractional order values α , β , γ , and θ , the temperature T_d , the gravity g , and the collision frequency β_0 and β_1 on the properties of nonlinear dust acoustic waves by a gravity field in dust plasma.

Data Availability

No data is used in our research.

Conflicts of Interest

The authors declare that there are no conflicts of interest regarding the publication of this paper.

Acknowledgments

This work was supported by Nature Science Foundation of Shandong Province of China (No. ZR2018MA017) and China Postdoctoral Science Foundation funded project (No. 2017M610436).

References

- [1] J. X. Ma, "Dusty plasmas," *Physics*, pp. 244–250, 2006.
- [2] F. Li, "Dust plasma physics," *Physics*, vol. 9, pp. 518–521, 2006.
- [3] N. N. Rao, P. K. Shukla, and M. Y. Yu, "Dust-acoustic waves in dusty plasma," *Planet Space Science*, vol. 38, p. 543, 1990.
- [4] P. K. Shukla and V. P. Silin, "Dustion-acoustic wave," *Physica Scripta*, vol. 45, pp. 508–511, 1992.
- [5] R. L. Merlino, A. Barkan, C. Thompson, and N. D'Angelo, "Experiments on waves and instabilities in dusty plasmas," *Plasma Physics and Controlled Fusion*, vol. 39, no. 5A, pp. A421–A429, 1997.
- [6] R. Bharuthram and P. K. Shukla, "Large amplitude ion-acoustic solitons in a dusty plasma," *Planetary and Space Science*, vol. 41, pp. 17–19, 1992.
- [7] W.-S. Duan and Y.-R. Shi, "The effect of dust size distribution for two ion temperature dusty plasmas," *Chaos, Solitons & Fractals*, vol. 18, no. 2, pp. 321–328, 2003.
- [8] B. B. Kadomtsev and V. I. Petviashvili, "On the stability of solitary waves in weakly dispersive media," *Doklady Akademii nauk SSSR*, vol. 15, pp. 539–541, 1970.
- [9] S. Singh and T. Honzawa, "Kadomtsev-Petviashvili equation for an ion-acoustic soliton in a collisionless weakly relativistic plasma with finite ion temperature," *Physics Fluids B: Plasma Physics*, vol. 5, no. 7, pp. 2093–2097, 1993.
- [10] M.-M. Lin and W.-S. Duan, "(2 + 1) dimensional nonlinear waves in a two-ion-temperature warm dusty plasma

- considering the dust size distribution,” *Chaos, Solitons & Fractals*, vol. 21, no. 2, pp. 325–333, 2004.
- [11] W.-S. Duan, “The Kadomtsev-Petviashvili (KP) equation of dust acoustic waves for hot dust plasmas,” *Chaos, Solitons & Fractals*, vol. 14, no. 3, pp. 503–506, 2002.
- [12] T. S. Gill, N. S. Saini, and H. Kaur, “The Kadomtsev-Petviashvili equation in dusty plasma with variable dust charge and two temperature ions,” *Chaos, Solitons & Fractals*, vol. 28, no. 4, pp. 1106–1111, 2006.
- [13] H. W. Yang, Z. H. Xu, D. Z. Yang, X. R. Feng, B. S. Yin, and H. H. Dong, “ZK-Burgers equation for three-dimensional Rossby solitary waves and its solutions as well as chirp effect,” *Advances in Difference Equations*, vol. 2016, no. 167, 2016.
- [14] M. Guo, Y. Zhang, M. Wang, Y. Chen, and H. Yang, “A new ZK-ILW equation for algebraic gravity solitary waves in finite depth stratified atmosphere and the research of squall lines formation mechanism,” *Computers & Mathematics with Applications*, vol. 75, no. 10, pp. 3589–3603, 2018.
- [15] L. Fu, Y. D. Chen, and H. W. Yang, “Time-space fractional coupled generalized Zakharov-Kuznetsov equations set for rossby solitary waves in two-layer fluids,” *Mathematics*, vol. 7, no. 1, p. 41, 2019.
- [16] M. Han, L. Zhang, Y. Wang, and C. M. Khalique, “The effects of the singular lines on the traveling wave solutions of modified dispersive water wave equations,” *Nonlinear Analysis: Real World Applications*, vol. 47, pp. 236–250, 2019.
- [17] J. T. Ha, H. Q. Zhang, and Q. L. Zhao, “Exact solutions for a Dirac-type equation with N-fold Darboux transformation,” *Journal of Applied Analysis and Computation*, vol. 9, pp. 200–210, 2019.
- [18] M. Liu, X. Li, and Q. Zhao, “Exact solutions to Euler equation and Navier–Stokes equation,” *Zeitschrift für Angewandte Mathematik und Physik*, vol. 70, no. 2, pp. 1–13, 2019.
- [19] H. K. Qi, L. D. Liu, and X. Z. Meng, “Dynamics of a nonautonomous stochastic SIS epidemic model with double epidemic hypothesis,” *Complexity*, vol. 2017, Article ID 4861391, 14 pages, 2017.
- [20] F. X. Song and H. W. Yang, “Modeling and analysis of fractional neutral disturbance waves in arterial vessels,” *Mathematical Modelling of Natural Phenomena*, vol. 14, no. 3, p. 301, 2019.
- [21] C. N. Lu, L. Y. Xie, and H. W. Yang, “Analysis of Lie symmetries with conservation laws and solutions for the generalized (3+1)-dimensional time fractional Camassa-Holm-Kadomtsev-Petviashvili equation,” *Computers & Mathematics with Applications*, vol. 77, no. 12, pp. 3154–3171, 2019.
- [22] Z. Z. Yue and Y. M. Zou, “New uniqueness results for fractional differential equation with dependence on the first order derivative,” *Advances in Difference Equations*, vol. 2019, no. 1, p. 38, 2019.
- [23] H. Yang, J. Sun, and C. Fu, “Time-fractional Benjamin-Ono equation for algebraic gravity solitary waves in baroclinic atmosphere and exact multi-soliton solution as well as interaction,” *Communications in Nonlinear Science and Numerical Simulation*, vol. 71, pp. 187–201, 2019.
- [24] S. M. Meng and Y. J. Cui, “Multiplicity results to a conformable fractional differential equations involving integral boundary condition,” *Complexity*, vol. 2019, Article ID 8402347, 8 pages, 2019.
- [25] Y. L. Li, F. W. Liu, I. W. Turner, and T. Li, “Time-fractional diffusion equation for signal smoothing,” *Applied Mathematics and Computation*, vol. 326, pp. 108–116, 2018.
- [26] S. Aman, Q. Al-Mdallal, and I. Khan, “Heat transfer and second order slip effect on MHD flow of fractional Maxwell fluid in a porous medium,” *Journal of King Saud University-Science*, 2018.
- [27] Q. M. Al-Mdallal and A. S. Abu Omer, “Fractional-order Legendre-collocation method for solving fractional initial value problems,” *Applied Mathematics and Computation*, vol. 321, pp. 74–84, 2018.
- [28] Q. Song and Z. Bai, “Positive solutions of fractional differential equations involving the Riemann-Stieltjes integral boundary condition,” *Advances in Difference Equations*, vol. 2018, Article ID 183, 2018.
- [29] Y. W. Ren, M. S. Tao, H. D. Dong, and H. W. Yang, “Analytical research of (3+1)-dimensional Rossby waves with dissipation effect in cylindrical coordinate based on Lie symmetry approach,” *Advances in Difference Equations*, vol. 2019, p. 13, 2019.
- [30] C. Lu, C. Fu, and H. Yang, “Time-fractional generalized Boussinesq equation for Rossby solitary waves with dissipation effect in stratified fluid and conservation laws as well as exact solutions,” *Applied Mathematics and Computation*, vol. 327, pp. 104–116, 2018.
- [31] C. Fu, C. N. Lu, and H. W. Yang, “Time-space fractional (2+1) dimensional nonlinear Schrödinger equation for envelope gravity waves in baroclinic atmosphere and conservation laws as well as exact solutions,” *Advances in Difference Equations*, vol. 2018, p. 20, 2018.
- [32] X. Meng, F. Li, and S. Gao, “Global analysis and numerical simulations of a novel stochastic eco-epidemiological model with time delay,” *Applied Mathematics and Computation*, vol. 339, pp. 701–726, 2018.
- [33] Y. Tian, Y. Wei, and S. Sun, “Multiplicity for fractional differential equations with p -Laplacian,” *Boundary Value Problems*, vol. 2018, p. 127, 2018.
- [34] B. Kilic and M. Inc, “The First Integral Method for the time fractional Kaup-Boussinesq System with time dependent coefficient,” *Applied Mathematics and Computation*, vol. 254, pp. 70–74, 2015.
- [35] B. Lu, “The first integral method for some time fractional differential equations,” *Journal of Mathematical Analysis and Applications*, vol. 395, no. 2, pp. 684–693, 2012.
- [36] N. Shang and B. Zheng, “Exact solutions for three fractional partial differential equations by the (G'/G) method,” *International Journal of Applied Mathematics*, vol. 43, no. 3, pp. 1–6, 2013.
- [37] B. Zheng, “ (G'/G) -expansion method for solving fractional partial differential equations in the theory of mathematical physics,” *Communications in Theoretical Physics*, vol. 58, no. 5, pp. 623–630, 2012.
- [38] Y. Zhou and W. X. Ma, “Complexiton solutions to soliton equations by the Hirota method,” *Journal of Mathematical Physics*, vol. 58, no. 10, Article ID 101511, 2017.
- [39] W.-X. Ma and Y. Zhou, “Lump solutions to nonlinear partial differential equations via Hirota bilinear forms,” *Journal of Differential Equations*, vol. 264, no. 4, pp. 2633–2659, 2018.
- [40] Y. Gurefe, E. Misirli, A. Sonmezoglu, and M. Ekici, “Extended trial equation method to generalized nonlinear partial differential equations,” *Applied Mathematics and Computation*, vol. 219, no. 10, pp. 5253–5260, 2013.
- [41] S. M. Guo, L. Q. Mei, Y. Li, and Y. F. Sun, “The improved fractional sub-equation method and its applications to the space-time fractional differential equations in fluid mechanics,” *Physics Letters A*, vol. 376, no. 4, pp. 407–411, 2012.

- [42] R. Zhang, L. Yang, J. Song, and H. Yang, "(2+1) dimensional Rossby waves with complete Coriolis force and its solution by homotopy perturbation method," *Computers & Mathematics with Applications*, vol. 73, no. 9, pp. 1996–2003, 2017.
- [43] M. Tao, N. Zhang, D. Gao, and H. Yang, "Symmetry analysis for three-dimensional dissipation Rossby waves," *Advances in Difference Equations*, vol. 2018, article 300, 2018.
- [44] A. Biswas, "1-Soliton solution of the generalized Zakharov-Kuznetsov equation with nonlinear dispersion and time-dependent coefficients," *Physics Letters A*, vol. 373, no. 33, pp. 2931–2934, 2009.
- [45] M. Guo, H. Dong, J. Liu, and H. Yang, "The time-fractional mZK equation for gravity solitary waves and solutions using sech-tanh and radial basis function method," *Nonlinear Analysis: Modelling and Control*, vol. 24, no. 1, pp. 1–19, 2019.
- [46] C. M. Khalique and G. Magalakwe, "Combined sinh-cosh-Gordon equation: Symmetry reductions, exact solutions and conservation laws," *Quaestiones Mathematicae*, vol. 37, no. 2, pp. 199–214, 2014.
- [47] E. Misirli and S. M. Ege, "A new method for solving nonlinear fractional differential equations," *New Trends in Mathematical Science*, vol. 1, no. 5, pp. 225–233, 2017.
- [48] B. J. Zhao, R. Y. Wang, W. J. Sun, and H. W. Yang, "Combined ZK-mZK equation for Rossby solitary waves with complete Coriolis force and its conservation laws as well as exact solutions," *Advances in Difference Equations*, vol. 2018, no. 1, p. 42, 2018.
- [49] M. Guo, C. Fu, Y. Zhang, J. X. Liu, and H. W. Yang, "Study of ion-acoustic solitary waves in a magnetized plasma using the three-dimensional time-space fractional Schamel-KdV equation," *Complexity*, vol. 2018, Article ID 6852548, 17 pages, 2018.
- [50] S. A. El-Wakil and E. M. Abulwafa, "Formulation and solution of space-time fractional Boussinesq equation," *Nonlinear Dynamics*, vol. 80, no. 1, pp. 167–175, 2015.
- [51] W.-S. Duan, "3+1 dimensional envelop waves and its stability in magnetized dusty plasma," *Chaos, Solitons & Fractals*, vol. 27, no. 4, pp. 926–929, 2006.
- [52] N. D'Angelo, "Dust acoustic waves excited by gravity in a collisional plasma," *Physics Letters A*, vol. 304, no. 3–4, pp. 102–105, 2002.
- [53] Q. Zhao and S.-K. Liu, "Application of Jacobi elliptic functions in the atmospheric and oceanic dynamics: Studies on two-dimensional nonlinear Rossby waves," *Chinese Journal of Geophysics*, vol. 49, no. 4, pp. 965–970, 2006.
- [54] J. X. Ma and J. Liu, "Dust-acoustic soliton in a dusty plasma," *Physics of Plasmas*, vol. 4, no. 2, pp. 253–255, 1997.
- [55] J. Y. Wang, X. P. Cheng, Y. Zeng, Y. X. Zhang, and N. Y. Ge, "Quasi-soliton solution of Korteweg-de Vries equation and its application in ion acoustic waves," *Acta Physica Sinica*, vol. 67, Article ID 110201, 2018.